Neotectonics of the Sumatran Fault And Paleogeodesy of the Sumatran Subduction Zone

Thesis by Danny Hilman Natawidjaja

In Partial Fulfillment of the Requirements for the Degree of Doctor of Philosophy



California Institute of Technology Pasadena, California

2002 (Defended September 27, 2002)

© 2002 Danny Hilman Natawidjaja All Rights Reserved

Abstract

Under the Sumatran plate boundary the Australian-Indian plate is subducting at about 60 mm/yr in the direction N11⁰E. The oblique convergence is partitioned into trench-parallel slip—accommodated largely by the Sumatran fault zone and trench-perpendicular slip—accommodated by the subduction zone. Our detailed map of the Sumatran fault zone (SFZ) shows that the Sumatran fault is highly segmented. The influence of these fault segmentations on historical seismic source dimensions suggests that the dimensions of future events will also be influenced by fault geometry. The largest geomorphic offsets along the Sumatran fault zone are about 20 km, and may represent the total offset across the fault. If so, the present SFZ may just be 2 Ma old. The shape and location of the Sumatran fault and the active volcanic arc are highly correlated with the shape and character of the underlying subducting oceanic lithosphere.

We utilize coral microatolls in west Sumatra to document evidence for deformation of the underlying subduction interface. Microatolls are very sensitive to fluctuations in sea level, and thus act as natural tide gauges. They record not only the magnitude of vertical deformation associated with earthquakes (paleoseismic data), but also continuously track long-term aseismic deformation that occurs during intervals between earthquakes (paleogeodetic data). Numerous microatolls from the region around the equator record a simple pattern of tilt away from the trench axis in 1935 related to an M_w7.7 earthquake. About 115 km from the trench axis, uplift was nil. Nearer to the trench, uplift progressively increased trench-ward to at least 90 cm. Farther than 115 km from the trench, submergence of up to 35 cm occurred. We model these paleogeodetic data by a 2.3 m slip event on the interface between 88 and 125 km from the trench axis. A large aseismic event or "silent earthquake" in 1962 is among the most interesting phenomena discovered in the coral record, and is the second largest short-lived event recorded throughout the equatorial region. Furthermore, paleogeodetic data reveal that the *interseismic* deformation rates have varied both temporally and spatially. For two centuries prior to 1935, the rates of long-term submergence above the soon-to-fail rupture were relatively low, indicative of rapid aseismic slip on the subjacent subduction interface. During the 25 years following the 1935 event, submergence rates dramatically increased. Modeling of these data suggests that much of the patch that ruptured in 1935 locked up in the decades after the earthquake. For the last four decades, the rates above the 1935 rupture have been lower than they were in two and half decades following the 1935 event, but are higher still than they were in the decades prior to 1935.

Acknowledgment

I would foremost like to thank my advisor, Kerry Sieh, for giving me financial support, guidance, and the opportunity to work on this exciting research in Sumatra. He was involved in every step of this study. He introduced me to the study of active faults when we worked together on the Sumatran fault in Indonesia prior to my arrival at Caltech. Kerry later infected me with his enthusiasm for studying coral microatolls and reconstructing the geodetic history of the Sumatran subduction zone.

I owe a debt of gratitude to Hiroo Kanamori who has always been keen to help me with many valuable discussions on the subduction zone study. He also helped me quantify the uncertainty of our coral paleogeodetic data, an essential feature of this study. Joann Stock was on my advisory committee, and helped me with valuable suggestions. Thanks are also due to the other members of my thesis committee—Jason Saleeby, who served as my academic advisor, Mark Simons and Tom Heaton, who provide valuable suggestions for improving the interpretation and presentation of the paleogeodetic data, and Jess Adkins, who gave valuable suggestions on the study of the corals.

There are many people without whom the work that has led to this thesis would have been impossible. I thank Steve Ward at U.C. Santa Cruz who helped us with the modeling of our paleogeodetic data. I learned valuable lessons about modeling from intensive discussions with him. My gratitude is also due to Larry Edwards at University of Minnesota, who performed the U-Th radiometric analysis of our coral samples.

I am very proud of the members of the Sumatran team, *a.k.a.* the M.I. (Mission Impossible) team, who were always highly motivated, hard working, and helpful in every

way. Our fieldwork would not have been very productive without their superb teamwork. Bambang W. Suwargadi handled most of the bureaucratic and administrative paperwork that otherwise would have slowed our progress. John Galetzka (USGS) and Dudi Prayudi (LIPI) never gave up on solving problems with our engines and power supply and many other technical obstacles. Without John's expert hand, it would have been impossible to collect all those big coral slabs. Bambang and Imam Supriyanto helped arranging the boat rental and preparing field equipments. Imam, his wife (Susi) and their family were always very kind and helpful. Their home in Padang (West Sumatra) became our second home. They kindly provided their garage for a storage space for our equipment and samples as well as for a workshop. We thank the Fishery Department of Bung Hatta University in Padang and the owner of the Padang Diving boat for lending us their boats. We also appreciate the dedication of their boat crews who made our journey pleasant, safe and productive

I would like to thank Hery Harjono, director of The Research center of Geotechnology of the Indonesian Institute of Sciences (LIPI), Jan Sopaheluwakan, the Deputy of Natural Sciences of LIPI, and Suparka, a vice chairmain of LIPI, and many other people at LIPI, who provided essential administrative support for conducting this research in Indonesia. Hery Harjono was enthusiastic and supportive throughout the study. Hariadi Permana, Iskandar Zulkarnain, and Jedi S. Widarto helped us in planning the field work. My thanks are also due to all my friends at LIPI who were consistently kind and helpful.

I thank Linette Prawirodirdjo, Jeff Genrich and Yehuda Bock at Scripps Institute of Oceanography for inspiring and pleasant interactions throughout our collaborative study on Sumatra. I have gained valuable knowledge from our one-day discussion with them and with Joe Curray when we visit Scripps in early 2000. My thanks are also due to Mike Gagan from Australian National University (ANU) for his participation in our fieldwork in 1999, and to Nerilie Abram for her valuable input to our coral study via our e-mail correspondence and during her visit to Caltech in 2001.

Caltech is a truly remarkable place full of extraordinary people. I could write a separate chapter to thank many people here. In particular, I would like to thank Tony Soeller and Joanne Giberson, who kept the GIS Lab up and running. Tony provided many useful scripts for the creation of the digital map of the Sumatran fault. I thank Jim O'Donnell and Susan Leising, who provide the best library service of any that I have known. My gratitude is due to Suefawn Barnett, who provided administrative support for this Sumatran project since my arrival at Caltech. Karolyn Knoll helped us prepare for the fieldwork in 2002. Donna Sackett and many other administrative staff members generously provide administrative services whenever needed. All the graduate students and post-doctoral fellows are brilliant people and always keen to discuss any topic. Jascha Polet and Magali Billen, and Anu Venkatraman help me with GMT problems. Jascha also provide an English translation for an old report in Dutch about the 1935 historical earthquake in Sumatra. Leo Eisner gave of his time to discuss some seismologic and math principles over a few beers. Edwin Schauble and Anke Frederick provided valuable discussions. Nathan Niemi and Mike Oskin help with solving problems in the Arc/Info. My officemates—Jing Liu, and Bruce Hsu always kept the atmosphere in our office pleasant and friendly. Eric Cowgill, Todd Ehlers and Nadine McQuarrie contributed to warm and inspiring discussions in our weekly tectonic group meeting.

I am gratefull to Simon LeVay who significantly improved the grammar and clarity of the text. Caltech proofreaders also provided valuable corrections to the grammar as well as the consistency of the text.

Finally, I am incredibly indebted to my family, particularly to my mother and father, who are endless sources of love and support. Lastly, I would like to express my sincere love and gratitude to my wife, Pramesti Resiandini, who has stood closely by me through the years of joy and difficulties and hard work that lead to this day. She also helped me in reformatting the thesis draft.

Table of content

Chapt	er 1. Introduction	•••••
1.1.	Motivation: Scarcity of data for understanding the earthquake cycle	1-2
1.2.	Opportunities in the Sumatran plate boundary	1-3
1.3.	Content and organization of this thesis	1-5
	1.3.1. Neotectonics of the strike-slip Sumatran fault	1-6
	1.3.2. Paleogeodesy and paleoseismology of the Sumatran subduction zone	1-7
1.4.	References	1-8
Chapt	er 2. Neotectonics of the Sumatran fault, Indonesia	
2.1.	Abstract	2-2
2.2.	Introduction	2-3
	2.2.1. Plate tectonic environment	2-3
	2.1.2. Motivation of this work	2-6
2.3.	A modern map of the fault	2-7
	2.3.1. Resources and methods	2-8
	2.3.2. Geometry of the fault	2-9
	2.3.3. Major segments of the Sumatran fault	.2-10
	2.3.4. Other related structures	. 2-29
2.4.	Discussion, interpretations, and speculations	2-30
	2.4.1. Historical and future seismicity	.2-31
	2.4.2. Offsets across the Sumatran fault and the evolution of dextral slip alor	ng
	the Sumatran margin	. 2-32
	2.4.3. Tectonic model of the Sumatran plate margin	. 2-51
	2.4.4. Relationship of the Sumatran fault to the modern volcanic arc	. 2-55
	2.4.5. Relationship of the Sumatran fault to the subduction zone	.2-60
2.5.	Summary, conclusions, and remaining questions	.2-61
2.6.	Acknowledgments	. 2-65
2.7	Deferences	2 66

-	ter 3. Paleogeodetic records from microatolls above the centr	
Suma	tran subduction zone	
3.1.	Introduction	3-2
	3.1.1. Motivation	3-2
	3.1.2. Sumatran active subduction	3-4
3.2.	Coral microatolls as paleoseismic and paleogeodetic instruments	3-7
	3.2.1. General	3-7
	3.2.2. The synthetic microatoll	3-9
3.3.	Method	3-11
3.4.	Paleogeodetic and paleoseismic sites	3-13
	3.4.1. Bendera site	3-13
	3.4.2. Badgugu site	3-19
	3.4.3. Barogang site	3-26
	3.4.4. Pono site	3-33
	3.4.5. Antinang site	3-42
	3.4.6. Memong site	3-44
	3.4.7. Tofa site	3-51
	3.4.8. Tanjung Anjing site	3-54
	3.4.9. Penang site	3-59
	3.4.10. Bai site	3-62
	3.4.11. Lago site	3-66
	3.4.12. Masin site	3-70
	3.4.13. Lambak site	3-74
	3.4.14. Sambulaling site	3-77
	3.4.15. Telur site	3-84
3.5.	Synopsis	3-85
3.6.	References	3-86

4.1.	Overview	4-2
4.2.	Analysis of uncertainties in HLS records	4-3
	4.2.1. Uncertainties associated with local effects and short-term regional	
	oceanographic fluctuations	4-3
	4.2.2. Ambiguities due to erosion	4-6
	4.2.3. Determination of submergence and emergence rates	4-8
4.3.	THE 1935 EVENT	4-10
	4.3.1. Overview	4-11
	4.3.1. Dating of the event	4-12
	4.3.2. Magnitude and pattern of vertical deformation	4-13
	4.3.3. Paleogeodetic source parameters of the 1935 event	4-16
	4.3.4. Elastic dislocation model of the 1935 event	4-19
4.4.	THE 1962 EVENT	4-17
	4.4.1. Overview	4-22
	4.4.2. Magnitude, duration and pattern of vertical deformation	4-22
	4.4.3. Elastic dislocation model of the 1962 event	4-25
4.5.	Deformation in the intervening decades	4-28
	4.5.1. Introduction	4-28
	4.5.2. Paleogeodetic evidence for deformation in the intervening decades	4-32
	4.5.3 Elastic modeling of slow deformation in the three periods: pre-1935,	1935–
	1962, and post-1962	4-35
4.6	Summary of Paleogeodetic records and of elastic models	4-40
4.7.	DISCUSSION	4-45
	4.7.1. Expenditure of the subduction slip budget throughout the 20th century	ry 4-47
	4.7.2. Implication of paleogeodetic behavior for rheology of the subduction	1
	interface	4-51
	4.7.3. Structural reasons for the contrast between the Equatorial patch and	the
	interface farther south	4-55
	4.7.4. Comparison with other subduction zones	4-57
4.8]	References	4-19

Chapter 5. A 250-year-long paleogeodetic record of subduction:	from
Sumatran coral heads	
5.1. Abstract	5-2
5.2. Introduction	5-3
5.2.1. Motivation	5-3
5.2.2. Active Tectonics of the Sumatran subduction	5-4
5.2.3. Paleogeodetic records from the Equatorial region	5-5
5.3. The longest paleogeodetic record from near the Equator	5-6
5.4. The slab analysis	5-9
5.4.1. The heads	5-9
5.4.2. HLS history	5-12
5.5. Interpretation and Discussion	5-19
5.5.1. Insights from interpreting the 20th-century record	5-20
5.5.2. Emergence events in 1743 and 1797	5-21
5.5.3. Disturbances in 1833 and 1861	5-21
5.5.4. Slow submergence between 1797 and 1935	5-22
5.5.5. The 1935 event (M _w 7.7)	5-23
5.5.6. The 200-year-subduction history	5-24
5.5.7. Summary and conclusion	5-26
5.6. References	5-27

List of figures

Figure 1.1 Map of the principal tectonic elements of the Sumatran plate boundary	1-11
Plate 2.1 Map of the Sumatran fault and related features.	2-76
Figure 2.1 Regional tectonic setting of the Sumatran fault.	2-77
Figure 2.2 Data upon which the Sumatran fault map compilation is based	2-78
Figure 2.3 An example of the approximately 1:100,000-scale aerial photographs we	used
to compile most of our map of the Sumatran fault.	2-79
Figure 2.4 Map of 20 geometrically defined segments of the Sumatran fault system	and
their spatial relationships to active volcanoes, major graben, and lakes	2-80
Figure 2.5 Sumatran fault and related structures near the Sunda Strait	2-81
Plate 2.2 Shaded-relief map of the Sumatran fault where it crosses the western flank	c of a
highly dissected volcano at about 4.2°S.	2-82
Plate 2.3 Map of the Sumani and Sianok segments near the Singkarak graben	2-83
Figure 2.6 Map of small and large geomorphic offsets along the Sumatran fault	2-84
Figure 2.7 Two of the most compelling large geomorphic offsets along the Sumatra	.n
fault, the 21-km dextral offsets of the Tripa and Meureubo Rivers in north Sum	atra.
	2-85
Figure 2.8 Hypothetical evolution of the Singkarak graben and bounding normal fa	ults.
	2-86
Plate 2.4 Geologic maps of offset bedrock units along three sections of the Sumatra	n
fault	2-87
Figure 2.9 Stretching of the forearc sliver plate near the Sunda Strait	2-88
Figure 2.10 A plausible history of deformation along the obliquely convergent Sum	atran
margin	2-89
Plate 2.5 Geometric and structural details of the Sumatran fault, the forearc basin, o	uter-
arc ridge, and volcanic arc, suggesting the division of the Sumatran plate margi	n
into northern, central, and southern domains	2-90
Figure 2.11 Plot of the distance of volcanic centers from the Sumatran fault showing	ıg
that the volcanic arc has not influenced the location of the fault	2-91
Figure 3.1 Map of the principal tectonic elements of the Sumatran plate boundary	3-90

Figure 3.2	Index map to the coral paleogeodetic sites.	3-91
Figure 3.3	Seismicity in the central Sumatran subduction zone.	3-92
Figure 3.4a	The computer simulation of 100 years of growth of a coral microatoll	located
in a su	ıbmerging area.	3-93
Figure 3.4b	The computer simulation for a microatoll located in a stable region, b	out
which	experiences a sudden submergence.	3-93
Figure 3.4c	The computer simulation for a microatoll located on an intertidal reef	that is
emerg	ging	3-94
Figure 3.4d	The computer simulation for a microatoll located at the site that has a	long-
term s	tability but the coral experiences a sudden emergence event	3-94
Figure 3.5a	General site map at Bendera bay, southwest Tanabala	3-95
Figure 3.5b	Detailed map of the Bendera site	3-96
Figure 3.6a	Elevations of perimeter crests of the ancient and the living microatoll	s3-97
Figure 3.6b	Shapes and relative positions of the three types of microatolls in Bend	dera
site		3-97
Figure 3.7a	Sampled ancient microatoll (H1). The cup-shaped geometry implies	that a
rapid s	submergence had occurred prior to the 1935 event.	3-98
Figure 3.7b	Drawing of the Tb97 slab collected from H1	3-98
Figure 3.7c	e HLS records recovered from the Tb97 are plotted as a function of time	e 3-98
Figure 3.8a	Drawing of the radiograph of the Tb00A1 thin section	3-99
Figure 3.8b	HLS history recovered from the Tb00A1 slab.	3-99
Figure 3.9a	Schematic diagram showing a combine coral stratigraphy from Tb97	and
from T	Γb00A1 slabs.	3-100
Figure 3.9b	The combine HLS history recovered from The ancient and the living	heads
span t	he entire 20th century.	3-100
Figure 3.10	Map of the east-Badgugu site.	3-101
Figure 3.11	a Schematic beach cross section and the two populations of microatol	ls.3-102
Figure 3.11	b Relative elevations of tops of microatoll's perimeters	3-102
Figure 3.12	2a Cross section of the hat-shaped Bdg00B1 head.	3-102
Figure 3.12	2b HLS history of Bdg00B1 slab from east Badgugu site	3-102
Figure 3.13	B HLS history from west Badgugu site.	3-103

Figure 3.14 Surveyed crest points of the head H6 from the center to exterior 3-103
Figure 3.15 Barogang site map. 3-104
Figure 3.16a Detailed map of the modern hat-shaped microatolls at Barogang 3-105
Figure 3.16b Cross sections of the modern hat-shaped microatolls at Barogang 3-105
Figure 3.16c Elevations of the perimeter crests of the central bowl and the brims3-105
Figure 3.17a Radiograph of the Brg00A1 slab showing excellent contrast of annual pairs
of dark and light bands
Figure 3.17b Drawing of the BrG00A1 radiograph showing the coral band stratigraphy
of the hat-shaped head
Figure 3.17c HLS history reconstructed from the Brg00A1 slab
Figure 3.18 Topography of H3 that has a relatively preserved upper surface of the central
bowl
Figure 3.19a Coral stratigraphy of the Brg97 slab showing a submergence event in 1962.
Figure 3.19b Combined HLS histories of Brg97 and Brg00A1 for the period from 1955
to 1997
Figure 3.20a General map of Pono site
Figure 3.20b Detailed map of the surveyed microatolls
Figure 3.21a Photos of the modern heads, taken in mid-1997 when the microatoll
perimeters were still alive
Figure 3.21b Cross sections of the selected modern heads above (except H5) showing
lower central flats and prominent emergence for the past few decades 3-110
Figure 3.22a Plan-view maps of the large microatolls. Their topography shows a very
low relief indicative of generally near-stable conditions
Figure 3.22b Cross sections of the large microatolls above. The interiors displays a few
lower flats implies general stable conditions were interrupted by sudden
submergences. 3-111
Figure 3.23a Tops of most of the microatolls are concordant. The elevations of the tops
of living rings in 1997 are generally within 2cm of each other
Figure 3.23b Comparisons of the elevations of similar crests and troughs across the
heads

Figure 3.24a Cross section o	f H2 showing rapid submergence in 1962, a stable pe	eriod
between 1969 and 1983	, and rapid or sudden emergence about 1983-1986.	3-113
Figure 3.24b HLS history de	educed from Pn97A1 slab.	3-113
Figure 3.24c and d Average	rate if the effect of the mid-1980s emergence step is	}
removed		3-113
Figure 3.25a Cross section of	of the head H10 – Pn00A3.	3-114
Figure 3.25b Plots of HLS r	ecords of the east wing as a function of time	3-114
Figure 325c Plots of HLS re	ecords of the west wing.	3-114
Figure 3.26a Combined HL	S histories of Pn00A3 and Pn97A1.	3-115
Figure 3.26b Combined HL	S graph after correction for a possible 7cm local sett	lement
of the Pn00A3 head dur	ring the 1984 earthquake	3-115
Figure 3.27 Map of the Anti	inang site.	3-116
Figure 3.28 (a) Trace of a ra	ndiograph of the At99A1 slab. (b) Deduced HLS hist	ory
		3-116
Figure 3.29 Map of the Mer	nong site	3-117
Figure 3.30 (a) Graphical re	presentation of relative elevations of 31 microatoll p	erimeter
crests. (b) Table of relat	tive mean elevations of perimeter crests	3-117
Figure 3.31 (a) and (b) Map	s of the two largest and oldest microatolls at the site.	3-118
Figure 3.32 (a), (b), and (c)	Tracings of radiographs from the two slabs and the	eir HLS
histories		3-119
Figure 3.33 (a) Map view of	f modern eads at Memong	3-120
Figure 3.34 Site map at Tofa	a displays populations of both modern and Mid-Holo	ocene
heads		3-121
Figure 3.35 (a) Analysis of	Tf99C1 slab. (b) Tf99B1 slab. (c) HLS histories	3-121
Figure 3.36 (a) Map of the T	Tanjung Anjing site. (b) Head cross sections of Porito	es
microatolls. (c) Survey	ed elevations of head's crests.	3-122
Figure 3.37 (a) and (b) Trac	es of the radiographs of slabs from Tanjung Anjing.	(c) HIS
histories		3-123
Figure 3.38 Map of the site	in Penang Island.	3-124
Figure 3.39 (a) and (b) The	slabbed modern head and its cross section. (c) Relati	ve
elevation of the crests o	of living rings surveyed in mid-1997	3-124

Figure 3.40 (a) Analysis the Pe97-1 slab. (b) HLS history of the Pe97-1 slab	3-124
Figure 3.41 (a) The site on a small islet at the northern tip of Bai Island	3-125
Figure 3.42 (a) The "cabbage" head. (b) The cross section of the Ba97B-1 slab	o. (c) HLS
history.	3-125
Figure 3.43 Map of the Lago site. (b) Schematic beach cross section. (c) Detail	ed map of
the field of the modern Porites surveyed in 1999 and 2000.	3-126
Figure 3.44 (a) Profiles of selected microatolls and measurements of perimeter	crest
elevations of 21 heads. (b) Relative elevations of the perimeter crest	3-127
Figure 3.45 Slabs from head H17 (a) Lg99A1 and Lg00A1, collected in 1999 a	and 2000.
(b) Plot of the HLS history recovered from Lg99A1 and Lg00A1	3-128
Figure 3.46 (a) General map of Masin site. (b) Detailed map of surveyed mode	rn
microatolls. (c) Cross- sections of the selected heads. (d) Elevation of the	
perimeter's crests	3-129
Figure 3.47 (a) Plan-view map of head H19 at masin. (b) Trace of the radiogram	ph of the
Msn00A1 slab. (c) HLS history derived from the slab.	3-130
Figure 3.48 (a) Coral stratigraphy from the modern head at Lambak site. (b) A	graph of
HLS history	3-131
Figure 3.49 (a) Map of site at Sambulaling. (b) Survey of crests of living rings	s in 1997.
	3-132
Figure 3.50a Internal growth structures of Sm97-2 slab	3-133
Figure 3.50b Cross section of the modern head H2 (Sm97-1).	3-133
Figure 3.50c Graphical representation of a combined HLS history derived from	the old
and modern microatolls	3-133
Figure 3.51 (a) Chiseled sample from a small living head (Te97-1) in Mid-199	7 at the
Telur site. (b) HLS history for the past 15years	3-134
Figure 4.1 HLS histories of all sites, plotted with the aligned time scale and the	e same
scaling	4-68
Figure 4.2 Non-tectonic HLS die-downs during El-Nino and Ocean Dipole sea	sons 4-69
Figure 4.3 HLS die-downs that occurred locally.	4-70
Figure 4.4a Three sites with particularly good HLS records.	4-71

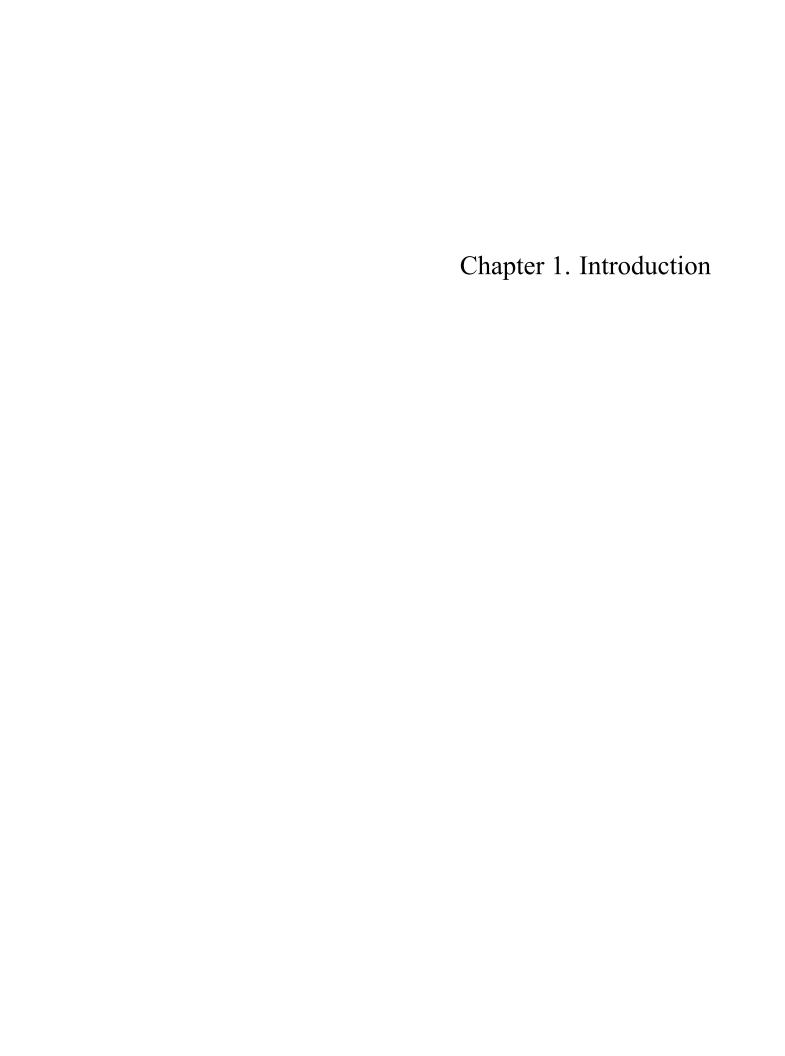
Figure 4.4b	Angsa site: numerous living microatolls showed pristine micro-topograp	phy.
		. 4-71
Figure 4.5	Erosion adds additional uncertainty to the rate calculations	. 4-72
Figure 4.6	Graphical representations of coral degradations.	. 4-73
Figure 4.7	Vertical displacements during the 1935 event	. 4-74
Figure 4.8	Date ranges of the December 1935 event based on visual ring counting	. 4-75
Figure 4.9	Date ranges for the 1935 event, based upon U-Th dates	. 4-75
Figure 4.10	A comparison of vertical deformations for the 1935 event from microate	olls
and fro	om a seismologic-based elastic model.	. 4-76
Figure 4.11	Difference between measured uplift determined from microatolls and th	ne
uplift p	predicted by the elastic dislocation model.	. 4-77
Figure 4.12	Two-D fit to microatoll data for the 1935 event	. 4-78
Figure 4.13	Date ranges for the 1962 event based on visual ring counting	. 4-79
Figure 4.14	Map of the 1962 emergence event	. 4-80
Figure 4.15	Map of Submergence that occurred in 1962.	. 4-81
Figure 4.16	The 2-D elastic dislocation that fits of the data of the 1962 emergence e	vent.
		. 4-82
Figure 4.17	Data of the 1962 submergence.	. 4-82
Figure 4.18	Superposition of the slips on the subduction interface from the 2-D elas	tic
disloca	tion models of the 1962 event	. 4-82
Figure 4.19	Paleogeodetic records derived from HLS records, but corrected for a 2	
mm/yr	global sea-level rise.	. 4-83
Figure 4.20	Average rate of deformations prior to 1935.	. 4-84
Figure 4.21	Average rates of deformations from 1935 to 1962.	. 4-85
Figure 4.22	Average rates of modern deformations (1962-2000).	. 4-86
Figure 4.23	a Sketch showing the parameters of an idealized elastic dislocation mode	el of
interse	ismic deformation at a subduction zone.	. 4-87
Figure 4.23	b Sketch showing contributions to vertical motions from individual sour	ces.
		. 4-87
Figure 4.24	Elastic dislocation models of slow vertical deformation prior to 1935	. 4-88

xviii

Figure 4.25	Elastic dislocations modeling of slow vertical deformation for the period	l
from 19	935 to 1961	4-89
Figure 4.26	The 2-D elastic dislocation models of modern interseismic deformations	
(1962-2	2000)	4-90
Figure 4.27	Summary of Paleogeodetic records of vertical deformations for the 20th	
century	·	4-91
Figure 4.28	Summary of the elastic dislocation models of the 20th-century paleogeod	detic
history.		4-92
Figure 4.29	Seismic and aseismic slip history on the subduction interface from 1900	to
2000 ba	ased on paleogeodetic data and elastic dislocation models.	4-93
Figure 4.30	Hyphothesis of the eastward moving of the subducting IFZ (Investigator	
Fractur	e Ridge) along the Sumatran subduction.	4-94
Figure 5.1a	Map of the principal tectonic elements of the Sumatran plate boundary	5-31
Figure 5.1b	Index map and the regional geological structures.	5-31
Figure 5.2	The two fossil microatolls that constitute the majority of the Badgugu reco	ord.
		5-32
Figure 5.3 V	West Badgugu site map.	5-33
Figure 5.4 I	Relative elevations of perimeter crests of microatolls at Badgugu	5-34
Figure 5.5 A	Analysis of four slabs from the West and East Badgugu sites	5-35
Figure 5.6	The HLS histories of the three longest coral slabs suggest that the physica	.1
behavio	or of the subduction before 1935 appears to have unchanged since 1800.	5-36
Figure 5.7 A	A graphic presentation of a complex history of seismic and aseismic slip of	on
the sub	duction interface for the last 200 years	5-37

List of tables

Table 2.1. The Sumatran Fault's Major Segments	2-74
Table 2.2. Selected Small Offsets Along the Sumatran Fault (From North to South) . 2-75
Table 2.3. Proposed Large Offsets Across the Sumatran Fault	2-75
Table 3.2 C-14 absolute age for the Mid-Holocene heads	3-54
Table 3.1. ²³⁰ Th ages of the central Sumatran microatolls analyzed in Chapter 3	. 3-135
Table 4.1 Vertical displacement in the 1935 event	4-15
Table 4.2 Vertical displacements of the 1962 event.	4-23
Table 5.1 The ²³⁰ th ages of the samples from microatolls in west Badgugu	5-30



1.1. Motivation: Scarcity of data for understanding the earthquake cycle

Understanding the sequential rupture of active faults is a fundamental unrealized goal in earthquake science. A key reason for slow progress is that relevant data bearing on how strains accumulate in the blocks surrounding faults and how faults release accumulated strains are difficult to obtain. Hence, physical models of the cycle of strain accumulation and relief remain loosely constrained. Common outstanding questions concern the regularity of fault rupture, repeatability of the pattern of slip on a fault, and the roles of geologic structure and rheology in governing ruptures. Clearly, answers to these and related questions are essential to progress in both the practical and academic realms of earthquake science. A thousand years hence, modern geodetic and seismologic instrumental records will likely have provided most of the requisite data. In the meantime, there will be a pressing need to collect paleoseismologic and paleogeodetic records for clues to the long-term behavior of faults.

Paleoseismology has contributed to understanding serial fault ruptures. But progress is being hampered by the imprecision and incompleteness of most records and by the difficulty of data acquisition. Data sets longer than one earthquake cycle are rare and generally incomplete and imprecise [Sieh, 1996]. Records are commonly incomplete due to poor preservation of ruptures in the geologic record. And even where excellent evidence of past earthquake events exist, for example, for the San Andreas Fault [Sieh et al., 1989], the Cascadian subduction zone [Atwater, 1992], and for the Nankai subduction zone [Ando, 1975], paleogeodetic data for interseismic periods are lacking.

Furthermore, paleoseismic dating precision is seldom better than ± 30 yr; thus, correlation of events is often speculative. For example, along the San Andreas, where four sites contain complete or nearly complete records of ruptures for the past millennium, large dating uncertainties make correlation of events along strike highly subjective [*Grant*, 1996; *Sieh*, 1996].

Moreover, the development of individual paleoseismic sites is so time-consuming that even on "celebrated" faults, such as the San Andreas faults, the North Anatolian faults and the Cascadian subduction zone, the distance between good sites is commonly a hundred km or so. This obstacle renders tests of the repetition of slip functions less conclusive than one would desire [Sieh, 1996]. Above the Sumatran plate boundary, we have an unusual opportunity to address these problems. Along the Sumatran fault, one of the largest and most active strike-slip faults in the world, we investigate the effect of fault geometry and discontinuities on earthquake ruptures. And along the Sumatran west coast and the outer-arc islands, we utilize coral microatolls as stable, long-lived "instruments" to document paleoseismic and paleogeodetic evidence for seismically and aseismically failing segments of the underlying subduction interface.

1.2. Opportunities in the Sumatran plate boundary

West Sumatra is an oceanic/continental plate boundary that consists of two fault systems, the mostly dextral strike-slip Sumatran fault system and a predominantly dipslip subduction interface [Fitch, 1972; McCaffrey, 1991]. Oblique northward convergence of the Indian and Australian plates toward Southeast Asia occurs at about 60 mm/yr [Prawirodirdjo, 2000; Prawirodirdjo et al., 1997]. The plate convergence

partitions into trench-parallel slip that is being accommodated largely by the Sumatran fault and trench-perpendicular slip accommodated by the subduction interface [Fitch, 1972; McCaffrey, 1991].

The Sumatran fault has generated nearly a dozen earthquakes of 7≤M≤7.7, as well as many smaller events, over the past century (Fig. 1.2). Unlike the San Andreas Fault, the Sumatran Fault is highly segmented. Thus, it offers an unusual opportunity to study the effects of segmentation on fault ruptures [*Rice*, 1992]. In our delineation of the geometry of the fault, we found evidence that the size and termini of these historic ruptures were generally limited by large dilatational stepovers. These divide the fault into 19 segments ranging in length from 60 to 200 km. Our best estimates of the rupture zones of these historical events are depicted as yellow ellipses in Figure 1.2.

The Sumatran subduction zone has produced two very large earthquakes—in 1833 (M9) and in 1861(M8.5). These dominate the historical seismicity of the subduction interface (Fig 1.2). Historical records of shaking and tsunami suggest that these events involved rupture of all or most of the interface between about 2° N and 5° S [Newcomb and McCann, 1987]. The M7.7 earthquake of 1935 and M7.2 earthquake of 1984 also involved rupture of the subduction interface, but in a zone sandwiched in between those involved in the 1833 and 1861 ruptures [Rivera et al., 2002]. The most recent large event is an M 7.8 earthquake in June, 2000 (Fig. 1.2). This was a complex event near the southern end of the 1833 rupture. Abercrombie [submitted 2001] has found that it involved rupture of the subduction interface and a strike-slip fault within the down-going oceanic slab. This is consistent with activity on N–S oceanic fractures to the west [Deplus et al., 1998]. The presence of fringing coral reefs on the islands of the

outer-arc ridge, only about 100 km from the trench, provides a good opportunity to study earthquake cycles of the Sumatran subduction interface [Sieh et al., 1999; Zachariasen et al., 1999; Zachariasen et al., 2000]. Using microatolls as natural tide gauges, we are able to recover the magnitude and geographic pattern of vertical deformation associated with past major earthquakes, as well as of the continuing slow deformation in the intervals between seismic events. Furthermore, because exposures of microatolls are more accessible than most paleoseismic data, we have been able to explore a large number of sites throughout a 150 by 450 km region in just a few years.

1.3. Content and organization of this thesis

This work is divided into five chapters. Chapter 2 contains the results of our neotectonic study of the Sumatran fault. The chapter is a reformatted version of a paper that was published in the *Journal of Geophysical Research* [vol.105, December 2000]. The content of the chapter is identical to that of the paper, except that some of the figures that were published in black and white appear in color here. The remaining chapters contain our paleoseismic and paleogeodetic studies of Sumatran subduction. These will not have been published by the time of the thesis defense. The data and analyses in this thesis are more comprehensive and complete than will be possible in the papers that will be distilled from them.

1.3.1. Neotectonics of the strike-slip Sumatran fault

The primary objective of our work on the Sumatran fault (Chapter 2) was to map the entire 1600 km long fault at a scale that would be large enough to enable assessment of the role of fault geometries and discontinuities in rupture processes. Secondary objectives were to study the tectonic evolution of the fault system and its interactions with the active volcanic arc through which it courses. We also intended to determine if and how the millennial slip rate of the fault varied along strike, to test the hypothesis that slip should vary along strike because of the curvature of the plate boundary [McCaffrey, 1991; McCaffrey, 1992]. This work never progressed beyond its initial stages [Natawidjaja and Sieh, 1994; Sieh et al., 1994; Sieh et al., 1991].

I intended to include the most thorough analysis of the historical record of large earthquakes along the Sumatran fault, to test the influence of large stepovers and jogs in the fault on the locations of rupture termini. Although I have collected much data, this aspect of my work is still too preliminary to be presented as a separate chapter. However, some aspects of evidence that I had collected were integrated into Chapter 2.

My advisor, Kerry Sieh, had initiated work on the Sumatran fault a few years before my arrival at Caltech. He had mapped about half of the Sumatran fault segment at a scale of 1:50,000. My involvement in this work began in 1993, and we first went to the field together in 1994, specifically to collect data that would enable us to determine geological slip rate along the fault. In my second and third years as graduate student at Caltech (1996–1998), I continued working on the Sumatran fault and finished mapping the entire fault using additional 1:50,0000-scale topographic maps and aerial photos that I

had brought from Indonesia. Analyzing so many aerial photographs and compiling my data on such a large number of maps inspired us to experiment with digital compilation of data. This began as a task that my advisor hired technician Carolyn White to accomplish, using Arc/Info. I completed this work for the entire Sumatran Fault.

1.3.2. Paleogeodesy and paleoseismology of the Sumatran subduction zone

Chapters 3 through 5 focus on the paleogeodetic and paleoseismic signals of subduction processes recorded in coral microatolls of the fringing reefs of western Sumatra. The data upon which this work is founded were collected in three month-long field excursions in 1997, 1999, and 2000. Chapter 3 and 4 comprise the largest part of my dissertation. These two chapters are the result of our work on microatolls near the Equator, where a large (M7.7) rupture of the subduction interface in 1935 is well recorded in the coral morphology and stratigraphy. These were the best data we obtained to rigorously test and develop the method first attempted using Sumatran microatolls a few hundred kilometers further south by *Zachariasen* [1998a].

Chapter 3 is predominantly a detailed description and analysis of each paleogeodetic site and of the individual paleogeodetic histories derived from each coral slab. The dates of my paleogeodetic time series are constrained by U-Th disequilibrium analyses performed in the laboratory of our collaborator, R. Lawrence Edwards, at the University of Minnesota. In Chapter 4, we synthesize the paleogeodetic data from the individual microatolls and sites. This synthesis has two aspects: a treatment of uncertainties in the microatoll "instrument," and a simple initial attempt to physically

model the data. We collaborated with Steve Ward at the University of California, Santa Cruz, to develop the elastic dislocation models that appear in this chapter. Our initial, less conclusive collaboration with Ward, using just the data collected in 1997, has already been published [Sieh et al., 1999]. Additional investigation of the 1935 earthquake, using historical seismograms, was carried out in collaboration with by Luis Rivera, during his year-long visit to Caltech in 2000 [Rivera et al., 2002]. Chapter 5 is a smaller chapter in which I present and interpret a very long paleogeodetic record derived from an extraordinarily large microatoll from the Equatorial region. The reason for separating the description and analysis of this microatoll record into a separate chapter is that it is about a century and a half longer than the record of any of the other microatolls. Thus, it records the effects of the giant earthquakes of 1833 and 1861 and other ancient events in addition to the record of the 20th century. This record provides a uniquely long glimpse at long-term variations in subduction processes.

Our study area for paleogeodetic works actually includes southern Sumatran subduction where the 1833 historical earthquake have ruptured the subjacent subduction interface in this region, such as indicated in Figure 1.2. However, this part of the study is working in progress still, and is not intended to be part of this thesis, therefore is not presented here.

1.4. References

Abercrombie, R.E., The June 2000, M_w7.9 earthquake in south of Sumatra: deformation in the India-Australia Plate, *Journal of Geophysical Research*, submitted 2001.

- Ando, M., Source mechanisms and tectonic significance of historical earthquakes along the Nankai through, Japan, *Tectonophysics*, *27*, 119-140, 1975.
- Atwater, B., Geologic evidence for earthquakes during the past 2000 years along the Copalis River, southern coastal Washington, *Journal of Geophysical Research*, 97, 1901-1919, 1992.
- Deplus, C., M. Diament, H. Hebert, G. Bertrand, S. Dominguez, J. Dubois, J. Malod, P. Patriat, B. Pontoise, and J. Sibilla, Direct evidence of active deformation in the eastern Indian oceanic plate, *Geology*, *26*, 131-134, 1998.
- Fitch, T., Plate convergence, transcurrent faults, and internal deformation adjacent to southeast Asia and the western Pacific, *Journal of Geophysical Research*, 77, 4432-4462, 1972.
- Grant, L., Uncharacteristic Earthquakes on the San Andreas Fault, *Science*, *272*, 826-827, 1996.
- McCaffrey, R., Slip vectors and stretching of the Sumatran fore arc, *Geology*, *19*, 881-884, 1991.
- McCaffrey, R., Oblique plate convergence, slip vectors, and forearc deformation, *J. Geophys. Res.*, *97*, 8905-8915, 1992.
- Natawidjaja, D., and K. Sieh, Slip rates along the Sumatran transcurrent fault and its tectonics significance, *Abstract in Proceeding of Conference on Tectonic Evolution of Southeast Asia, Geol.Soc. of London*, 1994.
- Newcomb, K.R., and W.R. McCann, Seismic history and seismotectonics of the Sunda Arc, *Journal of Geophysical Research*, *92*, 421-439, 1987.
- Prawirodirdjo, L., A geodetic study of Sumatra and the Indonesian region: Kinematics and crustal deformation from GPS and triangulation, University of California, San Diego, San Diego, 2000.
- Prawirodirdjo, L., Y. Bock, R. McCaffrey, and e. al., Geodetic observations of interseismic strain segmentation at the Sumatra subduction zone, *Geophysical Research Letters*, *24*, 2601-2604, 1997.
- Rice, J.R., Chapter 20. Fault Stress States, Pore Pressure Distributions, and the Weakness of the San Andreas Fault, in *Fault Mechanics and Transport Properties of Rocks*, Academic Press Ltd., 1992.

- Rivera, L., K. Sieh, D. Helmberger, and D.H. Natawidjaja, A comparative study of the Sumatran subduction-zone earthquakes of 1935 and 1984, *Bulletin of the Seismological Society of America*, *92*, 1721-1736, 2002.
- Sieh, K., The repetition of large-earthquake ruptures, in *Proc. Natl. Acad. Sci.*, pp. 3764-3771, 1996.
- Sieh, K., Y. Bock, L. Edwards, F. Taylor, and P. Gans, Active tectonics of Sumatra, *Geo. Soc. of Amer. Bull.*, 26, A-382, 1994.
- Sieh, K., Y. Bock, and J. Rais, Neotectonic and paleoseismic studies in West and North Sumatra, *AGU 1991 Fall Meeting Program & Abstacts*, 72 (44), 460, 1991.
- Sieh, K., M. Stuiver, and D. Brillinger, A more precise chronology of earthquakes produced by the San Andreas fault in southern California, *Journal of Geophsical Research*, *94*, 603-623, 1989.
- Sieh, K., S.N. Ward, D.H. Natawidjaja, and B.W. Suwargadi, Crustal deformation at the Sumatran subduction zone, *Geophysical Research Letters*, *26* (20), 3141-3144, 1999.
- Zachariasen, J., Paleoseismology and Paleogeodesy of the Sumatran Subduction Zone: A Study of Vertical Deformation Using coral Microatolls, Ph. D. thesis, California Institute of Technology, Pasadena, California, 1998.
- Zachariasen, J., K. Sieh, F.W. Taylor, R.L. Edwards, and W.S. Hantoro, Submergence and uplift associated with the giant 1833 Sumatran subduction earthquake: Evidence from coral microatolls, *Journal of Geophysical Research*, 104, 895-919, 1999.
- Zachariasen, J., K. Sieh, F.W. Taylor, and W.S. Hantoro, Modern vertical deformation above the Sumatran subduction zone: paleogeodetic insights from coral microatolls, *Bulletin of the Seismological Society of America*, *90* (4), 897-913, 2000.

Chapter 2. Neotectonics of the Sumatran fault, Indonesia

Kerry Sieh

Danny Natawidjaja

California Institute of Technology

 $Reformatted\ from\ \textit{Journal\ of\ Geophysical\ Research}$

Volume 105, Pages 28,295-28,326, December, 2000

2.1. Abstract

The 1900-km-long, trench-parallel Sumatran fault accommodates a significant amount of the right-lateral component of oblique convergence between the Eurasian and Indian/Australian plates from 10°N to 7°S. Our detailed map of the fault, compiled from topographic maps and stereographic aerial photographs, shows that unlike many other great strike-slip faults, the Sumatran fault is highly segmented. Cross-strike width of step overs between the 19 major subaerial segments is commonly many kilometers. The influence of these step overs on historical seismic source dimensions suggests that the dimensions of future events will also be influenced by fault geometry. Geomorphic offsets along the fault range as high as ~20 km and may represent the total offset across the fault. If this is so, other structures must have accommodated much of the dextral component of oblique convergence during the past few million years. Our analysis of stretching of the forearc region, near the southern tip of Sumatra, constrains the combined dextral slip on the Sumatran and Mentawai faults to be no more than 100 km in the past few million years. The shape and location of the Sumatran fault and the active volcanic arc are highly correlated with the shape and character of the underlying subducting oceanic lithosphere. Nonetheless, active volcanic centers of the Sumatran volcanic arc have not influenced noticeably the geometry of the active Sumatran fault. On the basis of its geologic history and pattern of deformation, we divide the Sumatran plate margin into northern, central and southern domains. We support previous proposals that the geometry and character of the subducting Investigator fracture zone are affecting the shape and evolution of the Sumatran fault system within the central domain.

southern domain is the most regular. The Sumatran fault there comprises six right-stepping segments. This pattern indicates that the overall trend of the fault deviates 4° clockwise from the slip vector between the two blocks it separates. The regularity of this section and its association with the portion of the subduction zone that generated the giant $(M_w 9)$ earthquake of 1833 suggest that a geometrically simple subducting slab results in both simple strike-slip faulting and unusually large subduction earthquakes.

2.2. Introduction

2.2.1. Plate tectonic environment

The Sumatran fault belongs to a class of trench-parallel strike-slip fault systems that work in concert with subduction zones to accommodate obliquely convergent plate motion [Yeats et al., 1997, Chapter 8]. Other strike-slip faults that occur in similar settings include the left-lateral Philippine fault (parallel to the Luzon and Philippine trenches), Japan's right-lateral Median Tectonic Line (parallel to the Nankai trough), and Chile's Atacama fault (parallel to the South American trench).

For its entire 1900-km length the Sumatran fault traverses the hanging wall block of the Sumatran subduction zone, roughly coincident with the active Sumatran volcanic arc (Fig. 2.1). On its northeastern side is the Southeast Asian plate, separated from the Eurasian plate only by the slow slipping Red River fault of Vietnam and southern China [Allen et al., 1984]. On its southwestern side is the Sumatran "forearc sliver plate" [Jarrard, 1986], a 300-km-wide strip of lithosphere between the Sumatran fault and the

Sumatran deformation front. At its northwestern terminus the Sumatran fault transforms into the spreading centers of the Andaman Sea [*Curray et al.*, 1979]. At its southeastern end, in the Sunda Strait, the fault curves southward toward the deformation front [*Diament et al.*, 1992].

The basic kinematic role of the Sumatran fault is rather simple: It accommodates a significant amount of the strike-slip component of the oblique convergence between the Australian/Indian and Eurasian plates. The pole of rotation for the relative motion between the Australian/Indian and Eurasian plates is in east Africa, ~50° west of Sumatra [Prawirodirdjo et al., this issue, Prawirodirdjo, 2000; Larson et al., 1997]. Northern Sumatra is closer to this pole than is southern Sumatra. Thus the orientation and magnitude of the relative-motion vector vary significantly along the Sumatran portion of the plate boundary (Fig. 2.1). At 6°S, 102°E it is 60 mm/yr, N17°E [Prawirodirdjo et al., this issue]. At 2°N, 95°E, it is 52 mm/yr, N10°E. Furthermore, because the shape of the plate boundary is arcuate, the nature of relative plate motion changes markedly along its strike. At the longitude of central Java the strike of the subduction zone is nearly orthogonal to the direction of relative plate motion, so any component of strike-slip motion need not be large [McCaffrey, 1991]. At the latitudes of Sumatra, however, the strike-slip component of relative plate motion must be significant because the direction of relative plate motion is substantially oblique to the strike of the subduction zone.

Fitch [1972] suggested that the right-lateral component of this oblique convergence is the cause for the right-lateral Sumatran fault. *McCaffrey* [1991, 1992] added more substance to this hypothesis with his discovery that slip vectors of moderate earthquakes along the Sumatran portion of the subduction zone are nearly perpendicular

to the strike of the plate boundary. He noted that if these vector directions are representative of long-term slip trajectories along the subduction interface, then subduction itself is only slightly oblique and most of the dextral component of plate motion must be accommodated elsewhere.

The Sumatran fault is the most obvious candidate for accommodation of the remaining component of dextral slip. The Mentawai fault, discovered offshore by *Diament et al.* [1992], complicates this slightly. This major, submarine, trench-parallel fault lies between the Sumatran fault and the trench and may also have accommodated a significant amount of the dextral component of plate motion.

The combination of an arcuate plate boundary and a distant pole of rotation suggests that the rate of dextral slip along the Sumatran fault increases northwestward [Huchon and Le Pichon, 1984; McCaffrey, 1991]. Observations near the northwestern and southeastern termini of the Sumatran fault support this contention. Curray et al. [1979] suggested that the rate of opening across the spreading centers of the Andaman Sea (Fig. 2.1) has averaged about 37 mm/yr for the past 11 Myr. They proposed that most of this motion has been carried to the southeast by the Sumatran fault. Reanalysis of these data yields the same rate; total opening in the past 3.2 Myr is ~118 km (J. Curray, written communication, 1999). The slip rate inferred for the Sumatran fault near its southern terminus, however, appears to be far lower than 37 mm/yr. Bellier et al. [1999] calculate a rate of ~6 mm/yr near the southern end of the fault from an offset channel incised into a dated Pleistocene tuff.

2.1.2. Motivation of this work

Despite its ranking as one of Earth's great strike-slip faults, its high level of historical seismic activity and its major role in the active tectonics and seismic hazard of Southeast Asia, the Sumatran fault has not been well characterized. What attention the fault has received has been predominantly from a great distance, mostly at plate tectonic scales. Until recently, the geometry of the fault was known only to first-order (see, for example, the small-scale maps of *Fitch* [1972], *Bellier et al.* [1997] or *McCaffrey* [1991]. More detailed studies have been limited to local studies, such as *Tija's* [1977] and *Katili and Hehuwat's* [1967] work on exemplary offset drainages.

The Sumatran fault has generated many historical earthquakes with magnitudes M≥ 7, but because most of these happened more than a half a century ago, they have not been well documented. *Reid* [1913] used geodetic measurements from before and after the 1892 Sumatran earthquake as support for his concept of elastic rebound. *Berlage* [1934] described the effects of the 1933 earthquake in south Sumatra. *Visser* [1927] described the effects of the 1926 Padangpanjang earthquake in west Sumatra, and *Untung et al.* [1985] and *Natawidjaja et al.* [1995] recently reported dextral offsets formed during the nearby 1943 Alahanpanjang earthquake.

The paucity of detailed maps of the fault, the scarcity of data on historical large earthquakes, and the lack of reliable estimates of slip rates are unfortunate. They seriously hamper attempts to forecast the seismic productivity of the fault and efforts to understand quantitatively its role in the oblique convergence of the Sumatran plate boundary.

Our first task in this study, then, has been to construct a modern map of the active components of the Sumatran fault. To be of use in seismic hazard assessment and in understanding the neotectonic role of the fault, the scale of the map needed to be large enough to clearly discriminate major fault strands and the discontinuities and changes in strike between strands.

Our second task, which will be described in a future paper, will be to determine the slip rate of the fault at several localities to determine whether or not the actual slip rates conform to current kinematic models. Such rates would also serve as a long-term average for the interpretation of geodetic data from Global Positioning System (GPS) networks that now span the fault [Genrich et al., this issue] and historical triangulation data [Prawirodirdjo et al., this issue].

2.3. A modern map of the fault

To map the Sumatran fault efficiently and reliably, we have relied primarily upon its geomorphic expression. Geomorphic expression is especially reliable for mapping high slip rate faults, where tectonic landforms commonly develop and are maintained at rates that exceed local rates of erosion or burial [Yeats et al., 1997, Chapter 8]. Examples of geomorphologically based regional maps of active faults include active fault maps of Japan, Turkey, China, Tibet, and Mongolia [Research Group for Active Faults, 1980; Saroglu et al., 1992; Tapponnier and Molnar, 1977] as well as most maps of submarine active faults.

Admittedly, the geomorphic expressions of active faults with slip rates that are lower than or nearly equal to local rates of erosion or burial is likely to be obscure. This is especially likely if the faults are short, have small cumulative offset, or have no component of vertical motion. Because of our reliance on geomorphic expression, our map of the Sumatran fault undoubtedly excludes many short, low-rate active fault strands.

2.3.1. Resources and methods

The grossest features of the Sumatran fault have long been known from analysis of small-scale topographic and geologic maps. More detailed small-scale maps of the fault, based upon analysis of satellite imagery, have been produced more recently [Bellier et al., 1997; Bellier and Sebrier, 1994; Detourbet et al., 1993]. The unavailability of stereographic imagery, however, limited the resolution and the reliability of these small-scale maps. Specifically, the lack of stereoscopic coverage precluded the recognition of important small tectonic landforms, unless they were favorably illuminated. Conversely, inactive faults lacking small, late Pleistocene and Holocene tectonic landforms may have been mapped as active, based upon the presence of older and larger tectonic landforms.

Our mapping of the Sumatran fault is based primarily upon inspection of 1:50,000-scale topographic maps and 1:100,000-scale aerial photographs. Where these were not available or were of unsuitable quality, we utilized 1:250,000-scale geologic maps and radar imagery. Figure 2.2 displays the coverage of materials that we used.

Figure 2.3 displays representative stereographic pairs of the 1:100,000-scale aerial photographs. These photos display the fault at about 0.3°S, where it offsets stream channels that are deeply incised into a thick pyroclastic flow deposit. After interpreting these and other stereopairs, we compiled our interpretations onto 1:50,000-scale topographic maps (or 1:250,000-scale topographic maps, where the larger-scale maps were unavailable). Where stereographic aerial photographs were unavailable, we interpreted active fault geometry and sense of slip directly from the 1:50,000-scale topographic maps.

These data were then digitized and attributed, using the Geographic Information System (GIS) software, Arc/Info. The resulting GIS database includes fault geometry, sense of fault slip, and photo centers. Plate 2.1, constructed from the database, depicts all of the salient features of the Sumatran plate boundary that we mapped and compiled.

2.3.2. Geometry of the fault

The overall shape of the Sumatran fault across Sumatra is sinusoidal (Fig. 2.1). The northern half of the fault is gently concave to the southwest, whereas the southern half of the fault is concave to the northeast. Over the 1650-km subaerially exposed length of the fault, the "amplitude" of the sinusoidal trace is ~55 km.

Ornamenting the broad, sinusoidal shape of the Sumatran fault are numerous smaller irregularities. Though smaller, these have dimensions of the order of tens of kilometers and are therefore tectonically and seismologically significant.

The greatest of these is a feature that we call the Equatorial Bifurcation (Fig. 2.1 and Plate 2.1). This forceps-shaped feature is present between the Equator and about 1.8°N latitude. It is characterized by the bifurcation of the Sumatran fault toward the southeast into two principal active strands. The two strands are distinct from each other even at their point of bifurcation (about 1.8°N). The greatest separation of these two branches is ~35 km, near 0.7°N. The western branch of the bifurcation does not rejoin the eastern branch farther south; instead, it dies out geomorphically at about 0.35°N.

Other large irregularities include sub parallel geomorphically expressed fault traces at about 5.5°N, 4°N, and 3.5°S. The Batee fault, a right-lateral fault that may have displaced the island's western shelf ~150 km since the Oligocene [Karig et al., 1980], diverges southward from the Sumatran fault at about 4.6°N. A 75 km long fold-and-thrust belt, exhibiting clear geomorphic evidence of youthfulness lies about 40 km west of the Sumatran fault at about 1.3°N. All of these features are described in section 2.3.

2.3.3. Major segments of the Sumatran fault

Superimposed upon the broad sinusoidal geometry of the Sumatran fault are more than a dozen discontinuities, ranging in width from ~5 to 12 km (Plate 2.1). Major local changes in strike also occur. Most of the discontinuities are right steps in the fault trace and thus represent dilatational step overs. However, a few contractional bends also occur. Theoretically, these discontinuities and bends in the fault are large enough to influence the seismic behavior of the fault [*Harris et al.*, 1991; *Harris and Day*, 1993]. The relationship of historical ruptures to these geometrical segment boundaries will be

the subject of a future paper (D. Natawidjaja and K. Sieh, manuscript in preparation, 2000).

We have used these second-order geometric irregularities to divide the Sumatran fault into 19 segments (Fig. 2.4 and Plate 2.1). Each segment bears the name of a major river or bay along the segment. In so naming the various segments, we have abandoned the usual practice of retaining names that have precedence in the scientific literature. The nomenclatural morass inherited from numerous earlier studies includes many fault names derived from nearby cities, districts, basins, and rivers. These include Banda Aceh Anu, Lam Teuba Baro, Reuengeuet Blangkejeren, Kla-Alas, Ulu-Aer, Batang-Gadis, Kepahiang-Makakau, Ketahun, Muara Labuh, and Semangko [e.g., see *Katili and Hehuwat*, 1967; *Cameron et al.*, 1983; *Durham*, 1940]. Since many of these overlap our geometric segment boundaries or include only parts of our segments, we have abandoned them in favor of a more systematic and precise nomenclature.

For the entire group of active fault segments, from Aceh in the north to the Sunda Strait in the south, we have chosen the name "Sumatran fault," first used by *Katili and Hehuwat* [1967]. This name represents best the dimension of the structure. Earlier names for the fault are "Semangko" and "Ulu-Aer," suggested by *Van Bemmelen* [1949] and *Durham* [1940]; but these refer to local features. "Great Sumatran trough system" was first used by *Westerveld* [1953]. Since "great" is not used for other faults of similar dimension, we suggest that it not be used for the Sumatran fault. In keeping with convention generally accepted in California, where "San Andreas fault system" refers to the San Andreas and its many auxiliary faults, we use "Sumatran fault system" (SFS) for the Sumatran fault and other structures that are related to the accommodation of strike

slip along the Sumatran plate margin. These would include the Batee fault, the Toru fold-and-thrust belt, and the Mentawai and the West Andaman faults in the forearc region (Fig. 2.1). For discrete, individual segments along the Sumatran fault, we suggest the particular names in Figure 2.4.

In sections 2.3.1-2.3.19, we describe each segment, beginning in the south. Each description focuses on the geomorphic expression of the segment and its terminations. Discussion of important historical earthquakes is minimal because the association of earthquakes with segments will be the focus of a future paper. Likewise, we do not focus on the slip rates of the various segments because this also will be the principal topic of a future paper.

Plate 2.1 displays the fault at a scale that is appropriate for the detailed discussion that follows. (This plate and its database are also available as postscript and GIS (ArcView) files at www.scecdc.scec.org/geologic/sumatra).

2.3.3.1. Sunda segment (6.75°S to 5.9°S)

Bathymetric maps of the Sunda Strait, between Java and Sumatra, reveal that the southernmost portion of the Sumatran fault is associated with two prominent south striking fault scarps on the seafloor [Nishimura et al., 1986; Zen et al., 1991; Pramumijoyo and Sebrier, 1991]. These scarps form a submarine graben, ranging in depth to 1800 below sea level (Fig. 2.5). The large vertical displacements of the seafloor and the orientation and location of the faults suggest that their sense of slip is normal and dextral. Focal mechanisms from a local seismic network [Harjono et al., 1991] and from the Harvard Centroid Moment Tensor (CMT) catalogue support this interpretation. They

show normal-fault mechanisms on the western side of the graben. Furthermore, faults appear on both sides of the graben in three seismic reflection profiles [Lassal et al., 1989].

The graben widens southward, toward the subduction zone, but loses bathymetric expression ~130 km from the trench, near where one would expect it to intersect the floor of the Sumatran and Javan forearc basins (Fig. 2.5). A belt of fault scarps and folds of the inner trench slope continues across the southward projection of the graben, but the outer-arc ridge and forearc basin that are prominent in the offshore of Sumatra and Java are absent in this region. Instead, these features appear to converge upon each other and to be replaced by a narrow, 150-km-long plateau across the projection of the graben. The lessening of sliver-plate width occasioned by the absence of the forearc basin and outer-arc ridge appears to be accommodated by a landward deflection of the trench axis (Figs. 2.1 and 2.5).

Huchon and Le Pichon [1984] were the first to propose that the disappearance of the outer-arc ridge and the forearc basin across the southern projection of the Sumatran fault indicates stretching parallel to the Sumatran fault. They also speculated that the subtle bending of the trench toward the Sunda Strait indicates arc-normal thinning of the region between the trailing edge of the Sumatran forearc sliver plate and the crust offshore from Java. This would be consistent with the northwestward translation of the forearc sliver plate along the Sumatran fault. We attempt to quantify this stretching in section 3.

2.3.3.2. Semangko segment (5.9°S to 5.25°S)

From beneath the waters of Semangko Bay at about 5.9°S to a 6-km-wide dilatational step over that has produced the Suoh Valley at about 5.25°S, the principal trace of the Sumatran fault runs almost linearly along the southwestern side of Semangko Bay and the Semangko Valley (Plate 2.1 and Figure 2.4). The prominent northeast facing escarpment along the 65-km length of this segment attests to a significant component of dip slip, southwest side up. An earthquake on July 26, 1908, may have involved rupture of all or most of this segment [*Berlage*, 1934].

2.3.3.3. Kumering segment (5.3°S to 4.35°S)

This 150-km-long segment runs between the dilatational step over at Suoh Valley to a contractional jog at 4.35°S. Near the center of this segment, the waters of Lake Ranau occupy a late Pleistocene caldera and conceal about 9 km of the trace (Plate 2.1 and Figure 2.4). The southern part of the Kumering segment traverses the drainages of the Werkuk and upper Semangko rivers. A less active southeastward continuation of this segment may form the northeastern flank of the Semangko Valley [*Pramumijoyo and Sebrier*, 1991], but we did not have adequate materials to determine its activity there.

North of Lake Ranau, a 40-km-long reach of the fault traverses the headwaters of the Kumering River. The trunk stream of this large river does not cross the fault; instead, its two major tributaries flow toward one another across the trace of the fault and flow northeastward away from the fault from their confluence. This relationship of large stream channels to the fault is common along much of the Sumatran fault; not uncommonly, the headwaters of a principal stream are near the fault, and none of the

larger channels of the drainage network cross the fault trace. In these cases, dextral offsets of the stream channels are either ambiguous or small.

The northwesternmost 15 km of the Kumering segment deviates westward from the trend of the rest of the segment and is part of a 10-km-wide contractional jog. This portion of the segment displays a significant component of reverse slip, as evidenced by a high escarpment and a mountainous anticline north of the fault trace. Aerial photography available to us did not reveal the continuation of the fault trace northwest of 4.35°S, through the rest of the contractional bend.

High intensities indicate rupture of many tens of kilometers of the Kumering segment during the Ms 7.5 Liwa earthquake of June 24, 1933 [*Berlage*, 1934]. Deadly phreatic explosions occurred 2 weeks after the earthquake within the Suoh Valley [*Stehn*, 1934].

A geomorphically less prominent sub parallel strand of the fault exists 2.5 km to the southwest of the principal active trace south of Lake Ranau [Natawidjaja, 1994; Widiwijayanti et al., 1996]. The devastating M_w6.8 Liwa earthquake of 1994 was generated by this less prominent trace. The most severe damage and the aftershock region coincided with a 25 km reach of this secondary trace.

2.3.3.4. Manna segment (4.35°S to 3.8°S)

This 85-km segment deviates only a kilometer or two from being rectilinear but has rather obscure terminations on both ends (Fig. 2.4). The Manna segment appears discontinuous on Plate 2.1 because the trace is obscure locally on the aerial photographs

and topographic maps. The southern end of the segment abuts the contractional bend mentioned above. The northern end of the segment is obscure beyond about 3.8°S but appears to be within a geometrically complex right (dilatational) step in the fault.

Exceptionally clear 2.4 ± 0.2 km dextral offsets of two large streams (Air Kanan and Air Kiri) exist on the dissected western flank of an extinct volcano southeast of Pajarbulan (Plate 2.2). We encountered surprisingly well-preserved small tectonic landforms beneath the jungle canopy during an excursion in the drainages of these two streams.

A destructive earthquake occurred in the vicinity of this segment on June 12, 1893. The area of greatest damage coincided with the central part of the Manna segment [*Visser*, 1922].

2.3.3.5. Musi segment (3.65°S to 3.25°S)

This 70-km segment of the Sumatran fault comprises several highly discontinuous fault segments (Fig. 2.4 and Plate 2.1). Despite good coverage with 1:100,000-scale aerial photography, we could not identify clear geomorphic traces along much of this segment.

The longest continuous trace that we were able to map traverses the southwestern flank of the large, active stratovolcano, Bukit Kaba. Stream channels cut into the youngest flows there are offset ~700 m. We have used these channels to determine the slip rate of 11 mm/yr for the Musi segment (D. Natawidjaja and K. Sieh, manuscript in preparation, 2000).

The destructive, Ms 6.6 Kepahiang earthquake occurred along this segment at about 3.6°S on December 15, 1979. We heard eyewitness accounts of minor cracking along the fault when we visited in 1993, but we saw no convincing evidence of tectonic surficial ruptures from 1979.

2.3.3.6. Ketaun segment (3.35°S to 2.75°S)

This 85-km-long segment consists of a linear trace with several discontinuities and stepovers of about a kilometer in dimension (Plate 2.1 and Figure 2.4). The segment's southern end is at a 6- to 8-km-wide dilatational step over onto the Musi segment. An inactive or less active continuation of the Ketaun segment may extend beneath the stratovolcanic edifice of Bukit Kaba. This possibility is suggested by the presence of a geomorphically subdued fault, southeast of the volcano and ~25 km east of the central Musi segment. The northern end of the Ketaun segment is within a 6-km-wide contractional step over. Within this contractional step over the topography rises several hundred meters above the surrounding landscape.

Two major rivers cross the Ketaun segment, the Ketaun in the south and the Seblat in the north. The Seblat river valley appears to be offset dextrally ~17 km, and the Ketaun river valley may be offset ~23 km. A moderate earthquake on March 15, 1952 (M6.2, U. S. Geological Survey (USGS)), produced high intensities along the Ketaun segment [*Kraeff*, 1952].

2.3.3.7. Dikit segment (2.75°S to 2.3°S)

This is a predominantly linear, 60-km-long segment with several short, obscure sections along its northern few kilometers (Plate 2.1 and Figure 2.4). It shares a contractional step over with the Ketaun segment on its southeastern end. Its northwestern termination is at one of the larger dilatational step overs along the Sumatran fault. On the southwestern flank of this 11-km-wide step over, the Dikit segment disappears into the edifice of the small stratovolcano Kunyit. This is one of the few clear associations of a dilatational step over and a volcano along the Sumatran fault.

The small diamond-shaped caldera of Dipatiampat is offset ~500 m by the fault. Just north of the small caldera lake, at about 2.65°S, the main trace appears to form an enigmatic dogleg. The Dikit River Valley follows the fault for ~20 km. We are not convinced that this represents a dextral offset of 20 km, because the construction of two large volcanic edifices has undoubtedly obscured older drainages on the block northeast of the fault.

2.3.3.8. Siulak segment (2.25°S to 1.7°S)

Clear dilatational step overs demarcate the terminations of this 70-km-long segment (Fig. 2.4 and Plate 2.1). The 11 km wide stepover at the southeastern end is the widest dilatational step over along the Sumatran fault, but our aerial photography did not reveal its structural details. The northern terminus of the Siulak segment is a 4-km-wide step over on the western flank of the great active stratovolcano Kerinci. West dipping normal faults cut lavas of Melenggok volcano there, and appear to transfer slip from the Siulak segment to its northwestern neighbor.

Along the Siulak segment's southeastern reach, Lake Kerinci and the alluvium of a broad valley obscure the fault trace for ~30 km. Two large earthquakes have caused severe damage along the Siulak segment of the Sumatran fault. On June 3, 1909, most of the region traversed by this segment was devastated by an earthquake judged to have a magnitude of about Ms 7.7 [*Abe*, 1981]. The zone of greatest damage during the M7.0 earthquake of October 6, 1995, was within the broad valley northwest of Lake Kerinci (Indonesian newspaper *Kompas*, October 7, 1995).

2.3.3.9. Suliti segment (1.75°S to 1.0°S)

This 95-km-long segment has a comparatively straight fault trace, which terminates on both the northwest and southeast at dilatational step overs within volcanic edifices (Fig. 2.4 and Plate 2.1). The northwestern step over, at Lake Diatas and Talang volcano, is 4 km wide. The details of the central reaches of the segment are obscure because the fault traverses the narrow valley of the Suliti River headwaters for more than 50 km. How much of this course of the fault along the Suliti River valley represents a dextral offset is unknown because the trunk stream does not cross the fault. Along the southernmost part of this segment, tributaries of the Liki River are offset several hundred meters.

The first of two large earthquakes of June 9, 1943 (M_s 7.1 [*Pacheco and Sykes*, 1992]), may have involved rupture of the northern part of the Suliti segment, judging from serious damage to Muaralabuh village, 25 km northwest of southeastern terminus of the segment [*Natawidjaja et al.*, 1995].

2.3.3.10. Sumani segment (1.0°S to 0.5°S)

This 60-km-long segment runs northwestward from the volcanic terrane of Lake Diatas to the southwestern flank of Lake Singkarak, which occupies a structural graben, rather than a volcanic caldera (Fig. 2.4 and Plate 2.1). Two opposing arcuate normal oblique faults form topographic scarps that rise 400 m above the surface of the lake (Plate 2.3). Ancient upland surfaces, with drainages flowing away from the lake, are clearly truncated by the steep scarps bounding the lake basin and thus appear to have been faulted down below the waters of the lake.

Failure of the Sumani segment produced the second of two large earthquakes (Ms 7.4 [Pacheco and Sykes, 1992]) on June 9, 1943 [Natawidjaja et al., 1995]. Shaking intensities indicate that the northwestern end of the fault rupture was beneath the lake. Eyewitness accounts led *Untung et al.* [1985] to conclude that right-lateral offsets of up to 2 m occurred near the town of Solok, but Natawidjaja et al. [1995] could only verify offsets of ~1 m. Analysis of geodetic data supports a meter or so of dextral slip [Prawirodirdjo et al., this issue].

High intensities in the vicinity of Lakes Dibawah and Diatas suggest that the entire southeastern part of the segment also ruptured, and perhaps even the northwestern part of the Suliti segment.

The first of two large earthquakes on August 4, 1926 was most severe in the narrow zone along the Sumani segment. Another earthquake, on October 1, 1822, was most severe between the Marapi and Talang volcanoes (Wichman, as cited by *Visser* [1927]). Thus this earthquake may well have involved rupture of the Sumani segment.

Genrich et al. [this issue] show that strain accumulation during the early to mid-1990s is consistent with 23 ± 5 mm/yr of dextral slip on this segment.

2.3.3.11. Sianok segment (0.7°S to about 0.1°N)

This predominantly straight and continuous segment runs ~90 km from the northeast shore of Lake Singkarak, along the southwest flank of the great stratovolcano Marapi to a 10-km-wide right step over at the Equator (Plate 2.1 and Figure 2.4). Its southern 18 km, on the flank of Lake Singkarak, is arcuate and must have a significant component of normal faulting down toward the lake. Geomorphic expression of the fault is particularly interesting along the Sianok segment because it traverses the flank of Marapi volcano and the young, 200-m-thick pyroclastic flow deposit of Maninjou volcano. Stream channels flowing off Marapi display clear dextral offsets that range from ~120 to 600 m. The trunk channel of the Sianok River is incised into the Maninjou Tuff and display offsets of ~700 m (Fig. 2.3). We have been able to use these offsets to determine a dextral rate of slip of ~11 mm/yr (D. Natawidjaja and K. Sieh, manuscript in preparation, 2000).

The second of two large earthquakes on August 4, 1926, was most severe along the southeastern portion of the Sianok segment. This is consistent with *Visser's* [1927] observation of fault rupture between Bukittinggi and Singkarak. *Genrich et al.* [this issue] show that strain accumulation across this segment in the early to mid-1990s is consistent with dextral slip of 23 ± 3 mm/yr.

2.3.3.12. Sumpur segment (Equator to 0.3°N)

Data along this 30-km-long segment and its northwestern neighbor are scant. Our map is based predominantly upon 1:250,000-scale geologic maps [*Rock et al.*, 1983, *Aspden et al.*, 1982] and poorly reproduced 1:50,000-scale topographic maps.

Both termini of the Sumpur segment are at large dilatational steps. Thus, between the Sianok and Barumun segments, the fault experiences a 35-km-wide, double-dilatational step over. The northwestern step is associated with a high west facing escarpment and the adjoining wide valley of the Sumpur-Rokan River.

2.3.3.13. Barumun segment (0.3°N to 1.2°N)

This 115-km-long segment is broadly concave toward the southwest and forms most of the northeastern leg of the Equatorial bifurcation (Fig. 2.4 and Plate 2.1). The southeastern 40 km of the Barumun segment forms the boundary between a high west facing escarpment and the broad depression of the Sumpur River. We interpret this escarpment and adjacent depression to be evidence of a significant component of extensional dip slip on this portion of the Barumun segment. We place the northwestern end of the Barumun segment somewhat arbitrarily at an abrupt 15° bend in the trace of the fault, near the headwaters of the Barumun River.

Only along its northernmost 35 km have we been able to inspect 1:100,000-scale aerial photography. There the fault traces display clear geomorphic evidence of strike slip. The channel of the Barumun River may be offset about 20 km, but this offset is not compelling because the trunk stream does not cross the fault.

2.3.3.14. Angkola segment (0.3°N to 1.8°N)

The southwestern branch of the Equatorial Bifurcation consists of a continuous fault with an abrupt 30° bend at about 0.65°N (Fig. 2.4 and Plate 2.1). Geomorphic expression is particularly clear between about 0.8°N and 0.5°N. Katili and Hehuwat [1967] used offsets of tributaries to the Angkola River at about 0.55°N to demonstrate right-lateral offsets ranging from 200 to 1200 m along this segment. The northern 30 km of the Angkola segment consists of a set of discontinuous faults on the southwestern flank of the Sarulla graben. Although large-scale aerial photographs do show minor, discontinuous faulting at about 0.35°N, the lack of through going geomorphic expression of the western branch south of 0.5°N shows that the fault is significantly less active there. The western segment does not rejoin the northeastern strand just north of the Equator. Geologic mapping supports this interpretation, and suggests that total slip on the western branch cannot be large [Rock et al., 1983]. Geodetic measurements spanning the early to mid-1990s suggest that modern strain rates are higher in the vicinity of the Angkola segment than on the main segment farther east [Genrich et al., this issue]. Combined slip at depth at a rate of 23 ± 4 mm/yr satisfies the geodetic measurements.

The Angkola segment of the Sumatran fault produced the famous earthquake of 1892, during the establishment of the first primary triangulation network in the region. Differences in angles measured just before and after the earthquake enabled *Müller* [1895] to calculate that coseismic right-lateral dislocations of at least 2 m had occurred along a northwest trending line coincident with that portion of the fault trace between 0.45°N and 1.2°N. These geodetic data, along with those from the 1906 San Francisco earthquake and 1891 Mino-Owari earthquake inspired, *Reid* [1913] to formulate the theory of elastic rebound [*Yeats et al.*, 1997, Chapter 8]. *Prawirodirdjo et al.* [this issue]

have reanalyzed the Dutch data and conclude that the dextral slip was 4.5 ± 0.6 m. The most serious damage reported in 1892 was along the fault in the valleys of the Gadis and Angkola Rivers, between Malintang and Lubuk Raya volcanoes [*Visser*, 1922].

2.3.3.15. Toru segment (1.2°N to 2.0°N)

Major bends in the fault trace delimit this segment of the Sumatran fault (Fig. 2.4 and Plate 2.1). We define the southern terminus to be at a regional bend of 15° at 1.2°N. The topographic high east of the bend suggests that this is a contractional bend.

The northwestern termination of the Toru segment occurs at a 15° regional bend in the fault, which is coincident with a 2.5-km dilatational step over. We can be confident that this bend is dilatational because the segment to the northwest does not display net vertical deformation across the fault and the bend coincides with the Tarutung depression.

Northwest of Sibual-buali volcano, a 30-km-wide caldera northeast of the fault is truncated by the fault. The other half of the caldera, southwest of the fault, must be concealed beneath young volcanic deposits. The geomorphic expression of the fault in the vicinity of the truncated caldera is unusually complex. Significant components of dip slip occur on faults that splay northward from the main trace into the caldera. The Toru segment has not produced a major historical earthquake, but right-lateral slip near the northern end of this segment did generate the M6.4 Pahae Jahe earthquake of 1984.

2.3.3.16. Renun segment (2.0°N to 3.55°N)

This longest segment of the Sumatran fault traverses the western flank of the 80-km-long Toba caldera, alleged to be the largest Quaternary caldera on Earth [Chesner et al., 1991]. Much of the Renun segment traverses the thick pyroclastic flow deposit of that 73,000-year-old eruption. The regional expression of this 225-km-long segment is linear, except for a dogleg along its northwesternmost 30 km, where the segment forms the southwestern flank of the Alas Valley graben. This graben, 45 km long and 9 km wide, is one of the largest graben along the Sumatran fault. West of Lake Toba, the fault consists of several 30- to 40-km-long strands, arranged en echelon, with across-strike separations of only a kilometer or so. Although the right-stepping nature of the en echelon pattern suggests that the fault is experiencing a minor component of transtension in the upper crust, the step overs are associated with horsts, not graben.

The southeasternmost part of the Renun segment exhibits a well-defined 2-km offset of the 73,000-year-old Toba Tuff, which we have used to determine a 27 mm/yr slip rate for the fault [Sieh et al., 1991; D. Natawidjaja and K. Sieh, manuscript in preparation, 2000]. GPS measurements across the southern portion of this segment suggest slip rates of 24 ± 1 mm/yr below ~ 9 km. Across the northern portion of the Renun segment, geodetic rates appear to be 26 ± 2 mm/yr [Genrich et al., this issue].

The Renun segment was the source of three major earthquakes early in the twentieth century. Accounts of these events are very sparse, however, and the limits of the rupture can only be guessed from poorly constrained isoseismal contours. *Visser* [1922] reports that shaking during the February 22, 1916, earthquake was very strong in the Tarutung valley and that the radius of strong shaking was ~200 km. The January 24, 1921, earthquake had a region of severe shaking similar to that of the earthquake of 1916.

The radius of shaking for the earthquake of April 1, 1921, was twice as large [*Visser*, 1922].

2.3.3.17. Tripa segment (3.2°N to 4.4°N)

Marked irregularity and curvature, mountainous terrain, and spectacular dextral offsets of major rivers characterize this 180-km-long segment (Fig. 2.4 and Plate 2.1). The location of the main trace of the fault is well constrained by spectacular offsets of the Kuala Tripa and Meureubo Rivers. Each of these deeply entrenched rivers displays a clear offset of ~21 km (Figs. 2.6 and 2.7 and Tables 2.2 and 2.3).

The segment's southeastern terminus is the northeastern flank of the extensional Alas Valley graben. Its northwestern limit is a 9-km-wide restraining bend, which displays south-side-up faults with a significant component of reverse slip. One could argue that an appreciable contractional jog at 4.0°N and a major change in strike at 3.85°N justify dividing this segment further.

Parallel to and ~15 km northeast of the central portion of this segment (between 4.0° and 4.25°N) is another active strike-slip fault. This 55-km-long fault trace is also well defined by aligned river valleys and stream offsets. Stream patterns suggest that this fault may converge with the main active trace at the northwestern terminus of the Tripa segment. However, we could find no clear large-scale geomorphic evidence of this, nor does the 1:250,000-scale geologic mapping suggest it [Cameron et al., 1983].

An earthquake on September 19, 1936, occurred along the southeasternmost part of the Tripa segment (M_s 7.2 [Newcomb and McCann, 1987]). A smaller, more recent shock (m_b 6.0, November 15, 1990) occurred near the middle of this segment.

2.3.3.18. Aceh segment (4.4°N to 5.4°N)

This 200-km-long segment of the Sumatran fault has a smooth sinusoidal shape and lacks major discontinuities or sharp bends (Fig. 2.4 and Plate 2.1). The southeastern two thirds traverse mountainous terrain and are well expressed by aligned major river canyons and stream offsets. Dextral separations of ~25 and 20 km on the Geumpang and Woyla River channels are not compelling evidence for offset, but they are similar in magnitude to the size of clear offsets of the Tripa and Meureubo Rivers farther southeast (Fig. 2.7). The northwestern portion of the Aceh segment traverses a region of low relief and is obscure on 1:100,000-scale aerial photographs. Geomorphic expression of the fault is subtle and stream offsets appear to be absent there. Although some published maps show the Sumatran fault running along the southwestern flank of the Aceh Valley and continuing into the sea across the northwestern coast [Curray et al., 1979; Page et al., 1979], we see no geomorphic evidence of active faulting within 25 km of the coastline. Therefore, we, are not convinced that the fault is active northwest of about 5.4°N. Geomorphic evidence for inactivity is compatible with geodetic observations that strain is accumulating at no more than a few millimeters per year across the fault [Genrich et al., this issue].

2.3.3.19. Seulimeum segment (5.0°N to 5.9°N)

This segment represents the principal active trace of the Sumatran fault through northern Aceh province (Fig. 2.4 and Plate 2.1). The active trace is marked by sharp escarpments and dissected young volcanic deposits on the southwestern flank of Seulawah Agam volcano. Small tributaries of the Seulimeum River are clearly offset a few hundred meters. Along the central part of this segment, young folds appear to be offset ~20 km (Figs. 2.6 and 2.7 and Tables 2.2 and 2.3).

Clear evidence of recent activity along the southeastern 22 km of this segment is absent from our aerial photos, but we infer that the fault continues through the long, narrow valley of the Baro River along this reach to an intersection with the Aceh segment at about 5°N. Northwest from the coastline, bathymetry [*Curray et al.*, 1979; J. Curray, written communication, 1999], focal mechanisms (Harvard CMT catalogue), geomorphic expression of faulting on Weh Island, and evidence on a seismic reflection profile [*Peter et al.*, 1966; *Weeks et al.*, 1967] suggest that the fault continues under water.

It is interesting that dextral movement along the Seulimeum segment has produced no deflection of the Aceh segment at their intersection. It is difficult to imagine how many kilometers of dextral slip on the Seulimeum segment could have occurred without at least a broad deflection in the Aceh segment.

A large earthquake in 1936 (M 7.1-7.3 [Newcomb and McCann, 1987; Soetardjo et al., 1985]) severely damaged the city of Banda Aceh, but the source of the event is unknown. An earthquake in 1964 (M_s 6.5, National Earthquake Information Center (NEIC)) damaged Krueng Raya more severely than Banda Aceh. Since Krueng Raya is closer to the Seulimeum segment, the Seulimeum segment of the Sumatran fault may

have generated this event. In contrast to the geomorphic evidence for recent dextral slip along the Seulimeum segment, *Genrich et al.* [this issue] show that strain accumulation across this segment in the early 1990s could be nil.

2.3.4. Other related structures

2.3.4.1. Batee fault

The Batee fault is a major right-lateral strike-slip fault that diverges from the Sumatran fault at about 4.65°N. Between its intersection with the Sumatran fault and the coastline, the fault traverses the 1000-m-high southwestern escarpment of the Barisan range. *Karig et al.* [1980] have shown that this structure continues onto the continental shelf and offsets the edge of the continental shelf ~150 km and the eastern edge of the outer-arc ridge ~100 km.

One strand of the Batee fault terminates before reaching the northern part of Nias Island (Plate 2.1). Another strand runs along the northern coast of Nias and appears to offset the inner trench slope and outer-arc ridge (Plate 2.1). Except very locally, the Batee fault does not appear to be active on the mainland of Sumatra. Although several large river channels display dextral deflections of up to 10 km, smaller ridge lines and channels exhibit no offset. We suspect that these large deflections are, indeed, dextral offsets, but the lack of clear small offsets suggests either no activity in the past few tens of thousands of years or activity at a rate much lower than along the Sumatran fault. This interpretation conflicts with the 12 ± 5 mm/yr estimate of dextral slip rate of *Bellier et al.* [1995]. We question the validity of their approach, which uses an empirical relationship

of channel length and age to derive an age for a channel. This age is then divided into the measured offset to determine a rate.

2.3.4.2. Toru fold and thrust belt

Between about 1.0° and 1.5°N lies a geomorphologically remarkable set of active folds and faults that strike roughly parallel to the Sumatran fault but lie 15 to 40 km farther southwest (Plate 2.1). The principal manifestations of this fold-and-thrust belt are a northwest striking anticline and syncline. The syncline underlies a 25-by-10-km swamp, and the anticline appears as a 30-by-15 km fold in Mio-Pliocene sediment. The Gadis River and its tributaries meander across the syncline and then traverse the anticline as an antecedent stream.

In addition, several smaller northwest striking reverse faults appear to break the anticline (Plate 2.1). The anticline also is cut by small north striking strike-slip faults. However, these faults are so small and closely spaced that they do not appear on Plate 2.1.

2.4. Discussion, interpretations, and speculations

In this paper, we have defined the geometry and geomorphology of the Sumatran fault. There are now several questions that these refinements allow us to address. These include the implications of the fault's historic behavior and geometry for the evaluation of future seismic hazard and questions about the total offset across the Sumatran fault and its role in oblique convergence during the past many millions of years. Other questions

concern the geometric and kinematic relationship of the Sumatran fault to the neighboring subduction zone and the relationship of arc volcanism to strike-slip faulting. We address each of these four questions in turn, below.

2.4.1. Historical and future seismicity

In the preceding discussion, we have described very briefly what is known about large earthquakes along the Sumatran fault. Even these highly abbreviated accounts suggest that geometric segmentation influences seismic rupture of the Sumatran fault. In contrast to the San Andreas fault in California [Lawson et al., 1908; Sieh, 1978], the Sumatran fault appears to produce earthquakes with rupture lengths no greater than a hundred kilometers or so. We speculate that this contrast in behavior results from the contrast in continuity of the two fault systems: The San Andreas fault has only one step over discontinuity with a cross-strike width greater than a kilometer (near San Gorgonio Pass [Allen, 1957]), whereas the Sumatran fault has at least 12. The San Andreas has only two large bends (near Monterey Bay and at Tejon Pass) [Jennings and Saucedo, 1994], whereas the Sumatran fault has about eight.

A more precise and detailed evaluation of the relationship of these irregularities and their relationship to historical ruptures is warranted but is beyond the scope of this paper. We have begun a thorough analysis of the historical accounts and hope to interest a seismologist in studying instrumental records in order to assess more fully the role of geometric segmentation in controlling rupture parameters. Until this future work is completed, one can obtain a crude sense of the influence of fault segments on historical ruptures by comparing *Katili and Hehuwat's* [1967] compilation of the felt regions of

historical earthquakes with our map of the fault. *Bellier et al.* [1997] have redrawn Katili and Hehuwat's map and include a few more recent earthquakes in their compilation of historical felt areas.

2.4.2. Offsets across the Sumatran fault and the evolution of dextral slip along the Sumatran margin

2.4.2.1. Exemplary small to moderate offsets

None of the geomorphic offsets across the Sumatran fault are greater than ~20 km, and most are far smaller (Fig. 2.6 and Tables 2.2 and 2.3). The smallest known offsets along the Sumatran fault are those associated with particular historic fault ruptures. These include offsets of a meter or two on the Sumani segment (0.75°S), during the 1943 earthquake [Untung et al., 1985] and up to about 4.5 m during the 1892 earthquake, on the Angkola segment (about 0.6°N) [Müller, 1895; Reid, 1913; Prawirodirdjo et al., this issue]. Our best examples of dextral offsets in the range of hundreds of meters to a couple kilometers are on or near the flanks of young volcanoes: Channels on the southwest flank of Kaba volcano (3.6°S) are offset ~700 m. The walls of Dipatiampat caldera (2.65°S) are offset ~500 m. Stream channels incised into the southwest flank of Marapi volcano display offsets ranging from 120 to 600 m. The Maninjou Tuff (0.4°S) has been offset 700 m (Fig. 2.3), and channels cut into the Toba Tuff (2.2°N) are offset about 2 km (Table 2.2). We have used three of these to determine the modern slip rate of the Sumatran fault, but full documentation of these rates is the subject of a manuscript in preparation.

As one would expect, highly dissected volcanic landforms are offset more than their younger neighbors are. The two offset streams cutting a dissected volcanic edifice at 4.2°S are good examples of this. They are offset about 2.5 km (Plate 2).

2.4.2.2. Largest geomorphic offsets

The largest plausible geomorphic offsets along the Sumatran fault are ~20 km (Table 2.3, Figures 2.6 and 2.7, and Plate 2.1). These include right-lateral deflection of the channels of the Ketaun River channel at 3.2°S, the Seblat River channel at 2.9°S, and the Tripa and Meureubu River courses at 4.1° and 4.4°N (PLATE 2.1). Late Cenozoic folds at 5.25°N may also be offset ~20 km. Furthermore, we speculate below that the Singkarak graben (at 0.6°S) has developed in response to 23 km of offset.

The two major offsets between 5° and 5.5°N provide the most compelling evidence from stream channels for large offset along the Sumatran fault (Fig. 2.7). The deeply incised trunk channels of both streams cross the fault at a high angle and have long, straight courses along the fault trace. The neighboring Woyla River drainage also appears to be offset ~21 km, but this offset is less certain because the match across the fault is of trunk channel to tributary channels. The drainage divide between the Woyla and Geumpang Rivers also appears to be offset by ~20 km.

One could propose 40- to 50-km offsets for the deeply entrenched channels of the Tripa and Meureubo Rivers, but this would leave implausible mismatches in the surrounding topography. Our proposed 20- to 30-km offset of an anticline/syncline pair at about 6.4°N, which is based upon a plausible offset of folded Pliocene, Miocene, and

Oligocene rocks [*Bennett et al.*, 1981] (Fig. 2.7), supports the interpreted 20-21 km offset of the Tripa and Meureubo Rivers.

Another large offset that we will consider in more detail is one we can infer from the geometry of the normal faults along the Singkarak graben at about 1.4°S. This is more speculative than the geomorphic offsets described above. In most cases, the length of a pull-apart graben along a strike-slip fault probably does not represent the total slip across the fault zone (for example, the 7-km-long step over mapped by *Zachariasen and Sieh* [1995] between two faults in California has only 300 m of total offset across it). The particular nature of the faults bounding the Singkarak graben suggests that it may be an exception.

Although the dextral fault segments coming into the step over from the northwest and southeast are misaligned by only \sim 3.5 km, the normal faults bounding the lake are separated by as much as 7.5 km (Plates 1 and 3). Because of their salad-tong geometry, we surmise that the normal faults represent collapse of shallow crust into the expanding rectangular region that is being produced by dextral slip on the misaligned lateral faults.

The predominance of volcanic rocks of Plio-Pleistocene age on the flanks of the graben indicates that the graben is no more than a few million years old. *Bellier and Sebrier* [1994] proposed that the Singkarak basin is an extinct pull-apart graben, inactivated when the trace of the Sumatran fault cut across the lake. The very steep scarps and youthful topography associated with the graben-bounding normal faults strongly suggest, however, that accommodation space continues to be created by dextral slip on the en echelon Sumani and Sianok segments. Furthermore, the location of the

1943 rupture is inconsistent with a competing model for the evolution of the fault by *Bellier and Sebrier* [1994].

We hypothesize that the normal faults should only be active adjacent to foundering crust within the accommodation space generated by dextral slip along the en echelon faults. A hypothetical evolution of these normal faults as the strike-slip displacement grew is depicted in Figure 2.8. Therefore, we propose, that the total offset on these two misaligned strike-slip segments is ~23 km, the length of the arcuate normal fault zones on either side of the lake.

This is, of course, not the only plausible evolution for the Singkarak pull-apart graben, but it is one that is consistent with ~20 km of total offset along the Sumatran fault. One could, for example, accept our inference that the lengths of the normal faults reflect the fault-parallel length of actively foundering crust but hypothesize that the length of the foundering region has remained unchanged at ~23 km since the faults initiated. This would imply that the length of the foundering region has no bearing on the amount of total offset. We favor our hypothesis because it is consistent with other evidence for ~20 km of total offset.

2.4.2.3. Total offset

Why are the largest geomorphic offsets no greater than ~20 km? Is it possible that these represent total strike-slip offset along the Sumatran fault? Or is there a limit to the size of geomorphic offsets related to the susceptibility of landforms to erosion and burial? We will give reasons below why 20 km might well be the total offset across the

fault, but we will also show that a total offset as great as \sim 100 km can not be ruled out at this time.

Indirect arguments for offset much greater than 20 km are as follows: One might expect that the great length of the Sumatran fault requires substantially greater total offsets than a couple tens of kilometers. It is certainly true that many very long strikeslip faults, such as the Alpine (New Zealand) and San Andreas (California) and many oceanic ridge-ridge transform faults display geologic offsets of hundreds of kilometers [Yeats et al., 1997, Chapter 8].

But this is not a strong argument for large offset, for two reasons. First, many other very long strike-slip faults have accrued only a few tens of kilometers of offset. An example is Turkey's 1500-km-long North Anatolian fault, which has a total offset of only 85 km [*Armijo et al.*, 1999]. Second, in a strict sense, the Sumatra fault is not one fault; rather, it is a fault zone that consists of many segments, which range in length from 60 to 220 km. Many strike-slip faults with lengths as short as these have accrued only a few kilometers to a few tens of kilometers of offset (for example, the San Jacinto fault in California is a zone with 24 km of dextral offset that consists of many disjunct segments, tens of kilometers long).

Another reason to suspect that total slip would be >20 km is the transformation of the Sumatran fault into the spreading centers of the Andaman Sea [*Curray et al.*, 1979]. This suggests that offset could equal the 460 km of spreading that has occurred there in the past 10 Myr. But we will see below that much of this offset has been carried by faults that splay into the forearc, west of the Sumatran fault zone.

Regardless of plausible analogues and the fault's connection to the spreading centers of the Andaman Sea, direct geologic evidence for total offset across the Sumatran fault is sparse and equivocal. *McCarthy and Elders* [1997] suggest 150 km of dextral slip, on the basis of similarities in isolated outcrops of crystalline basement on both sides of the fault in central Sumatra. *Katili and Hehuwat* [1967], however, infer that total dextral offset at three localities (near the Equator, 3°S, and 4°S) is only 20 to 25 km on the basis of regional-scale maps of late Paleozoic to early Cenozoic rocks (Plate 2.4). *Cameron et al.* [1983] suggest a 20-km dextral offset of Oligocene beds at about 4.1°N. Neither the larger nor the smaller offsets are adequately defended by sufficiently detailed mapping.

The geologic setting of the Sumatran fault supports the notion that geomorphic offsets might be limited to less than a few tens of kilometers and that these values could be significantly less than the total offset. The abundance of young volcanic cover, the spacing of major river channels, and the length of individual fault segments all limit the accumulation of geomorphically evident offset. Let us consider volcanic cover first. More than a quarter (~450 km) of the 1650-km-long Sumatran fault traverses young volcanic edifices and their thick pyroclastic deposits. Most or all of these volcanic constructions are probably far less than a half million years old, given their generally undissected nature. Even if the Sumatran fault carried all the dextral component of the relative plate motion vector (~30 mm/yr), no more than ~15 km of offset could have accumulated since their deposition. Burial of older offsets would have obscured or eliminated their clear geomorphic expression.

Clear geomorphic offsets are also limited by the length of individual fault segments, which range in length from ~35 to 220 km (Plate 2.1). Since the majority of the fault segments are right-stepping, graben are common along the fault. These grabens form intramontane valleys that occupy about ~350 km of the fault. As these basins form, streams divert into them. The Alas graben, between 3.1° and 3.9°N, has probably enabled such a diversion. The Alas River drains a 130-km reach of the fault into the 50-km-long graben before breaching the graben wall and flowing southwestward to the Indian Ocean. The flow of the Sumpur River, between about 0.1° and 0.75°N, has also been strongly influenced by subsidence along the fault; major tributaries flow into and across the Sumpur Valley before flowing eastward toward the Java Sea from their confluence at the fault.

A third limit to the size of geomorphic offsets is imposed by the spacing of major drainage channels that cross the fault. Cumulative offsets are unlikely to be greater than the spacing between major river channels because piracy occurs as trunk channels of one drainage system are offset to positions upstream from neighboring trunk channels [see, e.g., *Prentice*, 1988; *Allen et al.*, 1984; *Yeats et al.*, 1997, Chapter 8]. Along only a small percentage of the Sumatran fault are major stream channels spaced more than a couple tens of kilometers apart (Plate 2.1). Piracy of the headwaters of the Alasijani River by the Manna River, for example, may have occurred at about 4.1°S (Plate 2.1). Furthermore, where the Sumatran drainage divide is within just a couple kilometers of the Sumatran fault, large trunk stream channels do not cross the fault trace. In these places, the Sumatran fault traverses only smaller tributary drainages. Because tributaries are more closely spaced, geomorphic interference will result where offsets exceed a few

kilometers. Thus only about half of the Sumatran fault might be expected to express offsets greater than a few kilometers.

Nonetheless, there is reason to favor the hypothesis that the largest geomorphic offsets are, in fact, the total offset across the fault. The 20- to 21-km offsets of deeply incised channels in northern Sumatra probably record total offset since the initiation of uplift of the Barisan mountain range in this region, and that uplift is quite old. The age of initiation of uplift is poorly constrained, but sedimentation history of the forearc basin suggests that Sumatran sediment sources began eroding in late mid-Miocene time (about 10 Ma) [Karig et al., 1979; Harbury and Kalagher, 1991], and Cameron et al. [1980] document major activity of a range-bounding fault about 10 Ma. If this is true, then incision of the Tripa and Meureubo Rivers would also have begun about 10 Ma, and the 21-km offsets would necessarily reflect total offset since that time. The nearby 20-km offset of an Oligocene sedimentary unit proposed by Cameron et al. [1983] suggests that this may be the total offset since the Oligocene as well.

Our analysis of the Singkarak graben also suggests that 23 km is the total offset across the Sumatran fault since formation of the two bounding faults, the Sumani and Sianok segments. If the total offset across the fault were greater, proof would require discovery of an older fault, hidden beneath the younger sediments of the region.

2.4.2.4. Evidence of stretching near the Sunda Strait

A simple structural analysis of the forearc region near the southern terminus of the Sumatran fault provides support for ~100 km of total offset across the Sumatran fault

system. However, as we will show, not all of this, nor even a majority of it, need be associated with the Sumatran fault.

Two earlier papers discuss stretching of the forearc near the southern terminus of the fault. *Huchon and Le Pichon* [1984] were the first to suggest that arc-parallel stretching of the forearc region near the Sunda Strait is related to strike slip along the Sumatran fault. They hypothesized that the landward bend in the subduction deformation front and the absence of an outer-arc ridge and forearc basin south of the Sunda Strait (Fig. 2.5) indicate arc-parallel stretching of the forearc region. However, they did not use this to calculate plausible amounts of offset along the Sumatran fault. Instead, they accepted sparse and equivocal evidence for ~100 km of total offset along the fault and attempted to demonstrate that this offset is consistent with reasonable estimates of arc-parallel stretching. They did not attempt a rigorous assessment of the implications of the forearc geometry on total offset along the Sumatran fault.

Lassal et al. [1989] also attempted to quantify the stretching of the forearc region south of the Sunda Strait. They show three seismic reflection lines from a 80 x 50 km area in and on the flanks of the graben at the western entrance to the strait. They annotate these with five stratigraphic boundaries, whose geometry and ages they defend by reference to unpublished work. They claim (without discussion or argument) that an allegedly upper Miocene stratal package contains reef deposits (an indicator of shallow water). They assume an uppermost Miocene (5 Ma) age for the reefs and then use the depth of this packet of sediment to calculate the "stretching factor" since 5 Ma. This factor is described by Le Pichon and Sibuet [1981], who apply a stretching model of McKenzie [1978] to passive continental margins. The use of this model seems wholly

inappropriate to us since the parameters needed to calculate stretching are mostly unknown for the Sunda Strait. *Lassal et al* [1989], conclude by asserting, without any discussion or calculation, that this stretching factor "probably explains the opening of the strait since 5 Ma ago, with a maximum displacement of 50 to 70 km along the central Sumatra fault." Their paper is, in fact, so sparse on data and documentation that its conclusions are left undefended.

We propose a simple measure of extension across the graben of the Sunda segment, which establishes a minimum amount of dextral slip on the Sumatran fault. If we assume that the faults bounding the graben dip 60°, we can calculate the horizontal extension across the faults in the direction of the Sumatran fault. We calculate a 6.5-km lower bound on extension of the graben parallel to the Sumatran fault if we assume that the 2-km height of the scarp represents vertical throw across the faults. This assumption is manifestly an underestimate of total vertical throw, since hundreds of meters of deposits within the graben are clear on the seismic reflection cross sections. Thus 6.5 km is probably several kilometers less than the actual amount of extension across the Sunda graben. Several more kilometers of dextral slip could probably also be added to total slip along the Sumatran fault if the geometry and timing of faulting farther east within the strait and buried beneath >2000 m of volcanic debris (summarized by Huchon and Le Pichon [1984]) were known better. In summary, extension of the Sunda graben and filled graben farther east is consistent with dextral slip of the order of 10 km along the However, more detailed stratigraphic and structural data will be Sumatran fault. necessary to calculate extension across the graben more precisely.

Let us now attempt a quantitative analysis of stretching of the forearc region, to provide a maximum limit to dextral slip on the Sumatran fault during the past few million years. This analysis simply carries the geometrical observations of *Huchon and Le Pichon* [1984] to their logical conclusion. From simple volumetric balancing of the forearc wedge, we calculate ~100 km of stretching of the forearc parallel to the Sumatran fault.

As we discussed in section 2.3.1. (Fig. 2.5), the forearc basin and outer-arc ridge are attenuated in the region of the Sunda Strait. These two features disappear near the strait, and the deformation front bows landward. Following *Huchon and Le Pichon* [1984], we interpret this as an indication of fault-parallel stretching and fault-normal necking of the forearc region. Extensive seismic reflection studies and structural and stratigraphic information from the forearc and outer-arc regions north of the Equator show that the paired forearc basin and outer-arc ridge developed throughout the Miocene epoch but grew particularly rapidly during the Pliocene epoch [*Samuel et al.*, 1997; *Samuel and Harbury*, 1996]. Thus we infer that the deformation of these features has occurred within just the past few million years.

We begin with an estimate of the boundaries of the volume that has been stretched. The concavity of the deformation front and merging of the outer-arc ridge and forearc basin suggest that the current length of the deformed region, L, is ~356 km (Fig. 2.9). Hypocentral depths on or near the subduction interface constrain the northeast dipping base of the deformed forearc wedge. The deformation front and the base of the continental slope define the seaward and landward boundaries of the deformed region.

Using these boundaries, we calculate that the deformed crustal wedge has a volume V, of about $1.01 \times 10^6 \text{ km}^3$. We assume that this volume is equal to the original, undeformed volume V_o . By further assuming that the cross-sectional areas of the current southeastern and northwestern edges of the deformed region, A and B, have not changed since deformation began, we can calculate the original arc-parallel length of the deformed region. A and B are currently 2870 and 4970 km²:

$$L_o = 2 * V / (A + B) = 258 \text{ km}.$$
 (1)

The total amount of northwest-southeast stretching is:

$$\Delta L = L - L_0 = 356 \text{ km} - 258 \text{ km} = 98 \text{ km}.$$
 (2)

Since the Sumatran fault forms the northeastern boundary of the forearc sliver block, we are tempted to conclude that this estimate of stretching of the forearc equals the amount of right-lateral slip along the Sumatran fault. However, in fact, this 100 km is only an upper bound on offset of the past few million years since there is another structure in the forearc region that could also have accommodated some of this stretching. The Mentawai fault [*Diament et al.*, 1992], located between the forearc basin and the outer-arc ridge (Figs. 2.1 and 2.8 and Plate 2.1), could also have accommodated some of this motion. The linearity of this large structure suggests a significant component of strike-slip motion, but the magnitude of strike-slip motion, if any, has not been documented.

2.4.2.5. Plausible evolution of dextral slip along the Sumatran margin

Although knowledge of the geology of the Sumatran fault and other faults of the Sumatran fault system is incomplete, enough information exists to attempt a reconstruction of the system's deformational history over the past few million years (Fig. 2.10). The principal constraints on this history are: (1) the magnitude and timing of the discrepancy between spreading in the Andaman Sea and stretching near the Sunda Strait; (2) a range of plausible total offsets for the Sumatran fault; (3) the timing, style, and magnitude of deformation in the Sumatran forearc region; and (4) a southeastward decrease in the current rates of slip along the Sumatran fault. These constraints suggest that the Sumatran fault system has evolved significantly in the past several million years and that the current configuration of deformation is not representative of pre-Quaternary deformation.

One hundred kilometers of motion near the Sunda Strait contrasts markedly with the 460 km of opening suggested by *Curray et al.* [1979] for the Andaman spreading centers (Fig. 2.1). The contrast disappears, if one compares Andaman extension and Sundan offset for similar periods of time. Only about 118 km of Andaman extension may have accumulated in the past 3 Myr (J. Curray, written communication, 1999). This does not differ greatly from the 100 km of stretching of the forearc near the Sunda Strait for about the same period of time (i.e. since the rapid rise of the Sumatran outer-arc ridge in the early Pliocene). Hence the discrepancy between deformation in the Andaman sea and Sunda Strait during the past 3 Myr may be very small or nonexistent.

Nonetheless, the current rate of slip on the Sumatran fault appears to diminish significantly from northwest to southeast. Although new geodetic evidence suggests that there is no significant decrease between about 1°S and 2°N [Genrich et al., this issue], geologic slip rates across this section suggest a much larger decrease in rate, from 27 mm/yr (near 2.2°N) to 11 mm/yr (near 0.4°S) [Sieh et al., 1991, 1994; D. Natawidjaja and K. Sieh, manuscript in preparation, 2000]. Bellier and Sebrier's [1995] estimations of slip rate along the fault, based upon correlations of stream length with age, also decrease from northwest to southeast.

If the total offset along the Sumatran fault is only \sim 20 km and slip rates have been constant, then the northern part of the fault zone would be less than a million years old. South of the Equatorial Bifurcation, where late Quaternary slip rates appear to be \sim 10 mm/yr, 20 km of slip might have accrued in \sim 2 Myr.

Our calculation of ~100 km of fault-parallel stretching of the forearc near the Sunda Strait suggests that either the total offset along the Sumatran fault is much larger than 20 km or that another structure in the Sumatran fault system has accommodated ~80 km of the stretching. The only plausible other candidate for dextral slip would be the Mentawai fault, well constrained from seismic reflection data to run between the outerarc ridge and the forearc basin [Diament et al., 1992]. The linearity of the feature suggests that it is principally a strike-slip feature. Diament et al. [1992] also argue that the structure of the fault zone indicates that its sense is primarily strike-slip. In our opinion, the structural argument is a less compelling one because we are not convinced that the Mentawai fault zone exhibits the "flower" structure characteristic of strike-slip faulting. In fact, the position of the fault, on the northeastern flank of the outer-arc ridge,

is consistent with the fault being a backthrust, along which the outer-arc ridge has risen. The existence of a large homocline in the same position relative to the forearc basin and outer-arc ridge north of the Equator [Karig et al., 1980] (Plate 2.1) supports this interpretation. So it is with some reluctance that, in the evolutionary model below, we use the Mentawai fault as a strike-slip element of the Sumatran fault system.

A final constraint on the evolution of the Sumatran fault system is the Mio-Pliocene history of the forearc and outer-arc regions. The Andaman spreading centers were actively spreading at ~40 mm/yr during this period, yet we have no evidence of contemporaneous dextral deformation of the forearc sliver plate south of the Equator. How and where, in Pliocene and late Miocene time (about 2 to 10 Ma), was the dextral component of oblique convergence accommodated? *Matson and Moore* [1992] suggest that some of this discrepancy can be accommodated by the dextral-normal faults of the forearc region near Nias Island (Fig. 2.2 and Plate 2.1). We consider this possibility below.

Stratigraphic and structural studies by *Samuel et al.* [1997] and *Samuel and Harbury* [1996] show that broadening and uplift of the outer-arc ridge occurred early in the Pliocene epoch throughout the Sumatran forearc region. This is critical to reconstructing deformation of the forearc sliver plate because the early Pliocene growth of the outer-arc ridge produced an elongate feature that has been deformed in the subsequent several million years. The ridge is clear in the bathymetry of Plate 2.1. South of about 1°S, it is regular and 60 to 80 km wide. Its northeastern boundary is the Pliocene Mentawai homoclinal flexure. On the southwest the ridge is bounded by a plateau that sits at a depth of ~2400 m. We speculate that this plateau was formerly a

part of the Australian plate and that its northeastern edge is the former deformation front of the subduction zone. Similar features are also present between about 1.5°N and 3°N, near Simeulue Island.

Between 1.5°N and 2°S, the outer-arc ridge, the homocline, and the ancient deformation front and plateau are markedly disarticulated. *Karig et al.* [1980] observed that the Pliocene homocline on the east side of Nias is dextrally offset ~100 km by two strands of the Batee fault. We infer from bathymetry that the strand of the Batee fault northwest of Nias offsets the ancient deformation front ~50 km, from northwest of Nias to a position west of Nias (Plate 2.1). Farther south on the inner trench slope, between Nias and Siberut Islands, the deformation front may be offset by about an additional 50 km along another north striking fault.

Dextral offset of the eastern edge of the forearc basin by the Batee fault is ~150 km [Karig et al., 1980]. From paleontologically constrained seismic stratigraphy, Matson and Moore [1992] show that the Batee fault was active from the late Miocene through the Pleistocene epochs. Twenty to thirty kilometers of dextral slip appear to have occurred on the nearby Singkel fault in the late Miocene epoch. Thus it is reasonable to suggest that the first few tens of kilometers of the 150-km dextral offset on the northern portions of the Batee fault accrued in the late Miocene. However, the bulk of the slip must be late Pliocene and younger because the Pliocene homocline of Nias Island is offset ~100 km. This offset must have accrued over at least 1.5 Myr, since a shorter duration would require rates of dextral slip in excess of the rate of relative plate motion.

Plate 2.1 also shows a disruption of the outer-arc ridge and inner trench slope south of Nias Island, at the Pini basin and between Tanabala and Siberut Islands. The Pini basin experienced rapid subsidence beginning about 4 Ma. This subsidence is probably contemporaneous with activity of north striking faults that bound the basin [Matson and Moore, 1992] and with minor north striking dextral-slip faults on Nias [Samuel and Harbury, 1996]. A disruption in the inner trench slope farther south, along strike of the Pini basin, may represent a 40- to 50-km dextral offset of the same ancient deformation front mentioned above.

Figures 2.10a-10c depict a plausible evolution of the Sumatran fault and other structures of the plate boundary that is consistent with available geologic, geodetic, and seismographic data. Variations of this history are also possible; our principal intention is to show that the fault system evolved significantly in the past few million years. The main characteristics of this speculative history are as follows: (1) the current 15 mm/yr difference in Sumatran fault slip rate north and south of the Equator is very young (perhaps only100,000 years old), and (2) active normal- and dextral-slip (transtensional) faulting in the forearc and outer arc between 1°S and 2°N is an ancient (and perhaps current) analogue to the stretching at the southern end of the Sumatran fault.

Figure 2.10a shows the geometry of the region at about 4 Ma. Just prior to this time, relief between the forearc basin and the outer-arc ridge increased greatly across the homoclinal fold between the forearc basin and outer-arc ridge [Karig et al., 1980; Samuel et al., 1997; Samuel and Harbury, 1996]. We speculate that as the outer-arc ridge grew, the subduction deformation front jumped southwestward to its present location, from a deformation front still visible in the bathymetry, closer to the outer-arc ridge (Plate 2.1).

From 4 to 2 Ma, dextral slip on the Aceh segment and the Batee fault occurred at 37 mm/yr, and the homocline, outer-arc ridge, and inner trench slope were offset 37 km by a curved southern extension of the Batee fault, off the north coast of Nias Island, and 37 km more across the Pini basin. This is consistent with the stratigraphy of *Matson and Moore [1992]*. Several kilometers of arc-parallel elongation of Nias Island along north striking dextral-slip faults and conjugate sinistral-slip faults also occurred during this period [*Samuel and Harbury*, 1996]. Subduction south of the Equator was parallel to the relative plate motion vector and highly oblique to the deformation front. Subduction north of the Equator was mostly or wholly dip slip because most or all of the dextral component of plate motion was occurring along the Batee-Aceh fault.

About 2 Ma (Fig. 2.10b), both the Mentawai fault and the Sumatran fault formed. From 2 Ma to 100 ka, they carried ~40 mm/yr of the dextral component of oblique convergence south of the Equator, and the subduction interface accommodated only the dip-slip component. North of the Equator, 40 mm/yr of dextral slip was accommodated by the Sumatran fault (10 mm/yr) and Aceh-Batee fault (30 mm/yr).

Figure 2.10c depicts our suggestion for the current neotectonic partitioning of deformation. The Aceh-Batee fault is no longer active or is only minimally so. The Sumatran fault is slipping ~15 mm/yr faster north of about 2°N than south. The mass balance problem caused by this discrepancy is being taken up by a nascent belt of deformation that crosses the outer-arc ridge at the Equator. This deformation belt is superjacent to *Fauzi et al.'s* [1996] swath of exceptionally high seismic activity in the down going oceanic slab. It also encompasses the active Toru folds of the mainland coast, two young faults on and south of Nias and north-south graben that bathymetry

suggest may exist on the inner trench slope (Plate 2.1). Figure 2.10c is consistent with recent measurements of geologically measured Sumatran fault slip rates but is inconsistent with the rates of geodetic strain measured by GPS south of the Equator.

If the Sumatran fault is carrying only \sim 10 mm/yr of dextral slip south of the Equator [Sieh et al., 1994; Bellier et al., 1999], the remainder of the dextral component of slip must be taken up along either the subduction interface or by a fault within the forearc sliver. The GPS data show no sharp gradients in shear in the forearc region, so the remaining dextral component is probably accommodated by slip on the subduction interface [McCaffrey et al., this issue]. This portion of the dextral component, x, would be \sim 27 mm/yr (x = 58 mm/yr*sin 41° - 10 mm/yr, where 58 mm/yr is the magnitude of relative plate motion and 41° is the angle between the plate motion vector and the trench normal and 10 mm/yr is the slip rate on the Sumatran fault). Slip vectors for earthquakes on the subduction interface deviate from the trench normal by \sim 20°, on average. These suggest that the dextral component on the interface would be a bit less than our model predicts, only \sim 16 mm/yr.

The history depicted in Figure 2.10 is consistent with the timing of activity on faults both offshore and onshore Nias [Karig et al., 1980; Matson and Moore, 1992; Samuel and Harbury, 1996]. It also incorporates our observation that the Batee fault is not currently active along most of its exposed trace but retains clear evidence of 5-km dextral offsets of a few of the largest channels that cross it (Plate 2.1). Restoration of ~80 km of slip on the faults between 1°S and 2°N in the offshore region eliminates the dimple in the subduction deformation front west of Nias and Simeulue, just as restoration of ~80 km of slip on the combined Sumatran and Mentawai faults nearly eliminates the dimple

west of the Sunda Strait. Thus we suggest that the concavities of the deformation front west of Nias and west of the Sunda Strait are features inherited from Plio-Pleistocene dextral strike-slip motion in the forearc region.

2.4.3. Tectonic model of the Sumatran plate margin

Transtensional necking of the forearc region between 1°S and 2°N during the past 4 Myr has had a profound effect on all of the major elements of the plate margin there. The inner trench slope, outer-arc ridge, and forearc basin have been fragmented by this process. Even the shapes of the subduction interface, the active volcanic arc, and the Sumatran fault appear to have been affected. In fact, we can divide the Sumatran plate boundary into three tectonic domains, based upon their relationship to this Plio-Pleistocene transtension (Plate 2.5). The southern domain, which we suggest has been part of the forearc sliver plate only for the past 2 Myr, is the most simple geometrically and structurally. The central domain, which comprises all the transtensionally fragmented pieces, is the most complex.

The southern domain has the following characteristics: (1) the Sumatran fault displays a right-stepping en echelon pattern and courses above the 100- to 135-km isobaths of the subduction interface, (2) the locus of volcanism is predominantly northeast of or near the fault, (3) the forearc basin is remarkably simple, ~2 km deep and unbroken by major faults, (4) the outer-arc ridge is relatively narrow, forms a single antiformal high, and is geometrically simple, (5) the Mentawai fault and homocline, which separate the basin and ridge, are unbroken and relatively straight, and (6) the inner trench slope is relatively uniform and possesses a prominent plateau about half way

between the active deformation front and the outer-arc ridge. The source of the giant (M_w 9) subduction earthquake of 1833 was the subduction interface beneath much of this domain [Newcomb and McCann, 1987; Zachariasen et al., 1999]. Strains measured by GPS in the early to mid-1990s show that the outer-arc islands are moving parallel to the relative plate motion vector and that the subduction interface beneath the southern domain is currently fully locked [Prawirodirdjo et al., 1997; McCaffrey et al., this issue]. The Sumatran fault appears to be slipping at a rate of about 10 mm/yr in the Southern domain [Sieh et al., 1991, 1994; Bellier et al., 1999].

The northern domain is characterized by these features: (1) a geometrically irregular Sumatran fault, with both releasing and restraining bends, which resides above the 125- to 140-km subduction isobaths, (2) a volcanic arc on and north of the Sumatran fault, (3) a 1- to 2-km-deep forearc basin, (4) a very broad, structurally and bathymetrically complex outer-arc ridge, (5) a homocline along its southernmost few hundred kilometers that is similar to the Mentawai structure of the southern domain, and (6) a very narrow inner trench slope.

The central domain is distinguished by these features: (1) a 350-km-long section of the Sumatran fault that is markedly discordant with the subduction isobaths, (2) a volcanic arc that cuts dramatically across the Sumatran fault, (3) a topographically shallow (0.2-0.6 km deep) forearc basin, which has been fragmented into several blocks during oblique-normal faulting, (4) a fragmented outer arc, (5) a fragmented homocline between the outer-arc ridge and forearc basin, and (6) a fragmented inner trench slope. The giant (M_w 8.5) subduction earthquake of 1861 and numerous other large historic subduction earthquakes originated within this domain [Newcomb and McCann, 1987].

Strains measured by GPS in the early to mid-1990s indicate that the hanging wall block across the central domain is currently moving parallel to the subduction deformation front [*Prawirodirdjo et al.*, 1997; *McCaffrey et al.*, this issue]. The geologic rate of slip of the Sumatran fault increases markedly from southeast to northwest across the central domain, from ~11 mm/yr to ~27 mm/yr [*Sieh et al.*, 1991].

We suspect that transfersional fragmentation has dominated the central domain because the Investigator fracture zone has been subducting beneath the central domain for the past several million years. Its locus of impingement on the deformation front has migrated from the northern to the southern margin of the central domain during the past 5 Myr (Plate 2.5). This may be significant because fault activity in the hanging wall block of the forearc region appears to have been restricted during this period to the central domain (Fig. 2.10). Furthermore, the orientations of faults in the central domain are predominantly north-south, parallel to the topographic and structural grain of the underlying Investigator fracture zone. We hypothesize therefore that the topographic heterogeneity of the Investigator fracture zone beneath the central domain has led to disruption of the forearc and outer-arc regions. Currently, the Investigator fracture zone is also associated with a band of intense seismicity within the down going slab in the middle of the central domain (Plate 2.5) [Fauzi et al., 1996] and an abrupt change in the azimuth of GPS vectors on the outer-arc ridge [Prawirodirdjo et al., 1997, McCaffrey et *al.*, this issue].

The subduction interface curves broadly across the Central domain (Plate 2.5) [Fauzi et al., 1996]. The close association of this curve with the other elements of the central domain suggests cause and effect or at least a shared cause. Could flexure of the

downgoing slab have been produced by necking of the hanging wall block? Or did deformation within the downgoing slab lead to transtension in the forearc sliver plate? We suggest the former.

The existence of the 1500-km-wide boundary between Indian and Australian plates offshore western Sumatra and the Andaman Islands gives reason to suspect that the downgoing slab west of the Investigator fracture zone is deforming. This broad region of deformation abuts all of the central and northern domains. Gordon et al. [1990] calculate that the two oceanic plates are converging north-south at an angular rate of 0.3°/Myr about a pole of rotation in the central Indian Ocean. At the Sumatran deformation front this translates into a nominal 13-km north-south shortening of the downgoing slab in the past 3 Myr. The actual nature of lithospheric deformation west of the deformation front is quite uncertain, however. Simple north-south buckling is unlikely. Focal mechanisms and structure indicate a predominance of north-south left-lateral slip on north-south faults [Deplus et al., 1998]. To accommodate north-south contraction, these structures would need to be rotating clockwise, domino-like, to enable eastward extrusion of lithosphere [Gordon et al., 1990]. The precise locus of such deformation is unknown, and so its impact on the overriding central and northern domains is hard to assess. Nonetheless, it is plausible that the contrast in nature of the southern and northern hanging wall domains could have arisen, at least in part, from subduction of deforming oceanic lithosphere beneath the northern domain. It is hard to imagine, however, how dextral transfersion on north striking faults within the central domain could be related to sinistral slip and clockwise rotation on north striking faults in the subjacent subducting lithosphere, unless

eastward extrusion of the oceanic lithosphere has led to northwestward extrusion of the forearc sliver plate, as plate collision has done in Turkey and Tibet.

A more logical proposition may be that transtensional necking of the central domain has led to bending of the subducting slab. Trench-orthogonal thinning of the forearc appears to have drawn the deformation front and trench northeastward, tens of kilometers closer to the mainland coast. If this process had not also drawn the deeper parts of the subducting slab northeastward, the dip of the interface in the forearc and outer arc would be steeper than in the southern domain. The isobaths show the contrary, that the subduction zone beneath the central domain has a very similar cross-sectional profile to that beneath the southern domain. One test of this hypothesis would be to determine if the active volcanic arc in the central domain is substantially northeast of the late Miocene and Pliocene arc. If so, it would suggest that the subduction isobaths have moved northeastward in the past few million years.

2.4.4. Relationship of the Sumatran fault to the modern volcanic arc

Many have noted the proximity of the Sumatran fault to the volcanic arc and have suggested that it formed there because of the effect of magmatism on the lithosphere [e.g., *Fauzi et al.*, 1996; *Tikoff*, 1998]. Sumatra aside for the moment, however, most trench-parallel strike-slip faults are not coincident with their volcanic arcs. The Median Tectonic Line (Japan) does not have an associated arc; the Denali fault (Alaska) lies much farther from the trench than the Alaskan arc volcanoes; the Atacama fault (Chile) lies between the trench and volcanic arc; and the Philippine fault is tens of kilometers from the major Philippine arc volcanoes [*Yeats et al.*, 1997]. Furthermore, most volcanic

arcs along obliquely convergent margins do not sport large strike-slip faults. This general lack of association suggests that the alignment of the Sumatran volcanic arc and the Sumatran fault is purely a coincidence. In fact, *McCaffrey et al.* [this issue] have used finite element modeling of stresses across the obliquely convergent Sumatran plate boundary to show that formation of the trench-parallel Sumatran fault did not require the presence of the magmatic arc. Nonetheless, *Tikoff* [1998] has suggested that faults such as the Sumatran fault form above the locus of greatest strain gradient in the lower crust or mantle, occasioned by the magmatism of the volcanic arc. *Bellier and Sebrier* [1994] have claimed that numerous small and large volcanic cones and calderas occur at both current and ancient releasing step overs along the Sumatran fault.

We can test directly whether or not magmatism has influenced the location of the fault or, conversely, whether or not faulting has influenced the location of volcanism and magmatism. Plate 2.1 allows us to search for a relationship between the volcanic arc and the Sumatran fault, since it displays not only the most prominent traces of the Sumatran fault but also the youngest volcanoes. We mapped these volcanic features using the same sources we used to map the fault (Fig. 2.2). We limited our mapping to those features that have suffered minimal erosion, since highly eroded, older volcanic constructs are harder to recognize geomorphologically and mapping would have required a more substantial effort. The features we mapped exhibit very little erosional modification of their constructional landforms. Many have been active historically. Those that have been dated radiometrically are typically <100,000 years old (e.g., Toba caldera, 73 ka [Chesner et al., 1991], and Maninjou caldera, 60-90 ka [Nishimura, 1980]). In addition to mapping craters and calderas, which are indicators of volcanic source vents, we also

mapped the edges of the volcanic cones in order to display a crude measure of the output of individual sources.

At first glance, the most striking relationships between the Sumatran fault and the young arc volcanoes are that: (1) the average center line of the active arc is decidedly landward (northeast) of the Sumatran fault and (2) the local center line of the young volcanic arc switches back and forth across the trace of the Sumatran fault as it traverses the 1650-km length of Sumatra. Figure 2.11 shows these relationships. The 10-km separations northeast from the Sumatran fault are common, 25-km distances are not rare, and a few volcanoes are even farther northeast. Only two volcanoes are more than 10 km southwest of the Sumatran fault. From Figure 2.11 one can estimate that the averaged center line of the largest volcanic edifices is ~10 km northeast of the Sumatran fault. This skewed distribution of volcanoes relative to the Sumatran fault suggests that the modern magmatic arc has not created a weak crustal zone that has favored the concentration of shear. Perhaps the active volcanic arc has failed to influence the locus of faulting because the volcanic conduits "soften" only a small percentage of the length of the arc. Alternatively, perhaps magmatic plumbing beneath the Sumatran fault, associated with an unmapped, extinct volcanic arc, did influence the location of the fault.

The local center line of the volcanic arc varies along the strike of the Sumatran fault. It is a few kilometers northeast of the fault between 5.5°S and 0.4°S, swings southwest of the Sumatran fault between 0.4°S and about 2°N, and then swings to a position ~25 km northeast of the Sumatran fault between 2°N and 5.5°N. This broad disparity between the local center line of the volcanic arc and the Sumatran fault is another indication that modern arc magmatism has not guided the formation of the fault.

It also does not appear that individual volcanic conduits have influenced the location of particular fault segments. Only rarely do individual segments of the fault bisect volcanic centers or bend in their vicinity (counterexamples are Kaba and Dipatiampat). However, we would not expect such an association, since the volcanoes that we have mapped are far younger than the age of initiation of the mapped fault segments. We suspect that most of the uneroded edifices are less than 100,000 years old, whereas we have made a case that the fault planes we have mapped are probably ~2 Myr old. If the locus of faulting were influenced by magmatic softening of the crust, the magmatic plumbing that led to the concentration of strains beneath the Sumatran fault would have formed long before the young volcanoes on Plate 2.1. To test the hypothesis that magmatic concentration of shear stresses led to the formation of the fault within the arc, one would need to map the Pliocene and early Pleistocene volcanic centers. We may attempt this at a future date, but it is beyond the scope of our current efforts.

Despite the lack of influence of active magmatism on tectonism, tectonism is influencing magmatism, but only to a minor extent. This conclusion contrasts with that of *Bellier and Sebrier* [1994], who proposed that extensional pull aparts along the Sumatran fault have affected the location of the volcanoes. In fact, our map shows that only 9 of the 50 young volcanic vents shown on Plate 2.1 are located within 2 km of a mapped trace of the Sumatran fault (Fig. 2.11). These are, from southeast to northwest, Suoh, Seminung, Kaba, Dipatiampat, Kunyit, Melenggok, Talang, Sibual-buali, Seulawah Agam, and Pulau Weh. Kaba, Kunvit, Meleggok, Talang, Sibual-buali, Seulawah Agam, and Pulau Web are stratovolcanoes greater than about 10 km in diameter and, thus, embody the most substantial volumes. Suoh, Kaba, Kunyit,

Melenggok, Talang, and Sibual-buali are located within dilatational stepovers or on one of the bounding faults of a dilatational step over. One of these (Suoh) is a large phreatic explosion crater that formed 15 days after the large Semangko segment rupture of 1933 [Stehn, 1934], most convincingly in association with tectonic activity. Bellier and Sebrier [1994] proposed that Toba and Ranau calderas also formed at extinct extensional step overs along the Sumatran fault zone, but these hypotheses are not well founded. They are based solely on the use of SPOT imagery to map more ancient fault strands in the vicinity of these two calderas. Although lineations may exist along these alleged ancient faults, their documentation of the lineations is scant, and they present no geologic mapping to confirm their existence or to quantify the style, age, or amount of shear along them.

We suspect that the association of just 9 of the 50 young volcanoes with the Sumatran fault is a random occurrence. If one peppered an elongate rectangle (with the 1700-by-50 km dimensions of the volcanic arc) with a random distribution of 50 points and then ran straight lines randomly through its long dimension, several points would typically be within 2 km of each line. Thus the close association of several volcanoes with the Sumatran fault zone does not, by itself, demonstrate a genetic relationship. The close association of six of the eight close encounters with dilatational step overs does, however, suggest that tectonic step overs are influencing the locations of a few of the arc's volcanic centers.

2.4.5. Relationship of the Sumatran fault to the subduction zone

The general shape of the Sumatran fault mimics that of the deformation front offshore so faithfully that one wonders about a genetic relationship between the subduction interface and the strike-slip fault (Plate 2.5). North of the Equator, both structures are concave toward the southwest. South of the Equator, both are broadly concave toward the northeast. Along the entire length of the Sumatran fault on land, its horizontal distance from the deformation front varies no more than ~10% from 290 km (Plate 2.1 and Plate 2.5).

A similar coincidence exists between the shape of the Sumatran fault and that of the subduction interface downdip from its trace. This is clear from Plates 1 and 5, which show the 50-, 100-, and 200-km isobaths of the subduction interface. The contours are drawn on the top of the Wadati-Benioff zone, as defined by hypocentral locations in the International Seismological Center (ISC) catalog (as relocated by *Engdahl et al.* [1998]) and as determined by *Fauzi et al.* [1996] in their local seismic survey in the region of Lake Toba.

From about 6°S to the Equator, the relationship is particularly regular; the subduction interface lies 100 to 135 km below the Sumatran fault, except along the southernmost (Sunda) segment (Plate 2.1 and Plate 2.1). Between about 3.5°N and 6.0°N the subduction interface is 125 to 140 km below the Sumatran fault, except beneath the northern (possibly inactive) part of the Aceh segment. These depths in the north are, on average, ~20 km greater than depths south of the Equator. The relationship of subduction isobaths to the Sumatran fault is markedly aberrant between the Equator and about 3.5°N.

There the traces of the Sumatran fault and the subduction isobaths are markedly discordant; the depth of the interface beneath the Sumatran fault ranges from ~ 100 to 175 km.

Because of the well-behaved relationship of Sumatran fault to isobaths in the northern and southern domains, we propose that the Sumatran fault formed first in those two domains, as two separate structures. As displacement on the faults has grown, they have formed a linkage across the central domain and will one day become a single structure.

2.5. Summary, conclusions, and remaining questions

We have used stereographic aerial photography and topography to map 1650 km of the Sumatran fault (Figs. 2.2 and 2.3). The resulting map shows that the fault comprises numerous segments separated by dilatational and contractional step overs and abrupt changes in trend (Plate 2.1 and Figure 2.4). This segmentation appears to have influenced the rupture dimensions of historical large earthquakes and limited their magnitudes to ~7.5.

The largest geomorphically evident offsets along the Sumatran fault are between 17 and 23 km (Plate 2.3, Figures 2.7, and 2.9 and Table 2.3). These are predominantly deeply incised river channels, but one apparent offset of a fold pair and the accumulated offset across a major step over also fall within this range. A lack of detailed and complete mapping along the fault precludes confident matching of geologic units across the fault, but rock offsets suggested by *Katili and Hehuwat* [1967] and *Cameron et al.*

[1983] support the contention that the 20-km geomorphic offsets represent the total offset across the fault.

The distention of forearc structures and the trench near the Sunda Strait suggests ~100 km of arc-parallel stretching of the forearc sliver plate since the early Pliocene (Figs. 2.5 and 2.8). We propose that 20 km of this was accommodated by dextral slip on the Sumatran fault and that the Mentawai fault, a long, linear structure within the forearc region, accommodated the remaining dextral slip.

Our synthesis of data from the Sumatran fault, the volcanic arc, and the forearc region shows that the Sumatran forearc sliver plate consists of three tectonic domains with very distinct tectonic histories (Plate 2.5). The southern domain (from 7°S to 1°S) is the simplest and may have been accreted to the forearc sliver plate only about 2 Myr ago by the creation of the Sumatran and Mentawai faults. The northern domain (north of 2°N) is more complex, and its northern part has been experiencing arc-parallel translation for at least the past 10 Myr. The central domain is the most complex of the three and has been a region of transtension between the northern and southern domains since at least 4 Myr ago.

Geodetic measurements suggest that slip across the Sumatran fault between about 0.8° S and 2.7°N is nearly uniform at about 25 mm/yr [*Genrich et al.*, this issue]. These rates are incompatible with the 27 and11 mm/yr geologic slip rates that we have determined at 2.2°N and 0.3°S [*Sieh et al.*, 1991, 1994; D. Natawidjaja and K. Sieh, manuscript in preparation, 2000). We propose that the geologic difference in rates has arisen in just the past 100 ka or so, because structural evidence for accommodation of the

15 mm/yr difference is obscure. We suggest that a belt of auxiliary, transtensional deformation between the Sumatran fault and the trench is the nascent manifestation of this rate change (Fig. 2.10). This belt includes the western (Angkola) branch of the Equatorial Bifurcation, the Toru fold-and-thrust belt along the mainland coast, and submarine faults in the forearc basin, outer-arc ridge, and inner trench slope.

Although the Sumatran fault and the Sumatran volcanic arc share the same jungle, neither appears to have fundamentally affected the location of the other. Rather than being coincident, the fault and the arc intertwine (Fig. 2.11). The averaged center line of the volcanic arc is distinctly northeast of, not at, the Sumatran fault. Nevertheless, the few volcanic centers that are on or very near the Sumatran fault are predominantly at major extensional step overs, which may well have attracted a small percent of the arc volcanism. The dramatic bend in the modern volcanic arc between 0.7°N and 2.5°N is most probably the result of transtensional thinning of the forearc sliver plate in the past 4 Myr. We can not rule out the possiblility that the Pliocene and Miocene volcanic arc were less sinuous and closer to the locus of later strike-slip faulting.

The broad similarity in shape of the Sumatran fault and subduction interface suggests a genetic relationship. The broad, low-amplitude sinusoidal shape of the subduction interface is mimicked by the Sumatran fault, and along most of its trace the Sumatran fault lies above the 110- to 140-km isobaths of the subduction interface. These relationships are particularly regular north of 3.5°N and south of the Equator, in the northern and southern domains. We suggest that the Sumatran fault first formed as two separate faults in these two domains, and are in the process of linking together through the central domain and across the volcanic arc. We ascribe the disrupted nature of the

central domain's outer-arc ridge and forearc basins to its location above the Investigator fracture zone throughout the past 5 Myr.

Not unexpectedly, this work has generated as many questions as answers: What are the details of the creation and evolution of the three tectonic domains of the forearc sliver plate? How, for example, did deformation in the transtensional central domain evolve through the past several million years? Why did the Sumatran fault form where it did, 290 km from the subduction deformation front and 100 to 150 km above the subduction interface? Would careful, detailed mapping confirm total Sumatran fault offsets of only ~20 km? When did the contrast in slip rates along the Sumatran fault begin? Why is this gradient in rates not apparent in the geodetic data? Is it plausible that the Mentawai fault has a strike-slip component as large as 80 km? Did the two faults originate a mere 2 Myr ago?

Our map of the Sumatran fault can serve as a jumping-off point for careful analysis of the seismic hazard posed by this major structure. To what degree does the historical record of large earthquakes along the Sumatran fault demonstrate that large structural irregularities constrain rupture lengths? Would primitive instrumental records help constrain the source parameters of these large events of the first half of the twentieth century? Whether or not segmentation of the Sumatran fault has markedly influenced ruptures, answering these questions could profoundly affect our general understanding of the importance of structural geometry on seismic rupture processes.

2.6. Acknowledgments

This work began with an invitation by Yehuda Bock and his colleagues at the Indonesian **National** Coordination Agency for Surveying Mapping and (BAKOSURTANAL) to visit Sumatra. They were interested in establishing a better geologic context for their GPS geodetic studies, supported under NSF grants EAR-8817067 and EAR-9004376. Our initial reconnaissance, in 1991, supported by donations from the Caltech Associates, convinced us that geological work aimed at understanding the active tectonics of the fault could be very fruitful. In 1992, we initiated our own NSF sponsored project (EAR-9205591) to map and characterize the Sumatran fault. BAKOSURTANAL, through Bock, supplied most of our topographic coverage of the fault. We are grateful to Suparka and Hery Harjono at the Indonesian Institute of Sciences (LIPI) for helping us acquire many important aerial photographs and arranging fieldwork. Rudy Bachruddin at the Volcanological Survey of Indonesia (VSI) and Gunawan Burhan at the Geological Research and Development Centers (GRDC) also helped us by providing essential aerial photographs along portions of the Sumatran fault. Various private companies also allowed us access to topographic maps and aerial photographs. Paul Tapponnier (IPG Paris) shared topographic maps from the Singkarak region. We also benefited from conversations with Rob McCaffrey and Bob Kieckhefer and from an initial GIS compilation of our data by Carolyn White. Reviews of an early manuscript by Yehuda Bock, Joseph Curray, and Rob McCaffrey were very helpful. Finally, we greatly appreciate the thorough, thoughtful, and careful reviews of Jeff Freymuller, Eli Silver, and Paul Tapponnier.

2.7. References

- Abe, K., Magnitudes of large shallow earthquakes from 1904 to 1980: *Phys. Earth Planet. Inter.* 27, 72-92, 1981.
- Allen, C., A. Gillespie, H. Yuan, K. Sieh, Z. Buchun, and Z. Chengnan, Red River and associated faults, Yunnan Province, China: Quaternary geology, slip rate and seismic hazard, *Geol. Soc. Am. Bull.*, 95, 686-700, 1984.
- Allen, C.R., San Andreas fault zone in San Gorgonio Pass, southern California, *Geol. Soc. Am. Bull.*, 68, 315-350, 1957.
- Armijo, R., B. Meyer, and A. Hubert, Westward propagation of the North Anatolian fault into the northern Aegean: Timing and kinematics, *Geology*, *27*, 267-270, 1999.
- Aspden, J.A., W. Kartawa, D.T. Aldiss, A. Djunuddin, R. Whandoyo, D. Diatma, M.C.G. Clarke, and H. Harahap, The geology of the Padangsidempuan and Sibolga Quadrangle, Sumatra, report Geol. Res. and Dev. Centr., Bandung, Indonesia, 1982.
- Barka, A., The North Anatolian fault zone, Ann. Tectonicae, 6, 164-195, 1992.
- Bellier, O., and M. Sebrier, Relationship between tectonism and volcanism along the Great Sumatran fault zone deduced by SPOT image analyses, *Tectonophysics*, *233*, 215-231, 1994.
- Bellier, O., and M. Sebrier, Is the slip rate variation on the Great Sumatran fault accommodated by fore-arc stretching? *Geophys. Res. Lett.*, 22 1969-1972, 1995.
- Bellier, O., M. Sebrier, S. Pramumidjojo, T. Beaudouin, H. Harjono, I. Bahar, and O. Forni, Paleoseismicity and seismic hazard along the Great Sumatran fault (Indonesia), *J. Geodyn.*, 24, 169-183, 1997.
- Bellier, O., H. Bellon, M. Sebrier, Sutanto, and R. Maury, K-Ar age of the Ranau Tuffs: Implications for the Ranau caldera emplacement and slip-partitioning in Sumatra (Indonesia), *Tectonophysics*, *312*, 347-359, 1999.
- Bennett, J. D., et al., Geologic map of the Banda Aceh quadrangle, Sumatra, Geol. Res. and Dev. Cent., Bandung, Indonesia, 1981.
- Berlage, H., Jr., De aardbeving in zuid Sumatra van 25 Juni 1933: Waarremingen in het epicentrale gebied, *Natuurwet. Tijdschr. Ned. Indie, 94*, 15-36,1934.

- Cameron, N., M. Clarke, D. Aldiss, J. Aspden, and A. Djunuddin, The geological evolution of northern Sumatra, paper presented at Proc. 9th Indonesian Petroleum Association Annual Convention, Jakarta, 1980.
- Cameron, N., et al., Geology of the Takengon quadrangle, Sumatra, report Geol. Res. and Dev. Cent., Bandung, Indonesia, 1983.
- Chesner, C.A., W. I. Rose, A. Deino, R. Drake, and J. A. Westgate, Eruptive history of Earth's largest Quaternary caldera (Toba, Indonesia) clarified, *Geology*, *19*, 200-203, 1991.
- Curray, J., D. Moore, L. Lawver, F. Emmel, R. Raitt, M. Henry, and R. Kieckhefer, Tectonics of the Andaman Sea and Burma, *AAPG Mem.*, *29*, 189-198, 1979.
- Deplus, C., et al., Direct evidence of active deformation in the eastern Indian oceanic plate, *Geology*, 26, 131-134, 1998.
- Detourbet, C., O. Bellier, and M. Sebrier, La caldera volcanique de Toba et le systeme de faille de Sumatra (Indonesia) vue par SPOT, *C. R. Acad. Sci., Ser. II, 316*, 1439-1445, 1993.
- Diament, M., H. Harjono, K. Karta, C. Deplus, D. Dahrin, M. T. Zen Jr., M. Gerard, O. Lassal, A. Martin, and J. Malod, Mentawai fault zone off Sumatra: A new key to the geodynamics of western Indonesia, *Geology*, 20, 259-262, 1992.
- Durham, J., Oeloe Aer fault zone, Sumatra, Bull. Am. Assoc. Pet Geol., 24, 359-362, 1940.
- Engdahl, E., R. van der Hilst, and R. Buland, Global teleseismic earthquake relocation with improved travel times and procedures for depth determination: *Seismol. Soc. Am. Bull.* 88, 722-743, 1998.
- Fauzi, R. McCaffrey, D. Wark, Sunaryo, and P. Y-PrihHaryadi, Lateral variation in slab orientation beneath Toba caldera, northern Sumatra, *Geophys.Res.Lett.*, *23*, 443-446, 1996.
- Fitch, T. J., Plate convergence, transcurrent faults, and internal deformation adjacent to southeast Asia and the western Pacific, *J. Geophys. Res.*, *77*, 4432-4462, 1972.
- Genrich, J., Y. Bock, R. McCaffrey, L. Prawirodirdjo, C. Stevens, S. S. O.Puntodewo, C. Subarya and S. Wdowinski, Distribution of slip at the northern Sumatra fault system, *J. Geophys. Res.*, this issue.
- Gordon, R., C. Demets, and D. Argus, Kinematic constraints on distributed lithospheric deformation in the Equatorial Indian ocean from present motion between the Australian and Indian plates: *Tectonics 9*, 409-422, 1990.

- Harbury, N., and H. Kalagher, The sunda outer-arc ridge, north Sumatra, Indonesia, *J. Southeast Asian Earth Sci.*, 6 (3/4), 463-476, 1991.
- Harjono, H., M. Diament, J. Dubois, and M. Larue, Seismicity of the Sunda Strait: Evidence for crustal extension and volcanological implicationa, *Tectonics*, *10*, 17-30, 1991.
- Harris, R., and S. Day, Dynamics of fault interaction: Parallel strike-slip faults, *J. Geophys. Res.*, 98, 4461-4472, 1993.
- Harris, R., R. Archuleta, and S. Day, Fault steps and the dynamic rupture process: 2-D numerical simulations of a spontaneously propagating shear fracture, *Geophys. Res. Lett.*, 18, 893-896, 1991.
- Huchon, P., and X. Le Pichon, Sunda Strait and central Sumatra fault, *Geology*, 12, 668-672, 1984.
- Jarrard, R., Terrane motion by strike-slip faulting of fore-arc slivers, *Geology*, 14, 780-783, 1986.
- Jennings, C., and G. Saucedo, Fault activity map of California and adjacent areas with locations and ages of recent volcanic eruptions, Calif. Div. of Mines and Geol., Sacramento, 1994.
- Karig, D., S. Suparka, G. Moore, and P. Hehanussa, Structure and Cenozoic evolution of the Sunda arc in the central Sumatra region, *AAPG Mem.*, *29*, 223-237, 1979.
- Karig, D., M. Lawrence, G. Moore, and J. Curray, Structural framework of the fore-arc basin, NW Sumatra, *J. Geol. Soc. of London, 137*, 77-91, 1980.
- Katili, J., and F. Hehuwat, On the occurence of large transcurrent faults in Sumatra, Indonesia, *J. Geosci., Osaka City Univ., 10*, 5-17, 1967.
- Kraeff, A., The earthquake of the Tes region, Benkulen residency on March 15th, *Berita Gunung Berapi*, 1, 40-56, 1952.
- Larson, K., J. T. Freymueller, and S. Philipsen, Global plate velocities from the Global Positioning System, *J. Geophys. Res.*, *102*, 9961-9981, 1997.
- Lassal, O., P. Huchon, and H. Harjono, Extension crustale dans le detroit de la Sonde (Indonesie): Donnees de la sismique reflexion (campagne Krakatau), *Geophysics*, 309(2), 205-212, 1989.
- Lawson, A., et al., *The California Earthquake of April 18, 1906, Report of the State Earthquake Investigation Commission*, 451 pp., Carnegie Ins. of Washington, Washington, D.C., 1908.

- Le Pichon, X., and J. C. Sibuet, Passive margins: A model of formation, *J. Geophys. Res.*, 86, 3708-3720, 1981.
- Matson, R., and G. Moore, Structural influences on Neogene subsidence in the central Sumatra fore-arc basin, in *Geology and Geophysics of Continental Margins*, edited by J. Watkins, F. Zhiqiang, and K. McMillen, pp. 157-181, Am. Assoc. of Pet. Geol., Tulsa, Okla., 1992.
- McCaffrey, R., Slip vectors and stretching of the Sumatran fore arc, *Geology*, 19, 881-884, 1991.
- McCaffrey, R., Oblique plate convergence, slip vectors, and forearc deformation, *J. Geophys. Res.*, *97*, 8905-8915, 1992.
- McCaffrey, R., P. Zwick, Y. Bock, L. Prawirodirdjo, J. Genrich, C. W. Stevens, S. S. O. Puntodewo, and C. Subarya, Strain partitioning during oblique plate convergence in northern Sumatra: Geodetic and seismologic constraints and numerical modeling, *J. Geophys. Res.*, this issue.
- McCarthy, A., and C. Elders, Cenozoic deformation in Sumatra: Oblique subduction and the development of the Sumatran fault system, in *Petroleum Geology of Southeast Asia*, edited by A. J. Fraser, S. J. Matthews, and R. W. Murphy, *Geol. Soc. Spec. Publ.*, *126*, 355-363, 1997.
- McKenzie, D., Some remarks on the development of sedimentary basins, *Earth Planet. Sci. Lett.*, 40, 25-32, 1978.
- Molnar, P., and P. Tapponnier, Cenozoic tectonics of Asia: Effects of a continental collision, *Science*, *189*, 419-426, 1975.
- Muller, J. J. A., De verplaasting van eenige traiangulatie pilaren in de residentie Tapanuli (Sumatra) tengevolge de aardbeving van 17 Mei 1892, *Natuurwet. Tijdscht. Ned. Indie.,* 54, 299-307, 1895.
- Natawidjaja, D., Quantitative geological assessments of Liwa earthquake 1994, paper presented at Annual Convention, Indonesian Assoc. of Geophys. (HAGI), Bandung, Indonesia, 1994.
- Natawidjaja, D., Y. Kumoro, and J. Suprijanto, Gempa bumi tektonik di daerah Bukit tinggi Muaralabuh: hubungan segmentasi sesar aktif dengan gempa bumi tahun 1926 dan 1943, paper presented at Annual Convention, Geoteknologi-LIPI, Bandung, Indonesia, 1995.

- Newcomb, K. R, and W. R. McCann, Seismic history and seismotectonics of the Sunda Arc, *J. Geophys. Res.*, *92*, 421-439, 1987.
- Nishimura, S., Re-examination of the fission-track ages of volcanic ashes and ignimbrites in Sumatra, in *Physical Geology of Indonesian Island Arcs*, edited by S. Nishimura, pp. 148-153, Kyoto Univ., Kyoto, Japan, 1980.
- Nishimura, S., J. Nisida, T. Yokoyama, and F. Hehuwat, Neotectonics of the Strait of Sunda, Indonesia, *J. Southeast Asia Earth Sci.*, *1*, 81-91, 1986.
- Pacheco, J., and L. Sykes, Seismic moment catalog of large, shallow earthquakes, 1900-1989, *Bull. Seismol. Soc. Am..*, 82, 1306-1349, 1992.
- Page, B. G. N., J. D. Bennett, N. R. Cameron, D. M. Bridge, D. H. Jeffery, W. Keats, and J. Thaib, A review of the main structural and magmatic features of northern Sumatra, *J. Geol. Soc. London*, *136*, 569-579, 1979.
- Peter, G., L. Weeks, and R. Burns, A reconnaissance geophysical survey in the Andaman Sea and across the Andaman-Nicobar Island area, *J. Geophys. Res.*, 71, 495-509, 1966.
- Pramumijoyo, S., and M. Sebrier, Neogene and Quaternary fault kinematics around the Sunda Strait area, Indonesia, *J. Southeast Asian Earth Sci.*, *6*, 137-145, 1991.
- Prawirodirdjo, L., A geodetic study of Sumatra and the Indonesian region: Kinematics and crustal deformation from GPS and triangulation, Ph.D. Thesis, Univ. of Calif., San Diego, 2000.
- Prawirodirdjo, L. et al., Geodetic observations of interseismic strain segmentation at the Sumatra subduction zone: *Geophys. Res. Lett.* 24, 2601-2604, 1997.
- Prawirodirdjo, L., Y. Bock, J. Genrich, S. S. O. Puntodewo, J. Rais, C. Subarya, and S. Sutisna, One century of tectonic deformation along the Sumatra fault from triangulation and Global Positioning System surveys, *J. Geophys. Res.*, this issue.
- Prentice, C. Earthquake Geology of the Northern San Andreas Fault near Point Arena, California, Ph.D. thesis, California Institute of Technology, Pasadena, 1988.
- Reid, H., Sudden earth movements in Sumatra in 1892, *Bull. Seismol. Soc. of Am. Bulletin, 3*, 72-79, 1913.
- Research Group for Active Faults, *Main Active Faults in and Around Japan*, University of Tokyo Press, Tokyo, 1980.

- Rock, N. M. S., D. T. Aldiss, J. A. Aspden, M. C. G. Clarke, A. Djunuddin, W. Kartawa, Miswar, S. J. Thompson, and R. Whandoyo, The geology of the Lubuksikaping quadrangle, Sumatra, report, 60 pp. and map, Geol. Res. and Dev. Cent., Bandung, Indonesia, 1983.
- Samuel, M. A., and N. A. Harbury, The Mentawai fault zone and deformation of the Sumatran forearc in the Nias area, in *Tectonic Evolution of Southeast Asia*, edited by R. Hall and D. J. Blundell, *Geol. Soc. Spec. Publ. 106*, 337-351, 1996.
- Samuel, M., N. Harbury, A. Bakri, F. Banner, and L. Hartono, A new stratigraphy for the islands of the Sumatran forearc, Indonesia, *J. Asian Earth Sci.*, *15*, 339-380, 1997.
- Saroglu, F., O. Emre, and I. Kuscu, Active fault map of Turkey, Gen. Dir. of Miner. Res. and Explor. (MTA), Ankara, Turkey, 1992.
- Sieh, K., Slip along the San Andreas fault associated with the great 1857 earthquake, *Bull. Seismol. Soc. Am.*, 68, 1421-1428, 1978.
- Sieh, K., Y. Bock, and J. Rais, Neotectonic and paleoseismic studies in west and north Sumatra, *Eos Trans. AGU* 72(44), Fall Meet. Suppl., 460, 1991.
- Sieh, K., J. Zachariasen, Y. Bock, L. Edwards, F. Taylor, and P. Gans, Active tectonics of Sumatra, *Geol. Soc. Am. Abstr. Programs*, 26, A-382, 1994.
- Smith, W. H. F., and D. T. Sandwell, Global seafloor topography from satellite altimetry and ship depth soundings, *Science*, *277*, 1956-1962, 1997.
- Soetarjo, U., E. Arnold, R. Soetadi, S. Ismail, and E. Kertapati, *Ser. Seismol.*, vol. 5, 199 pp., *Indonesia*, Southeast Asian Assoc. of Seismol. and Earthquake Eng., (SEASEE), Series Editor and Program Coordinator: E.P. Arnold, USGS Denver, Colo., 1985.
- Stehn, C., Explosionen des Pematang Bata in der Suoh-senke (sud Sumatra) im jahre 1933, *Natuuk. Tijdschr. Ned. Indie, 94*, 46-68, 1934.
- Tapponnier, P., and P. Molnar, Active faulting and tectonics in China, *J. Geophys. Res.*, 82, 2905-2930, 1977.
- Tikoff, B., Sunda-style tectonics and magmatic arc processes, *Eos Trans. AGU*, 79(45), Fall Meet. Suppl., F222, 1998.
- Tjia, H., Tectonic depression along the transcurrent Sumatra fault zone, *Geol. Indonesia*, 4(1), 13-27, 1977.

- Tregoning, P., F. K. Brunner, Y. Bock, S. S. O. Puntodewo, R. McCaffrey, J. F. Genrich, E. Calais, J. Rais, and C. Subarya, First geodetic measurement of convergence across the Java trench, *Geophys. Res. Lett.*, *21*, 2135-2138, 1994.
- Untung, M., N. Buyung, E. Kertapati, Undang, and C. Allen, Rupture along the Great Sumatran fault, Indonesia, during the earthquakes of 1926 and 1943, *Bull. Seismol. Soc. Am.*, 75, 313-317, 1985.
- Van Bemmelen, R., *The Geology of Indonesia*, 732 pp., Gov. Print. Off., The Hague, Netherlands, 1949.
- Visser, S., Inland and submarine epicentra of Sumatra and Java earthquakes: Koninklijk Magnetisch en *Meteorologisch Observatorium te Batavia*, *9*, 1-14, 1922.
- Visser, S., De aardbevingen in de Padangse Bovalanden, *Natuurwet. Tijdschr. Ned. Indie.*, 87, 36-71, 1927.
- Weeks, L., R. Harbison, and G. Peter, Island arc system in the Andaman Sea, *Am. Assoc. Pet. Geol. Bull.*, *51*, 1803-1815,1967.
- Westerveld, J., Eruptions of acid pumice tuffs and related phenomena along the Great Sumatran fault-trough system, in *Proceedings of the Pacific Science Congress*, vol. 2, Pacific Science Congress, New Zealand, 1953.
- Widiwijayanti, C., J. Deverchere, R. Louat, H. Harjono, M. Diament, and D. Hidayat, Analysis of the aftershock sequence of the M_w6.8 Liwa earthquake, Indonesia, *Geophys. Res. Lett.*, 23, 3051-3054, 1996.
- Yeats, R., K. Sieh, and C. Allen, *The Geology of Earthquakes*, 568 pp., Oxford Univ. Press, New York, 1997.
- Zachariasen, J., and K. Sieh, The transfer of slip between two en echelon strike-slip faults: A case study from the 1992 Landers earthquake, southern California, *J. Geophys. Res.*, 100, 15,281-15,301, 1995.
- Zachariasen, J., K. Sieh, F. W. Taylor, R. L. Edwards, and W. S. Hantoro, Submergence and uplift associated with the giant 1833 Sumatran subduction earthquake: Evidence from coral microatolls, *J. Geophys. Res.*, 104, 895-919, 1999.
- Zen, M., Jr., D. Dahrin, M. Diament, H. Harjono, K. Karta, C. Deplus, M. Gerard, O. Lassal, J. Malod, and A. Martin, Mantawai-90 cruise result: The Sumatra oblique subduction and

strike slip fault zones, in *Geodynamic Processes in the Forearc Sliver Plate and General Topics*, edited by H. Prasetyo, pp. 46, Indonesian Assoc. of Geophys., Bandung, 1991.

Table 2.1. The Sumatran Fault's Major Segments

			•)				
o O	Segment	Latitude	Length, km	Large Historical Earthquakes, year(M)	Nature of Southern Termination	Geomorphic Features	Distance From Deformatio n Front, km	Depth to Benioff Zone, km
_	Sunda	8.75°S –5.9°S	~150	No record	submarine forearc	submarine graben	115-220	up to \sim 50
2	Semangko	-5.9°S - 5.25°S	65	1908	southern tip of Semangko Peninsula	east facing scarp	220-270	50-100
3	Kumering	5.3°S – 4.35°S	150	$1933 (M_s=7.5),$ $1994 (M_w=7.0)$	dilatational step over, 6 km width	Suoh geothermal valley	300	100-120
4	Manna	4.35°S – 3.8°S	85	1893	contractional bend, 17º deflection	mountainous range on east side of the fault, associated with possible folds and thrusts	275	120
2	Musi	3.65°S – 3.25°S	70	$1979 \text{ (M}_s=6.6)$	dilatational step over, 5.6 km width	valley /depression	260	115
9	Ketaun	3.35°S- 2.75°S	85	$1943 \text{ (M}_s=7.3), 1952 \text{ (M}_s=6.8)$	dilatational step over, 5–18.5 km width	depression valley and Kaba volcano	271	110-125
7	Dikit	2.75°S- 2.3°S	09	no record	complex fault discontinuity			
∞	Siulak	2.25°S– 1.7°S	70	$1909 \text{ (M}_s=7.6), 1995 $ (M _w =7.0)	dilatational step over, 11 km width	Lake Kerinci and Kunyit volcano	266	120-130
6	Suliti	1.75°S- 1.0°S	95	$1943 \text{ (M}_{s}=7.4)$	4.5-km-wide dilatational step over	small depression, calderas and young volcanic cone	273	130
10	Sumani	1.0°S – 0.5 °S	09	1943 (M_s =7.6), 1926 (M_s ~7)	4.5-km-wide dilatational step over	Lake Diatas, calderas, and Talang volcano	293	130
11	Sianok	$0.7^{\circ}S - 0.1^{\circ}N$	06	1822, 1926 ($M_s \sim 7$)	4.5-km-wide dilatational step over	Lake Singkarak	302	135–145
12	Sumpur	0°- 0.3°N	35	no record	12-km-wide dilatational step over	wide depression associated with normal faults	308	165–175
13	Barumun	0.3°N – 1.2°N	125	no record	23-km-wide releasing bend	long (Sumpur) valley along the fault	294	125-170
14	Angkola	0.3°N – 1.8°N	160	$1892 (M_s=7.7)$	complex structure	mountainous ranges on both sides of the fault	290	135–155
15	Toru	1.2°N - 2.0°N	95	$1984 \text{ (M}_s=6.4), 1987 $ ($M_s=6.6$)	contractional bend	uplifted hill on the east side of the bend	294	125–155
16	Renun	2.0°N – 3.5°N	220	1916, 1921 (m_b =6.8) 1936 (M_s =7.2)	3-km-wide dilatational step over	Tarutung Valley	286	100–125
17	Tripa	3.4°N – 4.4°N	180	1990 (M_s =6?) 1997 (M_w =6?)	9-km-wide dilatational step over	Alas Valley	295	125–150
18	Aceh	4.4°N – 5.4°N	200	no record	3-km-wide contractional step over	mountainous range, associated with active thrusts	323	105–130
19	Seulimeu m	5.0°N-5.9°N	120	1964 (Ms=6.5)	4-km-wide releasing bend and dilational step over	Small depression on dilational stepover	323	125-140

Table 2.2. Selected Small Offsets Along the Sumatran Fault (From North to South)

			Comments
	River/Lake Name	Offset, m	
a	Aceh River	750-1000	offset of several streams that incised young volcanic deposits on the southwest flank of Seulawah Agam volcano
b	Toru River	1700-2100	excellent offset of several streams deeply cut into the 73,000 year old Toba Tuff
c	Angkola River	1200-1400	offsets of a few streams on the northeast flank of the Sorik Merapi volcano
d	Angkola River (Ringkit branch)	1000-1300	offsets of several tributaries of the Angkola River
e	Sianok River	700	excellent offsets of several crossings of the Sianok River, deeply incised into the 60,000 year old Maninjau Tuff
f	Anai River	600	offsets of several channels on the southwest flank of Merapi volcano
g	Lake Dipatiampat	500	offset of north sidewall of the caldera lake
h	Musi River	700	excellent offsets of tributaries to the Musi River, on the southwest flank of Kaba volcano
i	Manna River	2400	offset of Air Kiri and Air Kanan (Plate 2) which drains an eroded volcanic edifice
j 	Werkuk River (Menjadi, Pisai, Rebu branches)	300	offsets of three channels that are deeply incised into the thick, Quaternary Ranau Tuff

Table 2.3. Proposed Large Offsets Across the Sumatran Fault

	Features	Offset,	Quality	Description
		km		
a	Quaternary folds	20	fairly good	offset of a few fold axes which deformed Pliocene, Miocene, and Oligocene strata
b	Meureubo River	21	excellent	dextral offset is clearly indicated by the deflection of the trunk channel
c	Tripa River	21	excellent	dextral offset is clearly indicated by the deflection of the trunk channel
d	Singkarak graben	20-22	N/A	based on an interpretation of the graben opening (Fig. 2.7)
e	Seblat River	17	good	clearly shown by a sharp deflection of the main channel
f	Ketahun River	23	good	clearly shown by a sharp deflection of the main channel

Chapter 3. Paleogeodetic records from microatolls above the central Sumatran subduction zone

3.1. Introduction

3.1.1. Motivation

Understanding earthquakes and forecasting future major destructive events is largely hampered by limited data on how seismic strain accumulates and is released in an earthquake cycle [Zachariasen et al., 1999]. The validity and utility of theoretical models can only be rigorously examined if long and detailed records of large earthquakes are available. Unfortunately, well-documented seismic histories that extend through more than one earthquake cycle are uncommon. Thatcher [1989], for example, found only twelve large fault segments in the circum-pacific region for which the record was relatively complete for the past single earthquake cycle. For subduction earthquakes, in particular, evidence is generally sparser because the seismic sources are under water.

Moreover, even in some areas where the history of coseismic deformation is relatively well documented, such as in Japan [Ando, 1975; Kanamori, 1973] data on slow strain accumulation during the interseismic periods is largely lacking. Because, unlike earthquake events, which produce very large signals in a very short timespan, the interseismic periods are characterized by much smaller deformation that accrues over tens, hundreds, or even thousands of years. Thus, to gather evidence of this slow deformation we need a very stable and long-lived instrument that is able to monitor it continuously.

This challenge has motivated us to use massive corals or "microatolls" that are abundant in the Sumatran Equatorial waters. Coral microatolls not only record the magnitude of vertical deformation associated with earthquakes (paleoseismic data), but also continuously track the slow aseismic deformation during the intervals between earthquakes (paleogeodetic data) [Sieh et al., 1999; Zachariasen, 1998b; Zachariasen et al., 2000]. Furthermore, the islands off the west coast of Sumatra, only 70 to 150 km off the trench axis, are ideally located to record surface deformation related to seismic and aseismic subduction. Large extents of the coastlines of these islands are fringed by coral reefs, in which massive corals flourish.

Most of our coral sites are on these forearc islands. The islands, composed primarily of deformed accretionary-prism sediments and coralline limestone, are the subaerial expression of the crest of the outerarc rise [Budhitrisna and Andi Mangga, 1990]. All of the Mid-Holocene microatolls found in the islands of Pagai, Siberut, Tanamasa, and Tanabala were less than 2 m above their modern counterparts ([Zachariasen et al., 1999], this chapter). Model of Holocene global isostatic adjustment to deglaciation suggests that sea level in this area reached a maximum of about 2 to 3 m above the present level about 5,000 years ago [Peltier and Tushingham, 1991; Zachariasen et al., 1999]. Thus, we suggest that there has been little, if any, net vertical displacement in the Holocene. In other words, most of the subduction deformations are being accommodated by the elastic deformation of earthquake cycles.

3.1.2. Sumatran active subduction

The Sumatran active plate margin sits over the subducting Australian oceanic plate that obliquely converges about 50 to 70 mm/yr (Fig. 1.1). The plate convergence largely partitions into the frontal component that is accommodated by slip on the subduction interface, and the right-lateral strike-slip component that is mostly accommodated by the 1600 km onland Sumatran fault ([Fitch, 1972; Katili and Hehuwat, 1967; McCaffrey, 1991; Sieh and Natawidjaja, 2000; Sieh et al., 2000], Chapter 2).

The Sumatran subduction zone accommodates the largest part of the plate convergence, and has produced numerous very large earthquakes in the past two centuries (Fig. 1.2). Two very large earthquakes, the 1833 event (M~9) and the 1861 event (M~8.5), dominate the historical seismicity of the subduction interface. Historical records of shaking and tsunamis suggest that these two events involved rupture of all or most of the interface between about 2^oN and 5^oS [Newcomb and McCann, 1987]. In the Equatorial region, the principal strain release for the last century is the M_w7.7–1935 historical earthquake (Fig. 1.2) [Rivera et al., 2002]. This earthquake also involved rupture of the subduction interface, but sandwiched in between the locations of the 1861 and the 1833 ruptures. Recently, in June 2000, the Bengkulu earthquake (M_w7.9) occurred near the southern end of the 1833 rupture. Abercrombie et al. [submitted 2001] have found that this recent event was complex: it involved rupture on the subduction interface, but was also coupled with a strike-slip fault within the down-going oceanic slab. This is consistent with activity on N-S oceanic fractures to the west [Deplus et al., 1998].

Recent upper crustal movements have been documented by the campaign-style GPS measurements that were obtained between 1989 and 1994 [*Prawirodirdjo*, 2000; *Prawirodirdjo et al.*, 1999]. These show that the large islands south of the Equator, in the area of the 1833 source rupture, moved in the direction of the relative plate-motion vector (Fig. 3.1). Models of these motions indicate that the subduction interface beneath these islands is currently fully locked [*Prawirodirdjo et al.*, 1997]. Thus, this portion of the subduction interface is efficiently accumulating seismic strain for the next major earthquake. *Zachariasen et al.* [1999] have suggested, based on sparse evidence from microatolls, that the recurrence interval of the 1833-like events is about 230 years. By contrast, those stations on the islands north of the Equator, above the 1935 source, experienced motions nearly parallel to the trench. These surface movements indicate significant aseismic slip on the interface. Data from our coral "instruments" are able to address both the stationary and variability of the seismic and aseismic behavior of the subduction interface through the course of the earthquake cycle.

3.1.2.1. Seismicity of the central Sumatran subduction during the 20th century

In this chapter and in the following chapter, we will focus on the Equatorial region of the Sumatran subduction zone, in which the 1935 event occurred. This part of the subduction interface is unique. From the point of view of seismicity, it is in the intervening region between the 1833 and 1861 seismic sources. In a tectonic framework, this central region is a distinct middle tectonic domain that separates the simpler tectonic domain to the south and the more complex domain to the north [Sieh and Natawidjaja, 2000].

The past century's seismicity in the region is shown in Figure 3.3. Prior to the 1935 event, almost none of the earthquakes had been recorded by teleseismic networks. For about 25 years after the 1935 event, the region appears to have been seismically quiescent. However, the lack of recorded seismicity before 1960 could simply reflect the lack of a modern global seismic network. During the 1960s, most of the small earthquakes clustered in a period from 1961 to 1962, in which we found paleogeodetic evidence for a very large "silent earthquake." During the 1970s, 1980s, and 1990s the occurrence of recorded small earthquakes increased slightly. A large earthquake also occurred during this period (1984, M_w7.1).

3.1.2.2. Coral microatolls of the central Sumatran subduction

In 1997, 1999, and 2000, we surveyed and collected 27 coral slabs from 15 sites in this Equatorial region (Fig. 3.2). Many of the slabs contain records of sea level for the past half-century. Eight of the bigger slabs enable reconstruction of the sea level history for almost the entire 20th century. Together, this paleogeodetic data suite illuminates the vertical deformation pattern of the 1935 event, as well as the pattern of continuous slow deformation before and after the event.

Our coral paleoseismic data for the vertical deformations associated with the 1935 event present a classical example of the upper crustal deformations that are produced by the seismic rupture on a subduction interface. The Tanabala Island that is closer to the trench rose by 90 cm. The eastern part of the region was sunk by as much as 35 cm. Moreover, our coral paleogeodetic data reveals that in the western part, where coseismic emergence occurred, slow submergence occurred during the decades before and after the

event. In the eastern region, which experienced coseismic submergence, interseismic emergence occurred, slowly raising the islands. Furthermore, the data reveals that the interseismic emergence and submergence rates have varied both temporally and spatially. This rich data set allows us to model the kinematics and other properties of the subduction interface in a fashion that can explain the observed vertical deformation history.

Among the most interesting phenomena we have discovered in the coral record is the occurrence of a large aseismic event or "silent earthquake" in 1962, 27 years after the 1935 event. This is especially interesting in the light of recent modern instrumental documentation of rapid aseismic events on subduction interfaces, such as in Cascadia [Dragert et al., 2001; Miller et al., 2002], South America [Lowry et al., 2001], and Japan [Heki et al., 1997; Hirose et al., 1999].

3.2. Coral microatolls as paleoseismic and paleogeodetic instruments

3.2.1. General

Microatolls act as stable, long-lived, natural tape recorders of sea-level changes with sensitivity down to about 1cm [Sieh et al., 1999; Zachariasen et al., 1999; Zachariasen et al., 2000]. Microatolls are superior to man-made tide gauges or geodetic networks in that they do not require us to emplace them to start the clock. Thus they can span much longer time periods, including pre-historic time. Furthermore, the microatolls

are more accessible than most paleoseismic sources and the raw data they contain can be acquired relatively easy.

Microatolls grow in the intertidal zones along the beaches. The upward growth of *corals heads* is limited by the lowest tide level, above which exposure cause coral death [Sieh et al., 1999; Taylor et al., 1987; Zachariasen et al., 1999; Zachariasen et al., 2000]. This maximum coral growth is termed "the highest level of survival" or "HLS" [Sieh et al., 1999; Taylor et al., 1987; Zachariasen et al., 1999; Zachariasen et al., 2000]. Therefore, fluctuations in sea level or HLS are accurately imprinted on the morphology and stratigraphy of microatolls. In west Sumatra, the HLS history recovered from corals is predominantly associated with the upper crustal deformations above the subduction interface. Thus microatolls serve as paleoseismic and paleogeodetic recorders [Sieh et al., 1999; Taylor et al., 1987; Zachariasen et al., 1999; Zachariasen et al., 2000].

Coral growth typically shows annual pairs of dark and light bands. This annual banding is seasonal density variations in coral skeletals caused by variations in sea temperature, rainfall, and other factors [Scoffin and Stoddart, 1978; Taylor et al., 1987; Zachariasen et al., 1999; Zachariasen et al., 2000]. The light bands (lower density cells) occurred during the rainy seasons (September to March), and the dark bands (higher density cells) are associated with the dry season (April – August). These annual bands are similar to tree rings in that they provide a yearly record of coral growth throughout the life of the coral, and thus provide an excellent time-series for constructing the sealevel history [Sieh et al., 1999; Taylor et al., 1987; Zachariasen et al., 1999; Zachariasen et al., 2000]. The annual bands are sometime visible to the naked eye, but are commonly

more pronounced in X-ray images of the coral thin slabs [Sieh et al., 1999; Woodroffe and McLean, 1990; Zachariasen et al., 1999; Zachariasen et al., 2000].

Other geological recorders of sea level that have been used in the past include coastal terraces [Bloom and Yonekura, 1985; Ota et al., 1990; Pirazzoli et al., 1993], eroded marine notches [e.g. Hantoro et al., 1994], and coral reefs [Chappell, 1983; Ota and Chappell, 1999; Ota et al., 1993; Ota and Omura, 1992; Pirazzoli et al., 1991]. These have helped to constrain long-term climatically induced sea-level changes, cumulative tectonic uplift, and sometimes the records of past earthquake, but not the details of deformation throughout the entire earthquake cycle. As geologic tide gauges, none of these show the promise of microatolls, which have internal age control and growth characteristics that are governed by sea level [Edwards et al., 1988; Taylor et al., 1987; Woodroffe and McLean, 1990; Zachariasen, 1998b; Zachariasen et al., 1999; Zachariasen et al., 2000].

3.2.2. The synthetic microatoll

To help understanding the natural response of our coral instrument, our collaborator, Steve Ward in the University of California at Santa Cruz, developed a computer program that simulates the natural process of coral growth. It is able to reproduce the shape of coral microatolls in various tectonic environments by incorporating the effect of tectonic submergence and emergence into the simulation [Fig. 3.4 a, b, c, d].

Based on the fact that coral growth is limited by annual lowest tide level or HLS, and any vertical motion will superimpose on the annual HLS fluctuation, we can define HLS as a function of time as in the following equation:

HLS(t) = Long-term tectonic rate (t) + Annual HLS Fluctuation (t) + Sum (coseismic steps)

Annual HLS fluctuation is simulated by a random Gaussian variable of zero mean and with a fixed standard deviation of 2 cm. This standard deviation value is estimated from the real HLS fluctuation recorded in the natural coral microatolls.

The virtual microatoll is programmed to grow at a fixed rate of 1 cm/yr. The program simulation will track the x (year) and z (elevation/HLS) position of every living coral in the outermost layers. When the simulation steps ahead one year and selects the next HLS for that year, it then scans all living coral surface position and *kills* any coral growth above the selected HLS. Thus, only coral bands that are below the HLS will survive and give rise to subsequent next growth bands.

The computer simulation image in Figure 3.4a demonstrates that coral heads maturing in a submerging area develop "cup-shape" morphology, because its living perimeter grows to a level that is higher than the interior, already dead coral bands. If the submergence is sudden, then the microatoll develops lower and upper flat surfaces, separated by a steep step representing the unrestricted growth of coral in the aftermath of the submergence (Fig. 3.4b). A coral head located in an emerging environment exhibits a conical shape because of the progressive fall of the upper growth limit as the coral expands outward (Fig. 3.4c). If the emergence is sudden, then the microatoll develops a "hat-shape" morphology (Fig. 3.4d). The hat "bowl" or elevated central head represents

the continued coral growth for the period before the emergence event. The hat "brim" represents the continued growth for decades after the event. The step from top of the bowl to the brim is a measure of the vertical displacement during the event.

3.3. Method

We surveyed the 1935-event region in mid-1997, 1999, and 2000. During our visit in 1997, abundant modern coral heads were still alive and healthy. The dead coral surfaces in the interior of the microatolls were ornamented by the glorious bright purple or brown tissues of the living coral around their exteriors. When we revisited the sites in mid-1999, most of these heads except the ones in Bendera had died. This massive coral mortality is related to the severe *El-Nino Southern Oscillations (ENSO)* and *Indian Ocean Dipole (IOD)* climate in 1997-98 [e.g. *Saji et al.*, 1999]. No detailed study has been done to ascertain why the corals did not survive. According to our interviews with local people, however, the coral reefs appear to have been killed by massive attacks of the red tides, a blooming of *phytoplankton* [*Indrawadi and Efendi*, 1999]. Certain species of this *phytoplankton* are poisonous.

Our survey at the site involved mapping the intertidal reef, documenting the height, shape and dimensions of the coral heads, and collecting slab samples from heads that were representative of the population of the area. We surveyed the site combining a hand-held GPS that has an accuracy of about 10 meters with a very accurate geodetic surveying instrument (an electronic total station) that has an accuracy of a few millimeters or less. To collect the slab samples we utilized a hydraulic chainsaw apparatus designed for underwater use. We installed and surveyed the nails on the upper

surfaces of the sampled microatolls prior to the cutting and the removal of the slabs, so that we could later determine the absolute horizontal level of the slab. In a few sites, with the collaboration of our colleagues at Australian National University (ANU), we also took drill-cores. The primary purpose of these cores was the investigation of paleoenvironments, but it also helped us constrain the ages of the fossil heads.

We selected sites where we found a population of coral heads that were representative of the entire surrounding area. We carefully looked for any evidence of land-locked beach pools. Our detailed topography surveys of the substrates told us if the water level behind the existing beach rampart did not correspond to that of the open sea surface. Thus we were able to ensure that the sea-level history we recovered from our samples was that of the open sea, not that of isolated beach pools [*Scoffin and Stoddart*, 1978]. We collected the samples from the heads that were undisturbed. A local disturbance to an individual head, such as tilting or subsidence, is relatively easy to recognize either by visual inspection of the head in the field or by its anomalous elevation relative to other surveyed points within and between heads in the site.

In the next section, we will describe the results of our survey at sites including detailed analysis of each slab sample. Site-by-site evaluation is important since the signal recorded at each individual site is unique to its position above the subduction interface. After we analyzed the sea level or HLS history of each individual site, we proceeded to the necessary data reduction and compilation. Finally, we will interpret the coral data to understand the deformation related to the subduction cycle.

We start at the site in the western section that is the closest to the trench axis, and then proceed to sites located farther from the trench.

3.4. Paleogeodetic and paleoseismic sites

3.4.1. Bendera site

3.4.1.1. Introduction

Our westernmost site, nearest the trench, is in Bendera Bay, near the western tip of Tanabala Island (Fig. 3.2). The site contains populations of both modern, living *Porites* microatolls and more ancient, dead *Porites* heads. Slabs from specimens representing each of these two populations enable construction of the site's HLS history for the entire 20th century.

Bendera Bay is 2.5 km wide and opens only to the north. Thus its shores are largely protected from the strong southwesterly swell of the dry season. Figure 3.5a is a map of the eastern shore of the bay. In general, the outer 100 meters of the shoreline consist of a shallow intertidal reef flat. Loose cobbles and small boulders that litter the outer part of the intertidal reef may well have been emplaced by a tsunami. Farther east, mangrove forest occupies much of the intertidal region. Where the mangrove forest is sparse, a beach berm is visible farther inland, beyond the mangroves.

The richest zone of dead, well-preserved heads within the intertidal zone occurs at the opening of a small embayment (Fig. 3.5a). The more protected part of the intertidal promontory that partially blocks the embayment is a graveyard of dead cup-shaped *Porites* microatolls (Fig. 3.5b). These heads stand up above the water during low low tides. Behind this promontory, and among the mangroves lining much of the small embayment, are numerous large, living *Porites* microatolls.

Well-preserved crests of the dead microatolls have nearly concordant elevations, about 55 cm above the elevations of the crests of the living microatolls (Fig. 3.6a). Thus it appears that an uplift of at least 55 cm has occurred. Head H18, which rests on the pebbly substrate between the principal fields of dead and living heads, exhibits both a raised, dead inner core and a living, lower partial rim (Fig. 3.6b). The hat-shape morphology of this head, though, is rather irregular and has been highly eroded. Thus, it suggests that the upper half-meter or so of this colony was raised above HLS, but the lower portions of the head remained below HLS. This lower perimeter of the head was thus able to survive and grow for many years after the uplift event, as described by *Taylor* [1987] and *Zachariasen* [2000].

3.4.1.2. Fossil heads

The family of dead microatolls resting on the promontory range in diameter from 150 to 250 cm and rise 20 to 40 cm above the substrate. We collected a slab sample of one of these heads, H1 (Fig. 3.5b). Unlike most of our slabs, this one spans the entire diameter of the microatoll (Fig. 3.7a). Therefore, it affords the unusual opportunity to compare the HLS history derived from two radiuses of the same head.

The annual bands in this head are exceptionally clear, so there are no ambiguities in the relative ages of bands. Figure 3.7b shows that the recovered bands grew over a

period of 50 years. In the cross section, the head appears to have begun as two separate, asymmetric heads. However, the microatoll is quite circular in plan view, so it may be that the two halves of the head seen in the cross section grew from an older raised rim, below the recovered part of the head.

U-Th analysis of a sample from the 29th band in from the perimeter of the microatoll yielded a date AD 1897±8 (Table 3.1). Thus, the outermost band formed AD 1926±8. This date is consistent with a date of death of 1935, the date of the largest earthquake in this region in the past 140 years [*Rivera et al.*, 2002]. We assumed this date for the outermost ring in assigning the band dates that appear on the cross section.

The cross section shows clearly a general submergence trend throughout the last 35 years of microatoll growth. The head (or heads) grew freely upward and outward from before the turn of the century until 1900. The first HLS impingement on the top of the head occurred in 1901. Upward growth then appears to have resumed until another impingement occurred at a higher level from about 1914 to 1925. Upward growth then resumed until an impingement at a still higher level in about 1931. Complete emergence killed the microatoll in 1935.

Figure 3.7c displays the HLS data graphically and allows us to compare and contrast the history revealed by each side of the head and the overgrowth in the middle of the head. The dots are levels where the tops of the coral bands were impinged by the annual lowest tides, and therefore represent HLSs. The bars represent the HLS surfaces that have been undergone a few centimeters of (bio) erosions. The smaller triangles are

elevations of the tops of the coral bands that freely grow outward and upward and that therefore represent the minimum elevation of HLSs.

Although all histories are similar, discrepancies of as much as 5 cm are apparent. For example, the HLS recorded on the right side of the head are up to 3 cm higher than those recorded on the left. This is either an indication of a true difference in the HLS across the top of the head or a significant bioerosion on the left side of the coral surface. Based on the shape of the surface across the head, we favor the latter. Intensive bioerosion commonly occurs on the dead central part of a microatoll and obscures the original shape of the old coral surfaces [e.g *Scoffin and Stoddart*, 1978; *Woodroffe and McLean*, 1990; *Zachariasen et al.*, 1999].

Although the apparent HLS elevations vary from side to side, HLS impingement dates and periods of free upward growths are nearly the same throughout the head. The left and right sides of the head yield least-squared average submergence rates of about 5.3 and 5.7 mm/yr, respectively (Fig. 3.7b). These values are calculated from all points except the values shown as small triangles when free upward growth was occurring. Combining all the HLS impingement we calculate an average submergence rate from 1901 to 1935 of about 5.4 mm/yr. If we calculate only the HLS where it is clearly uneroded, then the submergence rate from 1901 to 1935 is ~ 4.5 mm/yr. From here on, we will use the term "uneroded HLS" for the point where it is clearly preserved without erosion. In more detail, the submergence rate is probably not constant but a near stable condition from 1914 to 1925 in between two periods of much faster submergence. This may divide the history into three phases: 1901-1913 (fast submergence), 1914-1925 (near

stable), and 1927 - 1935 (fast submergence) and the submergence rates are \sim 9mm/yr, \sim 2.2 mm/yr, and \sim 10 mm/yr (using only the uneroded HLSs) (Fig. 3.7c).

3.4.1.3. Modern heads

Living microatolls in the field east of the promontory range in diameter from 130 to 350 cm at their crests and commonly rise about a meter above the substrate. In mid-2000, the living perimeter of these heads shows that these microatolls survived the devastating 1997 massive coral death event. But the living corallites died back to positions several centimeters below what would have been the natural HLS for 1997 had the environmental disaster not occurred.

Head H15 (Tb00A1), depicted in cross section in Figure 3.6b, is a good example of the morphology of these living heads. Its shape is typical for cup-shaped microatolls, with the lower inner flat filled partially with thin, complex younger overgrowths.

Figure 3.8a shows this cross section in more detail. This tracing of the slab collected from head H15 shows annual bands that formed from about 1927 to 2000. The errors shown for various annual bands indicate our estimate of potential error in counting back from the outer perimeter. The radiometric U-Th age of AD 1949 \pm 20 (Table 3.1) is consistent with our counting of the annual bands, but its large error renders the date of little value as a check on our counting.

Significant deaths of the upper part of the head appear in about 1936, the early-through late 1950s and early 1960s, about 1969, the mid-70s through 1980 and then several times in the 1990s, including early 1998. These impingements of HLS on the top

of the head are depicted as a function of time in Figure 3.8b. It appears that the head has been submerging throughout most of the past seven decades. A least-squared fit to HLS impingements yields rates of about 9 mm/yr during the 1930s, 40s and 50s and about 3 mm/yr submergence during the 1970s, 80s and 90s. Major emergences disrupted the general submergence in the mid-1930s, the early 1960s and about 1980.

3.4.1.4. Combining the records

Figure 3.9a and 3.9b shows HLS history of this site throughout the period spanned by both the fossil and the modern heads. The key observation is that there is an 85 cm difference in the elevation of the 1935 HLS levels between the two sampled heads. This is a measure of the emergence during the 1935 event. We use the term "event" as distinct from "earthquake." This distinction is important, because the coral record must reflect a longer period of time than the duration of the earthquake [Taylor et al., 1987]. It is more appropriate to consider this value to represent the net uplift that occurred over a few months.

Knowing from these heads the elevation of HLS prior to and just after the 1935 event, we can see that much of the promontory rose above HLS. Figure 3.5b shows that the pre-event HLS contour falls on the substrate near the foot of the modern sandy beach. The post-event HLS contour falls on the substrate 40 to 100 meters seaward of the modern beach. Thus it appears that almost the entirety of the reef flat rose above HLS in 1935 and the sea receded accordingly.

In addition to the magnitude of emergence during the 1935 event, the two HLS records reveal that the pre-seismic average rate of submergence (~5.4 mm/yr) is nearly

twice the current average rate (~2.8 mm/yr). Furthermore, it appears that the average rate of submergence in the 25 years after the 1935 event was higher still (~9.2 mm/yr).

This time-series may well be of use in understanding the accumulation and relief of strain in the Sumatran subduction zone. But it represents vertical deformation at only one point above the subduction interface. In the pages that follow, we describe several other sites where we have recovered records of the 1935 event and the decades before and after. Once we have described these time-series, we will be in a better position to model the source parameters of the 1935 event and the processes responsible for the preand post-seismic signals as well.

3.4.2. Badgugu site

3.4.2.1. Introduction

The broad bay on the southern flank of Tanabala Island contains two of our sites (Fig. 3.2). One is on the east flank and the other is on the west flank of a narrow northern arm of the bay. We present the eastern site first. This site has many "cowboy-hat" shaped heads that were living until the late 1990s and that record a large emergence in 1935. The brims of these hat-shaped microatolls consist of upward growth that has occurred in the years since 1935. The main body of these hats consists of growth that occurred prior to 1935. The site also contains at least one and perhaps two populations of older heads that sit at higher elevations within the intertidal zone.

The East Badgugu site encompasses a 500m wide, 800m long section of intertidal reef flat (Fig. 3.10). Its exposure to the southwest subjects much of its shoreline to very

large southwesterly waves during the dry season. Numerous loose coral blocks, ranging from a few tens of centimeters to 2 meters in diameter, litter the outer fringe of the reef in the southern part of the site. These blocks may well have been emplaced by tsunami, but we have not tested this hypothesis by determining ages for any of the blocks.

Modern, recently living heads reside predominantly along the outer margin of the intertidal flat (Fig. 3.10). Although many have small, living re-colonization, very few of these heads had living perimeters when we visited the site in July 2000. We assume that most of these heads died during the severe climatic episode of late 1997 and early 1998.

Older heads occur mostly in clusters farther inland and have upper surfaces that are higher than those of the modern heads. One population of older heads occurs in the southern sector. Head H1, depicted in cross section on Fig. 3.11a, is representative of this older population. These heads are thin and have rather flat pancake shapes. By contrast, the modern heads tend to be thicker, especially those that reside on the steeply sloping flank of the intertidal flat. Several heads in the northern sector of the site (e.g., H2, H3 and H4) also appear to be older than the modern heads, by virtue of their higher rims (Fig. 3.11b). We did not slab any of the older, higher heads, so the sea-level history they record remains uncertain.

3.4.2.2. Modern heads

Heads H6 and H7 are typical of many of the modern heads, in that they have *cowboy-hat* morphology (Fig. 3.11a). H6 and H7, in particular, root in deeper water, on the steep flank of a 20 m wide channel that breaches the reef flat in the middle of the site (Fig. 3.10). The cowboy-hat morphology is indicative of a large emergence in the course

of the growth of the microatoll. The summits of the brims of the cowboy hat are about 15 cm lower than the top of the hat and are about 30 cm lower than the tops of the older, pancake-shaped fossil heads (Fig. 3.11b). A large population of cowboy-hat microatolls in the northernmost sector of the site is probably correlative with H6 and H7 (Fig. 3.10), since their shapes and their elevations appear to be indistinguishable from those of H6 and H7.

HLS history from H6 and H7

A large slab collected from the flank of H7 provides an HLS history that spans most of the 20th century. Ages assigned by visual counting of the rings appear as dates written parallel to banding. To ensure accurate dating of the annual bands and HLS changes, we used the U-Th disequilibrium method [Edwards et al., 1987; Zachariasen et al., 1999]. The slab reveals that the brim of the hat represents growth of the microatoll after a large die down several decades prior to 2000 (Fig. 3.12a). This represents a sudden emergence event that killed all but the deepest corallites on the perimeter of the head. The lowest corallites of the perimeter remained below the HLS after the emergence and, thus, were able to continue growing until the complete death of the microatoll colony in the regional 1997-98 reef disaster.

Radiography of the slab generally reveals clear annual banding that enables recovery of an almost unambiguous time-series of growth throughout most of the 20th century. Visual counting uncertainties are no more than a few years within this series (Fig. 3.12a). The high density (i.e., dark band on the positive print of the X ray) of the

final partial growth band suggests that the microatoll died in the dry season (March - July). Thus, our best estimate for date of death is March-July of 1998.

We used the U-Th disequilibrium method to date samples 29, 70 and 83 rings in from the exterior of the slab. Assuming an early 1998 death for the outermost partial ring, these dated rings would have formed in AD 1968, 1928, and 1915. Three of the four U-Th radiometric analyses – AD 1963 \pm 8, 1926 \pm 11, and 1912 \pm 11 (Table 3.1) – are consistent with the visual ring counting. The U-Th date for the 1928 band – 1886 \pm 6 – is inconsistent with the visual count and must have resulted from a handling blunder.

Emergence in 1935

A visual count of annual bands from the early 1998 perimeter of the microatoll toward the interior yields a date of A.D. 1936 +1/-3 for the large emergence that initiated growth of the brim. The uncertainty in this date is due to a few ambiguous bands on the brim and modest erosion of the perimeter of the bowl of the cowboy hat. The youngest partially preserved band that antedates the emergence grew in 1933. The first band that unambiguously shows upward growth of the brim formed in 1937. The 1936 +1/-3 date of emergence suggests that emergence occurred in association with the large earthquake of December 28, 1935. The geometry of the slab constrains the amount of the 1935 emergence to be a minimum of 57 cm (Fig. 3.12a). We can improve our estimate of the magnitude of emergence by measuring the elevation of the pre-1935 rim on a less eroded nearby microatoll. The average elevation of the perimeter crest of the central bowl of microatoll H6 is about 5 cm higher than that of the H7 head. Thus, our best estimate of the amount of emergence during the 1935 event is about 62 cm or more.

It is interesting to estimate the change to the East Badgugu reef wrought by a 62cm emergence in 1935. Armed with the immediately pre- and post-event HLS elevations, we can estimate where the lowest tides (i.e., the base of the intertidal zone) would have impinged upon the reef substrate. The contour on the current reef that corresponds to the pre-1935 HLS runs along the sandy beach face, several hundred meters from the microatoll populations we have studied (Fig. 3.10). The immediately post-event HLS contour runs along the outer edge of the shallow reef flat. Thus all but the thin outermost fringe of the shallow reef flat rose into the intertidal zone during the 1935 emergence. Submergence since 1935 has moved the HLS contour slowly landward to its current position a few tens of meters landward of the edge of the reef flat.

HLS history prior to 1935

The central bowl of head H7 formed by nearly spherical growth, upward and outward, from well before 1900 until its upper surface reached HLS in about 1917(Fig. 3.12a). Once HLS was reached, microatoll growth began to record the HLS history of the site. The annual bands that formed in the two decades or so prior to 1935 indicate that HLS was nearly stable during that period (Fig. 3.12b). A least-square fit to the tops of the slightly eroded tops of each annual band yields an average rate of submergence of about 0.4 mm/yr.

This rate is so low that even modest bioerosion could well have obscured the actual rate significantly. A comparison with the survey of elevation of a nearby head, H6, suggests, in fact, that this is the case. That head has relatively well-preserved concentric

rings atop its central hat bowl. A least-square fit of the elevations of these rings yields a submergence rate of about 1.4 mm/yr (Fig. 3.13).

HLS history from 1935 to 1997

The shape of the brims of the modern cowboy-hat shaped microatolls indicates that these heads have been submerging during the last seven decades. These brims rise toward their perimeters. The annual bands in head H7 allow us to confirm and to quantify the history of this submergence.

Overall, H7 records a rise in HLS of about 40 cm since 1935 (Fig. 3.12b). But this rise has not been uniform. Rather, the rise appears to have been much faster in the decades following 1935 and slower in recent years. In fact, submergence of the microatoll after 1935 appears to have been so rapid that the head recorded only a brief HLS impingement from the mid-1940s to 1962. The 23 cm difference in elevation between the top of the 1936 and 1961 bands divided by their 26-year difference in age yields a *minimum* average rate of submergence of about 9 mm/yr for that period.

A significant emergence event in 1962 created a die-down of the brim to an elevation 9 cm below the top of the 1961 band (Fig. 3.12b). This is a minimum value for the emergence, since the top of the 1961 band is a lower limit for the HLS elevation just prior to the 1962 event. Growth then continued uninterrupted by HLS impingement until 1976. Average rate of HLS rise during that period was 16.3 mm/yr. HLS impingements in 1982-83 and in 1986-87 indicate nearly stable HLS from the mid-70s through the mid-80s. The average rate of HLS rise between 1976 and 1997 was about 5 mm/yr submergence.

Composite HLS history from 1900 to 1997

Fig. 3.12b depicts HLS history for the East Badgugu site from about 1917 until 1997. The general characteristics of HLS changes are these: 1) In the two decades prior to 1935, HLS was nearly stable and rates of submergence averaged about 1.4 mm/yr. 2) Emergence associated with the M 7.7 earthquake of December 1935 was about 62 cm. This amount would include any vertical changes in the 3 years before the event, since the annual bands of the three years have been eroded from the outer edge of the hat bowl. Furthermore, the 62 cm would include any submergence or emergence in the months following the event, since lowest annual tides do not commonly occur until June, July or August. 3) In the first few decades after the 1935 event, the head submerged rapidly. The average rate between 1935 and 1962 was at least 9mm/yr. 4) An emergence of at least 9 cm occurred in 1962. 5) A fast submergence rate of at least 16mm/yr followed the 1962 event. 6) Between 1975 and 1997, the head submerged at an average rate of 5 ± 1 mm/yr.

As a comparison we present a major feature of a paleogeodetic history from the site just across the bay at west Badgugu in Figure 3.13. Details of this site, however, will be presented more thoroughly in Chapter 5. The general history and timing are consistent with that of east Badgugu. The modern rate of submergence is not well defined because of very limited HLS clips between 1970 and 1997. On the other hand, the HLS history prior to 1935 is excellent, therefore the submergence rate is very well constrained to about 1.2 mm/yr. This rate is close to the submergence rate estimated from the survey points across head H6 (~1.4 mm/yr, Fig. 3.14).

We will examine the significance of this history of emergence and submergence once we have presented the data from several other sites, below.

3.4.3. Barogang site

3.4.3.1. Introduction

Barogang Island, a small satellite of Tanabala Island (Fig. 3.2), lies about 113 km from the trench axis. Our site occupies the shallow reef flat on the island's northeast shore. Numerous large modern heads form a 20 to 30 m north-south swath across the intertidal reef flat (Fig. 3.15). Like the modern heads of the East Badgugu site, just 30 km to the south, these microatolls display cowboy-hat morphology. As at the East Badgugu site, this morphology results from partial emergence of the microatolls in 1935. Thus these heads contain an HLS history that encompasses the 1935 event and the decades before and after. The bowl of each hat represents coral growth before emergence in 1935 and the brims record subsequent growth upward and outward. As at East Badgugu, the Barogang microatolls died *en masse* in the regional 1997-1998 reef disaster. The most obvious difference between the cowboy-hat heads at this site and at East Badgugu is that the vertical distance from the top of the bowl to the base of the brim at Barogang is half the value at East Badgugu. Thus, at first glance the magnitude of the 1935 emergence is only half that at Badgugu.

The intertidal reef flat at the site thins southeastward from a 150 m width in the north to just a few tens of meters in the south. It is protected from the strong southwesterly swells of the dry season by a rocky headland just to the north. A large

field of loose coral cobbles and small boulders in the northern part of the site attests, however, to strong, perhaps tsunamic, surf in the recent past. A pair of pancake-like heads (H1 and H2) lies near the beach, behind this field of rubble (Fig. 3.15). The upper surfaces of these heads are flat and unornamented with concentric rings and troughs, and much of each head has been eroded. All these attributes indicate that the heads are probably a few thousand years old. The elevation of the tops of these fossil heads varies from 14–45 cm above the tops of the modern heads.

3.4.3.2. Modern cowboy-hat heads

The family of modern cowboy-hat-shaped heads resides on a steeper and deeper section of the shallow intertidal reef and is well protected behind a 10- to 20-meter-wide zone of predominantly branching, foliose and platy coral reefs that fringe the outer edge of the reef (Fig. 3.15). The heads have diameters ranging from 3 to 4 meters and rise from about 30 to 60 cm above the substrate. Modern heads were still alive and healthy when we first visited the site in 1997, but none of them showed living perimeters when we visited again in July 2000. Thus they died in the period between August 1997 and July 2000. We assume that their final death occurred during the reef disaster of 1997-98. In our visit in 2000, we observed that re-colonization of living *Porites* has begun.

Figure 3.16a and 3.16b show our detailed mapping of the four best representatives of the cowboy-hat heads. In principle, the heads can be divided into two or three distinctive parts: the bowl, the lower brims, and the upper brims (color coded in Figure 3.16a and b). The bowl was constructed prior to 1935. The lower brims represent

growth from 1935 to 1962. The upper brims or the outer raised rim are representative of the coral growth in three and half decades after 1962.

Summits of the bowls of the cowboy-hat heads are remarkably concordant with differences of less than ± 4 cm (2σ), as depicted in Figure 3.16c. Summits of the brims are also concordant within ± 4 cm (2σ) but at an elevation about 5 cm lower than the tops of the bowls. In a crude sense, this implies that the upward growth of the brims in the past several decades has almost fully recovered the effect of the large emergence in 1935.

Many parts of the cowboy-hat microatolls have been broken. Most of the upper surface of the bowls has been degraded and rounded, especially around the edges, by bioerosion. The most prominent exception is head H3, half buried near the beach berm and still exhibiting concentric rings atop of the bowl (Fig. 3.16a,b). Average elevations of the top of the H3 bowl are, in fact, a few centimeters higher than that of the rest of the cowboy-hat heads. This is confirmation that erosion on most of the upper surfaces of the hat-shaped heads has diminished their elevations slightly.

One of the cowboy-hat heads in Figure 3.16a,b shows a tilted bowl (H13). The 1935 emergence killed the upper half of the central bowl but not the bottom part of the perimeter that was under the lowered HLS. The tilting must have occurred during or shortly after the 1935 emergence. Subsequently the brims grew asymmetrically around the perimeter and remain untilted. This head still had living perimeter when we visited the site in 1997.

HLS history

In July 2000, we took a slab from the head H5 (Brg00A1) as a good representative of the family of the cowboy-hat heads (Fig. 3.16a). The slab spans HLS history for the entire 20th century and the last decade of the 19th century. The positive print of the radiograph of the slab exhibits an extraordinarily sharp contrast between annual pairs of high-density (dark) and low-density (light) bands. Thus excellent annual banding ensured very accurate visual ring counting (Fig. 3.17a). However, as a test of our ring counting, we performed U-Th-disequilibrium dating of samples taken from the AD 1952, 1918 and 1888 rings. The U-Th dates 1953 ± 4 (2σ), 1921 ± 4 (2σ), and 1890 ± 4 (2σ) (Table 3.1), respectively, thus confirm the reliability of dates assigned by our visual counting of the annual bands (Fig. 3.17b).

Emergence in 1935

Inspection of the slab shows that the large emergence occurred sometime between AD 1927 and 1936 (Fig. 3.17b). The precise date of the emergence cannot be determined by inspection of the rings, because the rings in this span of years clearly have suffered modest erosion on the perimeter wall of the inner head. We can conclude that the emergence antedates 1936, because beginning in that year, the slab shows upward growth toward a higher HLS. The 1927–1936 constraint that the slab imposes on the date of the event is consistent with the date of the largest earthquake in this region on December 28, 1935.

Exact reconstruction of the amount of emergence associated with the 1935 event is also obscured by the erosion of the annual bands in the 1920s and 1930s. Because of

the erosion of the pre-1935 bands, for example, we cannot rule out the possibility that emergence began in the years just prior to 1935. If we assume, nonetheless, that the entire emergence occurred during the December 1935 event, we can project the trend of nearly stable HLS for the first three decades of the 20th century forward to 1935 and determine an HLS elevation. The elevation difference between this point and the base of the brim is about 30 cm (Fig. 3.17c). This, we suggest, represents the total emergence during the 1935 event. This contention is supported by the fact that the preserved upper surface of the head H3's bowl indicates a continuous submergence from its center toward the perimeter edge (Fig. 3.18), thus it indicates that the 1935 large emergence was sudden.

HLS history prior to 1935

The upper surface of the microatolls has suffered from bioerosion, for we do not, in general, see the small cusps and concentric rings that are apparent on uneroded heads. Nonetheless, bioerosion appears modest, except from about 1915 to 1935, and the gross pattern of HLS ups and downs is clear. A steep slope atop the annual bands that formed AD 1894 to 1902 indicates a few years of fast submergence around the turn of the century. HLS between about 1902 and 1915 is nearly stable at an average rate of about – 0.4 mm/yr (Fig. 3.17c). We are not certain that this rate persisted through the 1920s and early 1930s, because of the large amount of bioerosion of the tops of those annual bands. However, we suspect that a low rate of submergence did persist up to 1935, because a nearby microatoll, H3, appears to record a low rate right up to the emergent event. We surveyed the elevations of the preserved concentric ridges and troughs atop the upper surface of the H3 bowl (Fig. 3.18). A steep outward rise in the surface near the center of

the head may well represent the rapid submergence we see in the slab between 1894 and 1902. The remaining 40 cm diameter of the central portion of the head may well be growth in the third of a century leading up to the 1935 event. Burial of the pre-1935 perimeter by sand may have preserved the perimeter better than the perimeter of the slabbed head. Thus, the record of the 1920s and early 1930s may be preserved here. A least squares fit to points along these 45 cm surface yields an average rate of about 0.8 mm/yr submergence. This is our best estimate for the average submergence rate for the 33 years prior to 1935 (Fig. 3.18).

1935–1962

The geometry of the surface of the brim exhibits predominantly fast submergence during the several decades following 1935 (Fig. 3.17b). The total submergence is about 25 cm, but this did not accumulate uniformly. In the first three decades after the 1935 event, initially fast submergence of about 6 mm/yr decayed to a slower rate of about 0.6 mm/yr (Fig. 3.17c).

1962 event

A prominent emergence of about 10 cm occurred in 1962. Submergence was rapid following this emergence so that 10.5 cm of unrestricted upward growth occurred before HLS again impinged on the microatoll in 1969. It is indeterminate whether this submergence occurred in a single event after the 1962 emergence or whether it occurred over a longer increment of the 7-year-long period. Regardless, dividing the total submergence of 10.5 cm between 1962 and 1969 by the number of years yields an average submergence rate of about 11.5 mm/yr (Fig. 3.17c).

HLS history 1969–1997

Since 1969, upward coral growth has been restricted by HLS. It appears that from about 1969 to 1980, the average rate of submergence was a mere 2.2 mm/yr. Small emergences in 1987 and 1995 are associated with El-Nino events in those years. These complicate the calculation of a rate for the latest two decades. The average rate from 1980 to the present, however, has been only about 2 mm/year (Fig. 3.19c). We can check the HLS history derived from the large slab for the past four decades by comparing it with two independent records that we obtained from microatolls H3 and H13 (Fig. 3.17). A survey of the heights of ridges on the outer brim of H3 also yields a mean rate of submergence that is very low (Fig. 3.18)

Furthermore, in July 1997, we collected a slab from microatoll H13 (Brg97 slab in Figure 3.16a). Only the upper, outer brim was collected (Fig. 3.16a). Visual counting of clear annual banding retrieves a complete time series back to AD 1962, the 35th ring counting in from the 1997 living ring. The dark shade of the first few millimeters of the 35th band implies that our best estimate for the birthday of this outer most wing was probably in the beginning of the dry season, March–July in 1962 (Fig. 3.19a). Uninterrupted growth occurs from 1962 until the first HLS impingement in 1974. Upward growth from this time onward is much slower. The average rate is about 2.1 mm/yr, with small emergence in 1987 and 1995.

Combining modern HLS record

Figure 3.19b compares the HLS histories from the two slabs (datum for each record is the highest points on the 1997 ring). The two HLS histories are very similar.

Details differ, but by and large the dates and the values of rises and falls in HLS are consistent. In particular, elevation differences of each uneroded HLS at 1962, 1985 and 1995 rings of the Brg97 and Brg00A1 records are generally less than 1 cm. Both heads show a diminishing of rates from the early 1970s to 1997. A least squares fit to all HLS of the two records yields a modern average submergence rate of about 2.15 mm/yr.

3.4.3.3. Summary of HLS history at Barogang

The submergence rate prior to 1935 was less than 1 mm/yr at Barogang (Fig. 3.19c). During the 1935 event, an approximately 30 cm emergence occurred and killed the upper half of head H5. This was subsequently followed by a period of fast submergence freeing the coral to grow upward. Submergence, however, is not distributed evenly through the period from 1935 to 1997. The rapid submergence of the first two decades (~6 mm/yr) seems to decay to a slower rate prior to 1961 (~0.6). About 10 cm of emergence occurred in 1962, and then fast submergence resumed until 1969 (Fig. 3.19b). From 1969 to 1997 the submergence rate is much slower (~2.2 mm/yr).

3.4.4. Pono site

3.4.4.1. Introduction

The Pono site is on the fringing reef of the West Coast of Pono Island, 115 km from the trench axis (Fig. 3.2). The Porites microatolls we studied sit on a wide, sandy flat, a few hundred meters shoreward of the outer edge of the intertidal zone (Fig. 3.20a). They are protected from the full force of strong southwesterly breakers by the slightly

higher rampart on the reef flat to the southwest. On this rampart is a 200 m wide band of sparse debris and boulders of coral reefs that may be tsunamic in origin.

Most of the modern microatolls were still alive during our visit in July 1997 (Fig. 3.21a), but all were dead when we revisited the site in July 2000. These modern heads are 5 to 30 cm tall and 1 to 5 m in diameter. We expected that the larger ones would contain an HLS record that spans the 1935 event. In contrast to what we found at Barogang, Bendera and Badgugu, the Pono heads show a much smaller emergence step in 1935.

3.4.4.2. Morphology of microatolls

All of the heads display a relatively flat, pancake morphology, with one or more lower interior flats (Fig. 3.21 and Fig. 3.22). These shapes are a testament to decades of relative HLS stability, with only small fluctuations in lowest low tide. Those in the cluster H1 to H9 also have a prominent 10 cm emergence step about 15 cm in from their 1997 perimeters (Fig. 3.21a and b). This indicates a sudden emergence in the mid-1980s.

Our survey of the perimeter crests of H1 through H9 in August 1997 shows concordance within ± 2.3 cm (2σ) of their mean value (Fig. 3.23a). In July 2000 we surveyed the larger heads and found that, with only a few exceptions, the elevations of their perimeter crests and other crests and troughs are within a few centimeters of those of the heads H1 through H9 (Fig. 3.23a and b). Thus it appears that all of the heads we surveyed and sampled are contemporaneous.

3.4.4.3. A 50-year record from small microatolls and H2

We prepared a 50 cm long vertical slab from head H2 to determine a detailed HLS history. Fig. 3.24a depicts the pattern of growth bands revealed in that slab. The record is of near stability during the decade before 1962 and between 1969 and 1983 (Fig. 3.24b). The record between 1962 and 1969 is one of unhindered upward growth. This may indicate either sudden submergence or a sustained period of rapid submergence of about 6 cm in 1962. A 9 cm emergence event appears in the record in 1986. In the decade following 1987, Head 2 indicates emergence at an average rate of about 2.4 mm/yr (Fig. 3.24b). Figures 2.4.6c and d illustrate the average rates of submergence and emergence one calculates for the entire past three decades, if one first removes the emergence step of 1986.

3.4.4.4. A 100-year record from large microatolls and H10

In 2000, we studied larger microatolls a few tens of meters northwest and southwest of the H1–H9 cluster (Fig. 3.20b). Heads H10 and H16, representatives of these larger heads, are depicted in Figures 3.22a and 3.22b. All of these microatolls have a shallow cup-shaped morphology indicative of submergence at rates that, on average, have been low. Abrupt steps upward, however, suggest that they have been subjected to a couple of rapid submergence events. As we shall see in the slab of one of these heads, the highest, outermost flat represents coral bands that grew after 1961. The next flat toward the center formed between 1935 and 1962. The third flat toward the interior represents a period of growth prior to the 1935 event. This flat is a bit lower on average in H16 than in H10. We tentatively interpret this to be the result of settling of H16 into

the sandy substrate during the 1935 earthquake. H16 has a still-older step down to another flat, which forms the center of the head. Judging from the radius of the head, this central flat probably grew during a period of relative stability in the late 19th century.

In July 2000, we collected a diagonal slab across head H10 (Pn00A3), (Fig. 3.22). We chose this head, rather than the larger H16 head, because that 5 m head has been significantly degraded by bioerosion. The record from H10 is particularly valuable, because it extends farther into the past than the record of H2, and because we can compare HLS records from two radiuses

The 2 m long slab from H10 contains a continuous record of HLS variations through the 20th century. However, the geometry of the head is rather asymmetric (Fig. 3.25a). To determine the ages of the annual bands, we relied both on visual ring counting and U-Th age determinations. Two U-series disequilibrium analyses from the 62nd band inward on the western radius yielded dates AD 1933±2 and 1934±4 (Table 3.1). Using these dates and counting outward, we derive perimeter ages of 1995±2 and 1996±4. This is consistent with death in the regional environmental catastrophe of late 1997–early 1998. We assume, then, a date of AD 1997 for the outermost ring of the eastern wing in assigning the band dates shown in Fig. 3.25a. These show that the western radius contains growth bands from about 1926 to 1997.

To determine ages for the eastern radius, we first assumed those two small irregularities on the western radius in about 1935 and 1962 correlate with similar irregularities on the eastern radius. These assignments yield dates of 1957 and 1927 for bands that U-Th analyses indicate formed AD 1957±4 and 1927±6 (Fig. 3.25a and Table

3.1). Visual ring counting, then, shows that the eastern radius grew during the century between about AD 1886 and 1986. Both radii of H10 show a general submergence throughout the 20th century. That submergence, however, is "eventful," with abrupt submergence events in about 1935 and 1962. Long periods of nearly stable HLS occurred through most of the remainder of the microatolls growth history (Fig. 3.25a). Submergence of 5 to 8 cm occurred in the early 1930s. Emergence of 2 to 5 cm occurred in 1962, followed by submergence of 7 to 8 cm (Fig. 3.25 b and 3.25c).

HLS history prior to and during 1935 event

The lower flat on the eastern radius of H10 formed during growth between about 1890 and the early 1930s (Fig. 3.25a). The least-squares fit to all HLS on these bands yields an average submergence rate of about 1.1 mm/yr (Fig. 3.25c). The western radius' oldest bands record just the last few years of this period and are consistent with HLS levels on the East. The eastern radius records a small (2 cm) emergence in the early 1930s. This does not appear on the western radius. But both radii reveal a subsequent, prominent, fast submergence that enabled free upward growth for several years. The magnitude of the free upward growth is about 7.8 cm on the eastern radius and about 4.7 cm on the western (Fig. 3.25b-c). The U-Th dates constrain the onset of this submergence to AD 1931±4/7 and 1931±6. This is strong circumstantial evidence that the submergence is associated with the large earthquake of 1935.

HLS history between the 1930s and 1961

Both radiuses of H10 show relative stability of HLS between the disruptions of 1935 and 1961. However, the rates differ by a fraction of a millimeter per year. The

average rate on the western radius is ~0.1 mm/yr, and it is emergent. The average rate on the eastern radius is ~0.5 mm/yr submergence (Figs. 3.25b and 3.25c). This small discrepancy is easily attributable to differential bioerosion, since only an additional centimeter or two of bioerosion of the western radius would be required to produce the apparent difference between these two very low rates. Nonetheless, true differences as small as these could also be attributable to slight variations in HLS from one side of the microatoll to the other [*Zachariasen et al.*, 2000].

The 1962 event

The HLS disruption of 1962 in H10 mimics that of 1935 in that a lesser emergence event precedes the submergence event. As with the 1935 event, the precursory emergence is most prominent on the eastern side of the head. The magnitude is 4.7 cm on the eastern radius and 2.0 cm on the western radius. This difference could be a hint that micro-environmental conditions on the eastern side were more favorable to die-down than those on the western flank.

HLS history after 1962

HLS restricted the upward growth on both sides of the microatoll after 7 to 8 years of free upward growth after 1962. Only about a decade of growth at HLS occurred on the western flank before death of the perimeter in 1986. But growth continued on the eastern flank throughout the 1970s, 80s, and most of the 90s. The average rate of emergence recorded by HLS clips on the western flank is about 1.5 mm/yr (Fig. 3.25b).

3.4.4.5. Comparison and combination of HLS histories

Fig. 3.26a shows all three HLS histories we have recovered from the eastern and western flanks of H10 and from H2. This overlay of the records allows easy comparison between them. HLS histories recovered from the eastern and western sides of H10 are broadly consistent in pattern, magnitude and absolute elevation. The elevations of their HLSs during the stable periods before and after the 1935 and 1962 events differ by no more than a couple of centimeters. The systematically higher elevations of eastern-flank HLSs may reflect minor differences in bioerosion or microenvironmental controls of HLS across the head.

The pattern of HLS variation obtained from H2 (Pn97) is very similar to that of H10, with two odd exceptions: the absolute elevations for the first few decades are about 5 cm higher, and the 10 cm emergence of about 1986 appears only in H2 (Fig. 3.26a) and its nearest neighbors. If one inserts the 1986 emergence event of H2 into the records of H10, the three records become nearly identical in absolute elevation.

The only plausible explanation for the lack of an emergence event in the H10 records is that head H10 foundered 7 cm into its sandy substrate during the shaking associated with an M_w7.1 earthquake that shook the region in 1984, and the many heads that do display the emergence did not. The source of this large earthquake was only about 25 km to the north [*Rivera et al.*, 2002] so shaking would have been severe here.

3.4.4.6. Summary of HLS history of Pono site

Fig. 3.26b displays an HLS history of the Pono site, based upon the best information from all three records. The general pattern of the HLS history is one of slow submergence interrupted by two and perhaps three rapid small submergence events and

one small emergence event. The first fast submergence event may have occurred in about 1890. This is highly uncertain, however, because only the western record of H10 extends back that far and even that record contains only one HLS clip prior to the hypothesized submergence. From the 1890s to the 1930s, submergence occurred at an average rate of merely ~1 mm/yr submergence. In 1935, a sudden submergence of about 6 cm allowed unimpeded upward growth for several years. The eastern H10 record suggests that emergence of 2 cm occurred prior to the submergence event between 1935 and 1962, very slow submergence resumes. The rate appears to be about half that of the previous 3 decades. We use the eastern H10 record to assess the HLS period for this period, rather than an average of the eastern and western rates, because it appears that the western flank has been more eroded than the eastern flank. More severe bioerosion would explain the lower absolute elevations of HLS on the western flank, its lower rate of submergence, and its smaller emergence step in 1962. In 1962, emergence of about 5 cm occurred. This was followed by fast submergence, which enabled free upward growth through most of the 60s. All three records indicate that through the 1970s and early 80s, HLS was nearly unchanged—the site emerged slowly at ~ 1 mm/yr. The 10 cm emergence of about 1986 is the largest emergence event in the entire century. We attribute it to the Mw7.1 event in 1984. Although the emergence was recorded by the heads in 1986, uplift of such small magnitudes may well not record immediately, since an unusually low tide is necessary to produce an HLS clip [Taylor et al., 1987; Zachariasen et al., 1999]. Thus, we suggest that the emergence occurred during the 1984 event, which had a seismographically determined epicenter just 25 km to the north. In the decade after 1986,

the head was emerging rather than submerging. The average rate of emergence was \sim 3 mm/yr.

Our complete interpretation of this interesting history must wait until after our presentation of the remaining four sites. Nonetheless, we may speculate here upon the origin of the various periods and episodes of submergence and emergence. The submergence of the mid-1930s is, of course, most likely related to the 1935 M_w7.7 earthquake. *Rivera et al.* [2002] showed that this event occurred on the shallow-dipping subduction interface beneath Pono and neighboring islands. The small magnitude of initial emergence and subsequent submergence suggests that Pono sits close to the down-dip edge of the coseismic rupture. If a very small emergence did, indeed, precede a small submergence, we might suspect that slip initially occurred directly beneath the site, perhaps as a precursory aseismic event. Subsequent submergence would imply that Pono sits above a portion of the interface that did not slip during the earthquake.

The second rapid submergence, in about 1962, also appears to have been preceded by a smaller emergence event. Could it be that this represents a slow rupture of the underlying interface, followed by up-dip, trenchward aseismic rupture?

The emergence of the mid-1980s probably resulted from the $M_w7.1$ subduction event of 1984. Emergence at the site suggests that this earthquake involved rupture directly beneath the site. No other sites in our collection display evidence of this event, so the source region of the earthquake must have extended no more than ~ 15 km from Pono.

The three rapid events in the Pono record disrupt an interesting record of secular submergence. Throughout the first century of the record, from the 1890s to the mid-1980s, there is a distinct slowing of the rates—from about 1 mm/yr in the early 20th century to about zero in the 1970s and early 80s. The change to emergence after the mid-1980s is consistent with this trend. A number of mechanisms could be called upon to explain this slow variation from slow submergence to emergence. Perhaps the simplest would be the trenchward migration of the locked/unlocked transition of the subduction interface. Submergence would indicate that the transition is down-dip from the point on the interface directly beneath Pono. Emergence would imply that it has moved up-dip, past the site [Sieh et al., 1999]. We will explore this idea more thoroughly in Chapter 4.

3.4.5. Antinang site

3.4.5.1. Introduction

Antinang is one of islet that clusters around the northwestern tip of Tanamasa. This 1.5 km wide islet is located just 6 km north of the Pono site (Fig. 3.2). Mangrove swamps occupy most of the coast line in this area, but at the site the beach berm is open to the sea. Thick muddy substrate underlies almost the entire site. This leaves water with very poor visibility.

Numerous modern, recently dead microatolls populate the outer part of the intertidal zone (Fig. 3.27). We surveyed the upper surface elevations of some selected heads indicated in Fig. 3.27. Their crest elevations are concordant within $4 \text{ cm } (2\sigma)$.

To be thorough, we also examined some other modern coral populations nearby. The diameters of the modern heads in the mapped area are no more than 2 m but in other nearby locations are up to 3 m. Prominent flat to shallow cup morphology of these heads suggests stable to slow submergence.

Closer to the beach, within clusters of mangroves, numerous fossil heads stand out above the water (Fig. 3.27). Their crests are 60 to 100 cm above that of the modern heads.

3.4.5.2. HLS history of a modern head

We cut a 75 cm long slab from the perimeter to the center of head At99A1 (Fig. 3.27). This slab provides an HLS history from mid-1940s to 1997. We assume the outermost band to be 1997 for visual ring counting (Fig. 3.28a). Our age assignment is consistent with a U-Th date (1948±3) on the 1946 band (Table 3.1).

The upper surface of the coral growth bands implies an average submergence rate of about 2.6 mm/yr in the decade prior to 1960. A hiatus appears between 1960 and 1980. A least squares fit to HLS from 1980 to 1997 yields an average submergence of about 2.1 mm/yr submergence, close to that prior to 1960. It is important to note that the thick muddy substrate underlying the head(s) allows for the possibility of settling of the head and thus false HLS history. However, our visual inspection of the morphology of other modern heads at this site as well as in nearby areas confirms that this areas has been tectonically stable if not slowly submerging.

3.4.5.3. Mid-Holocene heads

We and our cooperative team from ANU took vertical drill-core samples from the center of the highest fossil head (At99A3). The C-14 radiometric analysis of this core yields a C-14 age of 4040±70 (or about 4600 BP after U-Th correction).

We also slabbed a large, fossil microatoll resting further landward (At99A2). The At99A2 head is an extraordinary well-preserved cup-shaped head. Elevation of its perimeter crest is approximately 66 cm above the mean elevation of that of modern heads. We perform a U-Th disequilibrium analysis of a sample from about the 40th band from the exterior of the slab, and it yields an age of 3600±12 BP. Together, these dates confirm that all of the fossil heads are of the mid-Holocene age. The slab analysis of the At99A2 slab is not presented here.

Model of glacio-eustatic sea level changes for this Equatorial region [Peltier in Zachariassen, 1998] predicts paleo—sea level in 3600±12 BP of about 2.5 m above the modern sea level. Thus, the difference in elevation between the fossil head (i.e., At99A2) and the predicted paleo—sea level yields a several-millennium-average submergence rate of about 0.5 mm/yr.

3.4.6. Memong site

3.4.6.1. Introduction

Memong Island is one of a cluster of several very small flat-topped islands that straddles the Equator (Fig. 3.2). None of the islands rises more than ten or so meters above sea level, and their flat reef surfaces tilt gently. A U-Th analysis on slightly re-

crystallized coral just beneath the surface on the neighboring island of Biang yielded an age of $202,000 \pm 1,500$ years. This stage 7 sea level surface is a gently east-tilting coral platform that rises about 4 meters above sea level on the western end of the island. It is covered almost entirely by coconut trees, which are cultivated by the inhabitants of the village in the center of the island.

Our site occupies a 150 m wide late-Holocene reef flat off the island's northern shore (Fig. 3.29). Cemented, undeformed sands of an ancient beach face lie just offshore of the modern beach. The outer few tens of meters of the intertidal reef form a rampart of predominantly foliose and branching coral. This protects the field of *Porites* microatolls that populates the central third of the intertidal reef.

Most of the *Porites* heads are only 20 to 30 cm thick, less than 1.5 m in diameter, and nearly flat-topped. Most of the heads appear to have grown in the latter half of the 20th century. The generally flat upper surfaces of the heads are evidence that sea-level changes on the island have been very small for the past century or so. Two larger heads provide a record that extends back into the 19th century. The record is one of very slow emergence, interrupted by emergence in about 1861 and submergence in 1935.

The perimeters of most of the heads were still alive and healthy during our visit in mid-1997. All of the heads were dead when we visited the site again in July 1999. We re-visited the site again in July 2000. Our surveys of the perimeter crests of many of the *Porites* microatolls suggest that all the heads are modern. Microatoll perimeter crests are concordant within ±5 cm (Fig. 3.30 and Plate 2.3.1).

3.4.6.2. HLS history from a large head, H14

The two largest heads at the site display similar morphologies. In each case, a wide and higher outer rim flanks a gently outward-sloping core. H21 (Fig. 3.29 and 3.31a) is almost circular, and its outer rim is nearly continuous. It has a diameter of about 3.5 m, which suggests that its record of HLS extends well into the 19th century. However, we did not slab this head.

Head H14 has an oval shape in plan view (Fig. 3.31b). Its long axis is also 3.5 m, but the raised outer rim is not contiguous around the entire perimeter. The center of H14 consists of an elevated, hemispherical core. Its elevated nature suggests a significant emergence event early in the growth history of the microatoll. Except atop this central core, the upper surfaces of H14 still display concentric ridges, which indicate that bioerosion has been quite modest.

We have collected two cross sectional slabs (Mm99A1 and Mm00A1) that span the entire long axis of H14 (Fig. 3.31b). These provide an opportunity to compare the HLS history of each radius.

The north radius

Slab Mm00A1 reveals a continuous HLS history from the middle of the 19th century to 1997 (Fig. 3.32a). Its clear annual banding leaves little ambiguity in the time series. A band that we assigned to 1865 by ring counting was U-Th dated to AD 1860±6 (Table 3.1), confirming that the precision of our visual counting of the bands is no worse than a few years over more than a century of growth.

The principal features of the HLS record from the north radius are a central dome that formed prior to about 1875, a broad middle flat that displays a very low rate of emergence between about 1885 and 1935, and an outer raised rim.

The central dome is eroded on top, as evidenced by the truncation of several annual bands. The youngest preserved annual band atop the central dome formed in about 1865. A die-down is evident in the stratigraphy at the beginning of 1874. This diedown is about 15 cm below the eroded top of the central hemisphere. Thus, this amount is a minimum value for an emergence that exposed the dome. We are unsure when in the period between about 1865 and 1874 the emergence of the central dome occurred because nearly a decade of growth has been removed by erosion. It is conceivable that it occurred in 1874. On the other extreme, the majority of the emergence may have occurred in about 1865, with an additional increment of a few centimeters in 1874. We would like to believe that emergence occurred during the great earthquake of 1861 [Newcomb and McCann, 1987], but both the visual ring counting and the U-Th date support an emergence event or episode several years later. Determination of the δ^{13} C record across the bands of the 1860s and 1870s might resolve this, since changes in light intensity have been shown to be associated with change in water depth at another of our sites [Mike Gagan, personal comm., 1999]. Furthermore, the great Indian drought of 1876 might show up as a spike in δ^{18} O values. Unfortunately, these analyses are beyond the scope of our current efforts.

A submergence event or episode enabled upward growth of about $10 \, \text{cm}$ between 1875 and 1885. From 1885 to 1935, steady emergence occurred at a rate of just $\sim 0.9 \, \text{mm/yr}$.

Another submergence event or episode began in 1935. The evidence for this is upward growth that commenced sometime between about 1935 and 1939. Slight erosion of the upper edges of the growth bands obscures a precise determination of the year of initiation of this upward growth. But steeply inclined growth undulations in the annual bands from 1935 to 1955 indicate that strong upward growth began in 1935. By 1975, at the latest, the HLS of the head was about 11 cm above its level in 1935. Growth was restricted to about this level until the death of the head. When we mapped the head in mid-1997, the outer edge was completely covered with living polyps. Substantial erosion of this perimeter occurred between 1997 and our visit in 2000.

The south radius

Slab Mm99A1 from the south radius of Head H14 tells a story that is similar to the one told by the north radius. However, this section is not as useful, because the HLS record between 1923 and 1965 is missing (Fig. 3.32b). This missing section precludes a visual determination of ages for those bands that formed prior to 1965. Instead, we must rely on one U-Th date and on a comparison of the morphologies of the north and south radii.

Emergence of the central hemisphere occurred after the growth of the ring dated 1864±3. This is consistent with emergence during the great earthquake of 1861, but appears to be significantly earlier than the 1865 to 1874 date range for the emergence suggested by analysis of the northern radius (Mm00A1). Furthermore, the emergence event seen in the 1874 band of the north radius is absent in the south radius. The annual-band ages shown on the south radius cross section assume that the emergence of the inner

hemisphere dates to the great earthquake of 1861. But in our analysis of this radius in Fig. 3.32c, we assume that the slow, steady emergence begins in 1885, as it does on the north radius. Clearly, if we wish to resolve what happened at the Memong site in the 1860s and 1870s, we will need to resolve this chronological conflict.

Despite the discrepancy in their age of emergence, the general growth pattern and gross morphology of the north and south cross sections resemble each other. Assuming that the visible HLS clips of the early emergence recorded on both sections are contemporaneous, their HLS histories appear to be identical in pattern, magnitude and relative elevation (Fig. 3.32c).

Disentangling the 1935 and 1962 events

The slow, persistent half-century of emergence evident in both radii ended in about 1935. The 1935 ring of the north radius marks the beginning of several decades of unhindered upward growth (Fig. 3.32a and c). This upward growth continued until 1975. The coral record, alone, only indicates that the submergence occurred at a rate of no less than a few millimeters per year, because this was the upward growth rate of the coral head in the decades following 1935. We suspect, though, that the 11 cm difference in elevation of the tops of the 1935 and 1975 growth bands is evidence primarily of sudden submergence during the 1935 event. If, as we have seen elsewhere in the region, there was also a rise of HLS in 1962, it is hidden in the record of this period during which the head was still striving to grow upward to HLS. Thus, any disturbance of 1962 can not be separated from that of 1935 in the Memong record. As a temporary and tentative solution, we assume that the magnitude of the 1935 disturbance is 7 cm, the vertical

distance between the 1935 surface and the 1962 surface on the north radius. We assume that the magnitude of submergence in 1962 equals the 4 cm vertical difference between the 1962 and 1975 bands (Fig. 3.32c).

3.4.6.3. HLS history of the past 35 years from a small head, H13

Most of the numerous smaller heads at the Memong site have a pancake shape morphology indicative of near-stable HLS for the past few decades. Head H13 is representative of these microatolls (Figs. 3.33a and b). We collected two slabs from this head (Fig. 3.33). These slabs, Mm97B1 and Mm99A2, span the entire diameter of the head. The eastern radius was collected in 1997, when the entire perimeter of the head was still alive. The western radius was collected in 1999, after the death of this and all neighboring microatolls.

The central core of the head was overturned in 1960 or 1962. Growth resumed in 1960 and in 1962 on the overturned head. On the east radius, upward growth reached HLS in 1966. On the west radius, HLS was not reached until 1977. The two HLS histories recovered from the east and the right radiuses are nearly identical (Fig. 3.33c). HLS estimates from the west radius are commonly a cm or so lower than those for the east radius. This appears to be due to slight bioerosion of the west radius, as evidenced by the smoother surface of the west radius, and truncations of individual bands there. A least-square fit to the HLSs of the east radius, for the period from 1966 to 1997, yields steady emergence at an average rate of about 0.3 mm/yr (Fig. 3.33c).

3.4.6.4. Combined history of sea level at Memong Island

Over most of the past 140 years, Memong Island has been experiencing slow emergence. Between about 1885 and 1935, emergence occurred at an average rate of about 0.9 mm/yr. Between 1966 and 1997, the average rate of emergence was about half this fast—about 0.4 mm/yr. The data suggest slight decadal variations about these average rates. However, these slight fluctuations may be within the noise level of the microatoll, so we hesitate to interpret them as tectonic variations in HLS.

These long periods of slow emergence are interrupted by three episodes of rapid emergence and submergence. During the 1860s and/or 1870s, at least 15 cm of emergence was followed by about 10 cm of submergence. Between 1935 and 1975 about 11 cm of submergence occurred. All of this may have occurred in association with the large earthquake of 1935 and the silent submergence event of 1962. We tentatively ascribe 7 cm to the former and 4 cm to the latter.

The physical significance of this HLS history will be considered after presentation of HLS histories for a few more sites, below.

3.4.7. Tofa site

3.4.7.1. Introduction

Tofa is a very small island at the northernmost part of a cluster of islets along eastern coast of Tanabala island (Fig. 3.2). The islet is only about 200 m wide and 400 m long located just about 200 m off shore Tanabala (Fig. 3.34). The west side of the isle slopes steeply toward the channel. A wide intertidal reef fringes the east and southeast sides of Tofa. A graveyard of numerous fossil heads occupies most of this broad shallow

reef platform. A cluster of modern heads inhabits the northwest corner near its outer edge. Another group of modern heads also populates a narrow intertidal flat on Tanabala shore across the channel.

The perimeter crests of the modern recently died heads were only several cm below the low tide at the time of our visit and are concordant within a range less than 3 cm (2σ) ; thus they appear to be of the same age. The heads are relatively small with diameters generally less than 1m and exhibit nearly flat tops indicative of insignificant changes in HLS throughout most of their lives.

3.4.7.2. HLS history from a modern head

We collected a 1 m long vertical slab that spans a radius cross section of one good representative of the modern heads (i.e., Tf99C1, Fig. 3.35a). The sampled head has an almost circular shape in plan view, but interestingly the slab geometry shows an off-center growth. This affords a longer HLS record on the southeast wing. The annual pairs of dark and light banding are fairly clear. Our visual counting has an ambiguity of only a few years within a 50-year time series; thus visual counting is relatively precise. We assume the exterior band is 1997. This head has begun to record HLS at the time of first HLS impingement in about 1948. For several decades thereafter, growth bands appear to have a nearly flat surface, indicating stability up until recent time. However, sudden or rapid submergence and emergence events disrupted this long-lived stability in the late 1950s, early 1960s, early 1980s, and early to mid-1990s.

We slabbed another modern head on the Tanabala shore (Tf99B1, Fig. 3.35b). This slab records HLS history only since the early 1980s. The history is similar to that of

Tf99C1 in that both show major HLS clips in the early 1980s, in 1988, and in 1993 that disrupted the predominantly stable HLS period (Fig. 3.35c).

We combined the HLS histories of the two slabs and presented them together in Figure 3.35c.

Pre-1962

A least squares fit to HLS from 1948 to 1958 indicates that the head has been slowly emerging at rate about 0.7 mm/yr (Fig. 3.35c).

1950s and early 1960s events

From 1958 to 1965, the head appears to have experienced three emergence/submergence events in about 1958, 1962, and 1965. A period of stability recorded between 1963 and 1964 intervenes in this flurry of submergence. The 1962 submergence event is one that is well recorded at many sites in the region. It appears that after the 1962 submergence the first HLS impingement occurred just two years later. This implies that the 1962-related submergence recorded at sites elsewhere may well have occurred in less than a year or two, assuming that the 1962 event represents one single slip event on the subduction interface.

Modern rate

The least-squares fit to the HLSs for the period of 1965-1997 yields an average emergence rate of about 0.3 mm/yr, only half as much as that prior to 1960.

3.4.7.3. Mid-Holocene heads

The tops of the fossil heads are about 20 to 70 cm above those of the modern heads. Most of their upper surfaces have been flattened by bioerosion. Among the few exceptions is the 90 cm in diameter head DC#2, which still preserves a non-microatoll hemispherical form. In contrast, the remnant morphology of a few heads including DC#6 (Tf99A6) suggests that they appear to be microatolls. The C-14 analysis of the coral drill cores yields ages ranges from about 2000 to 6000 B.P, thus confirming that they are all Mid-Holocene heads (Table 3.2).

Sample code	Elevation above mean value of modern head's crests (cm)	C-14 Dates uncorrected (year BP)
Tf99A2	56.7	-6110 ±70
Tf99A3	20.7	-2120 ±60
Tf99A4	69.5	-3940 ±70
Tf99A5	44.4	-4320 ±70
Tf99A7	55.8	-4260 ± 70

Table 3.2 C-14 absolute age for the Mid-Holocene heads (from M. Gagan, written. comm., 2000.)

3.4.8. Tanjung Anjing site

3.4.8.1. Introduction

Thick mangrove swamps occupy much of the protected East Coast of Tanamasa Island. Tanjung (Cape) Anjing, on the southeast corner of the island, is one of the few places along this long coast where we found a large population of *Porites* microatolls.

The site is a 60–100 m wide and 100 m long intertidal reef flat with numerous modern *Porites* heads (Fig. 3.36a). The cup-shape morphology of these microatolls is a testament to the dominance of submergence at the site (Fig. 3.36b).

All of the microatolls were dead when we visited in mid-2000. But the concordance of perimeter crest elevations suggests that they are of the same generation (Fig. 3.36c). A few *Goniastrea* heads (i.e., H4 and H5) display perimeter elevations 10 cm higher than that of the *Porites* heads, but it is typical for this genus to have HLSs about this much higher than those of *Porites*. A small cluster of highly degraded flattopped heads at the edge of the mangrove swamp rise to elevations about 25 cm higher than the elevations of the modern *Porites* heads (Fig. 3.36c). These are probably mid-Holocene heads, but we did not sample them.

3.4.8.2. HLS history from a modern Porites head

Microatoll H11 is the best representative of the population of modern heads (Fig. 3.36a). Its regular shape and 2 m diameter (Fig. 3.36b) enable reconstruction of an HLS history for much of the 20th century. The basic HLS record is of near stability punctuated by large emergence and submergence during both the 1935 and 1962 events.

Analytical problems

Interpretation of the HLS record is difficult, however. This stems from ambiguities in dating the annual bands and from rather intense bioerosion of the head. All of the modern heads appear to have suffered significant grazing and boring by predators, so we were unable to sample an unaffected head.

Furthermore, the annual growth bands are poorly developed. This yields unusually large uncertainties in age assignments from visual ring counting. We assume an outer perimeter age of 1997. Working inward, we find that the 1962 band is uncertain by 1 to 4 years, and the 1935 band is uncertain by 3 to 7 years.

To help overcome these problems, we took the unusual step of preparing two thin slabs from the thick sawed slab, rather than preparing just the customary single thin slab (Fig. 3.37a and b). We cut the thick slab from the south, so one of the thin slabs is from the west side and the other is from the east side of the thicker slab. The west-side cut is contiguous through the decade of the 1950s and early 1960 to mid-1960s, whereas the east-side slab is not. The east-side slab is contiguous through the 1960s, 1970s, 1980s, and 1990s, whereas the west-side slab is not. Together they give us a significantly more complete record.

We also dated an unusually large number of samples by U-Th, to constrain the ages of the annual bands better (Fig. 3.37a and b). Several of these ages, however, are also problematic or of limited use. A large uncertainty in the date of the 1959 band (1939±23) renders the analysis consistent with the visual counting, but not useful. The date for the 1941 band (1936±4) is marginally at odds with the ring count, but shows that our counting is not far off.

The three remaining dates are consistent with each other, but are incompatible with our ring counting. The two U-Th analyses of the 1938 band yield dates of 1923±5 and 1928±2 (Fig. 3.37a,b), several years older than our estimate. Last, a U-Th analysis of the 1913 band yields a date of 1902±5, also several years older than our estimate.

These three U-Th analyses suggest that our pick for the 1935 ring is off by about a decade. At the risk of letting our stratigraphic prejudices lead us into a blunder of observation, we choose here, tentatively, to accept our visual counting and ignore the U-Th analyses. To do otherwise would force us to assign a date in the mid-1920s to the largest submergence event in the record, which at all neighboring sites appears to have occurred in 1935.

The 1935 event and before

H11 grew freely upward and outward from about 1902 until at least the early 1920s (Fig. 3.37a and b). This growth appears in Fig. 3.37c as the small climbing triangles on the left side of the plot. HLS is poorly constrained during this period prior to initial HLS impingement.

Growth during most of the 1920s and early 1930s is unclear, because many of these annual bands were removed by erosion. This erosion occurred before 1940, because the void that represents the missing material was filled with new growth that post-date 1940 (Fig. 3.37a). Unfortunately, it is not at all clear that the head reached HLS prior to 1935. The upper surfaces of the annual bands that formed in the late 1920s and early 1930s may be eroded rather than limited by HLS impingement.

The 1935 event begins in both slabs as a die-down of at least 10 cm. This suggests that the site initially raised at least this amount. This emergence was followed by substantial submergence, which allowed the head to grow freely upward once again. Free upward growth continued until the next HLS impingement, in about 1948. This impingement is about 26 cm above the HLS impingement of 1935 (Figs. 3.37a, b and c).

HLS history between 1935 and 1962

The microatoll poorly constrains HLS during its free upward growth from 1935 to 1948. However, from 1948 to 1961, HLS impingements are common. HLS elevation does not change appreciably during this period, although the west-side cut shows a slight rise in the latter half of this period. The high degree of bioerosion on this head leads us to doubt the significance of this observation. The least-squares average rate of submergence during the period 1948 to 1961 is ~0.7 mm/yr (Fig. 3.37c).

The 1962 event

In 1962 (or 1961), HLS dropped 3 to 8 cm (Fig. 3.37a, b and c). This represents a minor emergence event. Quite soon thereafter, the microatoll submerged, which allowed free upward growth from 1962 until the early 1970s. The net effect of these events is submergence of about 10 cm.

HLS history between 1962 and 1997

Once the microatoll had reached the new HLS level, in the early 1970s, it was constrained to grow outward and inward. This growth continued until the death of the head, we presume in 1997. Although the net change in HLS for this quarter century is about nil, there is a record of initial submergence that is followed by emergence. For the first fifteen years of this period, the microatoll submerged at about 3.6 mm/yr. For the last decade, it emerged at 3.5 mm/yr (Fig. 3.37c).

3.4.8.3. Summary

Two submergence events dominate the HLS history at Tanjung Anjing. Both consist of an initial emergence event followed by a much larger episode of submergence. In the case of the 1935 event, the emergence/submergence pair was about 10 cm and about 26 cm in magnitude. In 1962 the emergence and submergence were about 8 cm and 13 cm respectively.

HLS behavior prior to 1935 is indeterminate, because bioerosion has obscured any HLS clips from that period. HLS from 1948 to 1961 is nearly stable (\sim 0.7 mm/yr). From the early 1970s to the mid-1980s HLS rises at \sim 3.6 mm/yr. From the mid-1980s to 1997, it falls at \sim 3.5 mm/yr.

3.4.9. Penang site

3.4.9.1. Introduction

Penang Island is located about 134 km from the trench. It is one of many small islands that lie northeast of Tanamasa Island, which shelters them from the swells of the Indian Ocean (Fig. 3.2). Several small, healthy *Porites* microatolls were living on the intertidal flat fringing the south west side of Penang, when we visited in mid-1997 (Fig. 3.38). These heads exhibited a low, central flat and an outward-sloping outer rim. Such morphology suggests a submergence event and subsequent long-lived emergence (Fig. 3.39b). A slab from the northern radius of a representative heads near the edge of the reef flat enables quantification of the site's HLS history (Fig. 3.39a). The concentration of giant tridacnid and other clams within living heads is unusually high at this site. Predation of the sampled head by the clams severely eroded the slab. This created

significant ambiguities in measuring HLS for some years in the interval 1950-1980 (Fig. 3.40a).

3.4.9.2. HLS history from Pe97-1

Nonetheless, analysis of the slab confirms our initial interpretation of the morphology of the heads: a submergence event or episode occurred prior to decades of emergence. Relatively clear annual banding enables reconstruction of an HLS time series with ambiguities of about 2 years.

The 1950s

Bio-erosion of the head's inner flat has almost completely obliterated the upper surface of the oldest part of the slab (Fig. 3.40a). Band ambiguity further limits reconstruction of the HLS history of the inner flat. We hesitantly interpret the last three annual bands of the inner flat as shown in Fig. 3.40b. The tops of the 1958 and 1959 bands appear to be close to the original, uneroded tops. The 1960 band appears to have escaped bio-erosion, unless it occurred prior to overgrowth of the 1961 band.

1960s event

We prefer to interpret the low top of the 1960 growth band as evidence of a small die-down near the beginning of that year. The magnitude of the die-down is only 2 or 3 cm, so a non-tectonic origin is not easily dismissed. Unhindered upward growth proceeded for 8 years after creation of the 1960 band. At the end of that period, HLS was 7 cm above the HLS level of 1960. Seven centimeters is, thus, a rough estimate of the submergence associated with this event or episode.

HLS history from 1968 to 1997

Despite significant bio-erosion of the record prior to 1980, the slab displays a clear history of progressive emergence in the 1970s, 1980s, and 1990s (Fig. 3.40ab). The average rate of emergence is about 3 to 4 mm/yr, comparable to that of Tanjung Anjing site for the last 15 years.

3.4.9.3. Summary

The Penang slab gives compelling evidence of rapid emergence in the three decades subsequent to 1968. It also yields an excellent estimate of the magnitude of submergence during the 1960s. Both the 1968 growth band and extrapolation of younger HLS elevations back to 1968 show that net submergence in this event or episode was about 7 cm. Extrapolation of the younger HLS trend back to the early 1960s yields a slightly larger value —about 7 cm.

Although this head suggests that the submergence event or episode began in early 1960, the record does not preclude initiation in 1962, the date suggested by records from several other sites. First, our band counting could be in error by 2 years. And second, even if our age assignments are precisely correct, the die-down in 1960 could be a non-tectonic event that was followed by two years of upward growth, back to the HLS level of the late 1950s. Tectonically induced submergence could, therefore, have begun in 1962.

3.4.10. Bai site

3.4.10.1. Introduction

East of the northern half of Tanamasa Island is a vast area of very shallow water and smaller islands (Fig. 3.2). Bai Island is the biggest of the islands of this miniature archipelago. The Bai site is only about 5 km north of the Penang site and about 250 m south of the southern tip of Bai Island. There, during the lowest tide of our visit, a 40 m long ridge of sandstone was exposed up to a few tens of centimeters above the sea surface (Fig. 3.41). Many thin microatolls sit on the bedrock substrate southwest of the ridge. The diameters of these heads reach 150 cm.

The tops of smaller heads dip radially outward, an indication of recent rapid emergence (Fig. 3.42a). The larger microatolls also show a pronounced outward dip on the top of their younger bands, but also contain a lower inner head (Fig. 3.42b). Thus, the general morphology of the heads is very similar to the morphology of the heads at Penang.

We collected a slab (Ba97-B-1) from the northeastern radius of one of the largest microatolls. The superb annual banding in this slab leaves no uncertainty in the assignment of band ages (Fig. 3.42b). The slab shows a marked contrast in the degree of preservation of the inner head and the raised perimeter. The outer perimeter is uneroded; the rises and falls evident in the cross section run around the entire microatoll. Thus they faithfully mark the small ups and downs of HLS in the past few decades. The inner head,

however, is pocked by the hollows created by boring clams. Its upper surface is most likely eroded by a few centimeters, and HLS cannot be constrained well.

We also collected the entirety of a small head, which we nicknamed "the cabbage," because of its resemblance in both size and shape to the vegetable (Fig. 3.42a). The annual growth bands of this head are also exceptionally clear and unaffected by erosion. The head contains a record of HLS during the period 1992–1997, which allows a comparison with the youngest portion of the record of the larger head.

3.4.10.2. HLS History

Ba97-B2 slab

The shape of the top of "the cabbage" testifies to a high emergence rate in the mid-1990s (Fig. 3.42c). The elevations of HLS on opposite sides of the head are nearly identical.

Ba97-B1 slab

The HLS history of the larger of the two heads is divisible into three periods, pre-1962, 1962–1973, and post-1973.

Pre-1962

The oldest part of the head consists of near-hemispherical bands added between the early 1930s and 1962. When the head was only a few years old, it appears to have been overturned. Ring counting indicates that this occurred in about 1935. The coincidence of overturning in the same year as the large earthquake may indicate that the

tiny head was overturned by shaking or tsunami. This is by no means certain, however.

And even if the turnover is seismogenic, it is of no great significance.

The eroded upper surface of the central hemisphere is diachronous. Bands from about 1954 to 1962 outcrop on its upper surface. Although this may reflect an emergence of about 5 cm over about 8 years, another plausible interpretation is that these bands have suffered partial erosion from the top of the head. If this is the case, then HLS is not well constrained by the tops of these annual bands. If the tops of these bands are close to HLS during those years, HLS during the late 1950s was rapidly dropping.

1962 event

The top of the 1962/63 growth surface is about 6 cm lower than the highest preserved remnant of the earlier 1962 band. (Fig. 3.42a). This is a minimum value for emergence in late 1962. If the 1962 and older bands used to extend over the top of the inner head, then the emergence might be as large as about 15 cm.

Upward growth began in 1962 and continued until the end of 1968, at which time a slight HLS clip occurred (Fig. 3.42c). Upward growth immediately resumed and continued until the end of 1973. It is important to note that growth during this period either did not extend radially inward or has been eroded from the inward-facing surface. Stunting of inward growth is common on the raised rims of submerging microatolls, so we suspect that in this case inward growth was minor or non-existent. We suspect that inward growth from raised rims is hindered by extreme temperatures in trapped shallow pools that form atop the low inner flat during lowest tides. Thus, the HLS clip that

occurred on this raised rim in late 1968 may reflect much localized death due to microenvironmental conditions rather than impingement of a truly regional HLS.

If the clip in 1968 did result from a regional HLS drop, the submergence that began in 1962 was at least 5 cm. If the 1968 clip is a local clip, then the submergence of the 1960s was at least 10 cm.

1973 to 1997

The upper surface of the outer raised rim exhibits remarkable preservation. Annual fluctuations in HLS are well preserved. The annual bands display a nearly monotonic decrease in HLS during this period. The average rate of emergence for the period is about 4.7 mm/yr (Fig. 2.13c). Superimposed upon this are higher-frequency, lower-amplitude fluctuations that we interpret as non-tectonic.

This rate of emergence is about 1 mm/yr higher than the rate observed at the nearby Penang site for the same period. It is, in fact, the highest observed rate for the last three decades in this region.

3.4.10.3. Summary

In 1935, when the head was only a few years old, it flipped over, possibly due to the shaking or the tsunami of the 1935 earthquake. The head then resumed growth, forming a hemisphere that first reached HLS sometime in the period 1954-1962. If the head reached HLS early in this period, emergence at a high rate is recorded by the down-stepping of successive annual bands, and about 5 cm of emergence occurred in late 1962.

If, instead, these bands have suffered partial erosion from the top of the head, then emergence of about 15 cm occurred in late 1962.

Unfettered upward growth dominates the period 1963–1973. A minor HLS clip in late 1968 could represent merely a local effect associated with stunting of inward-growing corallites. If so, the submergence of the 1960s could have occurred as one event, with a magnitude of at least 10 cm and perhaps about 13 cm. If the 1968 unconformity reflects a regional drop in HLS, then the submergence of the 1960s occurred in at least two events or episodes, nearly equal in size.

By 1974, the microatoll reached HLS once again. Numerous HLS clips in the succeeding two decades reveal a rather continuous emergence at the exceptionally high average rate of about 4.7 mm/yr.

3.4.11. Lago site

3.4.11.1. Introduction

The Lago site lies on a wide intertidal flat on the northeast side of Lago Island (Fig. 3.43a). The island is about a half kilometer in diameter and raises only about 2 m above sea level. The landward half of the intertidal flat is a deeper, sandy expanse nearly devoid of coral heads. The perimeter of the flat consists of a high-energy rampart of coral rubble and *in situ* branching corals. A wide field of massive *Porites* heads resides between the outer rampart and the landward pool (Fig. 3.43a, 3.43b).

During our visits to the site in mid-1999 and mid-2000, almost all heads were dead, but their high degree of preservation suggested that they had died recently. We suspected that the majority of the heads had died in late 1997, during the extreme event that killed so many of the West Sumatran reefs. Concordance in the elevations of perimeter crests supports the interpretation that almost all of the heads are modern (Fig. 3.44b).

A small cluster of highly degraded fossil heads outcrop near the base of the beach face. These do not appear to be microatolls and the elevations of their crests are about 50-60 cm above those of the modern population. Radiocarbon analyses on one of these heads (from DC#2 in Fig. 3.43) yielded 1350 ± 70 BP (uncorrected 14C date, from Nerilie Abrams at Australian National University, *written. comm., 2001*).

There are two basic forms among the modern heads. Those with a diameter between about 1 and 1.3 m have convex downward upper surfaces, which are suggestive of recent slow emergence. Heads H1, H4 and H16 are good representatives of this subpopulation (Fig. 3.44a). Larger heads, some with diameters as great as 3.5 m, have a cupshaped morphology, with a lower central flat about 30 cm below a 60 cm wide raised outer rim. This morphology suggests a significant submergence event some decades ago. Examples of this sub-population are Heads H14 and H17 (Fig. 3.44a).

3.4.11.2. Record from Microatoll H17

We collected two contiguous slabs from the southeast radius of one of the large heads, H17. We collected the outer rim in July 1999 and the central flat in July 2000.

The relationship of these two slabs was established from surveying of the upper surfaces of each slab prior to removal (Fig. 3.45a).

The annual bands in H17 are exceptionally clear, and so there is little ambiguity in assigning their ages by visual ring counting. We needed only to assume that the exterior ring formed in 1997. Two U-Th ages confirm the age assignments. The 1935 growth band yielded a date of 1936±4, and the 1882 growth band yielded a date of 1880±4 (Table 3.1).

Together, these slabs contain an HLS history that extends from about 1870 to 1997. The slabs reveal steady, slow emergence between 1870 and 1935 and from 1970 to 1997. These periods of stable emergence are interrupted by a large submergence event in 1935 and a lesser submergence in 1962.

HLS history in the decades prior to 1935

The central flat of H17 indicates that Lago was nearly stable in the decades prior to 1920 (Fig. 3.45a). The top of the central flat is devoid of the concentric rings that are characteristic of minor annual fluctuations in HLS. This suggests that bioerosion has removed a few centimeters of the central flat. Nonetheless, the top of the central flat slopes gently away from its center. This slope yields an average rate of emergence of about 1.1 mm/yr for the period 1873 to 1935.

A trough in the upper surface occurs at about the 1920 band. This exists throughout the entire 15 cm thickness of the sawed slab, so it does not appear to be an effect of bioerosion. Rather, it appears that the emergence of the prior decades reversed in the 15 years prior to the 1935 event. The average rate of submergence in these 15

years appears to have been about 3.3 mm/yr. Moreover, there is some indication that submergence accelerated further in the few years prior to 1935.

Submergence in 1935

None of the annual bands between 1935 and 1958 show HLS impingements. Instead, they display rapid, unconstrained upward growth. The difference in elevation between the 1935 and 1958 growth bands is 28 cm (Fig. 3.45a). We interpret this value as a rough indication of submergence magnitude during the 1935 event. However, this value also includes all post-seismic transients that might have occurred in months, years and decades after 1935. If we subtract two decades of emergence at the most recent or the pre-1935 rate, we estimate a slightly higher step associated with the 1935 event and its post-seismic transients —30 to 35 cm (Fig. 3.45.b).

Submergence in 1962

Just a few years after the initial post-1935 HLS impingement by the coral head, another period of free upward growth began (Figs. 3.45a and 3.45b). As at many other sites, this episode began in 1962. This upward growth ended in 1970, by which time the microatoll had grown upward an additional 8 cm. This is a rough measure of the magnitude of submergence during the 1962 event.

Modern emergence

For the past 30 years, the upper surface of the living perimeter of the head has been dropping at an average rate of about 2.5 mm/yr. This rate is twice as fast as the average emergence rate prior to 1935 (Fig. 3.45b).

3.4.11.3. Summary

Microatoll H17 provides a long, continuous record of sea-level change at Lago Island over the past 130 years. Between 1863 and 1920, the site was submerging steadily at a rate of about 1.1 mm/yr. In about 1920, this trend appears to have reversed, with submergence at an average rate of about 3.3 mm/yr continuing (and possibly accelerating) up to the date of the 1935 earthquake. The 1935 event and any transients in the subsequent two decades yielded a net submergence of the site of 30 to 35 cm. Submergence during the 1962 event amounted to about 8 cm. In the past three decades (1970 to 1997), emergence at an average rate of 2.5 mm/yr has been occurring.

The significance of this history will be considered in concert with the histories of the other sites in Chapter 4.

3.4.12. Masin site

3.4.12.1. Introduction

Masin is an islet off the southwest coast of Pini Island (Fig. 3.2). It is about 150 km northeast of the deformation front, farther than any of the sites we have discussed thus far. The subduction interface is about 40 km beneath the site (Chapter 2).

The Masin site is a sandy spit that juts northeastward into the strait from the islet and toward Pini Island (Fig. 3.46a). We first visited the site in 1997 but did not collect a slab until 2000. The couple of dozen *Porites* microatolls that we surveyed in 2000 are just a few of the hundreds that are present on the spit. Particularly large and thick heads,

some about 4m in diameter, rest on the steep southeastern flank of the sandy spit, at the brink of the spit's plunge into much deeper water. Eighteen surveyed heads, all on top of the sandy spit, have diameters between 1 m and 4 m, and their crests rise above substrate from a few tens of centimeters to a meter (Fig. 3.46b and 3.46c). The larger ones commonly have perimeters that overhang the substrate (for example, H19 in Fig. 3.46c). The nearly flat tops of these microatolls suggest that HLS has been nearly stable over the past few decades.

When we visited the site in mid-1997, many of the living perimeters showed signs of distress. In particular, the elevation of the upper limit of the "carpet" of living polyps (i.e., the HLS) fluctuated tens of centimeters around many of the head perimeters. We ascribed this to cyanide fishing, which our crew noted had been prominent in the early 1990s. When we revisited the site in 2000, all of the heads were dead.

Nonetheless, our visit in 1997 and our survey of the perimeter crests of 18 heads in 2000 convinced us that these heads are all part of the same modern population. Crest heights of all the surveyed heads are concordant within 5 centimeters of their mean (Fig. 3.46d).

3.4.12.2. Microatoll H19

We collected a 1 m long slab from the south radius of microatoll H19 (Fig. 3.46b and 3.46d). The morphology of this head is representative of the shape of many of the larger heads at the site, although some of the larger heads have a low, central flat (for example, H14, Fig. 3.46c). The annual banding within the slab is of average quality. Thus, we were able to assign ages without great difficulty. Our uncertainties of the

assignments are typically about a few years. We did not use U-Th analyses to check the reliability of our visual counting of the annual bands. We assumed that the outermost full band grew in 1997.

Initial HLS history

Analysis of the slab reveals a half-century of slow submergence, interrupted by slight drops in HLS in 1962 and about 1992. The slab also reveals a large submergence event in 1935 (Fig. 3.47b and 3.47c).

The oldest band present in the slab grew in about 1925. The band was growing horizontally, which suggests that the head had already reached HLS and upward growth had been restricted. In fact, the slab appears to contain an HLS impingement in 1930, nearly 30 cm below the upper surface of the microatoll.

The 1935 event

Another HLS impingement, barely recovered on the left edge of the slab, occurred in about 1935. The growth ring just above this impingement clearly wraps around the impingement.

Free upward growth of annual bands occurred from 1935 to 1943. This is consistent with submergence of about 18 cm in 1935. As elsewhere, we know only the date of inception of the submergence event or episode. We do not know the precise duration of the submergence event, but we know that it occurred more rapidly than vertical growth could keep up with it. Thus, in this case, submergence had to have been more than about 2 cm/yr for each of the years between 1935 and 1943. As with the other

sites, we suspect that most of the submergence occurred during the 1935 earthquake and during post-seismic transients within a year or two of that event.

Slow, steady submergence since 1943

Between 1943 and 1961, HLS was nearly stable. Submergence occurred at about 0.65 mm/yr. Similarly, from 1964 to 1991, submergence was very stable at about 0.95 mm/yr. Thus, if we extrapolate the post-1943 continuous submergence back to 1935 the size of the 1935 submergence event will be slightly smaller (Fig. 3.47c). Between 1991 and 1997, HLS also appears to have been stable or nearly so.

The 1962 event

The unusually clear record of HLS and its stability between 1943 and 1991 allows us to see quite clearly a slight perturbation in 1962. This begins with an emergence of about 10 cm, which appears on the outside of the 1961 ring. Within two years, by the end of 1964, the microatoll had grown back up to a new HLS, within only 1 cm of the pre-1961 level.

The 1992 event

A clear die-down of about 4 cm occurred in 1991/1992. This event is possibly related to an $M_w5.2$ earthquake that occurred in 1991 in this vicinity (Fig. 3.3). However, the die-down may also be induced by cyanide poisoning related to fishing practices that were common in the early 1990s but which have subsequently been made illegal.

3.4.12.3. Summary

The Masin site contains an exquisite record of slow submergence preceded by a major submergence event in 1935 and minor emergence events in 1962 and 1992. The magnitude of submergence in 1935 was about 18 cm. Emergence in 1962 was about 10 cm, but this recovered almost fully by late 1964. The 4 cm die-down of HLS in 1992 is possibly a tectonic event, but it may also be an effect of cyanide fishing, or it is a combination of two.

3.4.13. Lambak site

3.4.13.1. Introduction

Lambak site is on the northwest coast of Pini (Fig. 3.2), about 160 km from the trench. We could not map the site due to storminess and the threat posed by a waterspout on the day of our visit in 2000. The site is a broad intertidal reef, about 100 m offshore of the coastline and from the seaward edge of the intertidal reef. The reef flat is unusual in that it is broken by numerous deep but narrow, barely navigable channels that wend their way from the sea to near shore.

The shallow reef was a graveyard of dead coral, much of it killed in the mass dieoff of late 1997 and early 1998. Nonetheless, numerous young, well-preserved heads
with nearly concordant outer perimeters rested undisturbed just below lowest tide. Many
of these young heads were more than 2 m in diameter. Unfortunately, however, our chain
saw had recently broken, and so we were limited to the collection of a relatively small
slab using a carpenter's handsaw. The slab we collected includes an entire radius and the
center of the head. The GPS coordinate of the slab is at N 98.60184⁰ E, S 0.048⁰.

3.4.13.2. HLS history

Visual counting of the annual bands in the slab is rather difficult, since the annual bands are poorly developed. Thus, it bears relatively large ambiguities (Fig. 3.48a). We assume that the head died in late 1997. A U-Th date shows that our assumption is reasonable, as it yielded a date of 1987 ± 2 (Table 3.1) for the 1986 band.

Pre-1961

Erosion of the upper surface of the central core of the head eliminates any opportunity to infer HLS history prior to 1960. The 1961 band on the right side of the cross section (Fig. 3.48a) may be partially eroded or it may be intact. Both the 1962 and 1963 rings, however, appear to be intact and to record separate die-downs of several centimeters. The total die-down in these two years appears to be at least 6 cm (Figs. 3.48a and 3.48b).

1963-1970

Between 1963 and 1970, the microatoll experienced uninhibited upward growth (Fig. 3.48a). The raised outer rim that developed during this interval was alive on both its outward- and inward-facing flanks. The difference in elevation between the HLS impingement in early 1970 and late 1962 or early 1963, 9 cm, indicates the magnitude of the submergence event or episode.

1970-1997

HLS elevations at Lambak during most of the 1970s, 1980s and 1990s were stable; fluctuate only a few centimeters from year to year. An unusually large drop in

HLS occurred, however, in 1990±2. No other slab, except that in Masin, records this event, so it is not a regional event. An earthquake (M_w5.2) had an epicenter only a few km south of this site. This event might have caused a 5 cm emergence that we see in coral stratigraphy if, in fact, the seismic source is just beneath this area. However, we suspect that local pollution may also be the cause of this apparent emergence event. The reason for our suspicion is that the shape and magnitude of the HLS drop looks very similar to the one that occurred in 1992 in Masin, 10 km south of Lambak, and in the slowing of the growth rate of the younger bands (i.e., causing thinner bands). Thus, we suspect that the depressed growth bands may result from local poisoning, such as by cyanide fishing, as probably occurred in Masin.

3.4.13.3. Summary

The Lambak slab shows the regional emergence/submergence event of the 1960s very clearly. The amplitude of emergence is about 6 cm. The amplitude of the subsequent submergence episode is about 9 cm. One idiosyncrasy of this episode at Lambak is that the initial emergence episode may have begun in late 1961 and lasted until early 1963.

HLS during the 1970s, 1980s, and 1990s was stable, except for a 4 cm emergence in 1989. This event may well be attributed to the earthquake that occurred north of the site, but alternatively may result from poisoning, as we have documented on the other side of Pini Island at the Masin site.

3.4.14. Sambulaling site

3.4.14.1. Introduction

Sambulaling belongs to a cluster of small islands arrayed along the shallow lip of the deep fore-arc basin south of the Equator (Fig. 3.2). The islet is about 3 km wide and lies about 50 km southeast of Pini Island and 181 km from the trench.

Our site is on the intertidal reef that extends out 150 to 300 m from the eastern side of the island (Fig. 3.49a). The topography of the intertidal reef is typical of wide reef flats. A rampart of branching corals, tens of meters wide, forms the outer edge of the widest part of the reef. The highest living corals of the rampart appeared a few centimeters above water at low tide during our visit in mid-1997.

Porites heads occupy the region between the outer rampart and the shoreline. Their highest elevations were a few centimeters below low tide during our visit, and they were growing on a substrate a few tens of centimeters below low tide. The upward growth of these heads is not controlled by the height of the rampart, because breaks in the rampart exist between them and the open ocean to the northeast.

The reef supported dozens of living *Porites* microatolls, ranging up to about 1.5 m in diameter, during our visit in mid-1997. The perimeters of these heads were a continuous, velvety living golden brown or purple mantle. The highest living corallites on these perimeters are concordant within about ± 4 cm (Fig. 3.49b). The dead upper surfaces of the heads exhibit the low-amplitude concentric rings typical of uneroded microatolls (Fig. 3.50b). The shallow outward dip of these surfaces indicates that slow

emergence has been occurring for the past several decades. The larger of these living heads also contain a hollow and overgrowths that hide a lower central surface. This suggests a submergence episode some decades before our visit.

Near the beach berm is a smaller group of dead microatolls. These have a morphology that is distinctly different from the shape of the living heads. They exhibit a central flat, surrounded by a high raised rim (Fig. 3.50a). This shape suggests a rapid submergence a few decades prior to the death of the heads. The average elevation of the summits of the raised rims is about 5 cm higher than the elevations of the tops of the living perimeters of the living microatolls.

The differences in shape and elevation indicate that the two populations of heads are not contemporaneous. Our U-Th dates demonstrate, in fact, that the older heads died in the 1950s. We collected slabs from representative heads of each population to reconstruct the HLS history of the site.

3.4.14.2. HLS history from the old head, Sm97-2

Slab Sm97-2 is from a radius of microatoll H8, one of the dead, cup-shaped microatolls. The bands in the slab are relatively clear, so assignment of relative ages to the bands is relatively easy. Assigning absolute ages required U-Th analysis. We chose two samples, separated by 31 annual bands. The U-Th ages of these two bands, 1907 ± 1.4 and 1938 ± 1 (Table 3.1), are also 31 years apart. The age assignments on Fig. 3.50a are based upon the two absolute ages and visual counting. The oldest ring in the slab formed in about 1902 and the head died in about 1953.

During this half-century, HLS fluctuations sculpted the shape of the head's upper surface. Its predominant features are a lower central flat, which formed between about 1905 and 1935, and a raised rim, which formed between 1935 and 1953 (Fig. 3.50a). The upper surface of the dead microatoll is highly eroded, so a precise and detailed HLS history cannot be obtained from the slab. Nonetheless, several features are large enough to be preserved.

HLS history before 1935

The inner flat of the head appears to dip slightly toward the center of the head (Fig. 3.50a). This may indicate that submergence was occurring at a few millimeters per year between 1905 and 1920. However, this slope may be an erosional relict, so we place little trust in this interpretation.

A die-down in 1920 is very prominent in the cross section. The pre-1920 HLS level was reached by upward growth in about 1929. We do not see a die-down in 1920 at any of the other sites with slabs that span this period. Thus, we suspect that this is a very local die-down. Alternatively, it could be a regional tectonic event constrained to an area within about 50 km radius. However, seismic and historical records show no occurrence of a large earthquake in this vicinity during that time.

1935 event

Three decades of stable or nearly stable HLS ended in 1935. That year, after 2 or 3 cm of die-down, the head began to grow rapidly upward toward a higher HLS level (Fig. 3.50a). The head's first post-1935 HLS clip occurred in 1940 at an elevation 9 cm above the top of the 1935 band.

HLS history between 1940 and 1953

The outer raised rim of Sm97-2 is highly eroded, so details of the HLS history are uncertain. Nonetheless, it appears that HLS was stable between about 1940 and 1944. The tight curvature of growth bands that formed between 1945 and 1949 strongly suggests free upward growth to a higher HLS during that 5-year interval. HLS may well have been nearly stable between 1949 and 1951. This stability may have persisted until death of the head in about 1953. The cause of death of the microatoll is mysterious, but it was certainly not related to earthquakes, as there were no large earthquakes in the region that year.

3.4.14.3. HLS history from modern head, Sm97-1

Slab Sm97-1 was cut from a radius and center of H2, one of the living microatolls (Fig. 3.49a). Although its annual bands do not exhibit the pronounced dark/light alternation that we see in many other heads, the slab displays exquisite thin bands formed by rows of single cells, each band being about 1 mm thick. These appear to represent *monthly* growth bands, as groups of 12 to 13 bands constitute annual bands that are weakly expressed by density differences. Using these monthly bands, we assign dates for bands between the living perimeter of 1997 and 1951 (Fig. 3.50b). The imprecision of our date assignments is probably no greater than 4 years.

The principal features of the upper surface of the coral slab are these: an eroded central low involving the bands formed before 1960, a period of unhindered upward growth to a higher HLS between about 1961 and 1970, and a slowly descending HLS between about 1971 and 1997.

HLS history prior to 1961

Growth of the head in its earliest years, the decade or so before about 1951, is ambiguous. The growth bands are not concentric and appear to result from the coalescence of several small heads. Therefore, we hesitate to interpret this. From 1951 to about 1960, unhindered hemispherical growth occurred. The 1958 and 1959 bands were later partially eroded. The upper surface of the 1960 band may also have suffered erosion, but its truncation may, instead, be the result of a die-down of about 2 cm in late 1960 or early 1961.

Submergence between 1961 and 1971

Unhindered upward growth began with the 1961 band and continued until about the 1971 band. As our age assignment has an uncertainty of a few years (Fig. 3.50b), this submergence event/episode may have occurred in 1962. If so, it correlates with similar records in neighboring sites. Even if our visual ring counting is flawless, the year of initiation of the subsidence that allowed this period of unhindered growth could have been at any time within the first two years of the period, for the following reason: although the episode may have initiated as a 2 cm emergence, the magnitude of emergence is so small that it could well be ascribed to a typical non-tectonic annual variation in HLS. Furthermore, since the upward growth did not rise above the level of the prior HLS for about 2 years, these first two years of upward growth could also be ascribed to normal, non-tectonic variations in HLS. Thus, the year of initiation of submergence could be as late as about 1963.

HLS history from 1970 to 1997

HLS history for this period is exceptionally well constrained, because the upper surface of these annual bands is uneroded (Fig. 3.50b). The bumps and swales seen on the cross section continue uninterrupted around the entire head, forming a series of concentric circles that represent the minor annual fluctuations of HLS during this period. HLS clips of a few centimeters occur in about 1972/1973, 1974/1975, 1978, 1982/1983, 1989/1990, and in 1994. The times of this impingement are mostly consistent with the occurrence of the severe ENSO and IOD weather in the last three decades [Saji et al, 1999].

In between these years, upward growth occurred, but this did not fully compensate for the die-downs. Thus, HLS progressively declined over this period at an average rate of about 1.9 mm/yr. This represents an emergence rate.

3.4.14.4. Summary and discussion

The HLS record obtained from the Sambulaling site spans all but the first and last couple years of the 20th century. The record from the first half of the century is poorer than that for the latter half, due to bioerosion. Figure 3.50c depicts the composite history derived from the dead and the living microatolls. The record is dominated by submergence in the first half of the century and emergence in the latter half. The details are particularly complex.

From about 1905 to 1935, HLS appears to have been rising at an average rate of several millimeters per year. This could, however, be in part an artifact of bioerosion. An emergence event of about 7 cm disturbed the head in about 1920, but HLS had risen back to or slightly above its pre-1920 level by 1929. This event must be local, as it does not

appear at other sites. In or before 1929, the submergence trend may have reversed and emergence of a few millimeters per year may have begun.

A significant, rapid submergence event or episode began in 1935. We ascribe this to deformation associated with the M7.7 earthquake of that year [Rivera et al., 2002]. Erosion makes determination of the date of the next HLS impingement uncertain, but it probably occurred in about 1940, about 9 cm above the pre-1935 HLS level.

HLS was more-or-less stable for the period from about 1940 to 1944. A small submergence event initiated 5 cm of upward growth between 1944 and 1949. This event could be associated with a M7.1 earthquake in 1946 that had an epicenter about 50 km to the east, near the Sumatran coastline.

A net emergence of about 6 cm must have lowered the HLS from the level of the late 1940s in the dead microatoll to the level of the first impingement of HLS on the living microatoll in about 1961. The date of this emergence is poorly constrained. The last major submergence event occurred in about 1961, and initiated about 7 cm of unhindered upward growth between 1961 and 1971.

HLS during the last three decades has steadily dropped at an average rate of about 1.9 mm/yr. The pristine, uneroded surface of the head shows that this emergence occurred gradually over this period, because successive HLS hits every few years are progressively lower.

At this point we have developed HLS histories across the fore-arc from west to east. The site, described below, is the farthest from the trench.

3.4.15. Telur site

3.4.15.1. Introduction

Telur is an islet 5 km off the coast of the Sumatran mainland, near the Equator and the mainland port city of Air Bangis (Fig. 3.2). Our site is on the intertidal flat on the western side of the 250 m wide islet. We did not have the opportunity to construct a map of the site during our visit in mid-1997.

During our brief survey of the island, we collected with hammer and chisel an oriented chunk from the overhanging outer margin of a small, living microatoll near the shoreline. The GPS position of this head is at 99.35970°E, 0.12860°N. The outer portion of the microatoll exhibited concentric ridges and furrows with amplitudes of a centimeter or so. These indicate that the head is uneroded and should provide a reliable and precise history of HLS elevations.

3.4.15.2. HLS history of slab Te97

Slab Te97 is a small sample and records an HLS history for just the past two decades (Fig. 3.51a). Its annual banding is unclear except along the outermost 15 cm, where it is fairly visible. The precision of our ring counting is about ± 3 years for the overhanging portion.

The uneroded upper surface of the microatoll is nearly flat. A least squares fit to the HLS values yields an average submergence rate of ~0.4 mm/yr (Fig. 3.51b).

3.5. Synopsis

In essence, we have learned that time series of HLS fluctuations are consistent within and between heads at a site. Each site's HLS history is a unique time series of vertical motions above the subduction zone. Together, these HLS histories constitute a rich spatio-temporal paleoseismic and paleogeodetic database for investigating the earthquake cycle of a subduction zone.

We have provided detailed HLS histories for 26 coral microatolls from 17 sites ranging from 90 km to 170 km from the trench axis. The major features revealed by the microatolls are as follow. The 1935 historical earthquake is the largest seismic event recorded in many of the microatolls. The 1962 event is the largest non-seismic event in the HLS histories. Furthermore, decades of gradual change of HLS indicate slow subduction deformations between events. These slow inter-event deformations are opposite in sign to the events. Sites that experienced sudden emergence in 1935 were submerging slowly in the decades prior to the event. Similarly, sites that underwent fast submergence during and after the 1935 event were slowly emerging in the decades prior to the event.

In Chapter 4, we will assemble these HLS time series and analyze them as a single data set, in order to place quantitative constraints on the behavior of the Sumatran subduction interface. This analysis will include assessments of errors that are associated with the HLS data.

3.6. References

- Abercrombie, R.E., The June 2000, M_w7.9 earthquakes south of Sumatra: deformation in the India-Australia Plate, *Journal of Geophysical Research*, submitted.
- Ando, M., Source mechanisms and tectonic significance of historical earthquakes along the Nankai through, Japan, *Tectonophysics*, *27*, 119-140, 1975.
- Bloom, A., and N. Yonekura, Coastal terraces generated by sea-level change and tectonic uplift, in *Models in Geomorphology*, edited by M.J. Waldenburg, Allen and Unwin, 1985.
- Budhitrisna, T., and S. Andi Mangga, Geologi Lembar Pagai dan Sipora Sumatra (Geology of the Pagai and Sipora Quadrangle, Sumatra), Indonesian Geological Research and Development Centre, Bandung, 1990.
- Chappell, J.M., A revised sea-level record for the last 300,000 years on Papua New Guinea., Search (14), 99-101, 1983.
- Deplus, C., M. Diament, H. Hebert, G. Bertrand, S. Dominguez, J. Dubois, J. Malod, P. Patriat,
 B. Pontoise, and J. Sibilla, Direct evidence of active deformation in the eastern Indian oceanic plate, *Geology*, 26, 131-134, 1998.
- Dragert, H., K.L. Wang, and T.S. James, A silent slip event on the deeper Cascadia subduction interface, *Science*, *292* (5521):, 1525-1528, 2001.
- Edwards, R.L., J.H. Chen, and G.J. Wasserburg, 238U, 234U, 230th, 232th systematics and the precise measurement of time over the past 500,000 years, *Earth and Planetary Science Letters*, 81, 175-192, 1987.
- Edwards, R.L., F.W. Taylor, and G.J. Wasserburg, Dating earthquakes with high-precision thorium-230 ages of very young corals, *Earth and Planetary Science Letters*, *90*, 371-381, 1988.
- Fitch, T., Plate convergence, transcurrent faults, and internal deformation adjacent to southeast Asia and the western Pacific, *Journal of Geophysical Research*, 77, 4432-4462, 1972.
- Hantoro, W.S., P.A. Pirazzoli, C. Jouannic, H. Faure, and e. al., Quaternary uplifted coral-reef terraces on Alor-island, east Indonesia, *Coral Reefs*, *13* (4), 215-223, 1994.
- Heki, K., H. Miyazaki, and H. Tsuji, Silent fault slip following an interplate earthquake at the Japan trench, *Nature*, *386*, 595-598, 1997.

- Hirose, H., K. Hirahara, F. Kimata, N. Fujii, and S. Miyazaki, A slow thrust slip event following the two 1996 Hyuganada earthquakes
- beneath the Bungo Channel, southwest Japan, *Geophysical Research Letters*, 26 (21), 3237-3240, 1999.
- Indrawadi, and Y. Efendi, Kasus red tide di perairan Sumatera Barat, *Prosiding. Lok. Pengelolaan dan Iptek Terumbu Karang Indonesia*, 188-191, 1999.
- Kanamori, H., Mode of strain release associated with major earthquakes in Japan, *Annual Review of earth and Planetary Sciences*, 1973.
- Katili, J.A., and F. Hehuwat, On the occurence of large transcurrent faults in Sumatra, Indonesia, *Journal of Geoscience, Osaka City University*, *10*, 5-17, 1967.
- Lowry, A.R., K.M. Larson, V. Kostoglodov, and R. Bilham, Transient fault slip in Guerrero, southern Mexico, *Geophysical Research Letters*, 28 (19), 3753-3756, 2001.
- McCaffrey, R., Slip vectors and stretching of the Sumatran fore arc, *Geology*, 19, 881-884, 1991.
- Miller, M.M., T. Melbourne, and D.J. Johnson, Periodic slow earthquake from the Cascadia subduction zone, *Science*, *295*, 2423, 2002.
- Newcomb, K.R., and W.R. McCann, Seismic history and seismotectonics of the Sunda Arc, .Journal of Geophysical Research, 92, 421-439, 1987.
- Ota, Y., and J. Chappell, Holocene sea-level rise and coral reef growth on a tectonically rising coast, Huon Peninsula, Papua New Guinea, *Quat.Inter.*, *55*, 51-59, 1999.
- Ota, Y., J. Chappell, R. Kelley, N. Yonekura, E. Matsumoto, T. Nishimura, and J. Head, Holocene coral reef terraces and coseismic uplift of Huon Peninsula, Papua New Guinea, *Quat.Res.*, *40*, 177-188, 1993.
- Ota, Y., T. Miyauchi, and A.G. Hull, Holocene marine terraces at Aramoana and Pourerere, eastern North Island, New-Zealand, *New Zealand Journal of Geology and Geophysics*, *33* (4), 541-546, 1990.
- Ota, Y., and A. Omura, Contrasting styles and rates of tectonic uplift of coral reef terraces in the Ryukyuand Daito Islands, southwestern Japan, *Quat.Inter.*, *15/16*, 17-29, 1992.
- Peltier, W.R., and A.M. Tushingham, Influence of glacial isostatic-adjustment on tide-gauge measurements of secular sea-level change, *Journal of Geophsical Research*, *96* (B4), 6779-6796, 1991.

- Pirazzoli, P.A., U. Radtke, W.S. Hantoro, C. Jouannic, and e. al., Quaternary raised coral-reef terraces on Sumba-Island, Indonesia, *Science*, *252*, 1834-1836, 1991.
- Pirazzoli, P.A., U. Radtke, W.S. Hantoro, C. Jouannic, C.T. Hoang, C. Causse, and M.B. Best, A one million-year-long sequence of marine terraces on Sumba Island, Indonesia, *Mar.Geol.*, *109*, 221-236, 1993.
- Prawirodirdjo, L., A geodetic study of Sumatra and the Indonesian region: Kinematics and crustal deformation from GPS and triangulation, University of California, San Diego, San Diego, 2000.
- Prawirodirdjo, L., Y. Bock, J. Genrich, S.S.O. Puntodewo, J. Rais, C. Subarya, and S. Sutisna, One century of tectonic deformation along the Sumatran Fault from triangulation and GPS surveys, *submitted to J. Geophys. Res.* 17 November, 1999, 1999.
- Prawirodirdjo, L., Y. Bock, R. McCaffrey, and e. al., Geodetic observations of interseismic strain segmentation at the Sumatra subduction zone, *Geophysical Research Letters*, 24 (21), 2601-2604, 1997.
- Rivera, L., K. Sieh, D. Helmberger, and D.H. Natawidjaja, A comparative study of the Sumatran subduction-zone earthquakes of 1935 and 1984, *Bulletin of the Seismological Society of America*, *92*, 1721-1736, 2002.
- Saji, N.H., B.N. Goswami, P.N. Vinayachandran, and T. Yamagata, A dipole mode in the tropical Indian ocean, *Nature*, 401 (September 23, 1999), 360-363, 1999.
- Scoffin, T.P., and D.R. Stoddart, The nature and significance of microatolls, *Phil*□ *osophical Transactions of the Royal Society London, Series B*, 284, 99-122, 1978.
- Sieh, K., and D. Natawidjaja, Neotectonics of the Sumatran fault, Indonesia, *Journal of Geophysical Research*, 105 (B12), 28,295-28,326, 2000.
- Sieh, K., D. Natawidjaja, S. Ward, R. Edwards, B. Suwargadi, and J. Zachariasen, Paleogeodetic and paleoseismologic constraints on the earthquake cycle of the Sumatran subduction zone, in *Hokudan International Symposium and School on Active Faulting*, edited by K.T. K. Okumura, and H. Goto, pp. 459-463, Letter Press Co. Ltd., Hokudan, Japan, 2000.
- Sieh, K., S.N. Ward, D.H. Natawidjaja, and B.W. Suwargadi, Crustal deformation at the Sumatran subduction zone, *Geophysical Research Letters*, 26 (No.20), 3141-3144, 1999.

- Taylor, F.W., J. Frohlich, J. Lecolle, and M. Strecker, Analysis of partially emerged corals and reef terraces in the central vanuatu arc comparison of contemporary coseismic and nonseismic with quaternary vertical movements, *Journal of Geophysical Research*, 92, 4905-4933, 1987.
- Thatcher, W., Earthquake recurrence and risk assessment in circum-Pacific seismic gaps, *Nature*, *341*, 432-434, 1989.
- Woodroffe, C., and R. McLean, Microatolls and recent sea level change on coral atolls, *Nature*, *344*, 531-534, 1990.
- Zachariasen, J., Paleoseismology and Paleogeodesy of The Sumatran Subduction Zone: A Study of Vertical Deformation Using Coral Microatolls, California Institute of Technology, Pasadena, 1998.
- Zachariasen, J., K. Sieh, F.W. Taylor, R.L. Edwards, and W.S. Hantoro, Submergence and uplift associated with the giant 1833 Sumatran subduction earthquake: Evidence from coral microatolls, *Journal of Geophysical Research*, *104* (No. B1), 895-919, 1999.
- Zachariasen, J., K. Sieh, F.W. Taylor, and W.S. Hantoro, Modern vertical deformation above the Sumatran subduction zone: paleogeodetic insights from coral microatolls, *Bulletin of the Seismological Society of America*, *90* (4), 897-913, 2000.

Chapter 4. A synthesis of paleogeodetic records of seismic and aseismic subduction from central Sumatran microatolls

4.1. Overview

In Chapter 3, we assembled paleogeodetic records of 26 coral microatolls from 16 sites on the fringing reefs of the islands around the Equator. In this chapter, we first assess the errors associated with these data. After incorporating these errors, we construct HLS curves for each site. These curves are then used to model slip on the subduction interface associated with deformation during the 1935 earthquake, the 1962 aseismic event, and the remainder of the 20th century.

Figure 4.1 is a compilation of all the records. It facilitates comparison of the HLS histories by depicting them with their time scales aligned and with the same scaling of emergence and submergence relative to modern HLS. It is clear that the 1935 seismic event dominates the HLS history of several of the sites. We will see that the records contain a geographically coherent pattern of submergence and emergence for this event. The 1962 aseismic event is the second largest short-lived event recorded throughout the region. It commonly appears in the records as an emergence and subsequent submergence. The emergence is mostly less than 10 cm, but the submergence has substantially larger magnitude, up to about 25 cm. The shape, magnitude and coherent regional pattern of the 1935 and the 1962 events distinguish them from numerous other signals that are smaller in magnitude and in geographical extent. Figure 4.1 shows that rates of aseismic vertical deformation during the century vary markedly from site to site. Moreover, many sites show abrupt changes in rate associated with the events of 1935 and 1962.

In Chapter 3, we did not discuss in detail the sources of uncertainty inherent in our microatoll "instrument." The analysis that we embark upon in this chapter requires, however, that we do so now. Accurate determination of the magnitude of deformation in 1935 and 1962, for example, requires determination of the uncertainties in the levels of HLS both before and after these events. Similarly, calculations of rates of submergence and emergence during the remainder of the century require knowledge of the uncertainties in the data. The uncertainties that appear in Figure 4.1 were calculated according the procedures discussed below.

4.2. Analysis of uncertainties in HLS records

Paleogeodetic records from microatolls contain two principal sources of uncertainty. One source is non-tectonically induced variations in HLS. The other is the erosion of the upper surfaces of microatolls. Errors associated with the former are relatively easy to quantify. Errors due to erosion, however, are more difficult to assess. Once both eroded and uneroded data have been assigned errors, rates of submergence and emergence can be determined by use of a standard statistical procedure.

4.2.1. Uncertainties associated with local effects and short-term regional oceanographic fluctuations

A microatoll's HLS record serves as a proxy record of lowest annual low tides [Taylor et al., 1987; Zachariasen et al., 1999; Zachariasen et al., 2000]. Tectonic phenomena, global hydro-isostatic changes in sea level, regional oceanographic oscillations, and local variations in upward growth rate all contribute to an HLS history.

Thus, an HLS record is not, *ipso facto*, a record of tectonism. The non-tectonic signals in an HLS history must be considered first before assessment of the tectonic component.

Zachariasen et al. [2000] have observed that variations of HLS elevation around the Sipora and Pagai Islands within a single *Porites* coral heads are usually less than ± 3 cm, whereas the variation of average HLS elevation between microatolls from the same location is about 10±5 cm. From field work in 1997, our comparison of intra-head differences of uneroded living rings of microatolls shows that HLS elevations, approximated by the tops of living rings, vary by about ± 2.6 cm (2σ) within one head (e.g., Figs 3.14c, 3.21a, and 3.28). This is in agreement with the uncertainties estimated by Zachariasen et al. Our more intensive surveys in mid-1999 and mid-2000 show that intra-head variations in the elevation of the perimeter crests of recently dead, moderately eroded microatolls are also generally less than 3 cm. Thus we cannot expect to resolve tectonic events that produce signals less than or equal to about 3 cm. Moreover, our 1999 and 2000 surveys show that inter-head variations at a site vary by ± 5 cm (2 σ) (e.g., Figs 3.14c, 3.21a, and 3.28), a figure that significantly less than that reported by Zachariasen et al. [2000]. Hence, at those sites where we use more than one head to construct a record, as we have done to measure sudden emergence in 1935 at Bendera (Fig. 3.7a and b), we must allow for uncertainties of this magnitude. To further examine the sensitivity of the coral records, we compare HLS histories from the opposite side of the head (Figs 3.7c, 3.33) as well as those from different microatolls in a site (Figs. 3.19b, 3.35). Our comparison show that the relative elevations of the uneroded or slightly eroded HLS records in each HLS history recovered from two samples within one head, as well as

from between different heads, differ by no more than 2 cm. This is a test that supports our evaluation of the uncertainty due to local non-tectonic variations.

Broad oceanographically induced fluctuations in HLS are also non-tectonic and must be assessed. One might expect these to resemble tectonic events, because they could produce spatially and temporally coherent signals. Our records show, however, that the effect of even most severe climatic regional events during the El Nino-Southern Oscillation (ENSO) and the Indian Ocean Dipole (IOD) lowered HLS by no more than a few centimeters. The largest of these, in 1997, 1994, 1986/7, and 1982/3 [Saji et al., 1999] appear in our microatolls, but as minor disturbances (Fig. 4.2). Most of these diedowns recover by upward growth to prior levels within just a few years. To further distinguish these regional climatic events from tectonic signals, we found that they produce geographically incoherent patterns. That is, the magnitude of die-down is only grossly similar across the region.

At several sites, die-downs of up to a few centimeters occurred in years not associated with extreme climatic events (Fig. 4.3). At most of these sites, upward growth to the prior HLS level occurred quickly. At four sites, however, we cannot rule out local tectonic causes. Drops of about 4 and 5 cm at Masin and Lambak in about 1991 could be related to an M_w5.2 earthquake event (Ch.3, Fig. 3.3). The 5 cm HLS drop in early 1990s at Lago might also have been associated with this event. A 10 cm drop in HLS at Pono in 1986 that is not followed by recovery may be related to a nearby M 7.1 earthquake in 1984 [*Rivera et al.*, 2002]. *Taylor et al.* [1987] showed that for small uplifts, an HLS diedown could lag one year or more behind the event, because a subsequent very low lowest annual tide may not occur for several years.

Apart from the singular events just mentioned, our best-preserved slabs show annual fluctuations of a few centimeters. Few of these fluctuations correlate with those at nearby sites. Therefore they are not due to large or regionally extensive tectonic events. To quantify the uncertainty in the tectonic signal due to these fluctuations, we examine our three best-preserved records of HLS.

Figure 4.4a displays the records from Bai, Sambulaling, and Angsa islands. Figure 4.2 shows the locations of Bai and Sambulaling Islands. Angsa Island is very near the mainland coast, about 117 km southeast of Sambulaling, and therefore does not appear in the figure. From each HLS history, the long-term trend in emergence or submergence has been removed, so that the shorter fluctuations appear as residuals about the mean, long-term rate of change. Each point represents a clear, uneroded HLS clip in the record. The error bars shown represent the 2- σ deviation of each population of points from the dashed least-squares regression line. These values are ± 2.6 , ± 2.8 , and ± 2.7 cm for the three records. Hence, we consider the average of these values, ± 2.7 cm, to be representative of HLS variations for all of our records. So, in Figure 4.1 all uneroded or preserved HLS points (the large filled circles) appear with an error bar of this magnitude.

4.2.2. Ambiguities due to erosion

Recall that in our many HLS histories in Section 3.4, we took care to use a different symbol for the elevation of a clear HLS clip than we used for a lowest limit to HLS elevation (filled circles versus horizontal bars). A 2- σ error of ± 2.7 cm can be assigned to all of the uneroded HLS elevations in Figure 4.1, based upon the analysis of the uneroded heads in the preceding section. However, eroded points must bear errors

that include this value plus an estimate of the amount of erosion. How do we assign these errors?

A pristine microatoll has an upper surface ornamented by alternating concentric ridges and swales (Fig. 4.4b). The three slabs we have just analyzed from Bai, Sambulaling, and Angsa islands are good examples (Figs. 3.40b and 3.50b). We have found that the amplitude of this micro-topography usually is between 2 and 4 cm. Similar magnitudes of micro-topography are common on heads in Vanuatu [*Taylor et al.*, 1987] and on the Cocos Islands [*Smithers and Woodroffe*, 2000]. Viewed in cross section, it is clear that the concentric swales are associated with individual HLS clips that occurred during years of exceptionally low low tide (e.g., Figs. 3.40b and 3.48b). The concentric ridges represent unimpeded upward growth between HLS clips.

More often than not, however, these concentric bands are either subdued or absent, due to erosion. Erosion thus adds an additional level of uncertainty in interpreting the HLS record. If erosion occurs predominantly as a diffusive process, then degradation will occur qualitatively as shown in Figure 4.5. In this example we start in the upper panel with the young coral head from Sambulaling. Proceeding successively to lower panels, the ridges erode more rapidly than the swales, because of their more exposed position and greater ratio of surface area to volume.

Since the amplitude of the micro-topography of a head is 2 to 4 cm, 1 cm of erosion of the ridges will subdue but not eliminate the micro-topography, and the HLS clips, buried beneath the swales, remain uneroded. (Fig. 4.5, Stage 1). If concentric rings are barely apparent on the surface of the head, but HLS clips are still visible, then erosion of 2 to 4 cm has probably occurred (Fig. 4.5, Stage 2). If no expression of concentric

rings exists and HLS clips are not preserved, then erosion has probably equaled or exceeded 3 or 4 cm.

We use this analysis in assigning errors to each of the HLS records in Figure 4.1. Figure 4.6 shows graphically the result of this process. In the upper panel, HLS elevations from the pristine head from Sambulaling Island appear. In the lower panels, uneroded HLS points become progressive fewer. Each eroded point has an elevation equal to the measured elevation of the top of the annual band plus the estimated amount of erosion, which ranges from zero to 4 cm. The error is calculated as a function of the inherent fluctuation of HLS (±2.7 cm) and the estimated amount of erosion that the head has sustained, according to this formula:

$$\sigma_{eroded\ HLS} = \sqrt{(\sigma_{ol}^2 + \sigma_e^2)}$$

where σ_{ol} is the standard deviations of HLS fluctuations due to regional oceanographic and local causes, and σ_{e} is half of the estimated amount of erosion. Thus, smoother, more eroded heads have HLS estimates that are significantly larger than less eroded or uneroded heads (Fig. 4.1). Moreover, the observed elevation of the eroded HLS is also corrected for the amount of erosion according to this formula:

Corrected elevation of eroded HLS = observed elevation $+\sigma_e$

4.2.3. Determination of submergence and emergence rates

To isolate large tectonic signals in the HLS records, we eliminate uncorrelated fluctuations. These are commonly small in amplitude and duration, so we ignore them by calculating rates of change in HLS averaged over a decade or more.

Because we have calculated larger uncertainties for the HLSs of the more highly eroded heads, we avoid the paradoxical result that more-eroded heads would produce smaller uncertainties in rate of submergence or emergence. Consider, for example, the data from the uneroded head at the top of Figure 4.5e. Because the top of the head has not been smoothed by erosion, the data are more highly scattered about the mean rate of emergence. If data from the more-eroded surfaces in the lower panels had not been assigned progressively greater uncertainties, both the correlation coefficients and the uncertainties in emergence rate would have been inversely correlated with the amount of erosion.

Since the uncertainties are not necessarily the same for each point in an HLS history, the rates shown in Figure 4.1 are calculated from the best fits to the weighted data. Data points with lesser uncertainty are given larger error bars. The least squares regressions and associated $2-\sigma$ errors are calculated according to this formula:

Least-squares average rate of uplift = HLS rate changes as a function of time = (slope) b

$$b = \frac{(\sum_{i=1}^{n} W_i)(\sum_{i=1}^{n} W_i * X_i * Y_i) - (\sum_{i=1}^{n} W_i * X_i)(\sum_{i=1}^{n} W_i * Y_i)}{(\sum_{i=1}^{n} W_i)(\sum_{i=1}^{n} W_i * X_i^2) - (\sum_{i=1}^{n} W_i * X_i)^2}$$

[e.g. Bevington and Robinson, 1992; Taylor, 1982]

and standard error of $b = \sigma_b$, according to this equation:

$$\sigma_{b}$$
 =Scaling Factor x
$$\sqrt{\frac{\sum_{i=1}^{n} W_{i}}{(\sum_{i=1}^{n} W_{i})(\sum_{i=1}^{n} W_{i} * X_{i}^{2}) - (\sum_{i=1}^{n} W_{i} * X_{i})^{2}}}$$
 [e.g. Deming, 1964]

Where: Scaling factor = arbitrary number

 $X_i = \text{time axis (year)}; Y_i = HLS (cm);$

 $W_i = \frac{1}{\sigma_i}$, in which: σ_i = the estimated standard deviation of data

Note that, we do not use a common alternative method where σ_b is proportional to the average standard deviations (scattering) of data from the regression line [Bevington and Robinson, 1992]; but we determine σ_b proportional to the estimated errors of data.

In Figure 4.1, average rates calculated over longer periods appear alongside sloping arrows above the data. Average rates calculated over shorter periods appear directly above solid lines drawn through the data. Dashed lines through the data indicate that the calculated rates are less certain, and dotted lines indicate rates extrapolated into periods lacking data.

4.3. THE 1935 EVENT

In this section, we discuss in detail deformation recorded by the coral microatolls associated with the historically reported and instrumentally recorded large earthquake of December 1935. We use the date of this event to ascertain the reliability of our visual ring counting and U-Th dates. We then discuss in detail how we measured the values of uplift and submergence at the 9 sites that record the event. We, then, compare our data with model predictions based on source parameters obtained by our seismologic study [*Rivera et al.*, 2002]. And, finally, we use elastic dislocation theory to estimate the source parameters of the event based solely on the paleogeodetic records.

4.3.1. Overview

Historical evidence of the 1935 earthquake is sparse. Below is the only field observations that have been published [*Berlage Jr*, 1936]:

"A heavy earthquake hit the Batu islands (i.e., the islands of Tanabala, Tanamasa, Pini and other neighboring smaller islands) in December 28; 09:06.83 (1935). Reports were received from Northern and Southern Sumatra. The person in charge of the lighthouse on the little island of Bodjo [see Fig. 4.7] reported that the hill, on which the 60 m high light house stands, showed tears. Damage dimmed the light. Some walls of buildings next to the lighthouse cracked and roof tiles fell down, injuring two people. On Tello Island [see Fig. 4.7] several residential houses collapsed, a number of people therein were hurt, and some were seriously injured. The "person in charge" of the Batu Islands mentioned later that the islands Tanabala and Sigata [see Fig. 4.7] seem to have risen a little bit, since a reef fields [i.e., an intertidal reef] that used to be flooded at high tide, now remain dry. The coastal lights of Sigata and Moeara Siberoet were lightly damaged. On Sumatra the earthquake was also very strong. In the area of Padang the local phone lines were broken. Several walls cracked. Trees, telephone poles and light poles, and also the wires, moved. In several residential houses and shop, glasses fell down. In the Oranje hotel plaster fell down, while behind the main building an electrical cable snapped. In several parts of the city the light system broke. In the pool the water was moving around and flooded the edge of the pool. Cars were difficult to control and bounced across the road. In Sibolga some houses collapsed. However, no person was injured. Strangely enough the chief of the village of Moearakoeang in the residence of Palembang reported that on December 28 there were "flood waves" seen on the river Ogan "while there was no earthquake". The epicenter of the earthquake was registered world-wide and was located about 0.3°S, 97.9°E, just west of the Batu islands. A great number of aftershocks followed."

We did not find a historical report on tsunami that might be associated with this event. However, we observed and mapped many reef blocks and debris in intertidal reef flats in this region that were probably associated with this event. Local peoples that we interviewed during our field work in 1999 and in 2000 appear to confirm this hypothesis.

Nine of our paleogeodetic sites show clear evidence of vertical motion in about 1935 (Fig. 4.1). The pattern of deformation is consistent with the historical notes above. Figure 4.7 shows that the three sites closest to the trench emerged, whereas all sites closer to the mainland submerged. Emergence of nearly a meter occurred at Bendera, about 100 km from the trench. The Badgugu site and the Barogang site experienced lesser emergences. Emergence at Bendera, Badgugu, and Barogang are consistent with the Berlage's report that intertidal reefs in the western part of the Batu islands rose above water. The site with the greatest submergence, 34 cm, is Lago, about 140 km from the trench axis and about 30 km above the subduction interface. The domains of emergence and submergence join along a line that is approximately 114 km from the trench axis but not quite parallel to it (Fig. 4.7). The geographic extent and magnitude of this deformation constrain the dimensions of rupture that produced the pattern, in particular its downdip limit and the magnitude of slip.

4.3.1. Dating of the event

We have eight slabs from microatolls that were growing prior to the event, experienced it, but survived until the late 1990s. In each case, visual counting of annual bands inward from the outer surface of the slab yields dates for the event in the 1930s (Fig. 4.8). Uncertainties in counting range from 1 to 7 years, and the weighted average for the event is 1935.5 ± 0.6 . But our convention is to assign the beginning of a growth year to the beginning of the darker band of the annual dark/light pair. This means that the beginning of our growth year is in about March, the beginning of the annual dry season. Thus we must add about 2 months to the growth-year date to derive a calendar date of

 1935.8 ± 0.6 . The slab count with the least uncertainty gives a date centered on 1936. This strongly suggests that the deformation is related to the large earthquake ($M_w7.7$) of 28 December 1935 (1935.9).

U-Th dates from many of the slabs also constrain the date of the event. Sm97-2, for example, shows that a submergence of about 10 cm began within a year of 1935 (Fig. 3.50a). In total, 23 U-Th analyses (Table 3.1) constrain the date of the event (Fig. 4.8). Figure 4.9 shows that the age discrepancy between dates from U-Th analysis and those from visual ring-counting is generally less than 5 years and usually within the analytical precision of the U-Th analyses. The weighted average date of the event, based on the U-Th dates, alone, is 1935 ± 1.2 . The difference between the results of the two methods is insignificant (-0.8 ± 1.2 years, 2σ).

4.3.2. Magnitude and pattern of vertical deformation

Measuring the vertical deformation associated with the 1935 earthquake would be rather straightforward if all one had to do were to difference HLS values recorded immediately before and after the event. However, we must also use the uncertainties in these values to determine uncertainties in the magnitude of deformation. We must also, in most cases, extrapolate from older and younger HLS clips to estimate the HLS values just before and after the earthquake.

If the same head contains an HLS record for the periods both before and after the event, then we begin with the nearest data points both before and after the event. The uncertainties in the elevations of these points will be ± 2.7 cm, if the HLS is uneroded, or ± 2.7 cm plus the estimated amount of erosion. If these data points were recorded near the

time of the earthquake, then using the long-term submergence or emergence rate to extrapolate values just before and after the earthquake is inconsequential.

However, there is commonly a need to extrapolate to 1935 at sites where large submergence occurred. Since the coral grows upward at rates of only about 1 cm/yr, a submergence of many centimeters will require many years of free upward growth before the head again reaches HLS. Thus, post-earthquake periods roughly equal (in years) to the submergence (in centimeters) are devoid of HLS clips (e.g., Fig. 4.1e, i, j, m, n, and p). The Lago island site, where submergence was greatest in 1935, provides the most extreme example. Figure 4.1m shows that no HLS clips occurred until about 22 years after the event. In these cases, extrapolation of the most proximal HLS clip back to 1935, using the average rate of submergence or emergence influences the magnitude of the 1935 step, but by no more than a few centimeters.

At two sites, the HLS history is a composite assembled from more than one head. At Bendera and Badgugu, emergence was so great that the heads that record HLS before the event rose completely above the lowest annual low tide and died. Heads that record the post-1935 HLS history were well below lowest low tide until the event. In these two cases, we must also include inter-head uncertainties in HLS, which are about ± 5 cm. Thus the total uncertainty, a combination of the inherent uncertainty in the preserved HLS (i.e., ± 2.7 cm) and the inter-head HLS variations, is this:

$$\sigma_{ol(inter-head)} = \pm \sqrt{(2.7^2 + 5^2)} cm = \pm 5.7 cm (2\sigma)$$

Note that the solid, dashed, or dotted lines through the data in Figure 4.1 represent extrapolations used to calculate the magnitude of submergence and emergence for the

1935 event, but not the exact values. The actual calculation uses the least-squares average rates shown in Fig. 4.1, but we extrapolate back from the elevation of the first HLS clip after the event. The calculation and the values of submergence and emergence for the 1935 event appear in *Table 4.1*, and these are the values plotted in map view in Figure 4.7.

Table 4.1 Vertical displacement in the 1935 event (in centimeters). The 2- σ uncertainties due to (1) natural/local and oceanographic fluctuation, (2) erosion, and (3) extrapolation of rates to 1935 are σ _{on}, σ _e, σ _x, respectively.

	Pre-	Elev	σ_{e}	$\sigma_{ m ol}$	Post-	Elev	Ext.	σ_{x}	σ_{e}	σ_{ol}	Vert.	2σ
	1935	Corr	±	±	1935	Corr	Corr	±	±	±	Displ	±
	Elev		_	<u> </u>	Elev				-	_		
Bendera	53.0	2.0	2.0	5.7	-35.0	0.0	0.0	0.0	0.0	5.7	90	8
Badgugu-B	19.0	5.0	5.0	5.7	-42.0	0.0	0.0	0.0	0.0	5.7	66	13
Barogang	8.7	2.0	2.0	5.7	-24.2	0.0	0.0	0.0	1.0	5.7	35	8
Pono	-1.2	0.0	0.0	2.7	7.1	2.0	-0.2	0.9	2.0	2.7	-10	5
Memong	-12.0	1.5	1.5	2.7	-5.0	1.5	1.3	1.6	1.5	2.7	-8	5
Tj.Anjing	-35.4	0.0	0.0	2.7	-8.0	2.5	-2.3	3.4	2.5	2.7	-28	5
Lago	-27.5	1.0	1.0	2.7	0.4	1.0	6.0	2.3	1.0	2.7	-34	4
Masin	-17.6	0.0	0.0	2.7	0.2	2.0	-0.5	1.6	2.0	2.7	-19	4
Sambulaling	-17.3	0.0	0.0	2.7	-8.5	1.0	1.0	0.5	1.0	2.7	-11	4

The coral microatoll instrument has an odd "response spectrum." If emergence is approximately equal to the diurnal tidal fluctuations at spring tides (that is, about 1.5 m), most of the coseismic step should be recorded within a half day, since even at neap tides the head would be out of the water at least 75 cm right after the earthquake. If emergence is only about half of the magnitude of spring tides, then emergence might not begin to be recorded for as much as a week after the event, until the next spring tide produced the monthly lowest tides. The full extent of coseismic emergence might not be recorded for

as much as a year, since annual lowest low tides typically occur only in June, July or August. This could be the case at the Bendera site and the Badgugu site, where emergence was about 90 and 66 cm. Smaller emergences, of the order of 10 or 20 cm, would be less likely to appear immediately, but would most likely appear in the HLS record within a few years, since our records show that extreme annual lowest low tides vary by only a few centimeters and occur every few years. The fact that HLS was recorded within a year at all of our emergent sites (Fig. 4.1a, 4.1c and 4.1d) demonstrates that this analysis is fundamentally correct, and that any post-seismic transients hidden within our "co-seismic" emergence records would have occurred within about a year of the earthquake.

The submergence records of the 1935 event constrain post-seismic transients much more poorly. As Figure 4.1 shows, post-seismic periods ranging from 5 to 40 years contain no HLS clips.

4.3.3. Paleogeodetic source parameters of the 1935 event

The principal constraints provided by the paleogeodetic data on the 1935 event are these:

- A domain of emergence occurred outboard of about the 25 km isobath of the subduction interface (Fig. 4.7). Values of emergence increase systematically southwestward, toward the trench.
- A domain of submergence appears inboard of the same line. The magnitude of submergence is greatest at or about 10 km northeast of the
 25 km isobath and diminishes gradually toward the mainland.

- The hinge line separating domains of emergence and submergence runs near the western coast of Tanamasa Island. The best-fit hinge line strikes about N 41°W, several degrees more westerly than the trench, about 115 km to the southwest. This suggests that the event involved a small component of right-lateral slip on the subjacent subduction interface.
- Assuming a dip of 10° for the interface beneath the Bendera site (based upon its depth of 5 km below sea level at the trench and the location of the 25 km isobath, 115 km from the trench), we can make an elementary trigonometric calculation of slip. The 90 cm of uplift at the site yields a value of 2.1 meters of slip on the interface beneath the site. This must be considered a lower limit, since the dip of the interface beneath this westernmost site is probably less than the average dip over the region.

We can employ elastic-dislocation modeling to constrain further the parameters of fault rupture in the earthquake. *Rivera et al.* [2002] have already attempted this, but with a completely independent data set. They used historical seismograms of the 1935 event from four stations: De Bilt, Wellington, College, and Honolulu to constrain the source parameters of the earthquake. First, they studied the nearby $M_w7.2$ 1982 event, to be used as an empirical Green's function for the 1935 event. The focal mechanism of the 1982 event indicates that the source is a very shallow-dipping thrust fault, with a slip vector slightly oblique to the dip direction of the subduction interface. The source duration is around 16 sec, and the hypocentral depth is about 27 ± 2 km. The waveforms generated by the 1935 and the 1984 are nearly identical, but amplitudes for the earlier event are several times larger. Thus, these two events appear to have very similar

mechanisms, but the 1935 event has a duration of 30 sec and a seismic moment about 5 times larger that that of the 1984 event. By comparison with the size of the 1982 event, Rivera et al. estimate the seismic moment of the 1935 event to be $3.3 \times 10^{20} \text{ N}$ m (M_w =7.7). Furthermore, based on a shorter and higher source time-function recorded on the seismogram at Wellington, they conclude that rupture was *unidirectional* toward the southeast. Thus, assuming a rupture velocity of 2.0-2.5 km/sec for the 30-sec rupture, they estimate a rupture length of 60 to 70 km. Assuming a standard 2:1 ratio for strike length to dip length [*Geller*, 1976], they then calculate an average displacement of about 3 m. This value is not well constrained, offcourse, since it depends strongly on the assumed rupture velocity and shape ratio of the fault. Assuming extreme values for those parameters can give values for an average displacement as low as 1 m or as high as 10 m (and fault width of 90 or 9 km, respectively) [*Rivera et al.*, 2002].

Nonetheless, from these estimates of source parameters, *Rivera et al.*[2002] used elastic-dislocation theory to estimate the pattern of vertical deformation. They calculate elliptical uplift and submergence regions with peak amplitudes of about 70 and 35 cm, respectively (Fig. 4.10). A minor right-lateral component of slip yields a hingeline between the two domains that is slightly oblique to the strike of the subduction interface.

It is interesting to compare this model of vertical deformation with our paleogeodetic data. To first order, the model from the historical seismic data is consistent with the paleogeodetic data. The locations and magnitude of emergence and submergence are similar, as are the hingelines between emergence and submergence. The principal difference between the seismologically derived model and the paleogeodetic data is in the magnitude of deformation. Figure 4.11 shows that, with the

exception of the values at Pono, the paleogeodetic values of emergence and submergence are consistently greater than those of the model. The paleogeodetic values range from about 35 to 70% greater than the model values. Since the moment magnitude chosen for the model by *Rivera et al.*[2002] is near the upper end of their range of plausible values, this difference may be significant. Though, it can simply be accounted for the shortcoming of the fault parameters used by *Rivera et al*'s model.

4.3.4. Elastic dislocation model of the 1935 event

Elastic dislocation models have been quite successful in explaining sudden surface displacements associated with major seismic and aseismic events. These models are based on Voltera's formula, which was first applied by Steketee to the general study of dislocations in an elastic half-space [Steketee, 1958a; Steketee, 1958b]. Mansinha and Smylie [1971] further developed analytical expressions that enabled relating surficial displacement fields to slip on inclined faults. To relate interseismic deformation fields to slip on a subduction interface, Savage [1983] derived a simple two-D elastic half-space model for strain accumulation and release. The 2-D elastic model has been applied successfully to provide a solution for a surface deformation observed during a co-seismic event [e.g. Savage et al., 1998; Thatcher, 1984b]. We use a 2-D elastic model that is basically identical to the Savage's model to explain the vertical deformations of the 1935 recorded in microatolls.

The paleogeodetic data associated with the 1935 event vary principally as a function of distance from the trench (Fig. 4.7). More exactly, they vary as a function of distance from the hingeline. A 2-D treatment of these data should suffice, since they vary

little along strike. The results of our modeling are presented in Figure 4.12. The black dots are the 1935 uplift and submergence data derived from the microatolls. The black bars represent 2-σ uncertainties. The scale for these data appears on the upper part of the y-axis of the plot, in centimeters. The geometry of the subduction interface in the model is defined by a cubic polynomial fit to the location of the trench and the top of the Benioff-Wadati zone, based upon locations of seismic hypocenters from the relocated ISC: 1965-1998 [*Engdahl et al.*, 1998]. The scales for depth and position perpendicular to the trench appear along the lower part of the y-axis and the x-axis, respectively.

Figure 4.12 depicts the results of two 2-D models; in each case, the red patch on the subduction interface represents the location of the rupture, and the green line is the vertical deformation predicted by the inversion. In the upper panel (A), we projected the observed vertical deformations onto a cross section perpendicular to the average strike of the trench and isobaths. In this case, the paleoseismic data are moderately well fit by uniform slip of 2.5 m on a patch of the subduction interface 94 to 125 km downdip of the trench axis and 17 to 27 km deep. These model parameters are quite similar to those derived from the seismological study [*Rivera et al.*, 2002], (Fig. 4.11)]. However, the model underestimates the observed values at the three westernmost sites.

In the lower panel (B), we attempted to reduce the misfit that might be due to the slight obliquity of the hingeline by projecting the data onto a cross section perpendicular to the hingeline rather than perpendicular to the trench. The location of the rupture in this model is nearly the same as in the first model (88 to 125 km from the trench, 15 to 27 km deep). The magnitude of slip is a uniform 2.3 m. This model is an improvement, because two of the three westernmost points agree with the model deformation.

However, the point at Bendera (Tb) is still underfit (by about 10 cm), and the point at Barogang (Brg) is fit at the very edge of its lower error limit. We probably could fit these points better without degrading the fit to the other points by adding an additional few tens of centimeters of slip to the upper half of the rupture patch. We have not actually developed this inhomogeneous slip model, however, nor we have attempted to take into account any post-seismic transient slip or visco-elastic responses that might have occurred in months following the event.

Nonetheless, in both models, the downdip extent of the rupture is tightly constrained by our data. The updip limit of the rupture is less well constrained. We could extend the updip edge of the rupture by about 15 to 20 km trenchward without severely misfitting the data. Extending the updip limit by more than 20 km, however, results in an unacceptable misfit.

4.4. THE 1962 EVENT

Now we will analyze data related to the events of 1962. These events consisted of an emergence event followed by a submergence event. These events are not associated with any large earthquake; therefore, we consider them to be aseismic ruptures. Similar to the analysis of the 1935 event, we divide our presentation below into an overview, a section on the characteristics of the vertical deformation, and finally an interpretation using elastic models.

4.4.1. Overview

Short-duration deformations, in magnitude second only to those of 1935, appear in the paleogeodetic records during 1962 (Fig. 4.1). The time of the emergence phase is well constrained by visual ring counting to have occurred during the first half of that year (Fig. 4.13). The magnitude and extent of the deformation is much greater than could have occurred during a few small (M6 or less) earthquakes that occurred in the region in 1961 and 1962 (Fig. 3.2, Chapter 3). More probably, the moderate earthquakes were a minor seismic manifestation of this much larger episode of aseismic deformation.

Most of the sites reveal that the 1962 episode comprises two consecutive geodetic events; the first characterized by emergence of the sites and the second by their submergence. In both episodes, the magnitude of vertical deformation is a few times less than that of the 1935 event. Thus one would expect that if the source of the 1962 events were the subduction interface, the slip on the interface would have been just several tens of centimeters. Nevertheless, the submergence event of 1962 was of far greater geographic extent than the 1935 rupture, since it is also seen in records up to 400 km farther south (*unpublished data*).

4.4.2. Magnitude, duration and pattern of vertical deformation

Table 4.2 is a compilation of the values of emergence and submergence at the sites. All values were derived from the data presented in Figure 4.1 and Table 4.2 (in the manner described above for the 1935 event). At most sites, the magnitude of the initial emergence is smaller than that of the subsequent submergence. This fact manifests itself in many of the records as a distinct step up in HLS elevations after 1962 (in particular,

Fig. 4.1b, d, e, j, l, m and p). In addition to the distinctly higher HLS after 1962, at many sites the long-term rate of emergence or submergence changed appreciably at the time of the event (Fig. 4.1a, c, d, j, and m).

Table 4.2 Vertical displacements of the 1962 event. The values of the 1962 emergences are the sealevel drop from the HLS elevation before the event (pre-Event) to the HLS elevation after the emergence (post-Event) (measured in centimeters relative to the 1997 HLS). To estimate the amount of the 1962 submergences the submergence rates are extrapolated from the first HLS hit back to 1962.

	Pre-Event		Post-Event		First HLS hit			Extr. Corr.		Emergence		Submergence		Net Displ.	
	value	2σ	Value	2σ	Elev.	year	2σ	value	2σ	Value	2σ	Value	2σ	Value	2σ
Tb00A1	-12.5	2.9	-19.3	2.7	-7.7	1970	2.8	-2.6	1.5	6.8	4	-9	4.2	-2.2	5.8
Bdg99A3	-27.7	2.9	-33.3	2.7	-5.7	1983	2.9	-4.8	5.3	5.6	4.1	-22.8	6.6	-17.2	7.8
Bdg00B1	-17.9	2.9	-31.1	2.7	-8.4	1975	3	-7.1	4.5	13.2	4.2	-15.5	6	-2.3	7.3
Brg00A1	-16.3	2.9	-18.4	2.7	-8	1970	2.9	-2.2	0.5	2.1	4.1	-8.3	4	-6.2	5.7
Pn97 and Pn00A1	7.8	3.6	2.8	2.7	10.4	1972	3.1	-0.3	8.0	5	4.7	-7.3	4.1	-2.3	6.3
Tf99C1	4.6	2.9	1	2.7	2.8	1963	2.9	-0.1	0.1	3.6	4.1	-1.7	4	1.9	5.7
Mm00A1	-4.7	3	-4.7	2.7	-1.2	1975	3.2	0.7	8.0	0	4.4	-4.2	4.3	-4.2	6.1
Taj00A1	-5.3	4	-12.2	2.7	3.6	1975	4	5.7	3.4	6.9	5.7	-21.5	5.9	-14.6	8.2
Pe97-1	-6	3.4	-7.4	2.7	0.6	1968	2.9	2.7	1	1.4	4.5	-10.7	4.1	-9.3	6.1
Ba97	12.2	3.4	5	2.7	14	1973	3.4	4.8	1.3	7.2	4.8	-13.8	4.5	-6.6	6.5
Lg99A1	1.4	3.1	1.4	2.7	8.5	1970	3.1	2.3	0.9	0	4.3	-9.4	4.2	-9.4	6
Msn00A1	1.5	3.4	-7.9	2.7	0.6	1965	3.4	-0.2	0.3	9.4	4.8	-8.3	4.3	1.1	6.4
Lm99A1	0.6	3	-6.6	2.7	3.3	1971	3	1.2	8.0	7.1	4.2	-11.1	4.1	-4	5.8
Sm97-1	-1.2	2.9	-3.4	2.7	7.2	1971	2.7	1.9	1	2.2	4	-12.5	3.9	-10.3	5.6

Records from sites where the magnitude of the 1962 episode is small constrain the duration of the episode best, because the time required for the living perimeters to grow back up to HLS was short. The Masin site may provide our best constraint on the duration of the submergence event. It clearly indicates that the 1962-submergence event ended there no later than 1964 (Fig. 4.1n). The record from Tofa suggests a similarly short duration, but it is more ambiguous. Based upon the record from these two sites, we think that the entire episode took place in less than two years.

Maps of deformation during both the emergence and submergence events show distinct, contourable patterns. The emergence event appears to consist of two northwest-trending ridges, each a little over 10 cm high and separated by a swale of lesser uplift (Fig. 4.14). The swale between the two ridges is very close to the hinge line of the deformation in 1935. If this deformation resulted from slip on the subduction interface, then the ridges might be evidence for slip on the lower portion of the 1935 rupture and on a patch downdip from it. The swale suggests that these two patches were distinct, with minimal if any overlap.

The occurrence of strong ENSO and IOD events in 1962 [Saji et al., 1999] is reason to be cautious in interpreting this emergence event as being of tectonic origin. Such climatic events typically produce die-downs (i.e., emergence) of coral heads in this region, as Figure 4.2 shows. The magnitude of emergence during the strongest ENSO and IOD events of the past two decades, in 1982, 1986, 1994 and 1997 are commonly up to 3 cm in our records, but in some cases are close to 10 cm. Unlike the emergence event of 1962, however, these climatically induced emergences display no coherent geographic pattern. Nonetheless, emergence associated with the strong ENSO/IOD climatic event of 1962 probably contaminates the tectonic signal significantly. Still, the fact that the emergence pattern that we see in 1962 has a regional pattern and magnitudes greater than those commonly produced by the ENSO/IOD events suggests that it is predominantly tectonic in origin.

The deformation pattern of the subsequent submergence event is nearly a mirror image of the preceding emergence (Fig. 4.15). It consists of two northwest-trending synclinal troughs, separated by a long, narrow region of minimal submergence. The

synclinal axes appear to be in the same locations as the anticlinal crests of the prior emergence event. Furthermore, the location of the ridge between the zones of submergence is indistinguishable from the swale between the anticlinal ridges of the preceding emergence event. These coincidences suggest that slip during the submergence event was on parts of the subduction interface adjacent to those patches that slipped in the emergence event, as suggested in Figure 4.15. In this depiction, the two slip patches that produced the submergence event are immediately updip from the two slip patches that produced the emergence event. Together, the source of the western ridge and the western trough are coincident with, but of smaller magnitude than, the source of the 1935 earthquake.

The submergence event of 1962 also appears to have an odd extension that bends northward and eastward through Pini Island. We might interpret this as northwest-directed slip on the subduction interface. However, our data poorly constrain this sector of the submergence event, so we are not eager to speculate further about this part of the signal.

4.4.3. Elastic dislocation model of the 1962 event

We modeled the paleogeodetic emergence and submergence of the 1962 event in a similar fashion to what we did for the 1935 event. Our initial attempts, shown below, assume that 2-D representation of the data is adequate. All the data are projected onto a cross section perpendicular to the trench and interface isobaths. The maps of the data show clearly, however, that the data vary both as a function of distance from the trench and parallel to its strike. Thus, a 2-D representation is only a starting point for

understanding what happened during the 1962 episode, and modeling efforts are ongoing.

A suite of 3-D models will be attempted, but is beyond the scope of this thesis.

4.4.3.1 Modeling of the 1962 emergence

Figure 4.16 shows the results of 2-D modeling of the emergence event. The observed double-peaked emergence can be produced by slips on the three narrow patches in Fig. 4.16. The two patches nearer the trench are located on the center of and near the downdip limit of the 1935 rupture. Slip on these patches reaches maxima of about 50 and 170 cm. The bigger patch, about 20 km wide is much deeper than the 1935 rupture. It occurs at a depth of about 45 km, about 170 km from the trench axis. Maximum slip on this patch is about 120 cm.

The paleogeodetic data scatters rather widely around the model emergence curve. As mentioned above, this is primarily because of the variability of values perpendicular to the plane of the model cross section. In addition to this obvious limitation to the initial 2-D modeling, contamination of the data by the ENSO-IOD has not been removed. Because the emergence is only 2 or 3 times greater than the emergence that likely resulted from the ENSO-IOD event, we have a relatively low "signal to noise ratio." This may mean that our model overestimates by several tens of percent the slip on the three patches.

4.4.3.2. Modeling of the 1962 submergence

The model that we present here for the 1962 submergence episode is also 2-D. The data have been collapsed onto a cross section perpendicular to the trench (Fig. 4.17).

Like the emergence data, these data display considerable scatter because values also vary as a function of distance along strike. Uniform slips of 1.7 m on the shallowest interface from the trench to the islands and 1.2 m on the patch near the downdip edge of the 1935 rupture produce the double-troughed deformation pattern, such as suggested by paleogeodetic data. The model curve fits much of the data, but the two extreme submergence values are grossly underfit. These are the southernmost points in each trough. Thus a 3-D model slip patch would probably need to have greater slip to the south to fit these trough maxima. In fact, the steady southeastward increase in submergence values indicates that slip values on the patches would need to steadily increase southeastward as well. The principal insights provided by this initial, 2-D model are that two independent patches of slip are required to explain the double trough and that the amount of slip required must average a meter or two.

4.4.3.3. Summary of the 1962 elastic model

Figure 4.18 displays a summary of the results of the 2-D elastic-dislocation modeling of the emergence and submergence events in 1962. The double emergence ridges and submergence troughs of 1962 indicate slips on a total of five patches. The patches do not overlap. The elastic model suggests that within two years or less, about 0.5 to 1.7 m of rapid aseismic slip occurred on almost the entire interface above 60 km depth. The sequencing of submergence and emergence suggests that rupture propagated basically updip. Only a small, 20 km wide piece in the middle of the 1935 rupture and a large patch farther downdip, at a depth from 30 to 55 km, did not fail.

Contamination by the 1962 ENSO/IOD event might account for as much as one-third to one half of the magnitude of the emergence event, so the slips associated with that event might have been smaller than we modeled. Nevertheless, even if this is the case, the 1962 aseismic episode has slips much larger than slips associated with rapid aseismic ruptures observed in Cascadia [*Dragert et al.*, 2001; *Miller et al.*, 2002], in Mexico [*Lowry et al.*, 2001], and in Japan [e.g. *Heki et al.*, 1997].

4.5. Deformation in the intervening decades

4.5.1. Introduction

Although the rapid 1935 and 1962 events are prominent in the paleogeodetic records of Sumatran subduction, evidence of slow vertical deformation throughout most of the 20th century is also ubiquitous among the outer-arc islands. Generally, sites experienced slow vertical deformation opposite in sense to their co-seismic deformation in 1935. That is, places that submerged suddenly in 1935 *emerged* slowly throughout the rest of the century, and conversely, sites that emerged suddenly in 1935 *submerged* slowly during the remainder of the century. Basically, this suggests an interplay between strain accumulation and strain relief, as has been suggested for other subduction zones (e.g., Nankai trough, Japan [*Thatcher*, 1984a] and Alaska [*Plafker*, 1965; *Savage and Plafker*, 1991]. In detail, however, the pre-1935, 1935 to 1962, and post-1962 patterns of vertical deformation differ substantially from each other. These differences indicate decadal variability in the processes operating on and around the subduction interface.

In this section we investigate the basic signals of slow vertical deformation throughout the 20th century. The behavior is complex, in both space and in time. However, as we discuss below, it may be explained by different rates of slip on the principal locked patch of the interface and on adjacent downdip and updip patches.

4.5.1.1. Correction for global hydro-isostatic rise in sea level

Nearly all of the paleogeodetic records displayed in Figure 4.1 show significant emergence or submergence throughout the 20th century. But before we can analyze the tectonic signals in these records, a hydro-isostatic signal of about a millimeter or two per year must be removed. In general, sea level rose from about 21,000 years ago to the mid-Holocene because of the melting of glacial ice [e.g. Clark and Lingle, 1979]. An abundance of mid-Holocene coral heads within the intertidal zones of west Sumatra's fringing reefs indicates that sea-level peaked about 5,000 years ago [Zachariasen et al., 1999]. During subsequent millennia, sea level has been slowly dropping in low latitude due to isostatic adjustments of the crust in response to the melting glacial ice and concomitant rise in sea level [Clark and Lingle, 1979; Peltier and Tushingham, 1991]. Modeling suggests that along west coast of Sumatra, sea-level in mid-Holocene was about 2 to 4 m above its current level [Peltier and Tushingham, 1991, Peltier, written comm in Zachariasen, 1998]. The abundance of fossil mid-Holocene coral heads in the intertidal zone of the fringing reefs of Western Sumatra is generally consistent with this interpretation ([Zachariasen et al., 2000]; Chapter 3). However, the ages of mid-Holocene microatolls there range in age from 2000 to 6000 years, and most of these microatolls are less than a meter above their modern equivalents ([Zachariasen et al.,

2000]; Ch.3.4.5 and 3.4.7 herein]. This may indicate that in general the islands have tectonically submerged 1 to 3 m since the mid-Holocene. This slow, millennial tectonic subsidence, at rates of less than about 0.5 mm/yr, then, might be superimposed upon the much higher centennial rates that we have associated with elastic strain accumulation and relief.

Although sea level has, on average, been dropping over the past several millennia, an abundance of evidence shows that it has been doing just the opposite for the last century. Rates of sea level rise, determined from tide-gauge stations throughout the world, range from about 1.0 to 2.4 mm/yr [e.g., *Gornitz et al.*, 1982; *Peltier and Tushingham*, 1991]. This rise has been occurring for at least the past eight decades, but is less certain for the earlier part of the 20th century. This rise is believed to be a consequence global warming, which causes thermal expansion of the upper layers of the ocean and melting of the glacial ice [*Peltier and Tushingham*, 1989].

Clearly, our paleogeodetic records of the 20th century would include this non-tectonic submergence of about 1 to 2 mm/yr. Hence this signal needs to be removed prior to an analysis of the tectonic component. In the case of a submerging site, the effect will be to reduce the rate of submergence by 1 to 2 mm/yr. For example, the 6.1 mm/yr rate at Bendera (Fig. 4.1a) would be reduced to about 4 or 5 mm/yr. For an emerging site, however, the tectonic rate of emergence would be 1 to 2 mm/yr *greater* than the uncorrected rate. Thus, the observed 4 mm/yr rate of emergence at Bai (Fig 4.11) indicates a rate of tectonic uplift of 5 to 6 mm/yr. Records that have been experiencing submergence at rates of only 1–2 mm actually indicate tectonic stability or even slight

uplift. For example, when stripped of its hydro-isostatic signal, the 0.5 mm/yr submergence at Tofa (Fig. 4.1f) yields a tectonic uplift rate of 0.5 to 1.5 mm/yr.

In Figure 4.19 we apply an adjustment of 2 mm/yr to all of the records of Figure 4.1. An adjustment of 1 mm/yr is equally defensible, so we will also consider this correction in our modeling of the data, below. Note that with 2 mm/yr subtracted from the raw data in Figure 4.1, most but not all of the sites display rates of slow vertical deformation opposite in sense to the deformation of 1935. In the following discussion we will use the average rates of emergence and submergence shown in Figure 4.19.

4.5.1.2. Justification for dividing the century into three periods

Most of the site records show that rates of slow vertical deformation have not been constant throughout the century. For example, at Bendera the average rate of submergence in the three decades prior to 1935 was about 4 mm/yr (Fig. 4.19a). Within this period, decadal rates varied from as little as 1 mm/y to as much as 10 mm/yr. In the three decades between 1935 and 1961, the average rate was 7 mm/yr. And in the four decades following 1962, the average rate of submergence was about 1 mm/yr. In fact, 1935 and 1962 demarcate natural divisions in the history of vertical deformation for more than half of the sites. We thus separate our discussion of the records into three periods, pre-1935, 1935 to 1962, and post-1962.

4.5.2. Paleogeodetic evidence for deformation in the intervening decades

Below, we will discuss the paleogeodetic evidence of slow deformation in the intervening decades, beginning with the five decades prior to 1935.

4.5.2.1. Decades prior to 1935

In the decades prior to 1935, all but the westernmost site were uplifting (Fig. 4.20). Lago, the site with the greatest measured submergence in 1935, was experiencing the highest rate of uplift, 3.1 mm/yr. Bendera, the site with the greatest measured emergence in 1935, was experiencing the greatest measured subsidence, 4.1 mm/yr. The hingeline between uplift and submergence ran parallel to the subduction isobaths, except in the southern part of the area, where it turned north-south. The rate of tilt in the submerging region was lower than in the region of emergence. Use of a 1 mm/yr correction, rather than 2 mm/yr would shift the hingeline 5 km or so northeastward, toward the mainland. In either the 1 or the 2 mm/yr case, the hingeline is rather close to the hingeline of the 1935 event in the north, but deviate tens of km westward from the 1935 hinge in the south.

A few of the records contain clear evidence for changes in rate that were precursory to the 1935 earthquake (Fig. 4.19a, 4.1b, 4.1i, and 4.1m). Submergence at Bendera, for example, accelerated from about 1 to 8 mm/yr. Badgugu changed from an emerging to a submerging site. The rate of emergence at Memong slowed from about 3.3 mm/yr to near-zero. At Lago, emergence of about 4 mm/yr switched to submergence of about 4 mm/yr. These changes in the few years prior to the 1935 earthquake hint at

changes in the rate of slip on the subduction interface just before failure of the interface during the earthquake.

4.5.2.2. Decades between 1935 and 1961

The pattern of post-1935 rates is grossly similar to the pre-1935 pattern (compare Fig. 4.20 with 4.21). In both periods, tilt toward the southwest is predominant. However, post-1935 rates of submergence are nearly double the pre-1935 rates (Fig. 4.21). Another difference is the markedly higher rate of tilt across the northeastern third of Tanabala Island, near the hingeline, than to the southwest. Moreover, the deviation of contours in the southern part of the region is absent in the post-1935 period.

Post-1935 vertical deformations in the region of large co-seismic submergence, around Tanamasa Island, are unrecoverable, because most of the microatolls took more than a decade to grow up to their new HLS level. Nonetheless, contouring of submergence rates in the surrounding regions suggests that this region was sustaining tectonic emergence in the decades after the earthquake.

It is also important to note that the post-1935 data reveal few if any changes in rate in the two and a half decades after the earthquake. Thus a viscous response to the coseismic rupture and re-distribution of stresses seems to be absent. All of the well-constrained sites show that the rate of deformation remained constant (Fig. 4.1). The only exception to this is the Barogang site, where an immediately post-seismic rate of submergence of 6 mm/yr gradually rolls over into a 1.4 mm/yr rate of emergence by 1962 (Fig. 3.15c). This record also suggests that the rate of submergence in the year or two after 1935 could have been as high as 13 mm/yr. This record may be significant, because

it is one of only two good post-1935 records very close to the hingeline of the 1935 event. It suggests that rates of slip on the subduction interface may have varied over a couple of decades near the downdip tip of the rupture. Nonetheless, this would have to be a very local effect along just a part of the hingeline, because the other record from near the hingeline, at Pono, does not indicate a similar transient. Since the Barogang record must be recording only a very local transient, we ignore it in the modeling efforts presented below.

4.5.2.3. Decades between 1962 and 2000

This latest of the three interseismic periods contains the most complete record of vertical deformation. An HLS record for this latest period exists from almost all of our sites (Fig. 4.1). In map view, the data show a pattern of deformation that is broadly similar to that of the previous interseismic periods—southwestward tilt of the islands (Fig. 4.22). However, there is a significant difference. The modern rate of submergence near the southwestern coast of Tanabala is a mere 1 to 2 mm/yr, rather than the 4 and 7 mm/yr rates documented for the pre- and post-1935 periods. The trend of the hingeline between regions of emergence and submergence is very well constrained to be parallel to the trench and the isobaths of the subduction interface. As for the post-1935 period, there is no clear indication of time-dependent changes in rate since 1962.

Patterns within the area of emergence are also clearer than they are for the preand post-1935 periods. Two features stand out. First, very high emergence rates are occurring just off the east coast of Tanamasa. Although there are no data farther east, except along the coast of Pini island, we depict these sites of high uplift on or near the axis of a northwest-plunging ridge of emergence. Second, another ridge is demarcated by the three sites on and near Pini Island. This feature is interesting because it is nearly parallel to the long-axis of the Island, rather than parallel to the trench or outer-arc ridge.

Figure 4.22 is a map that shows the data for the modern period with a 2 mm/yr hydro-isostatic sea level correction. The figure also shows the kinematic behavior of the subduction interface that we think is responsible for the deformation pattern. In the next section, we invert the data for an optimum model of slip on the interface.

4.5.3 Elastic modeling of slow deformation in the three periods: pre-1935, 1935–1962, and post-1962

We model slow deformation using a 2-D elastic dislocation model, described in *Sieh et al.* [1999]. Elastic dislocation models have been used frequently to explain the observed surface deformation above subduction zones. They appear to provide good explanations of the kinematic behavior of subduction zones [*Kanamori*, 1973; *Savage*, 1983; *Savage*, 1995; *Thatcher*, 1984b; *Zachariasen et al.*, 2000].

We do not model these interseismic data with the standard procedure, first proposed by *Savage* [1983], in which aseismic and interseismic deformation is modeled as normal slip on the locked or partially locked portion of the interface superimposed upon a creeping interface. Instead, we explore different kinematic model, in which the slab descends between a lower and an upper interface into mantle asthenosphere. This model has significant limitations, of course, since it does not include post-seismic relaxations or other time-dependent effects. For example, our assumption of elastic behavior below about 30 km is surely unrealistic. Nonetheless, this is our first step

toward more geologically reasonable modeling of the subduction process. In the elastic modeling that we present here the shallow portion of the upper slipping surface may slip either seismically or aseismically.

The convergence rate V_{plate} is fixed at 4 cm/yr as constrained by the GPS data and global plate models. That is, we fix the downdip portion of the interface to slip continuously at 4 cm/yr. The slab thickness is arbitrarily set to 15 km thick at the trench, and it goes to zero at depth about 160 km, for reasons of mathematical convenience (Fig. 4.23a). Setting the thickness at 30 km will give solutions nearly identical to those produced by the 15 km thick model. This is because the interfaces at the top and a bottom of the slab produce signals that are nearly mirror images, and nearly cancel each another along most of the slab (Fig. 4.23b). In the limit of a slab thickness of zero, slip on the top and bottom interfaces will exactly cancel each another, and the model will be identical to the usual back-slip model [Savage, 1983].

The inversion searches for the best fit to the three or four remaining free parameters: the downdip distance from the trench to the updip tip of the principal locked zone (D_{lock}), the distance from the trench to the patch that is steadily slipping (D_{slip}), and the amount of slip on the different patches (Fig. 4.23a). To reduce free parameters, we initially fix D_{slip} at 27 km depth, because this coincides with the downdip limit of rupture in 1935. But if we cannot find a suitable fit to the data, we let D_{slip} vary.

4.5.3.1 Modeling of deformation rates prior to 1935

Figure 4.24 shows two models that best fit the pattern of slow deformation recorded by the microatolls in the decades prior to 1935. In each case, good solutions can be found in which the downdip limit of the principal locked patch is fixed at 125 km from the trench axis (i.e., $D_{\text{slip}} = 27 \text{ km}$). Farther landward slip on the interface, below D_{slip} , is at the assigned convergence rate (40 mm/yr). With these two parameters fixed, the three free parameters are the location of the updip tip of the locked patch (D_{lock}), the creep rate on the interface outboard of the locked patch (V_{out}), and the rate of creep on the "locked" patch (V_{plate}). In one case (Panel A) we assume a 2 mm/yr correction for hydro-isostatic sea level rise. In the other case (Panel B) we use a 1 mm/yr correction.

In both cases the "locked" patch is slipping at more than half of the plate rate and the interface farther outboard is slipping faster than the plate rate. The model in which we used the greater hydro-isostatic correction has lower submergence rates, and thus lower slip rates on both sections of the interface. These inverse solutions are tightly constrained by the observed peak emergence at Memong (Mm) and Lago (Lg). For example, if we fully lock the shallow (red and orange) patches, the predicted peak emergence value will increase to about 7.5 mm/yr, greatly overestimating the observed values. Moreover, the slope and magnitude of the submergence trough between Memong (Mm) and Bendera (Tb) places tight constraints on the amount and the proportion of the aseismic slip on the red and the orange patches. More sophisticated sensitivity tests seem unwarranted at this point, since we plan to move beyond simple elastic modeling to more rheologically realistic modeling in the near-future.

In the decade or so before the 1935 event, all three sites with high rates of either subsidence or uplift experienced large changes in rate. At the one site with a high pre-

1935 rate of submergence, Bendera, the submergence rate doubled, to about 8 mm/yr (Fig. 4.19). At Memong and Lago, long-term emergence of about 3 mm/yr and 4 mm/yr changed to about nil and 4 mm/yr submergence, respectively. This increase in the magnitude of the pre-1935 submergence peak implies that either the edge of the locked patch migrated downdip, the subduction interface outboard of the islands was creeping even faster in the final years before the earthquake, or the creep rate of the 1935 patch decelerated, or some combination of these three changes occurred. We suspect that the drop in the peak emergence rate at Memong and Lago (farther inboard) indicates that the eventual 1935 coseismic patch began to creep even faster before the earthquake. This would not be a novel or surprising observation, since accelerated slip before major seismic events has been observed in Japan [Kanamori, 1973; Stuart, 1988].

As data are scarce, we do not attempt to model quantitatively this short-lived preseismic deformation. Nevertheless, we can envision that the accelerated submergence at Bendera might well be due to migration of the downdip edge of the orange patch (Fig. 4.24) toward Bendera and/or accelerated creep on that patch. The diminishment of emergence at Memong and Lago could be attributed to updip migration of the D_{slip} . To produce the large submergence signal at Lago, however, might require creep acceleration on the soon-to-fail patch.

4.5.3.2 Modeling of deformation rates for the period from 1935 to 1961

The location of the hingeline separating domains of emergence and submergence in the post-1935 period differs no more than 5 km from that of the pre-1935 deformation (cf. Fig. 4.20 and 21). Therefore, we feel justified in starting our model iterations with

the same initial condition, namely that the updip edge of the fully creeping dislocation be fixed at 27 km depth, nearly beneath the hingeline. We could not, however, achieve a good fit to the emergence rate at either Masin or Memong with this constraint (Figs. 4.25a and b). An alternate model, in which the updip tip is allowed to move to a position 115 km from the trench, fits both points much better (Fig. 4.25c). This optimized model also has a boundary between a fast-creeping patch and a slowly-creeping patch 100 km from the trench.

The two principal differences between the behavior of the interface before and after the 1935 earthquake are these: 1) The central third of the 1935 coseismic patch stopped creeping at a high rate after the earthquake (the model yields a rate of 9 mm/yr).

2) The rate of slip on the patch between the trench and the islands slowed to about the plate rate after the earthquake. The high pre-1935 rate of slip within the lower third of the 1935 rupture continued after the earthquake. Another difference in the pre- and post-1935 records is in the behavior of the southernmost site, Badgugu (cf. Fig 4.20 and Fig. 4.21). In the post-1935 period, the rate of submergence of this site was more in line with the other sites, that is, the post-1935 Badgugu data does not require the southerly swing in the submergence contours like that seen in the pre-1935 data.

4.5.3.3 Elastic modeling of deformation rates for the period 1962-2000

Since the modern deformation rates around Tanabala and Tanamasa do not vary much along strike, we are well justifying to using a 2-D inversion. We exclude the two points from the reefs of Pini Island, since these data clearly reflect some other process. Each panel in Figure 4.26 shows a 2-D inversion of the modern data. In panel A, we lock

the entire interface between the trench and a point 135 km downdip. This fully locked scenario is unacceptable because it violates the low submergence rate at the westernmost point (Tb).

To produce a better fit to the data, we must allow some slip on the 1935 patch and a high slip rate on the patch farther outboard. The models depicted in Panels B and C fit the data much better. One uses a 2 mm/yr and the other a 1 mm/yr hydro-isostatic correction. In the class of models represented by these, the downdip limit of the locked patch is quite stable at 27 km depth, 125 km downdip from the trench. Recall that this is the lower limit of the 1935 rupture. In both optimal inversions, however, the outboard creeping section intrudes down dip into the 1935 coseismic patch, leaving a slow-slipping patch that is only about 12 to 17 km wide.

A comparison with the best-fitting models for the prior period, 1935–1961, shows only one principal difference in behavior between the two periods. Before 1962 the outboard patch was slipping at a rate near or slightly in excess of the plate rate. After 1962, the rate on the outboard interface dropped to only about half the plate rate, but extended about 10 km farther downdip.

4.6 Summary of Paleogeodetic records and of elastic models

Having analyzed individually the 1935 historical earthquake, the 1962 aseismic events, and all of the interseismic periods, we can now synthesize the paleogeodetic evidence and develop a plausible kinematics history of the subduction interface for the entire 20th century.

Figure 4.27 is a summary of vertical deformations during the 20th century. The main features are these:

- In the decades prior to the 1935 rupture (Fig. 4.27a) the islands tilted slowly trenchward. Submergence was highest in the west (up to 4 mm/yr, after correction for 2 mm/yr global sea level rise). Emergence was highest in the east. The hingeline ran NW–SE, except in the south, where it ran N-S through Tanabala Island. Deformation rates appear to be higher in the 5 to 10 years prior to 1935.
- During the 1935 earthquake (Fig. 4.27b) the islands tilted northeastward. The hinge line separating domains of emergence and submergence coincided with the pre-1935 hingeline in the north. The highest recorded coseismic emergence was at Bendera (90 cm). This site was experiencing the highest recorded submergence rate prior to 1935. The highest recorded coseismic submergence was at Lago (34 cm). This site was experiencing the highest recorded emergence rate prior to 1935.
- In the 25 years after the 1935 earthquake (Fig. 4.27c) the islands resumed their trenchward tilt but at rates much higher than before 1935. The hinge line appears to be coincident with that of the 1935 event. The tilt rates in the west were almost twice as fast as in the decades prior to 1935. The highest recorded emergence rate at Lago (1.5 mm/yr) is about half of that recorded in the decades prior to 1935 (3.1 mm/yr).

- Emergence during the 1962 aseismic event (Fig. 4.27d) varied from 2 to about 13 cm throughout the islands. The contouring of these values reveals double-ridge emergence. The western ridge crest ran above the 1935 rupture (in the middle of Tanabala Island). The eastern ridge crest ran about 15 km east of the submergence maxima of the 1935 event. The ridges plunge northeastward.
- The values of the subsequent submergence event in 1962 (Fig. 4.27e) are twice as large as the values of the preceding emergence. The double trough pattern of submergence is nearly a mirror image of the preceding double-ridge emergence. The troughs plunge southeastward.
- The pattern of southwesterly tilt continued after the 1962 event, but its rate changed markedly (Fig. 4.28f). Submergence in the west resumed but at a rate markedly lower than in the preceding decades. The highest submergence rate at Bendera decreased from 7 mm/yr to only ~1 mm/yr. The hinge line separating domains of emergence and submergence remained along the northeastern part of Tanabala Island: it was indistinguishable from the hinge lines of the slow deformation of 1935–1962 and of the 1935 event.

Figure 4.29 presents a summary of our best fitting 2-D elastic dislocation model for each interval. These models are not unique solutions. We have used a routine that search for plausible elastic-dislocation solutions using both 2 mm/yr and 1 mm/yr baseline corrections (for the global sea level rise). The models presented here are our most plausible model using 2 mm/yr baseline correction. The models with 1 mm/yr

baseline correction indicate a similar history. The main features of this first, simple attempt to model the data are these:

- In decades prior to the 1935 rupture (Panel A) the interface outboard of the islands may have been slipping at a rate slightly higher than the plate rate. The soon-to-fail patch beneath the islands was slipping aseismically at half of the long-term plate rate or slightly faster. The collapse of the pre-1935 emergence peak and deepening of the submergence trough in the decade prior to the earthquake suggests that the rates of slip on both patches increased significantly before the seismic rupture.
- During the 1935 earthquake (Panel B) the interface beneath Tanamasa and Tanabala, 88 km to 125 km from the trench axis, slipped about 2.3 m. An additional few tens of centimeters of slip on the shallower part of the rupture would produce a better fit to the westernmost point. These source parameters are consistent with the seismic inversion of Rivera et al. [2002], except that our value of slip is a few tens of percent greater. This may be due to the fact that the paleogeodetic measurements span more than just the seismic interval. Hence, the inversion of the coral data may include up to a year of post-seismic slip on the coseismic patch.
- In the 25 years after the 1935 earthquake (Panel C) the slip rate on the patch outboard of the islands continued at about or slightly greater than the plate rate. The core of the 1935 patch, a section only about 20 km wide, appears to have been fully locked during this period, but the updip portion of the 1935 patch was slipping at about plate rate.

- The double-ridged emergence event of early 1962 (Panel D) can be explained by slips of about 50 cm and 170 cm on two narrow patches beneath Tanamasa and Tanabala and by slip of about 120 cm on a 20 km wide patch much farther downdip, beneath the eastern part of Pini Island. The scatter in the data indicates that the two shallower patches were in the middle of and at the downdip limit of the 1935 coseismic rupture. The magnitude of slip is probably overestimated, given that an ENSO/IOD event in 1962 likely contributed to the emergence signal. Also, the 3-D character of the event means that the model parameters should be considered average values. Slip was greater to the southeast and less to the northwest.
- The double-troughed submergence that occurred later in 1962 (Panel E) could have been produced by an average slip of about 170 cm of slip on the subduction interface outboard of the islands and an additional 100 cm of slip on a smaller patch beneath the eastern part of Tanamasa Island. The outboard patch also involved the shallowest 15 km or so of the 1935 rupture. The smaller patch straddles the downdip edge of the 1935 rupture. As with the 1962 emergence event, the submergence in 1962 displayed a 3-D pattern. Thus our estimated values should be viewed as averaged values. Slip was greater to the southeast and smaller to the northwest.
- The behavior of the subduction interface changed abruptly after the
 1962 event. Panel F illustrates the behavior between 1962 and 2000.

Slip outboard of the islands abruptly slowed down to about half of the plate rate. The lower half of the 1935 patch began to creep again, at a rate of about 1 cm/yr.

Modeling of these paleogeodetic records is ongoing. We are planning to employ a broader range of models in the future, but those are beyond the scope of this thesis. The future models, for example, may allow upper mantle relaxation, visco-elastic deformation, and the dynamics of fault friction. We may also consider fitting the paleogeodetic data of each site more rigorously, although this would require modeling that would be able to produce time-series of vertical deformations that match the data of each site. It is obvious, then, that the present modeling results are provisional and might be improved. Our first attempts to explain the data do seem to demonstrate non-stationary of subduction processes in both space and time, and that a dense geodetic network operating over several decades would likely uncover more highly resolved spatio-temporal variations.

4.7. DISCUSSION

A primary goal of this thesis is to provide high-quality geodetic data that are applicable to the development and testing of theoretical models of the earthquake cycle. Data bearing on this phenomenon are rare. Previous data from other subduction zones include geodetic records from tide gauges and leveling from the Nankai trough, collected in the decades prior to and after the 1946 Nankaido earthquake [*Thatcher*, 1984a]. In the present study, we have succeeded in documenting the 20th-century paleogeodetic behavior of the Equatorial section of the Sumatran subduction interface.

Our coral records show that rates of vertical motions have varied markedly over the span of the 20th century (Fig. 4.27). We have used simple elastic dislocation models of the subduction interface to provide plausible interpretations of these records. This modeling is only the beginning of our effort to interpret the data. Further sensitivity analysis will be required to quantify the uncertainty of these models. We will also attempt to employ other types of modeling to interpret our data. Before heading to more sophisticated modeling, we now want to use the results of our initial elastic modeling to speculate on the significance of the data.

The elastic dislocation modeling basically suggests that the behavior of the subduction interface above a depth of about 30 km has varied markedly in time and space. Individual locations on the interface appear to have changed their behavior after the 1935 and 1962 events. Locations that ruptured seismically in 1935 slipped aseismically during other events and periods. What does this variability reveal about the nature of subduction processes, not only in western Sumatra but more generally as well?

To address this question, we divide the discussion into four parts. First, we construct a century-long slip budget for the shallow interface, to help visualize the behavior of the interface throughout the century and to see how the various sections are "spending" strain accumulations. Second, we then discuss possible rheological reasons for the behavior of the interface. Third, we propose a structural reason for the difference between the behavior of the Equatorial section of the interface and the long section to the southeast. Finally, we consider this record in the context of a burgeoning set of observations from other subduction zones in which transients have been recognized.

4.7.1. Expenditure of the subduction slip budget throughout the 20th century

Recent GPS geodetic measurements show that, by and large, decadal rates of strain accumulation across entire plate boundaries do not differ from plate rates averaged over a million years or so [Gordon et al., 1990; Larson et al., 1997; Larson et al., 1999; Royer et al., 1997]. Thus, rates of strain accumulation across entire plate boundaries do not appear to vary over a broad range of time scales.

However, within plate boundary zones, the varied behavior of structural elements complicates this perspective. Strain accumulation equals strain relief only if a fault's decadal slip rate accommodates all the strain accumulated during the decade (e.g., as along the central, creeping reach of the San Andreas fault [*Lisowski and Prescott*, 1981]). But most faults do not balance their accounts this frequently. Periods of strain accumulation without rupture may continue for centuries to millennia, and most strains may be relieved by slip that occurs in just seconds to days. These centennial and millennial imbalances between strain accumulation and relief within plate boundary regions are poorly understood, because data on serial fault rupture and strain accumulation over centuries and millennia are sparse.

The data we have obtained allow us to gain an increment of insight into the matter. Figure 4.29 shows a slip budget for the Sumatran subduction interface, based upon the elastic modeling of the previous section. The x axis is the distance downdip from the trench and the left y axis is slip that accumulated during the 20th century, according to the models in Figure 4.28. Faster slip events appear as warmer colors, and

periods of slower slip appear as cooler colors. The right-hand y axis shows the status of the interface relative to the slip that would have accumulated at the long-term plate rate. For example, the deeper part of the interface, more than about 130 km from the trench, experienced 100% of this amount, because we fixed its rate of slip at the long-term and GPS rate of 4 cm/yr.

The salient points of this display of the modeling results are these: The updip, shallow parts of the subduction interface have slipped significantly more than would have been produced by a century of slip at the plate rate. The nominal slip of this section is about 50% greater than would have accrued at the plate rate. Assuming a higher plate rate (e.g. 5 cm/yr) in the modeling will, however, will lower the difference. A large fraction (1.7 m) of this slip occurred during the submergence phase of the 1962 rapid slip event. Without this event, the cumulative slip for the century would have nearly equaled the 4 m predicted by the plate rate.

The edges of the patch that failed seismically in 1935 also experienced an amount of slip in excess of the 4 m that would have been produced by slip at the plate rate. Most of this excess (2.5 m) results from the seismic slip of 1935. But substantial slip (1.2 to 1.7 m) occurred during the submergence phase of the 1962 episode.

Only two small sections in the interior of the 1935 patch exhibit less slip than would have accrued at the plate rate. Neither of these thin patches experienced slip during the 1962 episode, and rates of aseismic slip in the decades before, during and after 1935 and 1962 were much less than the plate rate.

Balancing the excess of 20th-century slip along the shallowest section of the interface requires that the rate of slip be lower during a previous period. During the first

61 years of the century, the shallow section of the interface accumulated about 90 cm more slip than would have been required by plate convergence at 4 cm/yr. In the 1962 event, this interface slipped about 160 cm. From 1900 to 1962, the total slip accumulated on this interface, then, is 250 cm. Thus, it is reasonable to hypothesize that in the period 1900–1962 the interface relieved strains that had accumulated at the plate rate during at least the prior 60 years (i.e., 250/4 years). This estimate of accumulation time would increase by a factor of 3 (4/(4-2.7)), to about 180 years, if one assumes that the shallow interface was creeping at its current rate of 2.7 cm/yr prior to the 20th century. These calculations suggest that the rapid creep episode of 1962 does not repeat very often, perhaps only every other century or so. It is also seems likely that lengthy periods of excess slip, as occurred in the decades prior to and following the 1935 event, are rare.

The slip deficit that accumulated on the 1935 patch in the 35 years prior to the 1935 earthquake was about 50 cm, because the patch was slipping at about 2.5 cm/yr ((4-2.5)*35). At this rate, an additional 130 years would be required to accumulate strains that could result in 2.5 meters of seismic slip. We will see in the next chapter that this estimate is quite consistent with the date of the previous rupture of the 1935 patch, AD 1797.

The greatest excesses of 20th-century slip are on the upper and lower edges of the 1935 rupture patch. These sections experienced slip during both the 1935 and 1962 events and creep in the adjoining periods. The fact that these two regions of excess slip are on the edges of the 1935 rupture suggests that they may be the products of stress concentrations produced by the 1935 rupture.

The only sections with a 20th-century slip deficit are in the core of the 1935 rupture patch, where slip after 1935 has been nil or very slight (Fig. 4.29). The simplest hypothesis is that this section is accumulating strain that will be relieved in the future by either seismic or rapid aseismic slip. At current rates of aseismic slip (about 1 to 2.7 cm/yr), another 40 to 150 years would be needed to store strains that would be relieved by another 1935 event with 2.5 meters of slip.

The variation of slip behavior as a function of distance along the interface shows that calculations of a *percentage or a fraction of aseismic slip* for sections of this subduction interface must allow for variations down dip as well as along strike. The fraction of aseismic slips between the trench to 90 km downdip or so is 1.0 (or more). It also appears to be 1.0 farther downdip than about 130 km from the trench. The fraction of aseismic slip on the 1935 patch averages about 0.6 (i.e., 60% of the plate convergence is accommodated by aseismic slip on the 1935 patch), but the values varies within the patch and with time.

In conclusion, our 2-D elastic modeling, which explain our paleogeodetic data well, strongly suggests variations of slip behaviours on the subduction interface in both space and time. However, we are aware that we have not taken into account 3-D structure or variations of paleogeodetic data along the strike in our models. Therefore, such attempt will be warranted in the future.

4.7.2. Implication of paleogeodetic behavior for rheology of the subduction interface

The rheology of a subduction interface is strongly controlled by temperature, fluid pressures and mineralogical assemblages [e.g., *Hyndman et al.*, 1995; *Oleskevich et al.*, 1999]. These factors, in general, divide the subduction interface into three major zones: (1) an upper slow-slip zone, (2) a middle locked, seismic zone, and (3) a lower stable-sliding zone [*Hyndman and Wang*, 1995; *Kodaira et al.*, 2002; *Oleskevich et al.*, 1999]. This subduction zonation seems to explain adequately many observed deformations [e.g. *Dragert et al.*, 1994; *Freymueller et al.*, 2000; *Hyndman and Wang*, 1995; *Kanamori*, 1973; *Kodaira et al.*, 2002; *Oleskevich et al.*, 1999; *Thatcher*, 1984a].

The shallowest part of subduction zones are dominated by accreted unconsolidated sediments from the subducting oceanic crust [Goldfinger et al., 1996; Shreve and Cloos, 1986]. This outermost part of the interface is commonly capped by water-rich clays (e.g., smectites) and is highly overpressured, due to abundant trapped fluids from the overlying sediments and from the ocean. These weak-clay materials coupled with high pore pressures promote stable sliding [e.g. Moore and Saffer, 2001]. Thermal studies from subduction zones in southwest Japan, Alaska, and Chile show that the threshold temperature for the lower limit of this aseismic zone is about 100° to 150°C (4 to 10 km depth) [Hyndman et al., 1995; Moore and Saffer, 2001; Oleskevich et al., 1999]. Greater temperatures allow diagenetic to metamorphic processes, which release significant amounts of fluid from the subducted materials into pore space. In the process, zeolites and calcite replace the water-rich clays in the fault zone, and sediments above and under the interface become more dense by diagenetic cementation [Moore and

Saffer, 2001]. This transformation alters the mechanical behavior of the interface from aseismic (stable slip) to seismic (stick-slip), or from velocity strengthening to velocity weakening behavior [*Scholz*, 1990].

The downdip edge of the seismogenic zone (the lower brittle-ductile transition) generally reaches a temperature of about 350°–450° C [Hyndman et al., 1995; Oleskevich et al., 1999]. Below the seismogenic zone, convergence is generally accommodated by stable sliding [Hyndman et al., 1995; Kasahara et al., 2001; Oleskevich et al., 1999]. High-resolution tomography, seismic reflection surveys, and magnetotelluric studies reveal that this stable sliding is associated with a low-resistivity and highly reflective layer at the base of the overriding continental crust [Kodaira et al., 2002]. This is interpreted to be a water/fluid rich layer that is generated by dehydration of the downgoing, partially serpentinized upper mantle.

Modeling of our paleogeodetic data may suggest that these major mechanical boundaries of the interface are present, but may have not been stationary. The models may also suggest that fault patches do not have characteristic slips throughout the earthquake cycle (Fig. 4.28). For example, the upper and lower edges of the patch that ruptured seismically in 1935 re-ruptured in the 1962 slow event. The patch outboard from the islands that experienced stable slip for decades prior to and after the 1935 event slipped about 1.5 m during the 1962 event. The central part of the 1935 rupture zone, which slipped at more than half of the plate rate in the decades prior to 1935, ceased slipping after 1935. In 1962, slip on the 1935 patch accelerated to a rate of about a quarter of the plate rate, but this is still slower than the rate in the decades prior to 1935. The decadal to centennial changes in the behaviors of the interface seems to contradict

the notions that fault slips are characteristic, and that boundaries of stable and unstable sliding are fixed throughout an earthquake cycle [e.g. *Pacheco et al.*, 1993; *Thatcher*, 1984a]. The results of our 2-D model remains to be seen, however, since we have not yet explore a broader spectrum of modeling including 3-D aspects of rheological behaviour; but it is beyond this thesis.

Our paleogeodetic time series indicates that processes operating on and around the subduction interface changed markedly during the 1935 and the 1962 events. What conditions could have caused this? We have not investigated this phenomenon quantitatively, but we speculate that the slip events could have generated enough heat to alter the properties of the interface. In support of this hypothesis, previous studies show that a seismic rupture may only generate a very thin fault gouge or cataclastic rock plane, up to several millimeter width [Evans et al., in progress; Schulz and Evans, 2000]. This suggest that a moderately-sized slip event can generate a significant amount of heat in the fault zone [Kanamori and Heaton, 2000]. They show an example, assuming modest values of friction on the interface, in which the slip during a M=5 to 7 earthquake may raise temperatures by 1000°C and cause frictional melting. Heating of fluids within the fault zone may also lead to a change in properties. A small (100°-200°C) increase in temperature of the fluid in a fault zone may be large enough to elevate pore pressures and thus reduce the coefficient of friction of the fault surface to a lower value—one at which a M=3 to 7 earthquake can occur [Kanamori and Heaton, 2000]. Thus, it is plausible that large slip events, such as those in 1935 and in 1962, are capable of generating sufficient heat to modify the behavior of the subduction interface. One wonders how persistent this

change would be, of course. Would it last a decade or more? It must if is to explain the changes we have observed.

Despite evidence of complexities in subduction behavior, our models indicate that the shallowest parts of the interface from the trench to about 90 km landward (~15 km depth) has been slipping aseismically throughout the 20th century. This upper section, then, may represent an upper aseismic zone, such as postulated by standard subduction models [Kasahara et al., 2001; Kodaira et al., 2002; Moore and Saffer, 2001; Oleskevich et al., 1999]. The predicted major slip on this patch during the 1962 event, however, suggests that this outboard interface does not necessarily slip by continuous stable sliding, but is also capable of generating a cycle of strain accumulation and rapid aseismic release. This may indicate that the interface has a varying frictional strength.

Furthermore, our model tightly constrains the downdip edge of the 1935 rupture to a depth of about 25 km. The principal locked patches before and after 1935 can also be well fit by a downdip limit at 25 km. What kind of structure or rheology controls the downdip edge? Seismic refraction surveys around Nias, north of the Equator, revealed that the continental Moho is at about 25 km depth there [*Kieckhefer et al.*, 1980]. More recent seismic reflection surveys offshore of southern Sumatra also found the Moho to be at this depth [*Kopp et al.*, 2001]. Thus, it appears that the downdip edge of the seismogenic patch may correspond to the depth of the Moho. However, if the overriding crust bends down toward the subducting slab, the downdip edge of the locking may intersect the base of the upper crust rather than Moho. If so, this would be similar to the relationship observed in the Nankai subduction zone [*Kodaira et al.*, 2002].

In summary, our paleogeodetic model largely agrees with the general subduction model that postulates three major divisions of the subduction interface characterized by different mechanical behaviors [Kasahara et al., 2001; Kodaira et al., 2002; Moore and Saffer, 2001; Oleskevich et al., 1999]. Our model may suggest that the boundaries of these zones are not stationary, however, and that their percentage of aseismic slip may vary with time.

We have not yet tried to incorporate visco-elastic phenomena, such as mantle relaxation, into our model. However, the fact that linear regressions fit most of the HLS time series in the periods between events strongly suggests that rates of deformation in the intervening decades are not dependent on the time since perturbation by the seismic rupture of 1935 and the rapid aseismic events of 1962. Thus, the presence of viscous materials at the interface and the readjustment of the upper mantle appear to have negligible effects, given that they do not appear to influence the paleogeodetic time series.

4.7.3. Structural reasons for the contrast between the Equatorial patch and the interface farther south

Modeling of our paleogeodetic records suggests that the Sumatran subduction zone between 0.5°N and 1°S is largely aseismic. For the past four decades, the fraction of aseismic slip on the interface above 22 km and between 22 and 27 km depth are approximately 0.7 and 0.2 respectively (Fig. 4.26). On average, the fraction of aseismic slip on the shallow interface (above 27 km depth) is ~0.6. This is consistent with results from a campaign-style GPS study, undertaken from 1989 to 1994 [*Prawirodirdjo*, 2000;

Prawirodirdjo et al., 1997]. The GPS vectors showed that the islands at and north of the Equator moved sub-parallel to the trench during that period. Modeling of these vectors suggested that about 60% of the slip on the interface occurred aseismically (i.e., only 40% of the convergence is being stored as elastic strain) [Prawirodirdjo, 2000; Prawirodirdjo et al., 1997].

In contrast, the GPS vectors from stations on the islands south of the Equator showed movement in the direction of the relative motion of the subducting oceanic plate [Prawirodirdjo et al., 1997]. Modeling of these motions suggests that the subduction interface south of the Equator is fully locked [Prawirodirdjo et al., 1997]. This GPS result is consistent with the paleogeodetic model of subduction in this southern region [Zachariasen et al., 2000]. It is also consistent with the fact that this section of the interface generated a giant earthquake in 1833 [Newcomb and McCann, 1987; Zachariasen et al., 1999].

Prawirodirdjo et al. [1997] proposed that the high fraction of the aseismic slip of the northern region corresponds to the northwestward increase in the thickness of Bengalfan sediments in the trench [Curray et al., 1980]. They argued that subducting thick unconsolidated sediments expelled extra water into the subduction zone and thereby increased pore pressure and reduced normal stress on the interface. This observation alone, however, may not adequately explain the abrupt change in coupling and the coincidence with the disruption of fore arc structures (Chapter 2).

We suggest that the largely aseismic behavior between 0.5°N and 1°S relates to the impingement of the Investigator fracture zone (IFZ). Since the relative plate motion is about 7° more easterly than the axis of the IFZ, the junction of the IFZ at the trench has

been migrating southeastward along the trench. The eastward component of this is approximately 7 mm/yr (Fig. 4.30). During this migration the buoyancy and the topographic irregularity of the IFZ might well have led to the disruptions of the hanging wall block and the destruction of asperities on the subduction interface, as has been proposed for the subducting Nazca ridge along the Peruvian subduction zone [Spence et al., 1999]. In addition, hydrous minerals may have risen from the upper mantle and piped through the subducting IFZ and the WFSR to create a weaker interface [LeFevre and McNally, 1985; Sieh et al., 1999].

4.7.4. Comparison with other subduction zones

4.6.4.1. Temporal and spatial changes of the subduction behaviors

The concept that boundaries of the "stable" and "unstable" patches on a fault zone remain stationary through several earthquake cycles is mostly hypothetical. Our paleogeodetic data provides evidence that seems to contradict this hypothesis. Evidence from other subduction zones in support of our hypothesis is admittedly sparse. Nonetheless, it appears that some documented earthquake ruptures from other subduction zones overlap one another [e.g. *Ando*, 1975; *Kawasaki et al.*, 2001; *Lowry et al.*, 2001]. The major historical ruptures of the Nankai subduction zone, for example, have not always ruptured just one segment, but ruptured two or more adjacent segments at once [*Ando*, 1975]. The patch that ruptured in the 1944 Tonankai earthquake, in particular, seems to have been a portion of a much larger patch that ruptured in 1707 [*Ando*, 1975]. Of course we cannot put a great deal of confidence in such statements since most of the

findings were based on sparse data. In support of this notion, however, a GPS network in the Tokai region, Japan, recorded an ongoing continuous slow reverse motion since 27 March 2001 around Honsu Island above the Nankai subduction [http://cais.gsi.go.jp/tokai/sabun/index.html]. A preliminary model of these vectors indicates that this aseismic motion involved a slip on the rupture patch of the Tonankai earthquake [Ozawa et al., 2002]. Thus, the recent motions indicate that the "seismic" patch of the 1944 Tonankai earthquake may also slip aseismically. This may indicate that the behavior of the seismogenic zone has changed. However, the accuracy of the analysis in this preliminary report remains to be verified

Transient deformations that occurred before and after major events have been observed in other subduction zones, such as in Nankai [Ando, 1975; Thatcher, 1984a; Thatcher and Rundle, 1984] and Alaska [Freymueller et al., 2000; Savage et al., 1998]. In Nankai, the submergence rate, based on leveling and tide gauges, was lowest prior to the 1946 Nankaido earthquake. After the event, submergence was at its most rapid; it decayed gradually over the ensuing decades, but remained higher than the pre-1946 rate [Ando, 1975; Thatcher and Rundle, 1984]. This rapid post-seismic transient deformation, as well as its subsequent decay, were interpreted as the consequences of a visco-elastic response transient in the surrounding mantle [Thatcher and Rundle, 1984].

Post-seismic transients were also documented after the 1964 great Alaskan earthquake. The submergence rate averaged over the 10 years following the event (determined by leveling [*Brown et al.*, 1977]) was faster than the rate averaged over the 25 years following the event (determined from tide gauges [*Cohen and Freymueller*, 2001]). This indicates that the post-seismic transient decayed within a decade. From

1974 to 1989, the rate appears to have been linear [Savage and Plafker, 1991]. GPS measurements made between 1993 and 1997 indicate that a few localities in the eastern Kenai moved in reverse (i.e., trenchward) [Freymueller et al., 2000]. This reverse motion is interpreted as a continuing post-seismic response.

4.7.4.2. Variations in subduction behavior along strike (comparison to the Shumagin case)

The behavioral changes along the Sumatran subduction zone may be comparable to those observed in the Alaska-Aleutian subduction zone. The subduction interface subjacent to Kodiak Island, where the M_w9.2 Alaskan earthquake occurred in 1964, is entirely locked [Savage et al., 1999]. The neighboring segment to the southwest, which was the source of a smaller earthquake in 1938 (M_w8.2), appears to have experienced a small fraction (~0.2) of aseismic slip on the interface in the period between 1993 and 1997 [Fletcher et al., 2001]. The next adjacent segment to the south is the Shumagin segment. The GPS surveys from 1980 to 1991 and from 1991 to 1997 recorded very little strain accumulation [Larson and Lisowski, 1994; Lisowski et al., 1988] on this segment. The absence of elastic strain accumulation requires the subjacent interface to slip mostly in aseismic fashion.

Thus the major variation in the behavior of the Alaska-Aleutian subduction zone appears to be somewhat similar to that of the Sumatran zone. The cause of this variation remains unclear. It has been suggested, however, that it may be due to the occurrence of aseismic slip on a portion of the shallow interface [Beavan et al., 1984]. Another suggestion is that it may be due to mantle relaxation in the late stage of the cycle

[Lisowski et al., 1988]. The former may be similar to what could have been occurring in Sumatra.

4.7.4.3. Subducting oceanic ridges

We have discussed the possibility that the appearance of a high percentage of aseismic slip (from paleogeodesy) of the central and northern part of the Sumatran subduction zone is probably related to the subducting IFZ and WFSR since at least 10 million years ago. This is supported by evidence that the subduction of the oceanic ridges around the Pacific Rim appears to have lowered the seismic potential of the subduction zones [Kelleher and McCann, 1976].

It has been observed that a section of a subduction zone upon which an oceanic ridge is impinging shows either a long period of quiescence, less frequent large ruptures, or ruptures of smaller maximum size. Several documented historical ruptures, in fact, appear to have been terminated at points where ridges impinged on trenches [Nishenko, 1991]. For example, the southernmost limits of the great historical ruptures of the Nankai subduction zone coincided with the point where the Kyushu-Palau ridge is currently being subducted. The subduction zones south of this subducting ridge recorded fewer occurrences of large earthquakes.

Oceanic ridge subduction very similar to that of central Sumatra occurs in the South American continent where the Nazca ridge is subducting beneath Peru. The Nazca ridge impinged on the Peruvian subduction about 10 million years ago. Subsequently, it has swept about 800 km southward to its present position [Spence et al., 1999]. The

segment of the subduction zone where the ridge has impinged produces a smaller maximum rupture than does the neighboring segment.

4.8 References

- Ando, M., Source mechanisms and tectonic significance of historical earthquakes along the Nankai through, Japan, *Tectonophysics*, *27*, 119-140, 1975.
- Beavan, J., R. Billham, and K. Hurst, Coherent tilt signals observed in the Shumagin seismic gap: detection of time-dependent subduction at depth?, *Journal of Geophysical Research*, 89, 4478-4492, 1984.
- Berlage Jr, H.P., Aardbevingen, Natuurk. Tijdschr. v. Ned. Ind, 191-192, 1936.
- Bevington, P.R., and D.K. Robinson, *Data Reduction and Error Analysis*, 328 pp., MsGraw-Hill, New York, 1992.
- Boyd, T.M., J.J. Taber, A.L. Lerner-Lam, and J. Beavan, Seismic rupture and arc segmentation within Shumagin Island seismic gap, Alaska, *Geophysical Research Letters*, *15* (3), 201-204, 1988.
- Brown, L.D., R.E. Reilinger, S.R. Holdahl, and E. Balazs, Seismic crustal uplift near Anchorage, Alaska, *Journal of Geophsical Research*, 82, 3369-3378, 1977.
- Clark, J.A., and C.S. Lingle, Predicted relative sea-level changes (18,000 years B.P. to present) caused by late-glacial retreat of the Antarctic ice sheet, *Quaternary Research*, *11*, 279-298, 1979.
- Cohen, S.C., and J.T. Freymueller, Crustal uplift in the south central Alaska subduction zone: New analysis and interpretation of tide gauge observations, *Journal of Geophsical Research*, *106*, 11259-11270, 2001.
- Curray, J., F.J. Emmel, D.G. Moore, and R.W. Raitt, Structure, tectonics and geological history of the northeastern Indian Ocean, *in The Ocean Basins and Margins*, *edited by: A.E. Nairn and F.G. Stehli*, 6, p.399, 1980.
- Deming, W.E., Statistical Adjustment of Data, John Willey and Sons, 260pp, 1964.

- Dragert, H., R.D. Hyndman, G.C. Rogers, and K. Wang, Current deformation and the width of the seismogenic zone of the northern cascadia subduction thrust, *Journal of Geophsical Research*, *99*, 638-668, 1994.
- Dragert, H., K.L. Wang, and T.S. James, A silent slip event on the deeper Cascadia subduction interface, *Science*, *292*, 1525-1528, 2001.
- Engdahl, E., R.v.d. Hilst, and R. Buland, Global teleseismic earthquake relocation with improved travel times and procedures for depth determination:, *Seis. Soc. of Amer. Bull.*, 88, 722-743, 1998.
- Evans, J.P., Z.K. Shipton, K. Robeson, M.A. Pachell, and S.J. Lim, Slip Localization on narrow surfaces within exhumed fault zones: implication for earthquake rupture, in progress.
- Fletcher, H.J., J. Beavan, J.T. Freymueller, and J. Gilbert, High interseismic coupling of the Alaska subduction zone SW of Kodiak island inferred from GPS data, *Geophysical Research Letters*, 28 (3), 443-446, 2001.
- Freymueller, J.T., S.C. Cohen, and H.J. Fletcher, Spatial variations in present-day deformation, Kenai Peninsula, Alaska, and their implications, *Journal of Geophsical Research*, *105*, 8079-8101, 2000.
- Goldfinger, C., L.D. Kulm, R.S. Yeats, L. McNeill, and C. Hummon, Oblique strike-slip faulting of the central Cascadia submarine forearc, *submitted December 10, 1996: J.Geophys.Res.*, 1996.
- Gordon, R., C. DeMets, and D. Argus, Kinematic constraints on distributed lithospheric deformation in the Equatorial Indian ocean from present motion between the Australian and Indian plates, *Tectonics*, *9* (3), 409-422, 1990.
- Gornitz, V., S. Lebedeff, and J. Hansen, Global Sea level trend in the past century, *Science*, *215*, 1611-1614, 1982.
- Heki, K., H. Miyazaki, and H. Tsuji, Silent fault slip following an interplate earthquake at the Japan trench, *Nature*, *386*, 595-598, 1997.
- Hyndman, R.D., and K. Wang, The rupture zone of cascadia great earthquakes from current deformation and the thermal regime, *Journal of Geophsical Research*, *100*, 22133-22154, 1995.

- Hyndman, R.D., K. Wang, and M. Yamano, Thermal constraints on the seismogenic portion of the southwestern Japan subduction thrust, *Journal of Geophysical Research*, *100*, 15,373-15,392, 1995.
- Kanamori, H., Mode of strain release associated with major earthquakes in Japan, *Annual Review of earth and Planetary Sciences*, 1973.
- Kanamori, H., and T.H. Heaton, *Microscopic and macroscopic physics of earthquakes*, American Gephysical Union, 2000.
- Kasahara, J., A. Kamimura, G. Fujie, and R. Hino, Influence of water on earthquake generation along subduction zones, *Bulletin of The earthquake Research Institute, University of Tokyo*, 76 (3), 291-304, 2001.
- Kawasaki, I., Y. Asai, and Y. Tamura, Space-time distribution of interplate moment release including slow earthquakes and the seismo-geodetic coupling in the Sanriku-Oki region along the Japan trench, *Tectonophysics*, *330*, 267-283, 2001.
- Kelleher, J., and W.R. McCann, Buoyant zones, great earthquakes, and unstable boundaries of subduction, *Journal of Geophsical Research*, 81, 4885-4895, 1976.
- Kieckhefer, R.M., G.G. Shor Jr, and J.R. Curray, Seismic refraction studies of the Sunda trench and forearc basin, *Journal of Geophysical Research*, 85, 863-889, 1980.
- Kodaira, S., E. Kurashimo, J.O. Park, N. Tkahashi, A. Nakanishi, S. Miura, T. Iwasaki,
 N. Hirata, K. Ito, and Y. Kaneda, Structural factors controlling the rupture process
 of a megathrust earthquake at the Nankai trough seismogenic zone, *Geophysical Journal International*, 149, 815-835, 2002.
- Kopp, H., E.R. Flueh, D. Klaeschen, J. Bialas, and C. Reichert, Crustal structure of the central Sunda margin at the onset of oblique subduction, *Geophysical Journal International*, 147, 449-474, 2001.
- Larson, K., J. Freymueller, and S. Philipsen, Global plate velocities from the Global Positioning System, *Journal of Geophysical Research*, *102*, 9961-9981, 1997.
- Larson, K.M., R. Burgmann, R. Bilham, and J.T. Freymueller, Kinematics of the India-Eurasia collision zone from GPS measurements, *Journal of Geophsical Research*, 104, 1077-1094, 1999.
- Larson, K.M., and M. Lisowski, Strain accumulation in the Shumagin Islands; Results of initial GPS measurements, *Geophysical Research Letters*, *21*, 497-500, 1994.

- LeFevre, L.V., and K.C. McNally, Stress distributions and subduction of aseismic ridges in the middle America Subduction zone, *Journal of Geophsical Research*, *90*, 4495-4510, 1985.
- Lisowski, M., and W.H. Prescott, Short-Range Distance Measurements Along The San-Andreas Fault System In Central California, 1975 To 1979, *Bulletin of the Seismological Society of America*, 71 (5), 1607-1624, 1981.
- Lisowski, M., J.C. Savage, W.H. Prescott, and W.K. Gross, Absence of strain accumulation in the Shumagin seismic gap, Alaska, 1980-1987, *Journal of Geophsical Research*, *93*, 7909-7922, 1988.
- Lowry, A.R., K.M. Larson, V. Kostoglodov, and R. Bilham, Transient fault slip in Guerrero, southern Mexico, *Geophysical Research Letters*, 28 (19), 3753-3756, 2001.
- Masinha, L., and D.E. Smylie, The displacement fields of inclined faults, *Bull. Seismol. Soc. Amer.*, *61* (5), 1433-1440, 1971.
- Miller, M.M., T. Melbourne, and D.J. Johnson, Periodic slow earthquake from the Cascadia subduction zone, *Science*, *295*, 2423, 2002.
- Moore, J.C., and D. Saffer, Updip limit of the seismogenic zone beneath the accretionary prism of southwest Japan: an effect of diagenetic to low-grade metamorphic processes and increasing effective stress, *Geological Society of America Bulletin*, 29, 183-186, 2001.
- Newcomb, K.R., and W.R. McCann, Seismic history and seismotectonics of the Sunda Arc, *Journal of Geophysical Research*, *92*, 421-439, 1987.
- Nishenko, S.P., Circum Pacific seismic potential: 1989-1999, *Pure and Aplied Geophysics*, *135*, 169-259, 1991.
- Oleskevich, D.A., R.D. Hyndman, and K. Wang, The updip and downdip limits to great subduction earthquakes: Thermal and structural models of Cascadia, south Alaska, SW Japan, and Chile, *Journal of Geophysical Research*, *104*, 14965-991, 1999.
- Pacheco, J.F., R.S. Lynn, and C.H. Scholz, Nature of seismic coupling along simple plate boundaries of the subduction type, *Journal of Geophsical Research*, *98*, 14133-14159, 1993.

- Peltier, W., and A. Tushingham, Global sea level rise and the greenhouse effect: Might they be connected, *Science*, *244*, 806-810, 1989.
- Peltier, W.R., and A.M. Tushingham, Influence of glacial isostatic-adjustment on tide-gauge measurements of secular sea-level change, *Journal of Geophsical Research*, *96* (B4), 6779-6796, 1991.
- Plafker, G., Tectonic Deformation Associated with the 1964 Alaskan Earthquake, *Science*, *148*, 1675-1687, 1965.
- Prawirodirdjo, L., A geodetic study of Sumatra and the Indonesian region: Kinematics and crustal deformation from GPS and triangulation, University of California, San Diego, San Diego, 2000.
- Prawirodirdjo, L., Y. Bock, R. McCaffrey, and e. al., Geodetic observations of interseismic strain segmentation at the Sumatra subduction zone, *Geophysical Research Letters*, 24, 2601-2604, 1997.
- Rivera, L., K. Sieh, D. Helmberger, and D.H. Natawidjaja, A comparative study of the Sumatran subduction-zone earthquakes of 1935 and 1984, *Bulletin of the Seismological Society of America*, *92*, 1721-1736, 2002.
- Royer, J., R. Gordon, C. DeMets, and P. Vogt, New limits on the motion between India and Australia since chron 5 (11 Ma) and implications for lithospheric deformation in the Equatorial Indian Ocean, *Geophysical Journal International*, *129* (1), 41-, 1997.
- Saji, N.H., B.N. Goswami, P.N. Vinayachandran, and T. Yamagata, A dipole mode in the tropical Indian ocean, *Nature*, *401*, 360-363, 1999.
- Savage, J., A dislocation model of strain accumulation and release at a subduction zone, *Journal of Geophysical Research*, 88, 4984-4996, 1983.
- Savage, J.C., Interseismic uplift at the Nankai subduction zone, southwest Japan, 1951-1990, *Journal of Geophysical Research*, *100*, 6339-6350, 1995.
- Savage, J.C., and G. Plafker, Tide-gauge measurements of uplift along the south coast of Alaska, *Journal of Geophysical Research*, *96*, 4325-4335, 1991.
- Savage, J.C., J.L. Svarc, and W.H. Prescott, Deformation across the Alaska-Aleutian subduction zone near Kodiak, *Geophysical Research Letters*, *26* (14), 2117-2120, 1999.

- Savage, J.C., J.L. Svarc, W.H. Prescott, and W.K. Gross, Deformation across the rupture zone of the 1964 Alaska earthquake 1993-1997, *Journal of Geophsical Research*, 103, 21275-21283, 1998.
- Scholz, C., *The Mechanics of Earthquakes and Faulting*, 439 pp., Cambridge University Press, New York, 1990.
- Schulz, S.E., and J.P. Evans, Mesoscopic structure of the Punchbowl Fault, Southern California and the geologic and geophysical structure of active strike-slip faults, *Journa of Structural Geology*, 913-930, 2000.
- Shreve, R.L., and M. Cloos, Dynamics of sediment subduction, melange formation, and prism accretion, *J. Geophys. Res.*, *91*, 229-245, 1986.
- Sieh, K., S.N. Ward, D.H. Natawidjaja, and B.W. Suwargadi, Crustal deformation at the Sumatran subduction zone, *Geophysical Research Letters*, *26* (20), 3141-3144, 1999.
- Smithers, S.G., and C.D. Woodroffe, Microatolls as sea-level indicators on a mid-ocean atoll, *Marine Geology*, *168*, 61-78, 2000.
- Spence, W., E. Mendoza, E. R., C. G.L., and N. E, Seismic subduction of the Nazca ridge as shown by the 1996-97 Peru earthquake, *Pageoph*, *154*, 753-776, 1999.
- Steketee, J.A., On Volterra's dislocations in semi-infinite elastic medium, *Can. J. Phys.*, *36*, 192, 1958a.
- Steketee, J.A., Some geophysical applications of the elasticity theory of dislocations, *Can. J. Phys.*, *36*, 1168, 1958b.
- Stuart, W.D., Forecast model for great earthquake at the Nankai trough subduction zone, *Pure and Aplied Geophysics*, *126* (N0s 2-4), 619-641, 1988.
- Taylor, F.W., J. Frohlich, J. Lecolle, and M. Strecker, Analysis of partially emerged corals and reef terraces in the central vanuatu arc–comparison of contemporary coseismic and nonseismic with quaternary vertical movements, *Journal of Geophysical Research*, *92*, 4905-4933, 1987.
- Taylor, J.R., *An Introduction to Error Analysis*, University Science Books, Mill Valley, CA 94941, 1982.
- Thatcher, W., The earthquake deformation cycle at the Nankai through, southwest Japan, *Journal of Geophysical Research*, 89, 3087-3101, 1984a.

- Thatcher, W., The earthquake deformation cycle, recurrence, and the time-predictable model, *Journal of Geophsical Research*, 89, 5674-5680, 1984b.
- Thatcher, W., and J.B. Rundle, A viscoelastic coupling model for the cyclic deformation due to periodically repeated earthquakes at subduction zone, *Journal of Geophysical Research*, 89, 7631-7640, 1984.
- Zachariasen, J., K. Sieh, F.W. Taylor, R.L. Edwards, and W.S. Hantoro, Submergence and uplift associated with the giant 1833 Sumatran subduction earthquake:Evidence from coral microatolls, *Journal of Geophysical Research*, 104, 895-919, 1999.
- Zachariasen, J., K. Sieh, F.W. Taylor, and W.S. Hantoro, Modern vertical deformation above the Sumatran subduction zone: paleogeodetic insights from coral microatolls, *Bulletin of the Seismological Society of America*, *90* (4), 897-913, 2000.

Chapter 5. A 250-year-long paleogeodetic record of subduction from Sumatran coral heads

5.1. Abstract

We have recovered and analyzed a 250-year-long paleogeodetic record of vertical deformation from four coral microatolls above the Sumatran subduction zone. This record is the basis for construction of a slip history for the underlying subduction interface. Most of the record comes from the upper surface of one 8.5 m wide pancake-shaped *Porites* head. This disc records annual lowest low tide levels during the period from about 1746 to 1935. Two nearby heads yield the remainder of the record, from 1935 to 1997. The largest signal recorded is a 700 mm emergence associated with the M_w7.7 earthquake of 1935, which we have shown to be the result of about 2.3 m of slip on the subjacent subduction interface. Two lesser emergences occurred in about 1746 and 1797. The remainder of the record consists predominantly of long-term submergence. The average submergence rate between 1797 and 1935 is 1.2 ± 0.2 mm/yr. This low rate is difficult to explain without substantial quasi-stable sliding of the 1935 co-seismic patch. Modeling suggests that a rate of about 25 mm/yr, more than half the plate rate, fits the observed data best. High rates of submergence $(8.4 \pm 0.9 \text{ mm/yr})$ between 1935 and 1961 probably indicate that much of the 1935 co-seismic patch was fully locked during these post-seismic decades. Deceleration of the submergence rate to about 4.4 mm/yr sometime between 1960 and 1980 suggests a resumption of aseismic slip at about 9 mm/yr a rate still lower than that of the pre-seismic century. A plot of a 250-year-long slip history suggests that the interface has a complex history that includes co-seismic rupture, quasi-stable sliding and locking. These observations suggest that forecasts of future behavior will require geographically robust and very long-lived monitoring programs to record complex histories of deformation.

5.2. Introduction

5.2.1. Motivation

Modern observations have shown that the theory of "pure elastic rebound" does not explain the rich variety of earthquake behavior. For example, the occurrences of large earthquakes along the San Andreas Fault and other large faults have shown that they are clearly not periodic [Atwater, 1992; Sieh et al., 1989; Stein et al., 1997]. In fact, long periods of quiescence between flurries of large events suggest that large earthquakes occur in clusters rather than in regular cycles [e.g. Dawson, 2000; Rockwell et al., 2000]. Recently, modern GPS networks in Japan, Cascadia, and South America detected appreciable slips on the surfaces above subduction zones that did not emanate observable seismic waves [e.g. Dragert et al., 2001; Heki et al., 1997; Lowry et al., 2001]. These "silent earthquakes," which are not predicted by the elastic rebound theory, appear to be general features of fault behavior rather than exceptions.

Looking for clues in the past, people documented evidence of the past major earthquakes from any available source. However, this is hard to obtain anywhere in the world. Historical accounts of past earthquakes typically go back only 1-2 centuries. An exception is offered by the Nankai trough, for which historical earthquake records go back to AD 1000 [Ando, 1975], but even there, written documentation of individual earthquakes is largely incomplete. In the absence of historical records, the study of sedimentary layers in intertidal environments can establish the occurrence of earthquakes for thousands of years into the past, as has been accomplished in Cascadia [Atwater et al., 1996; Kelsey et al., 2002]. But evidence of how strain accumulates during the periods

between earthquakes is very rare, except for the last decade in areas where GPS networks have been installed [Fluck et al., 1997; Mazzotti et al., 2000]. The records may extend if tide gauges, geodetic leveling, or old triangulation networks existed [e.g. Freymueller et al., 2000; Thatcher, 1984a]. In short, even the most advanced physical modeling of the earthquakes cycle is based largely on inadequate data [Lyakhovsky et al., 2001; Mitsui and Hirahara, 2001; Scholz, 1990]. One of the key solutions to the problem is finding a long-lived instrument that continuously records slow strain accumulations as well as sudden strain releases during the earthquake cycles. This chapter presents an extraordinary long record of the vertical deformation above the Sumatran subduction zone, obtained from coral microatolls.

5.2.2. Active Tectonics of the Sumatran subduction

Along the Sumatran plate boundary the Australian-Indian plate is subducting at about 6 cm per year in the direction N11°E (Fig. 5.1). The campaign-style GPS monitoring between 1989 and 1990 and then between 1995 and 2000 illuminated a decade of modern crustal movement of the overriding plate[Bock, 2002; Prawirodirdjo et al., 1997]. The GPS data showed that the fore-arc islands were slowly moving away from the trench in a direction generally close to the plate vector. This indicates that the interface between the subducting and the overriding plates is generally locked, so that the subduction interface is currently accumulating strain [Bock, 2002; Prawirodirdjo et al., 1997].

Sparse historical accounts covering the last two centuries indicate that large earthquakes repeat along the Sumatran margin [Newcomb and McCann, 1987]. Two of

these rank among the world's largest historical earthquakes: one in 1833 (\sim M_w9) and the other in 1861(\sim M_w8.5) (Fig. 5.1). The former dominates the seismic history of the southern section of the subduction zone, and the latter is the dominant historical event in the region north of the Equator. The largest historical earthquake to strike the central region, sandwiched between these two giant earthquakes, was the M_w7.7 event of 1935 ([Newcomb and McCann, 1987; Rivera et al., 2002], Chapter 3 and 4).

5.2.3. Paleogeodetic records from the Equatorial region

Until the mass death of the coral reefs during the great fires of 1997, *microatolls* grew abundantly on the intertidal reefs of the west coast of Sumatra and its fore-arc islands (Chapter 3 and 4). This type of coral is very sensitive to fluctuations in sea levels, and thus acts as a natural tide gauge [*Taylor et al.*, 1987; *Zachariasen et al.*, 1999; *Zachariasen et al.*, 2000] (Chapter 3 and 4). Numerous microatolls from the region around the Equator record a simple pattern of tilt away from the trench axis in 1935 (Chapter 3 and 4). About 115 km from the trench axis, uplift was nil. Nearer to the trench, uplift progressively increased trench-ward to at least 90 cm. Farther than 115 km from the trench, submergence of up to 35 cm occurred (Fig. 4.1). We modeled these *paleogeodetic* data well with a 2.3 m slip event on the interface between 88 and 125 km from the trench axis (Section 4.3).

The component of plate vector that oriented parallel to the 1935 earthquake slip (i.e.,, nearly perpendicular to the trench axis) is about 4 cm/yr [*Prawirodirdjo et al.*, 1997; *Royer et al.*, 1997]. If the two slabs are fully coupled, then a 1935-like earthquake should repeat about every 75 years on average. In fact, a very-long-lived coral head that

will be presented in the following section recorded no 1935-like earthquake for at least 130 years prior to 1935 instead. This renders a very long period of quiescence.

Furthermore, for the past four decades, the long-term submergence rate above the 1935 rupture has been lower than that for the 3 decades following the 1935 event, but is higher still than the rate of the 3 decades before 1935 (Fig. 4.1). In the following section we will discuss a record that shows a very low rate of submergence preceding 1935 operated since mid-1700.

5.3. The longest paleogeodetic record from near the Equator

At the West Badgugu site, we have recovered an exceptionally long record of vertical deformation from two unusually large *Porites* microatolls, augmented by two nearby modern heads. The large microatolls are from a population of well-preserved and undisturbed heads that died from emergence during the 1935 earthquake. One of the modern microatolls has a record that spans the 1935 emergence, allowing us to tie together the more ancient and the modern paleogeodetic histories.

The microatolls are in a large bay at the south end of Tanabala Island (Fig. 5.1b). They sit in the middle of a broad intertidal platform, just offshore of Badgugu village, a group of bamboo and thatch dwellings scattered beneath coconut palms behind the beach. When we first visited the site, in mid-1999, we were attracted by a population of large pancake-shaped heads, whose upper surfaces were at a uniform elevation within the intertidal zone. With few exceptions, these heads displayed no tilt or other disruption. We cut slabs from the two largest of these heads, as shown in the photos (Fig. 5.2a and 5.2b). Concentric growth ridges are particularly clear in the photo of the smaller head but

are just as clear in the field on the larger head. As discussed earlier in this thesis (Chapter 4.1.2), these are clear indicators that the upper surfaces of the microatolls have sustained very little erosion. Nearer the center of each head, the rings are obscured, but protected, by later overgrowths.

Figure 5.3 is a map that provides a synoptic view of the intertidal platform. It shows that the platform extends 150 to 300 meters out from the narrow beach. The platform consists of an inner "lagoon" and an outer rampart. The rampart of loose cobbly to bouldery debris separates the open bay from the sandy to muddy "lagoon" that harbors most of the microatolls. The rampart is generally 20 to 30 cm higher than this sandy to muddy substrate, but blocks tens of centimeters to a couple meters high rest upon it (Fig. 5.3). We dated a sample from the largest block about 120 cm in diameter, expecting it to pre-date the 1935 earthquake and thus suggest construction of the rampart by a tsunami. Instead, we found that the perimeter of the coral block was alive as recently as 1980. Thus, it must have been emplaced on the rampart by exceptionally energetic surf within the past ten or twenty years.

Although the *Porites* heads within the waters of the "lagoon" are protected by the rampart, water circulates readily between the bay and the lagoon through a 200-m-wide breach in the rampart (Fig. 5.3). Hence, the *Highest Level of Survival or HLS* (Chapter 3) of the microatolls within the lagoon represent lowest low tides within the bay. This assertion is clearly supported by the fact that old microatolls #21 and #22, which are within the breach in the rampart, have HLS elevations that are indistinguishable from those of the microatolls within the lagoon.

Along the southern part of the breach in the bouldery rampart is a field of modern *Porites* heads and microatolls. All of these modern *Porites* heads were dead when we first visited in mid-1999. Presumably they are casualties of the great fire- and El Nino-induced death of the west Sumatran reefs of late 1997 (Chapter 3.3; [*Saji et al.*, 1999]). The zero contours on the map (Fig. 5.3) represents substrate elevations equal to the youngest HLS of the modern *Porites* heads growing in this small colony on the edge of the intertidal reef. Since this HLS represents the lowest annual tides, the map shows that most of the intertidal flat is exposed during lowest low tides.

Figure 5.4 is a compilation of the perimeter elevations of all the heads that we surveyed, modern and ancient. It shows that there are four populations of microatolls. Zero elevation in the figure (and on the site map) is the average elevation of the modern microatoll perimeters (heads 31 through 46). We sampled one of these at the site Well-preserved very small modern (but dead) Goniastrea heads, just landward of the breach in the rampart, have perimeter crests about 10 cm above the modern *Porites* values. It is typical of *Goniastrea* to grow about 10 cm higher than their contemporary *Porites*, because they are more tolerant of brief exposure above water ([Zachariasen, 1998b]; Chapter 3). Heads 7 through 23 represent the population of older heads that includes the two large ones from which we collected samples Bdg99A1 and Bdg00A1. The average perimeter elevation of the older heads is 35 cm above the modern HLS datum. A still older population of heads also exists. Their perimeters are only about 20 cm above the modern HLS. We sampled one of these heads (head # 6) for U-Th dating and determined an age of death of about AD 1335 \pm 69 but we have not been able to derive an HLS history from the slab, because it is severely eroded.

5.4. The slab analysis

The Badgugu record is a synthesis of HLS histories from four microatolls (Fig. 5.5). The bulk of the record comes from the largest head, which recorded HLS from 1740 to 1935. We are able to compare the youngest 75 years of this record with that from a nearby, smaller head. A small modern head gives a record of HLS for the period 1950 to 1997. And a head from the East Badgugu site, 2 km to the east, allows us to connect the old and modern records across the large emergence event of 1935.

5.4.1. The heads

Within the graveyard of pancake-shaped *Porites* microatolls in the West Badgugu lagoon is one exceptionally large microatoll. This is Head #15 in Figure 5.3. It is the largest head that we have sampled in all of our studies of the Sumatran reefs. We retrieved a 4.2-m-long slab (sample Bdg00A1) from a western radius of this head (Fig. 5.5D). Cutting of the slab revealed that the microatoll is only 40 to 50 cm thick and that it rests on a sandy substrate. The concentric growth bands of the outer meter are well preserved and visible in the field. The older HLS record of the microatoll is also well preserved, but younger overgrowths obscure it. These younger overgrowths are clear on the cross-section, resting as detached blocks on the older, contiguous body of the microatoll.

As a check on the reliability of visual band counts as a dating method, five bands from slab Bdg00A1 were sampled for U-Th dating (Table 5.1). The youngest U-Th date, on the 25-27th band in from the perimeter, confirms that the microatoll's death was related to emergence associated with the 1935 earthquake. If one assumes that the

outermost ring grew in 1935, then visual band-counting tells us that the 25-27th band grew in 1908-1910, well within its U-Th date range of 1907 ± 6 (Fig. 5.5D). The next-youngest dated band has a broad U-Th date range, 1918 ± 30 . Even so, our date based on band-counting is 4 years older than the older limit of this range. A U-Th date in the middle of the slab is also not very precise -1825 ± 27 . Our visual band count yields a date of 1826 for this band, squarely in the center of the U-Th date range. The band that we estimate formed in 1769 has a U-Th date of 1779 ± 9 . Our 1736 band yielded a U-Th date of 1734 ± 40 . These comparisons confirm that band-counting provides a satisfactory chronology of the slab.

The smaller fossil microatoll yielded an HLS record contemporaneous with the youngest 75 years of the long slab's record. This head, #20 on the site map, is only 25 meters west of the large head. The recovered slab (sample Bdg99A1) is from a northwest radius of the beautifully symmetrical microatoll (Fig. 5.2C) and extends almost to the center of the head. Four U-Th dates allow us to check the validity of our visual ring counting. The annual band that we estimate formed in 1899 was sampled twice; giving date ranges of 1907 ± 6 and 1898 ± 7 . Our age estimate falls two years outside of the former range but is squarely within the latter. The ring estimated to have formed in 1873 was also sampled twice; giving date ranges of 1868 ± 5 and 1866 ± 4 . Our preferred date is 3 years younger than the latter range, but at the youngest limit of the former range.

The modern sample from the West Badgugu site comes from head #43, on the edge of the intertidal flat (Fig. 5.3). The sample (Bdg99A3) is 70-cm wide and records HLS for the period from about 1950 to 1997 (Fig. 5.5B). We did not determine a U-Th date for any annual bands in this sample, because the rings are quite clear. Unlike the

record from the older two heads, this head consists of a small inner flat surmounted by a thick raised outer rim, a form indicative of rapid submergence.

The modern and fossil records from West Badgugu do not overlap in time—the fossil records stop at 1935, and the modern record begins in about 1950. We spanned this gap of 15 years with a record from the East Badgugu site, just 2 km to the east, across the bay. This site and record have already been described at length in Chapter 3, so we present only a short summary here.

The East Badgugu slab (Bdg00B1) comes from a *hat-shaped* microatoll, that is, a head with a high core and low outer rim. Figure 5.5A displays the shape of the sample, which was cut from a southeast radius of the microatoll. Visual ring counting from the perimeter ring inward shows that the low outer flange began to form in about 1935. The shape of the outer flange indicates rapid submergence in the subsequent decades. The nearly flat upper surface of the core of the head demonstrates that the site was nearly stable in the decades prior to 1935. Uplift in 1935 was about 67 cm, slightly less than at the West Badgugu site, 2 km to the west. In splicing this record into the West Badgugu HLS history, we have assumed that the 1997 HLS elevation of this sample and the modern sample at West Badgugu are identical. The overlap in the two records from 1950 to 1997 supports this assumption. We have used the East Badgugu record only back to 1935, because the size of the co-seismic step is clearly smaller than it is at West Badgugu.

5.4.2. HLS history

Together, the four coral slabs from the West and East Badgugu sites reveal a continuous HLS history for the period from about 1740 to 1997. That history is illustrated in Figure 5.5E. In general, the record is one of seismic emergence and interseismic submergence. The most prominent feature in the record is the 80-cm emergence associated with the earthquake of 1935. The submergence rate in the subsequent 25 years was very rapid—about 8.4 mm/yr. Submergence in the 40 years prior to the earthquake was very slow—a mere 1.2 mm/yr. Two modest emergence events appear in the record in about 1746 and 1799. Between these two events, the site was nearly stable. Between 1799 and 1935, submergence at an average rate of 1.2 mm/yr dominates the record. But this general trend is interrupted by three resolvable events, each about 10 cm in magnitude. Emergence and subsequent submergence occur in about 1833, most probably in association with the giant rupture of the subduction interface farther south in that year [Zachariasen et al., 1999]. Emergence and subsequent submergence also occur in about 1861, probably in association with the great subduction event to the north in that year [Newcomb and McCann, 1987]. An emergence and subsequent submergence in about 1876-1877 cannot be associated with an historical However, the disturbance may be related to oceanographic changes earthquake. associated with the great Indian drought of 1877 [Charles et al., 1997].

5.4.2.1. The 1743 event

The large head began to grow in about 1727. Its growth was radially upward and outward until about 1743. At that time, the top of the head died. The magnitude of this

emergence event is indeterminate, since the head had not reached HLS prior to the event. All we can say is that the emergence was 10 cm or greater. Submergence of about 10 cm followed the emergence, as evidenced by free upward growth of annual bands between about 1745 and 1750.

5.4.2.2. Stability from 1750 to 1797

During the latter half of the 18th century HLS at the West Badgugu site was unusually stable. Although HLS elevations fluctuate over a range of a few centimeters during these five decades, the errors inherent in determining the tectonic signal from coral HLS measurements are of about this magnitude (see Chapter 4.1.1). The average submergence rate through this period— 0.4 ± 0.6 mm/yr—is indistinguishable from HLS stability.

5.4.2.3. The 1797 event

An emergence event of about 17 cm ended this long period of stability. Ostensibly, the date of the event is about 1791, because the top of the 1791 annual band is about this much lower than the top of the 1790 band. However, we have learned from the experience of examining other heads that substantial erosion is not uncommon on the sides of a head that has been exposed by emergence (e.g., Chapter 3.4.3).

We suspect that the actual date of the emergence is closer to 1800, because this is the beginning of a short period of unimpeded upward growth. Such episodes are common after emergence events in this area (see Chapter 3). Furthermore, we suspect that the emergence event coincides with a large historical earthquake of 1797. The 6-

year uncertainty in our visual ring-counting at this distance in from the perimeter of the long slab certainly allows this hypothesis. We have an in-progress manuscript that describes evidence from microatolls that this earthquake was produced primarily by rupture of the subduction interface farther south.

5.4.2.4. Slow submergence between 1797 and 1877

During the eight decades since the beginning of the 19th century, the West Badgugu site submerged at an average rate of 1.2 ± 0.2 mm/yr. Although HLS fluctuates from year to year by as much as a few centimeters, these variations are well within the oceanographic and biological noise levels associated with microatolls (Chapter 4.1.1). Three exceptions are the distinctly larger geodetic signals in 1833, 1861, and in about 1877.

5.4.2.5. The 1833 event

A die-down of about 10 cm occurred in the early 1830s. The die-down is followed by a few years of rapid upward growth that fully recovers the drop in HLS. There is a suggestion in the HLS record that the submergence episode continued through about 1837 and even exceeded the magnitude of the initial emergence by a few centimeters. The timing of this modest emergence/submergence episode leads us to suspect that it is related to the giant earthquake of 1833, whose source was primarily to the south [Newcomb and McCann, 1987; Zachariasen et al., 1999] (Chapter 6 of this thesis). We discuss in the next section the implications of this small signal for delimiting the 1833 rupture and its effect on this site.

5.4.2.6. The 1861 event

Both fossil slabs show a few-centimeter HLS die-down in about 1860. However, the elevation of the HLS after the event in the shorter slab is about 10 cm lower than it is in the longer slab. This seems to reflect a very local subsidence or intra-head difference in the effect of whatever caused the die-down, because the deeper die-down on the shorter slab is followed by a longer period of rapid upward growth throughout the following decade. This rapid growth brings the HLS values for the two slabs into agreement by the early 1870s.

The historically documented occurrence in 1861 of a great earthquake centered on Nias Island, to the North, suggests the speculation that this small perturbation is related to that event. The fact that the initial emergence and the one we ascribe to 1833 have 28 annual bands between them lends further support to our contention that these two events are contemporaneous with the two large earthquakes. We will show in the following section that, regardless of the exact ages of the bands, the West Badgugu record clearly restricts the southern terminus of the principal 1861 source rupture to a position well north of Badgugu. Similarly, it clearly restricts the northern terminus of the principal 1833 rupture to a position well to the south.

5.4.2.7. The 1877 climatic event

The most pronounced of the three minor events in the mid-19th century is a die-down/re-growth episode in the mid-1870s. A die-down of about 10 cm is followed by rapid, unimpeded upward growth of 15 cm. The inception of the event is constrained from visual ring counting to be $1876 \pm 4/3$. It occurs 15 to 16 years after the emergence

that we ascribe to 1861, however, so we promote a date of 1876 or 1877 for the initial die-down. The historic record is adequate to allow us to conclude that there was no earthquake larger than about M 7.5 associated with this event. Instead, a severe drought in India, brought about by the failure of the Indian monsoon, occurred in 1877 [Charles et al., 1997]. So, It is most likely that the die-down is a result of depressed lowest low tides during that exceptional climatic event, such as also occurred in 1997 (Chapter 3.4.1).

5.4.2.8. Slow submergence from 1877 to 1935

For the six decades from about 1877 to 1935 the slow submergence resumed. The HLS-least-squares average rate of submergence is 1.2 ± 0.2 mm/yr, not significantly different from the rate for the first eight decades of the 19th century. Minor fluctuations over yearly to decadal periods may exist, but they would be small and within the range of non-tectonic noise in the coral records. An HLS die-down of about 5 cm appears in both fossil slabs in 1926, and recovered in a few years. These signals are marginally distinguishable from the non-tectonic fluctuations. The rate of submergence appears to pick up substantially in the ensuing decade, just prior to the 1935 event. The magnitude of this accelerating submergence is rather small, however, to conclusively constitute for a tectonic signal. However, evidence from the other sites supported this idea (Section 4.4).

5.4.2.9. The 1935 earthquake

At this site the sudden emergence in the 1935 event is about 80 cm (Fig. 5.5E). The entire intertidal reef, out to the current 40 cm contour on the site map (Fig. 5.3) rose

above lowest low tide levels during this event. Hence, subsequent re-colonization by *Porites* has been restricted to the margins of the intertidal flat (Fig. 5.3).

Many other sites also recorded the co-seismic emergence or submergence associated with the 1935 event (Chapter 3 and 4). From these data and from an inversion of historical seismograms [*Rivera et al.*, 2002], the source of the earthquake is known to be a roughly 35 by 70 km patch of the subduction interface, which sustained, on average, about 2.3 m of slip (Section 4.2). The Badgugu sites lie above the southern part of this co-seismic rupture.

5.4.2.10. Rapid submergence between 1935 and 1961

The HLS record of the decades immediately following the 1935 earthquake comes from the slab taken from the East Badgugu site. It shows that rapid submergence began within a year or so of the earthquake and continued unabated until about 1960. Free upward growth, with only a few HLS clips, characterizes the record for this period. The average rate of submergence is 8.4 ± 0.9 mm/yr. The existence of only a few HLS clips during this period indicates that the submergence rate was just slightly lower than the growth rate of the coral bands.

Many other fringing reefs in the surrounding area also contain records of vertical deformation during this period (Chapter 3). The regional pattern constrains elastic models well enough to show that a core of the 1935 patch was locked during the 25 years immediately after the earthquake (Section 4.4).

5.4.2.11. The 1962 Silent earthquake

The Bdg00B1 slab recorded that in 1962, the East Badgugu site sustained a diedown of more than 10 cm. A subsequent submergence allowed the microatoll to grow upward by about 15 cm until an HLS clip occurred in about 1975.

The 1962 event is a very prominent event throughout the region, as evidenced by its appearance in the microatolls of most neighboring reefs (Chapter 3). One might associate a small fraction of the emergent part of the episode with the strong 1961-El Nino/Indian Ocean Dipole event, but the emergence is appreciably larger than other emergences recorded by the microatolls in years with similar climatic events (Section 4.1). Furthermore, we argue that the distinct, contourable pattern of emergence indicates that it is principally a tectonic event (Section 4.3).

Moreover, the subsequent submergence is larger than the emergence event. This is another reason why the episode of 1962 is most likely a tectonic event. Elastic dislocation modeling of the emergence and submergence episode suggests that two dislocations propagating up-dip produced the deformation (Section 4.3).

5.4.2.12. Slower submergence rates during the period 1970-2000

The average rate of submergence after 1962 is markedly lower than the rate before 1962. Between the first HLS clip in 1975 and the death of the reef in 1997, the average rate of submergence was 4.4 ± 0.6 mm/yr. This rate is only about half the rate in the decades just after the 1935 event, but is nearly four times higher than the rate that dominated the interseismic periods of the 18th, 19th, and early 20th centuries. This pattern is similar to that seen at numerous other sites in the region (Chapter 3). Elastic

modeling of these data suggest that these rates are most consistent with the resumption of a high percentage of aseismic slip of the part of the patch that slipped co-seismically during the 1935 earthquake but locked up in the subsequent decades (Chapter 4).

5.5. Interpretation and Discussion

In Chapter 4, we utilized HLS histories from many sites on the outer-arc ridge, including the history from east Badgugu, to constrain the behavior of the subduction interface throughout the 20th century. The large number of sites and their geographic spread allowed us to place firm constraints on the changing behavior of the shallow subduction interface throughout the century. These data (in concert with a seismic inversion) constrain the source of the 1935 earthquake to a 65 x 30 km patch of the interface beneath the islands [Rivera et al., 2002], with an average slip of about 2.3 meters (Section 4.2). They also show that the behavior of the interface before and after the 1935 event was markedly different. In the decades before the 1935 event, low rates of submergence and emergence across the islands require quasi-stable sliding of the 1935 rupture patch at more than half the plate rate. High rates of submergence in the decades after the earthquake suggest that a significant portion of the 1935 patch locked up after the earthquake. The pattern of emergence and submergence during the 1962 episode is best modeled by a complex series of slips beneath the islands that vary in magnitude from a few centimeters up to 1.7 meter. Moderate submergence and emergence rates in the decades after 1962 indicate that half of the 1935 patch has begun to slip at 9 to 27 mm/y over the latest four decades.

The long Badgugu history sheds light on the behavior of the subduction interface before the 20th century, through the 19th and the latter half of the 18th century. But because the record is solitary, we lack the robust geographic coverage for these earlier times that we have for the 20th century. Thus, more assumptions will be necessary to interpret the older HLS history.

5.5.1. Insights from interpreting the 20th-century record

Our primary assumptions will be based upon what we learned from modeling the 20th-century histories. In general, sudden uplift of a site indicates sudden slip on the subjacent subduction interface. Sudden submergence generally indicates sudden slip on an up-dip section (Section 4.4.). For long-term patterns, a cross-strike sinusoidal pattern of submergence and emergence determined from paleogeodetic data indicates elastic strain accumulations of a portion of the interface. Higher amplitudes of the peak and trough indicate lower percentage of aseismic slip on the patch beneath the submerging sites. Conversely, lower amplitudes of the peak and trough generally indicate higher percentage of aseismic slip on the patch beneath the submerging sites. In the extreme case, a lack of vertical deformation indicates no deficit of slip on the subduction interface, that is, the down-going slab is stably sliding at the full plate rate and is decoupled from the over-riding plate.

The simplest interpretations would assume that the rates of vertical deformation or the magnitude of sudden events indicate the rate of slip or the magnitude of slip on the interface directly below the site. Lacking HLS records from other sites in the region, however, we cannot rule out a large array of more complex patterns of slip on the interface.

5.5.2. Emergence events in 1743 and 1797

The largest recorded emergence prior to the 80-cm emergence in 1935 is the 17-cm emergence of 1797. The amount of emergence in 1743 could be larger, but all that is certain is that it is greater than about 10 cm. The simplest interpretation of these events is that slip occurred on the underlying interface and that it was substantially less than the slip associated with the 1935 event. If we assume that these events had the same extent as the 1935 rupture, then average slip would have been about 0.5 meters ($\sim M_w 7.0$) in 1797 and at least 0.3 meters ($\sim M_w 7.0$) in 1743 . A larger magnitude of rupture farther from the site is certainly possible for each of these events. However, it is hard to imagine a scenario in which slip beneath the site is larger in either of these events than a few tens of centimeters. The lack of a prolonged period of rapid submergence following each event also suggests that these two events were much smaller or more distant than the 1935 rupture.

5.5.3. Disturbances in 1833 and 1861

The small die-downs of 1833 and 1861 suggest that a small amount of slip occurred on the underlying subduction interface in those years. If we assume that slip during these events was uniform over a rupture patch similar to that of the 1935 event then the 10 cm die-down in 1833 would imply about 30 cm of slip on the interface. Similarly, 5 cm of die-down in 1861 would imply about 15 cm of slip. This is miniscule

in comparison to the 13 meters of slip that *Zachariasen et al.* [1999] calculated for the 1833 rupture on the subduction interface 200 km to the south. But it does suggest that minor slip did occur this far north.

The rapid submergence events that followed the 1833 and 1861 die-downs are unlikely to have been caused by back-slip on the subduction interface. More likely, the submergence indicates a subsequent time-dependent phenomenon, either on the rupture surface or in the underlying crust and/or mantle lithosphere. Since rupture of a subduction zone produces an aureole of submergence around the source, post-seismic slip on adjacent (but not subjacent) parts of the rupture could produce submergence at the site.

5.5.4. Slow submergence between 1797 and 1935

Submergence at an average rate of about 1.2 mm/yr dominates the HLS history of the Badgugu site throughout the 130 years before 1935. We have already used data from several neighboring sites to interpret what was going on below the islands in the last 55 years of this period (Chapter 4, Fig. 4.1). Thus, the simplest initial interpretation of the entire record would be to assume that whatever was going on in the five decades before 1935 had been going on throughout the previous 100 years as well. This interpretation is supported by the linear long-term trend in the two other longest records in the 1935-submerged areas (Fig. 5.6). Our best-fitting models of pre-1935 behavior have most of the 1935 patch slipping at a rate between about 2.5 and 3 cm/yr, half or a little more than half the plate rate (Chapter 4, Fig. 4.21). The rate of slip on the interface between the

1935 patch and the trench ranges from 5.5 to about 7 cm/yr in these models, somewhat higher than the long-term relative plate rate.

However, the initial, simple 2-D model in Chapter 4 excludes the Badgugu data point, because it deviates noticeably from the overall trend. Figure 4.20 in Chapter 4 shows that all the other data can be fit with contours parallel to the trench and outer-arc ridge. The Badgugu data requires the contours to bend to a more southerly course. That is, the rate is much lower than expected, given the rates from the neighboring islands. This probably means that the rate of slip on the interface in the decades prior to the 1935 earthquake was markedly higher beneath the Badgugu site than Figure 4.22 suggests for the subduction interface farther north.

5.5.5. The 1935 event $(M_w7.7)$

The 1935 event dominates the seismic strain release in the last three centuries. Except for the signals associated with the neighboring giant earthquake in 1833 and 1861, no major seismic strain release occurred during the 135 years prior to 1935. This is a lower limit for the latest recurrence interval for a 1935-like earthquake. The smaller strain release in early 1743 and in 1797, compared with the 1935 event, may suggest that the slip and extent of rupture on the subduction interface are not the same from one rupture to the next—in other words, that the interface does not have a *characteristic earthquake*. Alternatively, if these two events are smaller earthquake superimposed upon a cycle of larger, 1935-style events, or if the events are manifestations of a larger magnitude earthquake in the neighboring subduction interface, then the 1935-event cycle must be longer than 130 years.

We could, in fact, calculate an average recurrence interval fro a nominal 1935 event, based on the slip deficit of the 1935 rupture patch in periods prior to 1935. Based on modeling, the slip deficit from 1797 to 1935 is about 1.0–1.5 cm/yr, if we use the global sea-level-rise correction of 1-2 mm/yr (Chapter 4, Fig. 4.22). A 1.5 cm/y slip deficit during the 138 years prior to 1935 yields 2.1 m, a value nearly as large as the slip that occurred during the 1935 event (Fig. 5.7). Using the 1 cm/yr figure for the slip deficit implies a seismic strain-accumulation period of about 230 years.

5.5.6. The 200-year-subduction history

Figure 5.7 graphically portrays a complex history of seismic and aseismic slip on the subduction interface for the last 200 years. This is based on the modeling in Chapter 4, Fig. 4.27 (using a global sea-level-rise correction of 2 mm/yr). The steady-state subduction on the down-dip interface that slips continuously at the plate rate (4 cm/yr) is represented by the graph on the right (east) side. The slip history on the shallow portion of the interface (closer than 130 km to the trench axis) is dominated by quasi-stable sliding.

The outboard interface between the island and the trench is entirely aseismic. The large 1962 silent earthquake comprises about 14% of the total slip. Curiously, the total slip exceeds the total plate convergence by about 360 cm. In defense of this model, one could argue that the excessive slip resulted from a slip deficit that had accumulated before 1743. Unfortunately, we have no record of slip history during that period. One for example could postulate that the modern submergence rate (which implies an accumulating slip deficit of about 1.3 cm/yr—Fig. 4.26) lasts for about 270 years before

the deficit reaches the pre-1935 level to enable plate rate keep up with the slip on the outboard.

Against such a proposition, one may argue that the data constraints upon the non-unique elastic dislocation solution may not be sufficient to determine the behavior of the outboard interface. For example, our 2-D preferred model for the pre-1935 deformation neglected the low submergence rate at Badgugu in order to fit most of the other data. If one inserts the Badgugu point and allows the predicted submergence to reach a compromise between the high submergence value at Bendera and low submergence value at Badgugu (Chapter 4, Fig. 4.21), then the slip on the outboard interface could be almost as low as the plate rate (~4.4 cm/y). Therefore the excessive slip would have been only 200 cm more than the total plate convergence.

The seismic slip during the 1935 event contributes about 40% of the total slip on the rupture patch from 1797 to 1935 (Fig. 5.7). Between 1935 and 1962, the central section of the patch that ruptured in 1935 was fully locked. That is, a slip deficit was accumulating at the plate rate. The outer portion of the 1935 rupture, however, was moving steadily with the down-dip and up-dip sections during that period. In this period (1935 - 1962), the strain that accumulated on the patch that ruptured in1935 was about 40% of the total plate convergence (i.e., the remaining 60% is accommodated by aseismic slip). After the 1962 event, the 1935 rupture patch continued slipping. Slips on the lower half of the patch decelerated to 9 mm/yr. Slips on the upper half moved with the up-dip extension at about 27 mm/yr (In short, in the years between 1935 and 2000, only a small portion of the patch that has experienced slip deficit (locked). In Figure5.7, the slip deficit is shown as two narrow troughs near the center of the 1935 patch.

5.5.7. Summary and conclusion

The 250-year record of the surface vertical motions above the Sumatran subduction zone reveals that the subduction process has had a complex history. A simple model of fault behavior cannot explain this complexity. Nonetheless, the slip history from 1797 to 1935 indicates that the amount of the slip deficit that accumulated during the 138 years prior to 1935 was about the same as the amount released in the 1935 event. Thus it might be consistent with a stick-slip mechanism. But this concept does not take into account the fact that the interface was sliding in a quasi-stable manner during the interseismic period.

Furthermore, uncertainty in the correction for the rise in global sea-level gives uncertainty to the estimation of the recurrence interval for a 1935-like event. The corrections that range from 1 to 2 mm/y yield the recurrence interval from 138 to 230 years. The two smaller events that occurred in about 1743 and 1797 may indicate that the subduction interface lacks a single, characteristic earthquake cycle. Alternatively, these events might be attributed to larger magnitude events on the adjacent subduction interface, or might be smaller events that superimposed on a longer cycle of characteristic, 1935-like earthquakes.

Lastly, it is clear that to fully understand the subduction process and to be able to predict the likelihood of future major earthquakes we need a geographically robust and long-term program to monitor the behavior of the subduction zone.

5.6. References

- Abercrombie, R.E., The June 2000, Mw7.9 earthquakes south of Sumatra: deformation in the India-Australia Plate, *Journal of Geophysical Research*, submitted 2001.
- Ando, M., Source mechanisms and tectonic significance of historical earthquakes along the Nankai through, Japan, *Tectonophysics*, *27*, 119-140, 1975.
- Atwater, B., Geologic evidence for earthquakes during the past 2000 years along the Copalis River, southern coastal Washington, *Journal of Geophysical Research*, 97, 1901-1919, 1992.
- Atwater, B., E. Hemphill-Haley, A. Long, S. Nishenko, I. Shennan, and M. Stuiver, Recurrence Intervals for Great Subduction-Zone Earthquakes of the Past 3500 Years in Southern Washington State, *To be submitted to Science*, 1996.
- Bock, Y., Investigations of Strain Accumulation at the Sumatran Fault and Subduction Zone from GPS Measurements, pp. 22, Scripps Institution of Oceanography, La Jolla, 2002.
- Boyd, T.M., J.J. Taber, A.L. Lerner-Lam, and J. Beavan, Seismic rupture and arc segmentation within Shumagin Island seismic gap, Alaska, *Geophysical Research Letters*, *15* (3), 201-204, 1988.
- Charles, C.D., D.E. Hunter, and R.G. Fairbank, Interaction between the ENSO and the Asian Monsoon in a coral record of tropical climate, *Science*, *277*, 925-928, 1997.
- Dawson, T., A 7000 Year Record of Paleoearthquakes on the Central Garlock Fault, near El Paso Peaks, California, M.S. thesis, San Diego State University, San Diego, 2000.
- Deplus, C., M. Diament, H. Hebert, G. Bertrand, S. Dominguez, J. Dubois, J. Malod, P. Patriat,
 B. Pontoise, and J. Sibilla, Direct evidence of active deformation in the eastern Indian oceanic plate, *Geology*, 26, 131-134, 1998.
- Dragert, H., K.L. Wang, and T.S. James, A silent slip event on the deeper Cascadia subduction interface, *Science*, *292*, 1525-1528, 2001.
- Fluck, P., R.D. Hyndman, and K. Wang, Three-dimensional dislocation model for great earthquakes of the Cascadia subduction zone, *Journal of Geophysical Research*, 102, 20539-20550, 1997.

- Freymueller, J.T., S.C. Cohen, and H.J. Fletcher, Spatial variations in present-day deformation, Kenai Peninsula, Alaska, and their implications, *Journal of Geophsical Research*, *105*, 8079-8101, 2000.
- Heki, K., H. Miyazaki, and H. Tsuji, Silent fault slip following an interplate earthquake at the Japan trench, *Nature*, *386*, 595-598, 1997.
- Kelsey, H.M., R.C. Witter, and E. Hemphill-Haley, Plate-boundary earthquakes and tsunami of the past 5500 yr, Sixes River estuary, southern Oregon, *Geological Society of America Bulletin*, 114, 298-314, 2002.
- Lowry, A.R., K.M. Larson, V. Kostoglodov, and R. Bilham, Transient fault slip in Guerrero, southern Mexico, *Geophysical Research Letters*, 28 (19), 3753-3756, 2001.
- Lyakhovsky, V., Y. Ben-Zion, and A. Agnon, Earthquake cycle, fault zones, and seismicity patterns in a rheologically layered lithosphere, *Journal of Geophsical Research*, *106*, 4103-4120, 2001.
- Mazzotti, S., X. Le Pichon, P. Henry, and S.-I. Miyazaki, Full interseismic locking of the Nankai and Japan-west Kurile subduction zones: An analysis of uniform elastic strain accumulation in Japan constrained by permanent GPS, *Journal of Geophsical Research*, 105, 13,159-13,177, 2000.
- Mitsui, N., and K. Hirahara, Viscoelastic simulation of earthquake cycle using a simple spring-dashpot-mass system with friction law, *Geophysical Research Letters*, 28, 4391-4394, 2001.
- Newcomb, K.R., and W.R. McCann, Seismic history and seismotectonics of the Sunda Arc, *Journal of Geophysical Research*, 92, 421-439, 1987.
- Prawirodirdjo, L., Y. Bock, R. McCaffrey, and e. al., Geodetic observations of interseismic strain segmentation at the Sumatra subduction zone, *Geophysical Research Letters*, *24*, 2601-2604, 1997.
- Rivera, L., K. Sieh, D. Helmberger, and D.H. Natawidjaja, A comparative study of the Sumatran subduction-zone earthquakes of 1935 and 1984, *Bulletin of the Seismological Society of America*, *92*, 1721-1736, 2002.
- Rockwell, T., A. Barka, T. Dawson, K. Thorup, and S. Akyuz, Paleoseismology of the Gazikoy-Saros segment of the North Anatolia fault, northwestern Turkey: Comparison of the

- historical and paleoseismic records, implications of regional seismic hazard, and models of earthquake recurrence, 2000.
- Royer, J., R. Gordon, C. DeMets, and P. Vogt, New limits on the motion between India and Australia since chron 5 (11 Ma) and implications for lithospheric deformation in the equatorial Indian Ocean, *Geophysical Journal International*, 129 (1), 41-, 1997.
- Saji, N.H., B.N. Goswami, P.N. Vinayachandran, and T. Yamagata, A dipole mode in the tropical Indian ocean, *Nature*, 401, 360-363, 1999.
- Scholz, C., *The Mechanics of Earthquakes and Faulting*, 439 pp., Cambridge University Press, New York, 1990.
- Sieh, K., M. Stuiver, and D. Brillinger, A more precise chronology of earthquakes produced by the San Andreas fault in southern California, *Journal of Geophsical Research*, *94*, 603-623, 1989.
- Stein, R., A. Barka, and J. Dieterich, Progressive failure on the North Anatolian fault since 1939 by earthquake stress triggering, *Geophys.J.Inter.*, *128*, 594-604, 1997.
- Taylor, F.W., J. Frohlich, J. Lecolle, and M. Strecker, Analysis of partially emerged corals and reef terraces in the central vanuatu arc - comparison of contemporary coseismic and nonseismic with quaternary vertical movements, *Journal of Geophysical Research*, 92, 4905-4933, 1987.
- Thatcher, W., The earthquake deformation cycle at the Nankai through, southwest Japan, *Journal of Geophysical Research*, 89, 3087-3101, 1984.
- Zachariasen, J., Paleoseismology and Paleogeodesy of The Sumatran Subduction Zone: A Study of Vertical Deformation Using Coral Microatolls, dissertation thesis, California Institute of Technology, Pasadena, 1998.
- Zachariasen, J., K. Sieh, F.W. Taylor, R.L. Edwards, and W.S. Hantoro, Submergence and uplift associated with the giant 1833 Sumatran subduction earthquake: Evidence from coral microatolls, *Journal of Geophysical Research*, *104*, 895-919, 1999.
- Zachariasen, J., K. Sieh, F.W. Taylor, and W.S. Hantoro, Modern vertical deformation above the Sumatran subduction zone: paleogeodetic insights from coral microatolls, *Bulletin of the Seismological Society of America*, *90* (4), 897-913, 2000.